# ANALYSIS OF THE EFFECTIVE PROPERTIES OF SMART COMPOSITE AND REINFORCED PLATES

by

ASHWIN KUMAR RAVICHANDRAN

Submitted in partial fulfilment of the requirements
for the degree of Master of Applied Science

at

Dalhousie University
Halifax, Nova Scotia
June 2021

© Copyright by ASHWIN KUMAR RAVICHANDRAN, 2021

# TABLE OF CONTENTS

# LIST OF TABLES

# LIST OF FIGURES

## ABSTRACT

In this thesis, an introduction to composite material is given for the understanding of its nature and behavior. Numerous types of composites and their properties studied further in the analysis are explained along with their graphical representation. A number of manufacturing methods are discussed for the production of these composites. Current problems in the usage of composites in a myriad of applications are reviewed. The difficulties in the industry due to the absence of data for long-term use of composites are put forward. The method acting as a solution to this issue called the asymptotic homogenization method is established, and the current literature available on this method is further elaborated. The asymptotic homogenization technique involves transforming a normal structural composite medium, anisotropic in nature, with varying elasticity, conductivity, thermal coefficients, and other influential coefficients into similar or homogenized coefficients with no variations in the properties. The resemblance of the method with the classical laminate theory for composites is also presented. This method helps us determine the local and global effective coefficients for composite plates and shells. Then, the mathematical equations used to predict these long-term properties of the composites are illustrated. A visual representation and explanation are also given for the number of different structures being considered in this analysis. Further, parametric inputs are given to those equations, and the variation of the properties along the thickness of the structures is represented. The aim is to calculate effective properties for a myriad of structures with different combinations of material and dimensional parameters to encourage the use of composites more spontaneously. The results are illustrated explicitly, and the variations are discussed. Applications are put forth for the structures with resemblance to the behavior and comparison to specific mechanical properties. This in turn will provide lots of data for the composite materials to be considered for more layman applications.

## LIST OF ABBREVIATIONS USED

MMC- Metal Matrix Composites

PMC- Polymer Matrix Composites

CMC- Ceramic Matrix Composites

FRP- Fiber Reinforced Polymer

CFRP- Carbon Fiber Reinforced Plastics

RTM- Resin Transfer Molding

RIM- Reaction Injection Molding

## ACKNOWLEDGEMENTS

I take this opportunity to acknowledge and have tremendous pleasure in thanking the following persons who have helped to make this thesis a successful one.

It is my pleasure to express sincere thanks and gratitude to my supervisor Dr. Alex Kalamkarov for being a great source of inspiration. It has always been a positive learning experience for me during his courses and interactions. He is a great deal of encouragement and motivation to me.

I would also like to thank Dr. Farid Taheri and Dr. Andrew Warkentin under whom I pursued my courses which were immensely helpful in gaining knowledge about the subject.

I am also very humbled in taking this opportunity to thank Dr. George Jarjoura and Dr. Pedram Sadeghian for accepting to be on the defense panel. I would also like to thank all the staff members and faculty encompassed in the Mechanical Engineering Department. I express my gratitude to the department and Dalhousie University for making all this possible.

Finally, I would also like to thank my parents, family members, and friends for being a pillar of support in all my educational endeavors and, in particular, my master's degree.

# CHAPTER 1 INTRODUCTION

## 1.1 COMPOSITE MATERIALS

Composite materials are materials created by binding different materials of unique physical and chemical properties. e.g. Kevlar Vest, Carbon Fibers. These different materials are existent in their original state and are just bound together as a whole to be called a composite. Composite materials have a wide range of applications such as aerospace, automotive, marine, and electronics due to their high strength-to-weight and stiffness-to-weight ratios, while researchers are working hard to find more common applications for them.

Composites are a constituent of reinforcement and a matrix. Reinforcement is the stronger and stiffer part of the composite, which deals with the carrying of the load, and the matrix is the softer phase that binds the reinforcements and the layers of it together. The matrix is also responsible for the attenuation of stresses from inside the composite to all phases of the composite so that the load-bearing capacity is increased. The objective is to move the applied loads to and among the filaments and shield the strands from threatening situations and rough handling. The matrix or resin is the low-strength connection in the composite. So, when the composite encounters loading, the matrix may split, de-bond from the fiber surface, or separate under far lower strains than usually desired. In any case, the matrix keeps the reinforcing strands in their legitimate direction and position with the goal that they can carry loads, disseminate loads uniformly among filaments, and give protection from crack development and other damages. Impediments in the matrix by and large decide the general service temperature restrictions of the composite.


**Figure 1.1 Composite Aircraft Structures [76]**

Until now, development and research of composites were done keeping in mind only the aerospace industry and other high-tech applications. The current decade and its technological advances have created the need for more efficient and highly complex materials to satisfy the need for more advanced applications. So, now composites are considered an everyday material to be used in all applications from bathroom fixtures, construction, automobile, and many more. The new challenges which are now being faced by researchers in using composite materials are that the long-term behavior characteristics of the composite are highly vague because of its inferiority in terms of highly used materials such as steel and concrete, which is well proven for their long-lasting properties in day-to-day life. There exists a constant need to analyze these long-term behavior characteristics of composites to make it possible to provide enough data to prove itself to be more worthy than the traditional materials. Glass fibers are the most common choice for composite parts. The best fiber for a particular application depends on the required strength, stiffness, and corrosion resistance.

## 1.2 CLASSIFICATION ACCORDING TO TYPE OF MATRIX

### 1.2.1 METAL MATRIX COMPOSITES (MMC)

Metal matrix composites comprise a metal (Al, Mg, and Cu) matrix loaded up with nano-ceramic particles (carbides, oxides, nitrides, and carbon nanotubes), highlighting physical and mechanical properties different from those of the framework (Riccardo and Maurizio, 2014). It is also defined by them that the MMC's are composites consisting of metallic alloys as the matrix such as aluminum, titanium, and copper. The reinforcements are more often particulate such as graphite, zirconium oxide, and aluminum oxide. MMC-type composites are highly suitable for fast-moving parts in aerospace and automobile industries, typically in jet engines, turbines, etc. MMCs can be utilized in different applications, for example, automotive designing, flight industry, and other light and substantial ventures. Light alloy composites are now used to manufacture valve trains, cylinder heads, chamber heads, driving shaft bearings in the auto industry [77].

### 1.2.2 CERAMIC MATRIX COMPOSITES (CMC)

As the name suggests, ceramic matrix composites use ceramics such as borosilicate as the matrix, with carbon or silicon carbide fibers acting as the reinforcement. This will make the ceramics less prone to fracture as it is a well-known fact that ceramics are tough materials, but they are prone to fracture very easily. Commonly known materials are Carbon-reinforced silicon carbide used in air and space vehicles with some application in the military. It is highly suitable for performance parts such as brakes, clutches, turbines, and nuclear reactors. Since the applications involve extreme temperatures, fibers other than carbon are avoided being used as a reinforcement.

### 1.2.3 POLYMER MATRIX COMPOSITES (PMC)

Polymer Matrix composites are different from CMC's in such a way that the fibers in CMC's gives them properties like making them stronger and less agile. But in PMC's the fibers makes the composite more brittle and also adds strength to the matrix. The matrix is usually plastic can be classified into thermoplastic - can be softened and reshaped comparable to polyamide, and thermoset - permanently shaped, such as epoxy resin. These thermosets give high temperature bearing capability to the composites and protection from other liquids, but they are not as strong as the thermoplastic resin. Thermoplastic resins are easier to make and are very much suited for cost-reduction and mass production. It also offers elite properties such as lightness, stiffness, strength and is resistant to corrosion. Parts based on thermoplastics include fiberglass, car bumpers, airplane parts. These materials are also the first choice for sporting goods that require agility.

Epoxy resins are utilized more than any other matrices in cutting-edge composite materials for basic aviation applications. Epoxies are well known for exhibiting better properties than polyesters in their protection from dampness and other natural impacts.

#### (a) FIBER-REINFORCED POLYMER (FRP)

Fiber-reinforced composite comprises the fiber in a dispersed manner, the matrix, and the medium in-between called the interface. Fiber strengthened polymer (FRP) are composites utilized in pretty much every sort of cutting-edge designing structure, with their use extending from airplanes, helicopters, and rockets through to vessels and ships. The use of FRP composites keeps on developing at an amazing rate.

These materials are utilized more in the current business sectors and expanding demand in the latest applications, such as biomedical gadgets and construction.

FRP composites are lightweight, non-destructive, show high explicit quality, are effectively built, and can be customized to fulfill performance prerequisites. Because of these invaluable qualities, FRP composites need new development and recovery of structures through its utilization as support in solid, connecting decks, measured structures, dies, and outside reinforcement for bolstering seismic overhaul. On account of FRP composites, ecological concerns have all the earmarks of being a boundary to its plausibility as an economical material, particularly while thinking about the fossil fuel consumption, air contamination. Adding to this case, the capacity to reuse FRP composites is restricted, and in contrast to steel and wood, primary segments cannot be reused to play out a similar function in another structure. Nevertheless, assessing the ecological effect of FRP composites in structural applications, explicitly through life cycle examination, may uncover immediate and circuitous advantages that are more effective than traditional materials. The classification of the matrix in the fiber-reinforced composites is clearly given in [7].

**(b) PARTICLE REINFORCED POLYMER (PRP)**

Particle reinforced composites, as depicted in the name, constitute particulate matter in various forms such as spheres, flakes, and powder randomly distributed in the matrix. In macroscopic terms, the material is isotropic as a result of the particles remaining roughly the same size. Viable examples of particulates used are Aluminum Oxide ($Al_2O_3$), Boron Carbide ($BC_4$), and Silicon Carbide (SiC). Particle reinforcement in composites is a less viable method for reinforcing than fiber reinforcement. Particulate strengthened composites accomplish benefits in applications requiring high stiffness and

can are satiable in quality and durability. In all cases, the enhancements are not precisely comparable to that in a fiber strengthened composite.

Particulate strengthened composites find applications where significant levels of wear obstruction are required, for example, street surfaces. The hardness of concrete is expanded altogether by including rock as a fortifying filler. The prime benefit of particle strengthened composites is their minimal cost and simplicity of creation and forming [8]. The most widely recognized particle reinforced composite is concrete, a blend of rock and sand generally reinforced by the inhibition of tiny stones or sand. Metals are regularly strengthened with ceramic to obtain higher strength at the expense of flexibility. At last, polymers and rubber are regularly strengthened with carbon dark, generally utilized in automobile tires.

### 1.3 CLASSIFICATION ACCORDING TO TYPE OF REINFORCEMENT

1) Particle Reinforced

    a) Huge Particles

    b) Dispersion Strengthened

2) Fiber Reinforced

    a) Continuous

    b) Discontinuous

3) Structural

#### 1.3.1 LAMINATES

Laminated composites are those composites that have an increased layer of reinforcement and matrix arranged in a sandwich, honeycomb, or any essential orientation influenced by the desired properties. Each layer is called the lamina, and the combination is called a laminate. The reinforcements can also be oriented at different

angles to improve the load-bearing characteristics of the composite further. The layers used can be of other materials, which will make a hybrid composite. The individual layers are mostly orthotropic, with properties differing among three mutually orthogonal axes. Their high solidarity to weight proportion and the adaptability to tailor-make different parts with quality far surpassing that of the parent constituent materials are their primary features. These designed materials are orthotropic for the most part and regularly show extremely novel reactions under basic stacking and mathematical arrangements.

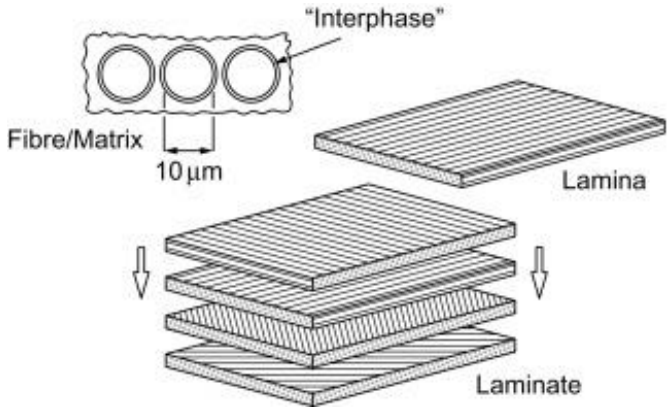


**Figure 1.2 Example of a laminate[42]**

The laminated composite structures essentially find applications in lightweight military vehicles and civil infrastructures as a result of their durability, ease of use, and high-performance characteristics. The technical shortcomings include involving less data when it comes to impact resistance attributes of the composite. They may undergo massive deformation under impact loading conditions and experience catastrophic damage themselves and the whole structure they are integrated into. Delamination is one of the significant problems in these kinds of composites. So, testing and analysis are often used to calculate the fiber-matrix bonding. Testing must be conducted obviously in the interface of the laminate where most shear properties are exhibited. Composite laminated are structured to provide optimum stiffness properties in the longitudinal axis

and along the other axes through a mix of varyingly oriented plies. Failure usually begins in the matrix of the laminates, leading to crack formation. Cracks are highly unstable and lead to propagation through the thickness and width of the composite in the loading direction. When loads are increased, failure occurs, causing significant damage if integrated into the critical part of the structure. It is essential to predict this data in the preliminary stages. Thus asymptotic analysis provides various analytical models suggesting the best usage of these high-quality composites, and a few orientations will be considered in the future sections.

### 1.3.2 SANDWICH PLATES

A sandwich composite is a unique plate where two thin sheets of composite material encompass a core material. The core material usually is a very lightweight, high stiffness material. The core material is capable of giving the composite high bending stiffness in a low-density layout.

Sandwich structures are generally utilized in lightweight development, particularly in aviation ventures as a result of their high explicit quality and solidity. The thin layers are usually made of steel, aluminum, composite, and the core of the sandwich might be plastics, foam, honeycomb, and balsa wood. The encompassing layers and the core are reinforced with resin to encourage the load transferring mechanisms between layers. This specific layered composition makes a fundamental component with high bending stiffness, lightweight, and optimum strength to weight ratios. Nevertheless, numerous turns of events and studies during these last years helped streamline the mechanical performance and thickness proportions for optimizing the ease of use for industrialists.

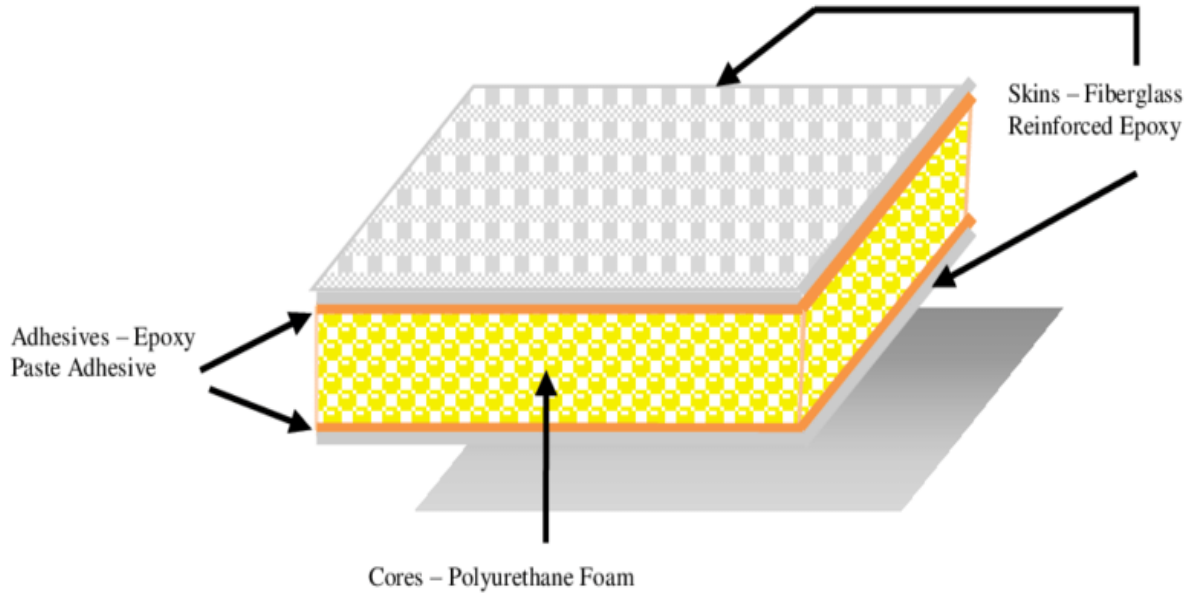


**Figure 1.3 Sandwich composite [33]**

The presence of the thick layer in the center called core implies that the deformation attributes of a sandwich shell are not the same as the relating qualities of a simple laminated shell or single-layer structure. For instance, the flexibility in the transverse direction of the core paves the conditions for a new unstable mode, whereby buckling of the face carriers into the core location may happen despite the fact that the general reaction of the structure may stay stable. Then again, because of the restricted flexural rigidity of the low-thickness core, the impacts of the local phenomena, for example, instability, load-incited thickness decrease, and so forth., on the global phenomena, for example, stability, bending, and so on., must be considered when planning with sandwich structures. The improvement of upgraded models that can viably influence the stresses, peak loads, and deformation under normal conditions is profoundly desirable. With the information on the effective deformation, stress, and performance of such structure, design characteristics at that point can be made available

to industrialists to encourage the use of these particular composites in a myriad of applications.

As shown in the image, the core consists of lightweight polyurethane foam and is embodied by a layer of adhesive and a fiberglass-epoxy reinforced composite skin on either side. The reinforced epoxy sheets can be manufactured by the hand lay-up method discussed further in section 1.7.1. Some common shapes of the cores being used in day-to-day applications are depicted in figures 1.3-1.5.

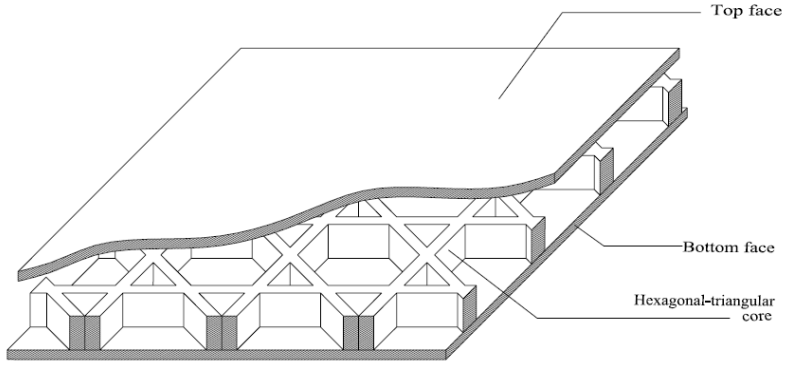


**Figure 1.4 Hexagonal-triangular core sandwich structure [34]**

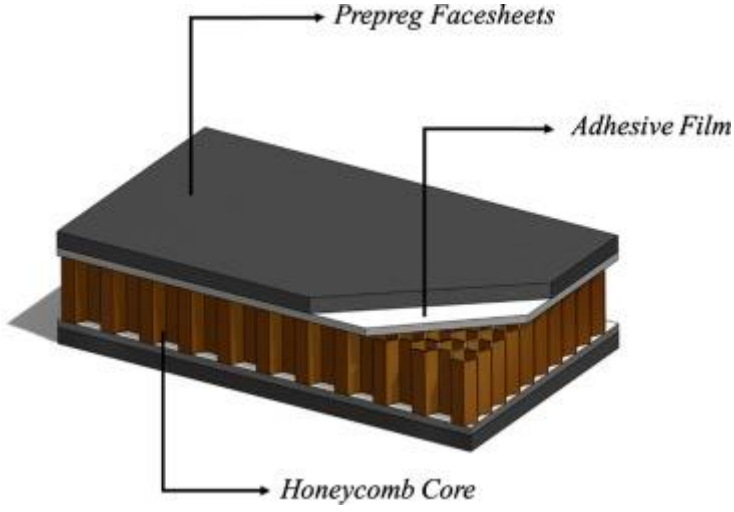


**Figure 1.5 Honeycomb sandwich structure [35]**

The core material assumes various shapes such as honeycomb, T rib, ∏ rib, triangular, diamond, star, hexagon, to name a few. According to the place of application,

the optimal design is assumed as the core to satisfy the performance characteristics. These rather advance high modulus, elevated strength, and low-density composite structures are only bound to be researched more and more because of the requirement of low weight materials in future applications. The thermal and mechanical behavior of these essential composite structures is an important facet purely because it will be used in applications that involve high temperatures, rapid temperature change, etc. So, for this reason, it is vital to obtain optimal solutions to thermoelasticity problems.

### 1.3.3 MAGNETOELECTRIC PLATES

The use of thin composites consisting of piezoelectric, piezomagnetic materials has increased drastically due to their potential for applications in streams like data storage, energy systems, magnetic sensors, etc. These particular composites exhibit some unique properties as a whole, which are seen in the macroscopic scale but are generally not potent on the micromechanical behavior of the individual components. This occurs as a result of coupling, which occurs in the form of magnetic, electrical, and thermal properties and is made possible through strain transfer between the components. So, these properties are fused to create new properties like pyroelectric, piezomagnetic, magnetoelectric, etc. A perfect example is the mechanical deformation of the piezoelectric phase when a field of electricity is induced in the piezoelectric-piezomagnetic phase of the composite. The strain overwhelms that particular phase and is transferred onto the piezomagnetic component creating a magnetic displacement. So here, a magnetic field is being created with an electric field application with the reversal also possible to perform. Similarly, the convergence of the thermal, electric and magnetic fields is referred to as pyroelectric and pyromagnetic effects.

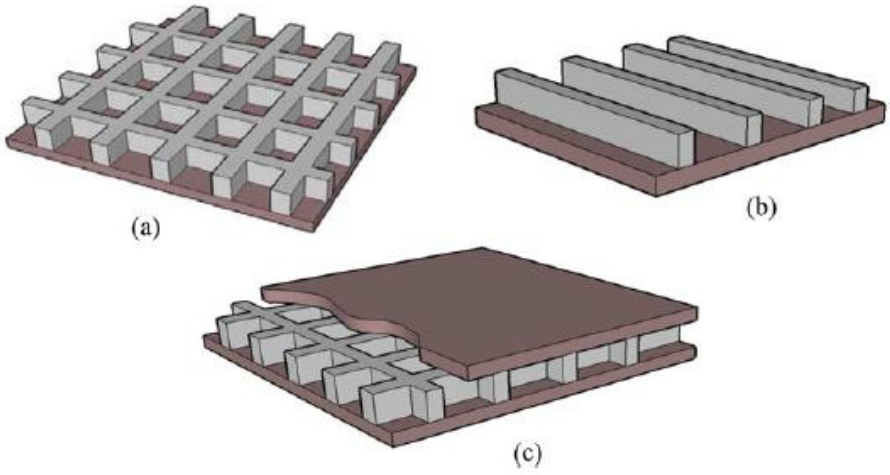


**Figure 1.6 Thin a) Wafer b) Rib c) Honeycomb filler reinforced plates [42]**

There is a scarcity of analytical models concerning composite reinforced structures such as rib or wafer reinforced, but some models are discussed in [42]. When the properties in the long term can be computed in the design phase, it is apparent that the integration of these unique magnetoelectric composites into new applications shall be achieved. Thus, newer mechanical models are being analyzed, and we will consider a few of these composites in this thesis. For the models to be effective, they are to be simple and have the capability of being used efficiently, effectively, and in less time.

### 1.3.4 THIN COMPOSITES

More often than not, composites in the form of thin plates and shells are highly preferred due to their optimal strength-weight ratio and their ease of manufacture using processes such as filament winding, as discussed in section 1.7.2. These thin composites are generally preferred for airplane bodies and shell structures. Engineers get attracted to these high-performance materials very easily as an alternative for mundane materials for numerous applications. For analysis and prediction of effective properties of these composites in the design stage, the asymptotic homogenization method remains a

desirable method due to its periodic or nearly periodic configuration with a single period being very small when compared to the global dimensions. For exceptional cases of plates where the thickness of the plate is in the same range as the reinforcements, a modified two-scale homogenization method must be applied.

### 1.3.5 GRID REINFORCED COMPOSITES

Grid reinforced composites are simple composites reinforced with a strong, high density, higher weight material. This reinforcement provides greater strength to the composite and improves the overall performance of the composite material in its application. The grids are placed in various angles and arrangements according to the characteristics needed. The most common example is the reinforcement of concrete with iron bars in the beams, pillars, and ceilings of buildings. The grid reinforcement is fully enclosed by a composite and is not visible in the outer area.

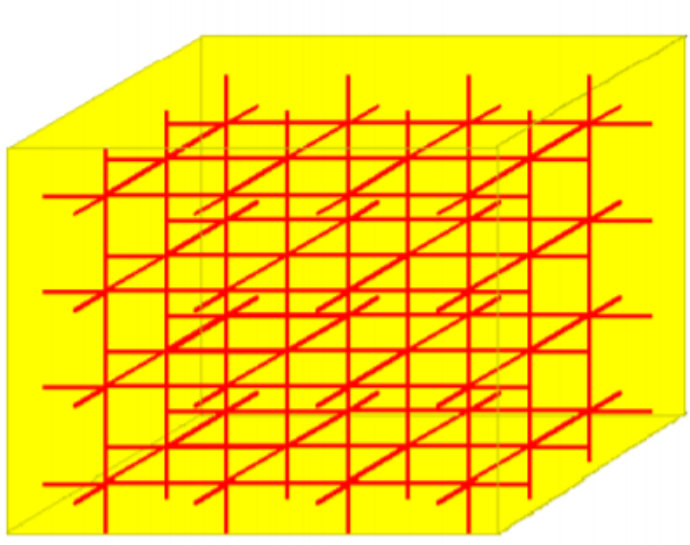

**Figure 1.7 Grid reinforced composite block [36]**

The most crucial incentive for using grid-reinforced composites is that they offer excellent unidirectional characteristics. The main structural components of these composites are nodes, ribs, and unit cells. They are regarded as a shell or skeleton

structure supported by a series of above-defined structural components. These structural supporting elements elevate stiffness property. Generally, the supporting elements run in two to four directions along with the shell, which forms a recurring arrangement. One of the benefits of using these composites is that in high-stress conditions, the propagation of cracks and the defects tend to settle within the unit cell in which the particular defect has occurred. In addition to the numerous advantages offered by these advanced composites, they are prone to buckling in the local/global coordinates. Manufacturing of these composites was a rigorous task in the past, but the advent of advancements in the filament winding and injection molding production techniques has, in a sense, alleviated that problem. Newer tooling techniques have decreased the manufacturing difficulties and increased its applications. The use of grid reinforced composites are gaining pace as they seem to eradicate the shortcomings of the simple laminated composites. Grid reinforcement is not a novel concept and was used mainly in spacecraft applications. Now, the operational engineers have found newer obligations to make use of these composites in many structures.

The general classification of grids includes arrangements such as tri-directional, quadri-directional, diagonal, ortho-grid, and angle-grid structures. Carbon fibers used as a reinforcement provide exceedingly satisfactory properties such as stiffness, lighter weight, capable of being used as flat and curved sheets used in the aerospace industry. General applications of the grid reinforced structures include high-speed applications as jet engine parts and structural applications such as launch-pads, panels, cargo containers, and slabs, etc. [37]

### 1.3.6 SMART COMPOSITE STRUCTURES

The smart composite materials in sync with the other types of composites are also predominantly being used in the shape of laminated and reinforced plates. It offers a wide range of advantages in any application for which it is being used. At the same time, it involves high complexity when it comes to the prediction of structural, material, geometrical characteristics when considering it in the preliminary stage. With the futuristic technology being made available day by day, there is growth in fields such as MEMS and radiocommunications, which as a chain reaction led to the development of high-performance sensors and actuators at affordable prices. Engineers found a way to integrate these sensors and materials to create smart material structures which elevated the control of properties of the composite materials. Smart Composites, as depicted in their name, are adaptive in nature and react to specific stresses and strains being induced on them with a capability to self-repair as conditions vary [15].

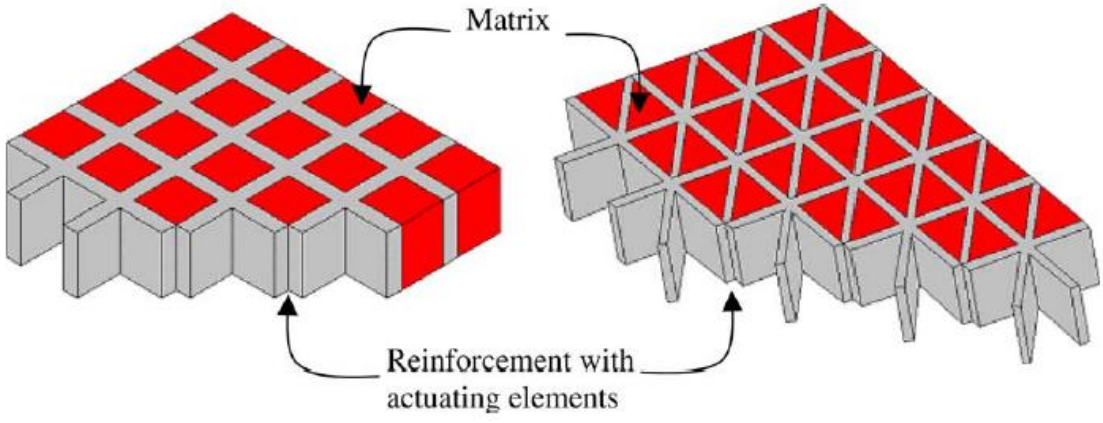


**Figure 1.8 Examples of smart structures with actuators [31]**

The function of smart structures is to be able to produce biological measures in mechanical systems under load. So, the sensors or actuators should be fitted in the skeletal system of the structure to induce or control the higher performance

characteristics. Features like learning and decision making are indigenous to these composites as it adapts to advanced conditions like the human motor system and can repair itself similar to the immune system in humans. Some mundane applications include shape memory alloys, piezomagnetic and piezoelectric panels, and electro magneto fluid systems [29].

The sensors and actuators have the capability to provide valuable data on the state and serviceability of the structure. They can effectively adapt to variability in the atmosphere such as magnetic power, loading, electrical, and thermal changes. Therefore, it can be said that these characteristics are required to be able to continually enhance and upgrade the structure's tendency for a particular purpose and ensure long-term dependability [17].

Often, in consideration of composite plates and shells, the reinforcing actuators or sensors are in the form of particles, ribs, wafers, fibers, etc., and spatially configured periodically. Thus, analysis by means of the asymptotic homogenization method is frequently used. Periodicity is exhibited in the tangential coordinates of the shell and not in the perpendicular coordinates. When the thickness of the shell has the same variance as the structural thickness and the thickness of the plate, the classical asymptotic homogenization method cannot be used. In that case, a modified approach is followed, as depicted in [38-40]. It is a relatively simple approach where individual variables are introduced for periodicity in the tangential direction. Another set of variables is introduced for the transverse direction, which is not in a periodic configuration.

The analysis of these smart composite structures must be carried out in a refined manner by considering that actuators and the distribution of the fibers comprise the smart material's microstructure. It can significantly manipulate the micromechanical behavior

of the smart material structure. It is essential to derive a fast and effective micromechanical model capable of depicting the structure's actual behavioral characteristics to inspire its use in various applications.[29]

## 1.4 FIBERS

**Glass fibers** are utilized for nonstructural, low-strength applications, for example, panels in airplanes and apparatus for elite applications such as rocket-engine cases and vessels. However, the sensitivity of the glass fiber to tackle dampness presents issues for different applications. The most usually utilized glass fiber is calcium aluminoborosilicate glass (E-glass). High silica and quartz filaments are likewise used for particular applications.

**Carbon strands** are the most popular and most broadly utilized reinforcing fiber in cutting-edge composites. Carbon fiber strengthened plastic (CFRP) materials are the future lightweight materials, generally welcomed in all ventures, including the car business, better than other light materials. Nonetheless, CFRP-based gadgets are costly due to the base material, which is carbon fiber. The early carbon filaments were created by the thermal decay of rayon forerunner materials. As of now, the most significant user of carbon fibers is the avionic industry since carbon strands are lighter and stronger than the other metals.

**Aramid fibers** are pleasant-smelling polyamide strands. The aramid fiber is a thermoplastic polymer like nylon, yet it decays when thermal energy is applied before it arrives at its calculated melting point. When polymerized, it forms strong, rigid, bar-like atoms that cannot be spun from a melt. Instead, they must be spun from a fluid glasslike solution. Early utilization of aramid strands included fiber wound engine cases and gas

pressure vessels. Aramid filaments have lower compressive qualities than carbon strands. However, their high explicit qualities, low densities, and durability keep them popular.

**Boron filaments** were the main elite reinforcement accessible for use in futuristic composites. They are, in any case, more costly and less appealing for their mechanical properties than carbon strands. Boron fibers are made by the deterioration of boron halides on a hot tungsten wire. Composites can likewise be produced using bristles scattered in a proper matrix.

## 1.5 ADVANTAGES OF COMPOSITE MATERIALS

- High strength and stiffness-to-weight ratio
- Low weight
- Excellent corrosion resistance
- Excellent fatigue resistance
- Can be "tailored to fit"

## 1.6 DISADVANTAGES OF COMPOSITE MATERIALS

- High cost of raw material
- Transverse properties may be weak
- Delamination
- Complex inspection methods
- Difficult to reuse

## 1.7 MANUFACTURING PROCESS

### 1.7.1 HAND LAY-UP METHOD

The Hand Lay up method is a widely used composite production process. It is very simple, and a layperson could perform this operation without any guidance. The

reinforcement, usually woven fabric, is combined with the resin by keeping layers of fabric and applying resin in between them (see figure 1.3 [11].

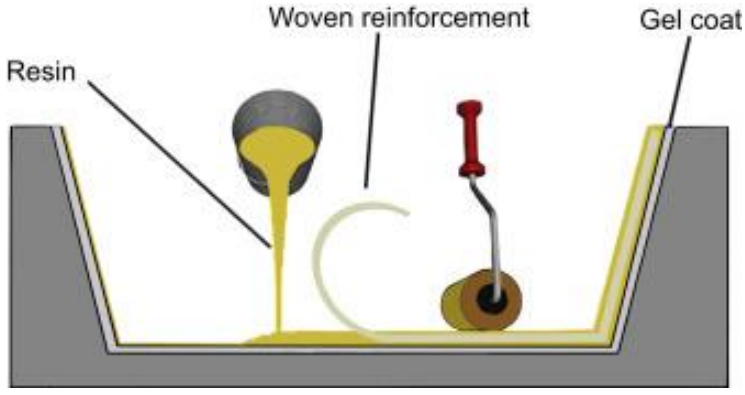


**Figure 1.9 Hand Lay-up setup [11]**

In this cycle, the fiber reinforcement is physically embedded into a one-sided form, where the resin is constrained through the thickness of the fiber mats utilizing hand rollers. An essential bit of leeway to the hand lay-up method is its capacity to manufacture huge, complex parts with a speedy process. Additionally, more advantages to this method are basic equipment and tooling that are generally more affordable as compared to other manufacturing processes. The hand lay-up process's first hindrance is that it is work concentrated, bringing high process durations and a low volume yield of parts. The idea of the hand lay-up cycle may likewise bring about parts with conflicting fiber directions. Another downside intrinsic to hand lay-up is that it tends to go out of shape when laminates of variable thickness are being used [12].

### 1.7.2 FILAMENT WINDING

Filament winding is a manufacturing procedure for most parts utilized for assembling open (chambers) or closed-end structures (pressure vessels or tanks). This cycle includes twisting fibers under strain created by the nip roller device, as shown in figure 1.10 over a rotating mandrel.

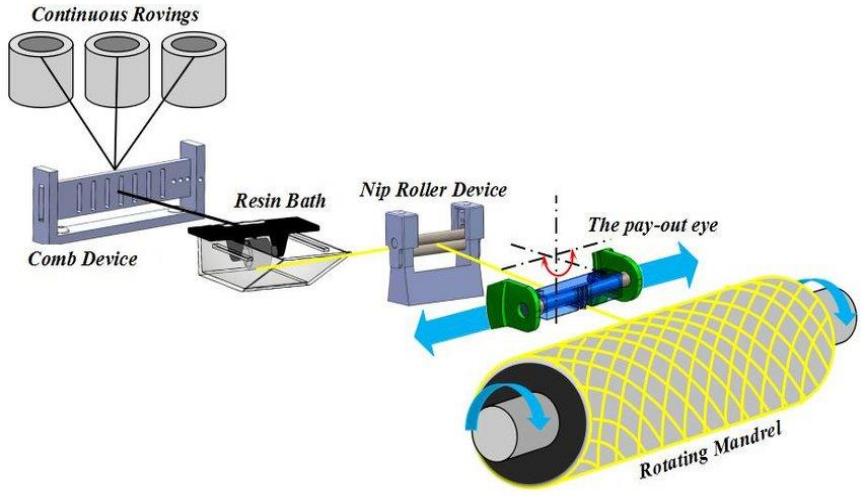


**Figure 1.10 Filament Winding [13]**

The mandrel turns around the axle while a pay-out eye on a carriage crosses on a level plane in accordance with the pivot of the rotating mandrel, laying down filaments in the ideal angles or arrangement. The most well-known fibers are glass or carbon and are impregnated in a resin shower as they are wound onto the mandrel. When the mandrel is wound up to the ideal thickness, the resin is allowed to dry. Depending on the resin's properties and curing time, the turning mandrel is frequently put in a thermal vessel or set under radiators until the part is cured. When the resin has dried out, the mandrel is taken out or extricated, leaving the hollow cylinder as the product. For certain products, for example, gas bottles, the 'mandrel' is a perpetual aspect of the completed item forming an inner lining to restrict gas spillage or as a hindrance to shield the composite from the liquid to be stored in it. Pipes and lightweight vessels that are wound can be cured with no human mediation [2].

### 1.7.3 PULTRUSION

Pultrusion is a composite manufacturing process where incessant fibers are impregnated with the thermoset polymer matrix through a heated-up die to shape composites. It has the capacity to run persistently to create segments with a consistent

cross-sectional profile for mass production, which is difficult utilizing other composite manufacturing techniques. The pultruded composites ordinarily involve as high as 70 % of fiber content, and the products are exceptionally rigid. Moreover, the simplicity of manufacturing and the cost-viability of this cycle makes it one of the effective procedures for the manufacture of fiber composite parts [14].

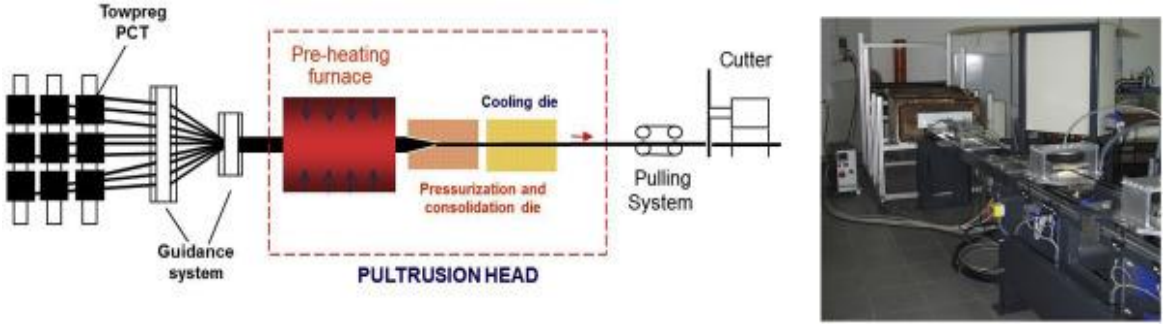


**Figure 1.11 Pultrusion Setup [75]**

The cycle begins with pulling the ceaseless fibers from the fiber creel and passing it through a resin shower. The composites are molded and cured in a heated die and finally cut by a shaper. Fiber creel is the equipment that sorts the fiber bobbins so that the fibers are effortlessly pulled without a tie-up, and the fibers can be glass fiber as well as natural fibres like balsa, jute, and so on. The size of fiber creels is subject to the amount of the fiber strand utilized to create the composite profiles. Every creel can uphold up to 100 fiber bobbins. The fibers are pulled from the creel into a resin shower and are inundated in the polymer resin in the resin bath. Complete submersion of fibers in the resin is guaranteed to evade deficient fiber wetting. The polymer resins utilized in the pultrusion procedure are commonly thermosetting polymers, for example, epoxy, polyester, vinyl ester, and phenolic, and their definitions are changed to suit the pultrusion operation. The unnecessary resin is collected onto a plate and diverted back to the pitch shower [14].

### 1.7.4 RESIN TRANSFER MOLDING

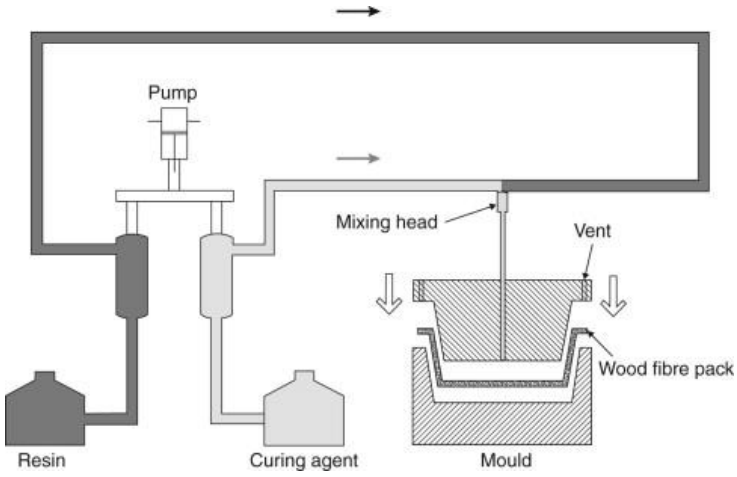


**Figure 1.12 Resin Transfer Setup [74]**

In resin transfer molding (RTM), the fiber reinforcement is put in a mold, and the resin at that point is presented by infusion. RTM, by and large, requires low-consistency resins, yet impregnation can be improved by vacuum-helped infusion. The resulting decrease in mold closure pressure makes the operation more apt for huge moldings, for example, vehicle body shells, and suggests that the molds themselves might be produced using lighter, less expensive materials, with impressive cost savings (light RTM). Another ongoing advancement is to infuse into a closed mold and complete the cycle with a pressurized step, permitting sped-up injection as well as higher fiber volume portions in the finished part. Nevertheless, although it is less expensive than prepreg preparation, RTM stays more restricted in its scope of utilization.

### 1.7.5 REACTION INJECTION MOLDING

Reaction injection molding (RIM) utilizes quickly responding parts blended only before infusion using a high-pressure impinging blender, allowing short process durations. Short fiber reinforcement may be presented in one or both reagents. It is comparable with press molding to assemble a range of small to medium-size cars and

homegrown components. RIM composites have various processing benefits, including concise process duration, low work, low mold bracing pressure, and low piece rate. RIM utilizes reinforcements to improve the properties of the pitch. With the utilization of reinforcements, polymerization shrinkage is diminished, thermal expansion is decreased, hang and droop of the composite at raised temperatures is limited, and other fundamental properties, for example, brittleness, rigidity, and ductile extension, are commonly improved. Processed filaments or flakes can be added legitimately to the resin before responding to the blending head.

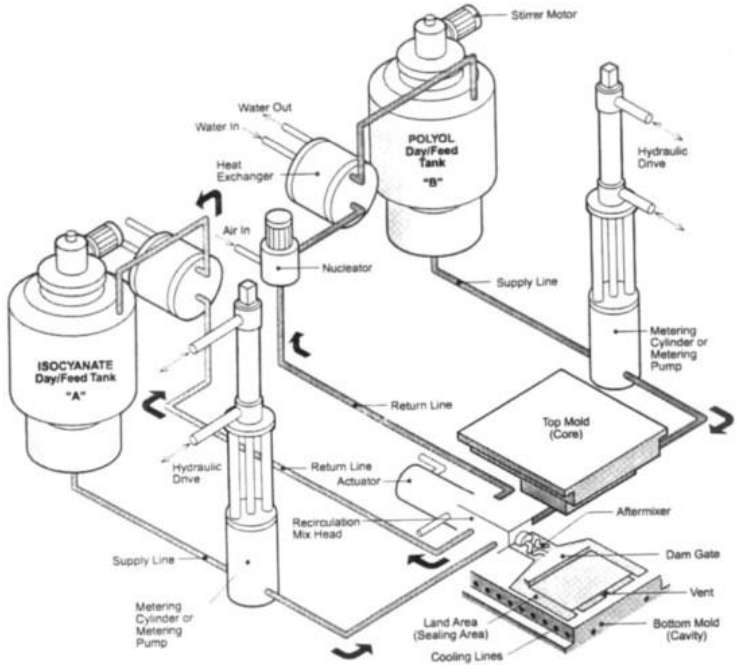


**Figure 1.13 Reaction Injection Molding [32]**

# CHAPTER 2 PROBLEM FORMULATION

Materials used for an application play a crucial role in deciding the characteristics of the part and how it can work. These materials are responsible for making up any required item from mobile phones to buildings. One or more materials together are used to make up the final structure required. Engineers choose these materials to comply with the requirements in all fields of work, from electronic to civil applications. The application influences the guidelines for selecting a particular material. Various factors being considered are lifespan, loading conditions, environmental conditions, impact resistance. A material needs to be analyzed highly before any real-life usage as it may involve massive amounts of investment and a considerable hazard to the users. It means that the material is chosen after scrutinizing it and with a comparison of where it has been used before. Steel, for example, is a vastly used material in engineering applications. As a result, there are lots of usage statistics available for engineers to use in order to make steel as their material and decide its properties, dimensions, etc. Steel, an alloy of iron, has been used for centuries for its well-proven properties, low cost, and easy availability. It has proven to be a sturdy and long-lasting material. Historically, steel is being used for rail tracks for decades requiring low maintenance and satisfying the required application without creating any hazard. It is also reusable by melting and can be shaped to fit into newer applications.

Tar, along with crushed stones, is the most commonly used material for the laying of roads. It can be considered a rudimentary composite. Nowadays, more futuristic materials are being looked upon to reduce the environmental effects leading to a greener planet. Recycled plastic roads are being tried as a substitute. It is a kind of composite where plastic is used as the base material with resin to hold it. Longer life

span and reduced usage of environmental resources are considered the benefits of going to this alternative.

Leading from that point, composites, as explained in the above application, can replace conventional materials in a vast number of applications. Deficiencies in conventional material can be satiated with the use of composites. The automobile and racing industry has been revolutionized by the use of composite materials, making it possible to achieve higher speeds in a lighter machine. The aerospace industry revolves around composites for about 60 percent of parts of an aircraft, with the number getting higher day by day. The focus now has been not just to use composites in such highly precise engineering applications but also on smaller layman applications. The challenging factor in reaching this astounding goal has been the lack of confidence among engineers in using these composites. This lack of trust exists because there is rudimentary data on the effective properties of the composites. Predicting the long-term behavior and fracture characteristics of the composite have also posed challenges to researchers. The thought process is such that using a known material with pre-existing data is naturally dominant rather than taking a chance with materials in which the properties cannot be fully understood. Composite materials have not existed as long as the other environmental materials have. The latest technological advances have created more revolutionary materials in the form of smart composite materials, which were introduced in the previous section. So, it is challenging to analyze and produce an adequate amount of data to encourage its use. Even though there is ample data available for short-term usage of composite material through rigorous testing and analysis, their characteristic behavior in terms of usage span is not readily accessible by engineers. One of the huge concerns is reliability.

Asymptotic homogenization method has been in focus among researchers to predict the long-term behavior and properties of the composite laminates and shells. A thin laminate with realistic dimensions is considered, and a unit cell is derived from it. The problems are solved, and after analytical calculations, the effective properties of the composite can be predicted. The asymptotic homogenization technique involves transforming a normal structural composite medium, anisotropic in nature, with varying elasticity, conductivity, thermal coefficients, and other influential coefficients into similar or homogenized coefficients with no variations in the properties. It is represented through a common set of effective coefficients. The characteristic data already available aids in the conversion of the structure to a homogenized medium. The related boundary value problems are dissociated and transformed into simpler problems related to the homogenized medium pertinent to a single unit cell. The unit cell problems permit the determination of the effective coefficients as discussed above of the homogenized medium.

In attempts to assuage this problem, asymptotic analysis of thin plates and shells has been in consideration, and optimal results have been obtained in various cases. This method is so effective as it manages to disintegrate the microscopic and macroscopic variables and provides an option to operate them independently. This influences the main differential equations to be dissociated into smaller, simpler equations, with each one having micro or macro variables. These equations characterize the behavior of the composite periodic layer. The microscopic and macroscopic variables are mediated as "fast" and "slow," respectively, with the fast variables involving type, size, geometry, and the constituents of the composite structure. In contrast, the slow variables

incorporate the globalized variables such as dimensions, loads, and boundary conditions of the composite.

The following section discusses the myriad of research done on this subject to make more data available for engineers to encourage the use of composites for their applications. These works make it possible for everyday engineers to customize the effective properties of a composite structure and make it pertinent to required applications by means of modification of some simple parameters such as geometric parameters, material properties, and dimensional parameters. This thesis is being written to continue providing data to engineers and bridging that gap further. Composite plates and shells of various magnitude and properties using different materials, for example, thin network structures, honeycomb sandwich structures, smart structures exhibiting piezoelectric, magnetic properties, are considered in this thesis, and a parametric analysis involving realistic dimensions and properties of these plates are conducted. Some of these structures were introduced and structurally explained in section 1 of this thesis.

This thesis also aims to ease the process of selection of materials for usage by the industrialists. This is achieved by considering realistic properties and dimensions for the composite and providing valuable data to the engineers. The process begins by calculating the effective properties of composite structures, predominantly thin plates and shells, including honeycomb structures, smart structures, thin networks, and prismatic plates. Magnetoelectric plates offering various properties such as piezomagnetic and piezoelectric etc., are also considered. These plates were briefly discussed in section 1 of this thesis. The characteristic data is calculated for the composite structures. The data is related to some realistic dimensions for the thin plates and shells. The variation of effective properties in comparison to the structural and

material data being inputted is depicted utilizing visual representations. The data aims to provide day-to-day engineers with ease of selection and encouragement for them to choose the highly efficient composite materials in place of their traditional materials, which are being used for a long period of time. Also, the engineers have only so much data that there is difficulty predicting the long-term usage characteristics of the composite materials. The calculation of the effective properties using the asymptotic homogenization method is solely aimed to alleviate that problem. The parametric analysis is being conducted based on the same asymptotic homogenization method. So, the data represented hopes to fill engineers with confidence in where and for which application these composites will be best suited.

# CHAPTER 3 LITERATURE SURVEY

In this thesis, we consider laminates and other various composite classifications. Laminates are layers of material laid over each other in tandem, varying the geometry and materials used according to the properties required. A parametric analysis is conducted in chapter 6 of this thesis for some of these composites. The effective properties are derived by solving the unit cell problems of the homogenized structure. Homogenization of the structures is performed using the pertinent asymptotic homogenization method. Realistic dimensions are assumed for the composite structures of various arrangements when conducting the parametric analysis. The effective properties are depicted employing graphs in which differential data is used for obtaining the optimal characteristics for individual applications. In most industrial applications, there is an automatic preference for composites manufactured in the form of thin plates and shells (laminates). This is because they can give viable properties that prove appealing to industries, one of which is an ideal strength-weight ratio. The requirement of composites in high precision and critical applications requires the composites to made using continuous geometry using polymer matrix and equally spaced reinforcements with significant effects on the properties. This complex manufacturing makes it daunting to determine the effective properties, which depend on various factors such as the spacing and distribution of fibers, geometry of the composite, and mechanical properties of the fundamental materials used to make up the composite. However, the analysis of composites using the asymptotic homogenization method to develop various micromechanical models has alleviated the problems in determining the characteristics at the design stage up to an extent. Some of the existing theory is discussed in brief in the current section.

Kalamkarov and Kolpakov [43] considered the fiber-reinforced angle ply composite shell and provided some valuable design data on the same. In their paper, the following issues have been described and solved. The design problem of the fiber-reinforced shell is solved. A method of design parameter calculation done using convex analysis is described. The number of layers required for solving the design problem is established. The authors put forth prescribed stiffness for which design problems can be solved. This analysis is conducted as there is a need for theoretical modeling capable of predicting both effective characteristics and microstructure of the processes occurring under various environments. The method used facilitates the prediction of both local and overall average properties using asymptomatic homogenization. Effective stiffnesses are calculated using this method.

Kalamkarov et al.[1] used the modified asymptotic homogenization method to develop a geometrically nonlinear elastic composite layer model. In this paper, a thin 3D periodically inhomogeneous composite layer with wavy surfaces was considered for analysis. The effective stiffness properties were calculated, and the mechanical stresses and displacements are also derived. It was shown that the unit cell problems in the transverse direction are not dependent on periodicity and are connected with the boundary conditions. Reddy [4] has widely studied the mechanics of composite laminated plates and shells. He provides solutions to various analytical problems of rectangular laminates using CLPT and FSDT in his study. He performed non-linear analysis, one-dimensional analysis and has proposed the classical laminate theory and the first-order theory.

Haldijiozi et al. [17] developed a comprehensive micromechanical model for a smart elastic thin plate with rapidly varying thickness. The asymptotic homogenization method was followed in view of his research. The noticeable thing is they had developed this model for a smart composite with the help of piezo-magneto thermal actuators used by means of a switch to create residual stresses to control the behavior of the composite structure. Haldijiozi et al. [16] followed up from their previous work adding important literature to the world of composites by proposing a micromechanical model for thin composite magnetoelectric plates providing analytical results for elastic, piezoelectric, piezomagnetic coefficients. He also investigated with his colleagues the piezo-magneto-thermo-elastic T ribbed and ∏ ribbed plates [18]. The aspects involving composite structures were studied in [19]. It provided an interesting result where some of the properties obtained from the structure were absent in the constituents of the composite. So, these were obtained only as a result of the whole composite and not related to the individual properties of the constituents used in the composites. Other notable works include Yi et al. [57], who used the asymptotic homogenization method for viscoelastic composites with periodic microstructures. Their work deals with highly complex computations and shows that the composites' necessary characteristics can be obtained optimistically using memory effects. A comprehensive asymptotic theory was developed for anisotropic inhomogeneous and laminated piezoelectric plates by Cheng et al. [58]. This was in specific applied to a composite with a rectangular piezoelectric plate which is put under electrical and mechanical loadings.

The same method was used by Challagula et al. [19] to develop the micromechanical model for smart orthotropic composite shells. Results for orthotropic

sandwich shells were given by Kalamkarov and Saha [20]. A two-scale asymptotic homogenization method in their work. Two sets of 'fast coordinates were taken and straightforwardly related to the 3-dimensional problem of a thin homogenous plate. One of the coordinates is engaged with the rapid periodic oscillation of properties in the composite, and the other is related to the minute thickness of the composite layer and accounts for no periodicity in the transverse direction.

In [21], Chalagulla et al. conduct a micromechanical analysis of a grid reinforced generally orthotropic shell. Homogeneous plates of quickly changing thickness have been concentrated autonomously by Kohn and Vogelius [22-24] with the assistance of strategies like those utilized by Caillerie [25]. Kalamkarov [26] has summed up the above two ways to deal with shells with - highly differing material properties and thickness. Literature concerning the important micromechanical models dependent on utilizing the asymptotic homogenization strategy can be found in Kalamkarov and Kolpakov [28]. The above-given models follow the structure of linear elasticity theory, which holds for minor bending problems of composite structures. As a result of research by Kalamkarov and Georgiades [13] and Hadjiloizi et al. [14], the overall asymptotic homogenization model was extended to the application of smart composite shells with intermittently organized actuators and differing thickness. Kalamkarov et al. [29] Saha et al. [30] gave a smart composite micromechanical model in application to honeycomb and sandwich structures, respectively. A formidable model based on the thermopeizoelastic behavior of prismatic composite structures made of orthotropic materials was given by Georgiades et al. [31].

In the following sections, we discuss the control of the behavior of the composites by means of an actuating element (piezoelectric material). We use it to

modify the properties slightly to benefit the application in which it is used. Luo and Tong [50] cover this control methodology by depicting the high precision shape control for the orthotropic plate using piezoelectric actuators. They use the finite element method for the simulation and tracking of the composite plate's behavior. Here, the adhesive layer is not considered, and the peeling and debonding may not be captured in this analysis. The FEA model was presented and validated. It was found that the shape control method was accurate and very efficient in inducing the required strains. Koconis et al. [51,52] have studied the static shape control of these piezoelectric actuators by voltage-oriented and shape-oriented methods. Nguyen and Tong [53] developed a method for the shape control of non-rectangular actuators. They sued a quasi-static approach, which is induced by means of modifying some input parameters like electric pulse, dimensional parameters of the actuators. They use the FEA method to analyze the characteristics of the composite plate and obtain good results in the area. Choi and Lee [54] illustrate the same shape control method for composite beams with actuators embedded in them. They use shape memory alloy wire as actuators, and the results obtained are favorable to encourage shape control.

Castillero et al. [55] also proposed a homogenization method based on a technique called periodic unfolding. They were able to analytically model the magneto-electro-elastic periodic structures similar to what we discuss in the future sections. The generalized equations for the effective properties of the laminated composite of the same type are also given in their work. Andrianov et al. [56] also used the asymptotic homogenization method proposed by others in a rather intriguing application to predict the wave dispersion and propagation. The type of composite used in their work was periodic composites, which are also being used in the future in this thesis. He and

Pindera [59] had worked on composites with viscoelastic nature to perform a locally precise asymptotic homogenization. They also put the composite and performed the procedure under anti-plane shear loading, and optimal results were obtained in coincidence with the numerical solutions. Pozos et al. [60] contributed to this stream by developing an asymptotic model for a composite with layered heterogeneous structure with orthotropic natured material. Two composite layers were connected with a soft adhesive, and the adhesive joints were analyzed. However, there is a significant void when a thin composite layer of a composite laminate with a plain surface is considered. The research being conducted on different reinforcements and composite layers and shells has given positive results to engineers for calculating required properties and making use of them in further applications. Following in the same path, this research could provide good results for encouraging the use of a simple laminated plate. This thesis aims to depict how the inhomogeneous composite layer's elastic properties are affected by the constituting materials' geometry and mechanical properties.

# CHAPTER 4 HOMOGNEISATION METHOD

In this chapter, the general homogenization model for a composite material is described. The homogenization method follows the rule of superposition. A composite material is considered and is analyzed with another known material that is believed to exhibit the same properties as the inhomogeneous composite material. The properties are superimposed together to obtain better results in the stress distribution.

## 4.1 ASYMPTOTIC HOMOGENISATION METHOD

Here, a thin three-dimensional composite layer of a periodic structure with a unit cell $\Omega_\delta$. Let us consider a thin layer of composite and analyze it locally by considering its unit cell. The unit cell is deemed to be occupying the domain $\Omega_\delta$. The depiction of the thin layer and its unit cell can be seen in figure 4.1. The thickness and scale of the composite material inhomogeneity are assumed to be small compared with the dimensions of the solid as a whole.

The unit cell $\Omega_\delta$ is determined by using the following inequalities.

$$\frac{-\delta h_1}{2} < \alpha_1 < \frac{\delta h_1}{2}, \frac{-\delta h_2}{2} < \alpha_2 < \frac{\delta h_2}{2} \; and \; \gamma^- < \gamma < \gamma^+$$

$$\gamma^{\pm} = \pm\frac{\delta}{2} \pm \delta F^{\pm}\left(\frac{\alpha_1}{\delta h_1}, \frac{\alpha_2}{\delta h_2}\right) \tag{4.1}$$

In the above equation, $\delta$ is the thickness of the composite layer. $S^+$ and $S^-$ are the upper layer and lower layer of the composite, along with which the function $F^{\pm}$ models the shape of the shell. $\delta h_1$ and $\delta h_2$ are the dimensions of the unit cell. In simple terms, it is taken as the width and breadth of the plate. When there are no reinforcements in the composite, the functions are set to zero, and $\delta$ will become the thickness of the composite layer. Generally, it is a minor value where $\delta << 1$.

The procedure followed in this process is that we take an inhomogeneous composite material and compare or take the material of anisotropic homogenous nature, showing approximately the same properties as the composite and performing stress analysis on it. These properties are, in turn, averaged using the asymptomatic homogenization method, which also gives relatively good results for the stress distribution. In the figure shown below, $\alpha_1$, $\alpha_2$, $\gamma$ are the orthogonal curvilinear coordinates such that $\alpha_1$ and $\alpha_2$ coincide with the main curvature lines of the mid surface of the carrier layer and $\gamma = 0$.

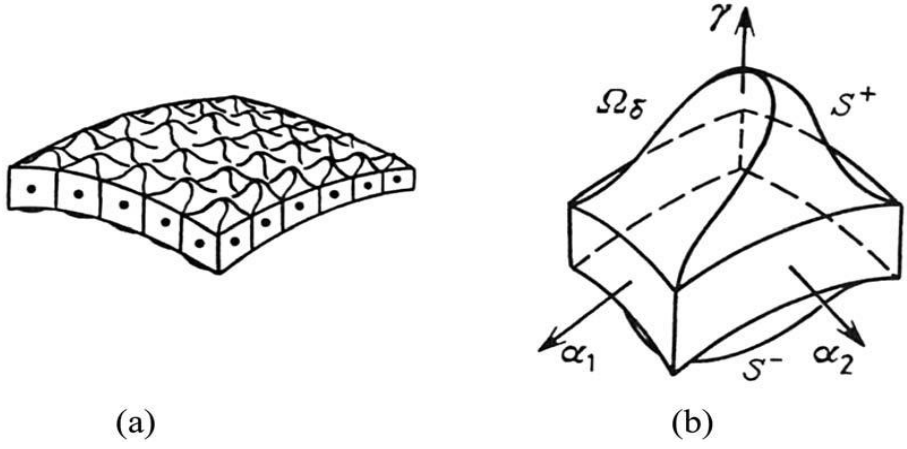


**Figure 4.1 a) Curvilinear reinforced composite shell b) Unit Cell $\Omega_\delta$**

Using the equations for the lame coefficients $H_1 = A_1(1 + k_1\gamma)$ and $H_2 = A_2(1 + k_2\gamma)$, we can get the relations describing the strain and displacements as

$$e_{11} = \frac{1}{H_1}\frac{\partial u_1}{\partial \alpha_1} + \frac{1}{H_1 A_2}\frac{\partial A_1}{\partial \alpha_2}u_2 + \frac{A_1 k_1}{H_1}u_3, \qquad e_{22} = \frac{1}{H_2}\frac{\partial u_2}{\partial \alpha_2} + \frac{1}{H_2 A_1}\frac{\partial A_2}{\partial \alpha_1}u_1 + \frac{A_2 k_2}{H_2}u_3,$$

$$e_{33} = \frac{\partial u_3}{\delta z}$$

$$2e_{12} = \frac{1}{H_2}\frac{\partial u_1}{\partial \alpha_2} - \frac{1}{H_2 A_1}\frac{\partial A_2}{\partial \alpha_1}u_2 + \frac{1}{H_1}\frac{\partial u_2}{\partial \alpha_1} - \frac{1}{H_1 A_2}\frac{\partial A_1}{\partial \alpha_2}u_1,$$

$$2e_{13} = \frac{\partial u_1}{\partial \gamma} + \frac{1}{H_1}\frac{\partial u_3}{\partial \alpha_1} + \frac{A_1 k_1}{H_1} u_1,\ 2e_{23} = \frac{\partial u_1}{\partial \gamma} + \frac{1}{H_2}\frac{\partial u_3}{\partial \alpha_2} + \frac{A_2 k_2}{H_2} u_2 \tag{4.2}$$

The equilibrium equations are given as shown below, and in this section, the subscripts 1,2 and 3 refers to $\alpha_1, \alpha_2, and\ \gamma$ respectively.

$$\frac{\partial(H_2\sigma_{11})}{\partial \alpha_1} + \frac{\partial(H_1\sigma_{12})}{\partial \alpha_2} + \frac{\partial(H_1H_2\sigma_{13})}{\partial \gamma} - \frac{H_1}{A_1}\frac{\partial A_2}{\partial \alpha_1}\sigma_{22} + \frac{H_2}{A_2}\frac{\partial A_1}{\partial \alpha_2}\sigma_{21} + H_2A_1k_1\sigma_{31} + H_1H_2P_1 = 0$$

$$\frac{\partial(H_2\sigma_{21})}{\partial \alpha_1} + \frac{\partial(H_1\sigma_{22})}{\partial \alpha_2} + \frac{\partial(H_1H_2\sigma_{23})}{\partial \gamma} - \frac{H_2}{A_2}\frac{\partial A_1}{\partial \alpha_2}\sigma_{11} + \frac{H_1}{A_1}\frac{\partial A_2}{\partial \alpha_1}\sigma_{12} + H_1A_2k_2\sigma_{32} + H_1H_2P_2 = 0$$

$$\frac{\partial(H_2\sigma_{31})}{\partial \alpha_1} + \frac{\partial(H_1\sigma_{32})}{\partial \alpha_2} + \frac{\partial(H_1H_2\sigma_{33})}{\partial \gamma} - H_2A_1k_1\sigma_{11} - H_1A_2k_2\sigma_{22} + H_1H_2P_3 = 0 \tag{4.3}$$

Where $P_i$, i = 1, 2, 3 represents the body forces in the composite and the $\sigma_{ij}$ terms are the stress components of the structure described as follows

$$\sigma_{ij} = c_{ijmn}e_{mn} \tag{4.4}$$

The shell surfaces are subjected to $\sigma_{ij}n_i = p^i$ where it is the stress tensor, unit vector, and the vector of the outer surface in order of the equation.

When we substitute the stress components into the boundary conditions, we get

$$\frac{\sigma_{11}}{H_1}n_1 + \frac{\sigma_{12}}{H_2}n_2 + \sigma_{13}n_3 = p_1$$

$$\frac{\sigma_{12}}{H_1}n_1 + \frac{\sigma_{22}}{H_2}n_2 + \sigma_{23}n_3 = p_2$$

$$\frac{\sigma_{13}}{H_1}n_1 + \frac{\sigma_{23}}{H_2}n_2 + \sigma_{33}n_3 = p_3 \tag{4.5}$$

Multiplying the above equations by $H_1$ and $H_2$

$$H_2\sigma_{i1}n_1^{\pm} + H_1\sigma_{i2}n_2^{\pm} + H_1H_2\sigma_{i3}n_3^{\pm} = \pm H_1H_2p_i^{\pm} \tag{4.6}$$

$n^{\pm}$ is the outward (+) / inward (-) unit normal vector.

When the surfaces $\gamma = \gamma^{\pm}$, the normal vector becomes

$$n^{\pm} = \left\{-\frac{\partial\gamma^{\pm}}{\partial\alpha_1}, -\frac{\partial\gamma^{\pm}}{\partial\alpha_2}, 1\right\}\left[1 + \frac{1}{H_1^2}\left(\frac{\partial\gamma^{\pm}}{\partial\alpha_1}\right)^2 + \frac{1}{H_2^2}\left(\frac{\partial\gamma^{\pm}}{\partial\alpha_2}\right)^2\right]^{-0.5} \tag{4.7}$$

Then, we move forward to introduce the fast coordinates of the problem,

$$y_1 = \frac{\alpha_1}{\delta h_1}, y_2 = \frac{\alpha_2}{\delta h_2}, z = \frac{\gamma}{\delta}, y = (y_1, y_2) \tag{4.8}$$

So, with the introduction of the new coordinate system, the inequalities defining the unit cell will take the form of,

$$\{-0.5 < y_1, y_2 < 0.5, z^- < z < z^+\}, z^{\pm} = \pm 0.5 \pm F^{\pm}(y)$$

and the vector is

$$n^{\pm} = \left\{\mp\frac{1}{h_1}\frac{\partial F^{\pm}}{\partial y_1}, \mp\frac{1}{h_2}\frac{\partial F^{\pm}}{\partial y_2}, 1\right\}\left[1 + \frac{1}{H_1^2h_1^2}\left(\frac{\partial F^{\pm}}{\partial y_1}\right)^2 + \frac{1}{H_2^2h_2^2}\left(\frac{\partial F^{\pm}}{\partial y_2}\right)^2\right]^{-0.5} \tag{4.9}$$

With the functions $c_{ijmn}(y, z)$ and $y = (y_1, y_2)$ being periodic to the unit cell in the normal coordinate system, the solution representing the non-homogeneity of the material is given as

$$u_i = u_i^{(0)}(\alpha) + \delta u_i^{(1)}(\alpha, y, z) + \delta^2 u_i^{(2)}(\alpha, y, z) + \cdots \tag{4.10}$$

Where $u_i^{(l)}(l = 1,2, \dots)$ functions with respect to $\alpha, y, z$ are also periodic to the unit cell. Assuming the asymptotic forms mentioned below with the consideration that the radii of curvature of the shell in the mid-plane are much larger than the shell's overall thickness.

$$k_1 = \delta K_2(\alpha), k_2 = \delta K_1(\alpha), k_1 + k_2 = \delta K_3(\alpha) \tag{4.11}$$

The relations for the external forces are also periodic to the unit cell and are given as

$$p_v^{\pm} = \delta^2 r_v^{\pm}(\alpha, y), p_3^{\pm} = \delta^3 q_3^{\pm}(\alpha, y), P_v = \delta f_v(\alpha, y, z), p_v^{\pm} = \delta^2 g_3(\alpha, y, z) \tag{4.12}$$

In the process of simplification, we introduce

$$\xi_1 = A_1 y_1, \xi_2 = A_2 y_2 \tag{4.13}$$

Taking into account relations (4.10), (4.11), and (4.12), we derive

$$e_{ij} = e_{ij}^{(0)} + \delta e_{ij}^{(1)} + \delta^2 e_{ij}^{(2)} + \cdots \tag{4.14}$$

where,

$$e_{11}^{(0)} = \frac{1}{A_1}\frac{\partial u_1^{(0)}}{\delta \alpha_1} + \frac{1}{h_1 A_1}\frac{\partial u_1^{(1)}}{\delta y_1} + \frac{1}{A_1 A_2}\frac{\partial A_1}{\delta \alpha_2} u_2^{(0)},$$

$$e_{22}^{(0)} = \frac{1}{A_2}\frac{\partial u_2^{(0)}}{\delta \alpha_2} + \frac{1}{h_2 A_2}\frac{\partial u_2^{(1)}}{\delta y_2} + \frac{1}{A_1 A_2}\frac{\partial A_2}{\delta \alpha_1} u_1^{(0)},$$

$$e_{33}^{(0)} = \frac{\partial u_3^{(1)}}{\delta z}$$

$$2e_{12}^{(0)} = \left(\frac{1}{A_2}\frac{\partial u_2^{(0)}}{\delta \alpha_2} - \frac{1}{A_1 A_2}\frac{\partial A_2}{\delta \alpha_1} u_2^{(0)}\right) + \left(\frac{1}{A_1}\frac{\partial u_2^{(0)}}{\delta \alpha_1} - \frac{1}{A_1 A_2}\frac{\partial A_1}{\delta \alpha_2} u_1^{(0)}\right) + \left(\frac{1}{h_2 A_2}\frac{\partial u_1^{(1)}}{\delta y_2} + \frac{1}{h_1 A_1}\frac{\partial u_2^{(1)}}{\delta y_1}\right)$$

$$2e_{13}^{(0)} = \frac{\partial u_1^{(1)}}{\delta z} + \frac{1}{A_1}\frac{\partial u_3^{(0)}}{\delta \alpha_1} + \frac{1}{h_1 A_1}\frac{\partial u_3^{(1)}}{\delta y_1}$$

$$2e_{23}^{(0)} = \frac{\partial u_2^{(1)}}{\delta z}\frac{1}{A_2}\frac{\partial u_3^{(0)}}{\delta \alpha_2} + \frac{1}{h_2 A_2}\frac{\partial u_3^{(1)}}{\delta y_2} \tag{4.15}$$

$$e_{11}^{(1)} = \frac{1}{A_1}\frac{\partial u_1^{(0)}}{\delta \alpha_1} + \frac{1}{A_1 A_2}\frac{\partial A_1}{\delta \alpha_2}u_2^{(1)} + K_2 u_3^{(0)} + \frac{1}{h_1 A_1}\frac{\partial u_1^{(2)}}{\delta y_1}$$

$$e_{11}^{(1)} = \frac{1}{A_1}\frac{\partial u_1^{(0)}}{\delta \alpha_1} + \frac{1}{A_1 A_2}\frac{\partial A_1}{\delta \alpha_2}u_2^{(1)} + K_2 u_3^{(0)} + \frac{1}{h_1 A_1}\frac{\partial u_1^{(2)}}{\delta y_1}$$

$$e_{22}^{(1)} = \frac{1}{A_2}\frac{\partial u_2^{(1)}}{\delta \alpha_2} + \frac{1}{h_2 A_2}\frac{\partial u_2^{(2)}}{\delta y_2} + K_1 u_3^{(0)} + \frac{1}{A_1 A_2}\frac{\partial A_2}{\delta \alpha_1}u_1^{(1)},$$

$$2e_{12}^{(1)} = \left(\frac{1}{A_2}\frac{\partial u_1^{(0)}}{\delta \alpha_2} - \frac{1}{A_1 A_2}\frac{\partial A_2}{\delta \alpha_1}u_2^{(1)}\right) + \left(\frac{1}{A_1}\frac{\partial u_2^{(1)}}{\delta \alpha_1} - \frac{1}{A_1 A_2}\frac{\partial A_1}{\delta \alpha_2}u_1^{(1)}\right) + \left(\frac{1}{h_2 A_2}\frac{\partial u_1^{(1)}}{\delta y_2} + \frac{1}{h_1 A_1}\frac{\partial u_2^{(2)}}{\delta y_1}\right)$$

$$e_{33}^{(1)} = \frac{\partial u_3^{(2)}}{\delta z}$$

$$2e_{13}^{(1)} = \frac{\partial u_1^{(2)}}{\delta z} + \frac{1}{A_1}\frac{\partial u_3^{(1)}}{\delta \alpha_1} - K_2 u_1^{(0)} + \frac{1}{h_1 A_1}\frac{\partial u_3^{(2)}}{\delta y_1}$$

$$2e_{23}^{(1)} = \frac{\partial u_2^{(2)}}{\delta z}\frac{1}{A_2}\frac{\partial u_3^{(1)}}{\delta \alpha_2} - K_1 u_2^{(0)} + \frac{1}{h_2 A_2}\frac{\partial u_3^{(2)}}{\delta y_2} \tag{4.16}$$

Substituting the above equations into stress and strain relation in (4.4), we get

$$\sigma_{ij} = \sigma_{ij}^{(0)} + \sigma_{ij}^{(1)} + \delta^2 \sigma_{ij}^{(2)} + \cdots \tag{4.17}$$

$$\sigma_{ij}^{(l)} = c_{ijmn}(y, z)e_{mn}^{(l)} where\ l = 0,1,2, \ldots \tag{4.18}$$

Substituting (4.15) in (4.18) we get

$$\sigma_{ij}^{(0)} = c_{ijn\mu}\frac{1}{h_\mu}\frac{\partial u_n^{(1)}}{\partial \xi_\mu} + c_{ijn3}\frac{\partial u_n^{(1)}}{\partial z} + c_{ijn\mu}\varepsilon_{n\mu}^{(0)} \tag{4.19}$$

In these relations,

$$\varepsilon_{11}^{(0)} = \frac{1}{A_1}\frac{\partial u_1^{(0)}}{\partial \alpha_1} + \frac{1}{A_1 A_2}\frac{\partial A_1}{\partial \alpha_2} u_2^{(0)}$$

$$\varepsilon_{22}^{(0)} = \frac{1}{A_2}\frac{\partial u_2^{(0)}}{\partial \alpha_2} + \frac{1}{A_1 A_2}\frac{\partial A_2}{\partial \alpha_1} u_1^{(0)}$$

$$\varepsilon_{12}^{(0)} = \varepsilon_{21}^{(0)} = \frac{1}{2}\left[\frac{A_1}{A_2}\frac{\partial}{\partial \alpha_2}\left(\frac{u_1^{(0)}}{A_1}\right) + \frac{A_1}{A_2}\frac{\partial}{\partial \alpha_1}\left(\frac{u_2^{(0)}}{A_2}\right)\right]$$

$$\varepsilon_{31}^{(0)} = \frac{\partial u_3^{(0)}}{\delta \alpha_1}, \varepsilon_{32}^{(0)} = \frac{\partial u_3^{(0)}}{\delta \alpha_2} \tag{4.20}$$

Then, the following notations are introduced

$$L_{ijn} = c_{ijn\mu}\frac{1}{h_\mu}\frac{\partial}{\partial \xi_\mu} + c_{ijn3}\frac{\partial}{\partial z} \tag{4.21}$$

$$D_{in} = \frac{1}{h_\beta}\frac{\partial}{\partial \xi_\beta} L_{i\beta n} + \frac{\partial}{\partial z} L_{i\beta n} \tag{4.22}$$

$$c_{in\mu}(\xi, z) = \frac{1}{h_\beta}\frac{\partial c_{i\beta n\mu}}{\partial \xi_\beta} + \frac{\partial c_{i3n\mu}}{\partial z} \tag{4.23}$$

$$D_{im} u_m^{(1)} = -c_{in\mu}\varepsilon_{n\mu}^{(0)} \tag{4.24}$$

With periodicity to coordinated $\xi_1$ and $\xi_2$ and the boundary condition l = 0, we get

$$\left(L_{ijm} u_m^{(1)} + c_{ijn\mu}\varepsilon_{n\mu}^{(0)}\right) N_j^{\pm} = 0 \ (z = z^{\pm}) \tag{4.25}$$

$$u_m^{(1)} = U_m^{n\mu}(\xi, z)\varepsilon_{n\mu}^{(0)}(\alpha) + v_m^{(1)}(\alpha) \tag{4.26}$$

$$D_{im} U_m^{n\mu} = -c_{in\mu} \ and \ \left(L_{ijm} U_m^{n\mu} + c_{ijn\mu}\right) N_j^{\pm} = 0 \ (z = z^{\pm}) \tag{4.27}$$

$$U_1^{31} = U_2^{32} = -z, U_2^{31} = U_3^{31} = 0, and\ U_1^{32} = U_3^{32} = 0 \tag{4.28}$$

$$b_{ij}^{n\mu} = L_{ijm}u_m^{(1)} + c_{ijn\mu}, where\ b_{ij}^{3\mu} \equiv 0 \tag{4.29}$$

$$\sigma_{ij}^{(0)} = b_{ij}^{\beta\mu}\varepsilon_{\beta\mu}^{(0)} \tag{4.30}$$

$$\varepsilon_{11}^{(0)} = \varepsilon_{22}^{(0)} = \varepsilon_{12}^{(0)} = 0 \tag{4.31}$$

$$u_1^{(0)} = u_2^{(0)} = 0, u_3^{(0)} = w(\alpha), u_3^{(1)} = v_3^{(1)}(\alpha), and\ u_\mu^{(1)} = v_\mu^{(1)}(\alpha) - z\frac{1}{A_\mu}\frac{\partial w}{\partial \alpha_\mu}$$

$$\text{Since } \sigma_{ij}^{(0)} = 0, \sigma_{ij}^{(1)} = L_{ijm}u_m^{(2)} + c_{ijm\nu}\varepsilon_{m\nu}^{(1)} + zc_{ij\mu\nu}\tau_{\mu\nu}$$

where,

$$\varepsilon_{11}^{(1)} = \frac{1}{A_1}\frac{\partial v_1^{(1)}}{\delta\alpha_1} + \frac{1}{A_1A_2}\frac{\partial A_1}{\delta\alpha_2}v_2^{(1)} + K_2w,$$

$$e_{22}^{(0)} = \frac{1}{A_2}\frac{\partial v_2^{(1)}}{\delta\alpha_2} + \frac{1}{A_1A_2}\frac{\partial A_2}{\delta\alpha_1}v_1^{(1)} + K_1w,$$

$$\varepsilon_{12}^{(1)} = \varepsilon_{21}^{(1)} = \frac{1}{2}\left[\frac{A_1}{A_2}\frac{\partial}{\partial\alpha_2}\left(\frac{v_1^{(1)}}{A_1}\right) + \frac{A_2}{A_1}\frac{\partial}{\partial\alpha_1}\left(\frac{v_2^{(1)}}{A_2}\right)\right]$$

$$\varepsilon_{31}^{(1)} = \frac{1}{A_1}\frac{\partial v_3^{(1)}}{\delta\alpha_1}, \varepsilon_{32}^{(1)} = \frac{1}{A_2}\frac{\partial v_3^{(1)}}{\delta\alpha_2} \tag{4.32}$$

$$\tau_{11} = -\frac{1}{A_1}\frac{\partial}{\delta\alpha_1}\left(\frac{1}{A_1}\frac{\partial w}{\delta\alpha_1}\right) - \frac{1}{A_1A_2^2}\frac{\partial w}{\delta\alpha_2}\frac{\partial A_1}{\delta\alpha_2}$$

$$\tau_{22} = -\frac{1}{A_2}\frac{\partial}{\delta\alpha_2}\left(\frac{1}{A_2}\frac{\partial w}{\delta\alpha_2}\right) - \frac{1}{A_2A_1^2}\frac{\partial w}{\delta\alpha_1}\frac{\partial A_2}{\delta\alpha_1}$$

$$\tau_{12} = \tau_{21} = -\frac{1}{A_1A_2}\left(\frac{\partial^2 w}{\delta\alpha_1\delta\alpha_2} - \frac{1}{A_1}\frac{\partial w}{\delta\alpha_1}\frac{\partial A_1}{\delta\alpha_2} - \frac{1}{A_2}\frac{\partial w}{\delta\alpha_2}\frac{\partial A_2}{\delta\alpha_1}\right) \tag{4.33}$$

$$D_{im}u_m^{(2)} = -C_{imv}\varepsilon_{mv}^{(1)} - \left(c_{i3\mu\nu} + zC_{i\mu\nu}\right)\tau_{\mu\nu} \tag{4.34}$$

$$(L_{ijm}u_m^{(2)} + c_{ijmv}\varepsilon_{mv}^{(1)} + zc_{ij\mu\nu}\tau_{\mu\nu})N_j^{\pm} = 0\ (z = z^{\pm}) \tag{4.35}$$

$$u_m^{(2)} = U_m^{lv}\varepsilon_{lv}^{(1)} + V_m^{(\mu\nu)}\tau_{\mu\nu} \tag{4.36}$$

$$D_{im}V_m^{\mu\nu} = -c_{i3\mu\nu} - zC_{i\mu\nu} \tag{4.37}$$

$$(L_{ijm}V_m^{\mu\nu} + z^{\pm}c_{ij\mu\nu})N_j^{\pm} = 0\ (z = z^{\pm}) \tag{4.38}$$

$$b_{ij}^{*\mu\nu} = L_{ijm}V_m^{\mu\nu} + zc_{ij\mu\nu} \tag{4.39}$$

$$\sigma_{ij}^{(1)} = b_{ij}^{\mu\nu}\varepsilon_{\mu\nu}^{(1)} + b_{ij}^{*\mu\nu}\tau_{\mu\nu} \tag{4.40}$$

$$\frac{1}{h_\beta}\frac{\partial b_{i\beta}^{\lambda\mu}}{\partial \xi_\beta} + \frac{\partial b_{i3}^{\lambda\mu}}{\partial z} = 0, \qquad \frac{1}{h_\beta}n_\beta^{\pm}b_{i\beta}^{\lambda\mu} + n_3^{\pm}b_{i3}^{\lambda\mu}\ at\ z = z^{\pm}, b_{ij}^{\mu\nu}N_j^{\pm} = 0\ (z = z^{\pm})$$

$$\frac{1}{h_\beta}\frac{\partial c_{i\beta}^{\lambda\mu}}{\partial \xi_\beta} + \frac{\partial c_{i3}^{\lambda\mu}}{\partial z} = 0, \qquad \frac{1}{h_\beta}n_\beta^{\pm}c_{i\beta}^{\lambda\mu} + n_3^{\pm}c_{i3}^{\lambda\mu}\ at\ z = z^{\pm}, b_{ij}^{*\mu\nu}N_j^{\pm} = 0\ (z = z^{\pm}) \tag{4.41}$$

Where $n_i^{\pm}$ are components of the normal to the upper and lower surfaces of the unit cell. It is possible in this method to calculate both the local and global properties of the composite layer by first solving the properties associated with the 3-dimensional local problems set on the unit cell. Subsequently, solving a two-dimensional boundary value problem for a homogenous anisotropic shell with the effective stiffness moduli, we get

$$N_\beta = \delta\langle b_{\beta\beta}^{\lambda\mu}\rangle\epsilon_{\lambda\mu} + \delta^2\langle c_{\beta\beta}^{\lambda\mu}\rangle\tau_{\lambda\mu}$$

$$N_{12} = \delta\langle b_{12}^{\lambda\mu}\rangle\epsilon_{\lambda\mu} + \delta^2\langle c_{12}^{\lambda\mu}\rangle\tau_{\lambda\mu}$$

$$N_\beta = \delta^2\langle b_{\beta\beta}^{\lambda\mu}\rangle\epsilon_{\lambda\mu} + \delta^3\langle c_{\beta\beta}^{\lambda\mu}\rangle\tau_{\lambda\mu}$$

$$N_\beta = \delta^2\langle b_{12}^{\lambda\mu}\rangle\epsilon_{\lambda\mu} + \delta^3\langle c_{12}^{\lambda\mu}\rangle\tau_{\lambda\mu} \tag{4.42}$$

Where β assumes values 1 and 2, and $\lambda, \mu$ = 1,2. The functions involving b and c can be calculated from the solution of local problems on the unit cell. Here $\xi_1 = \alpha_1 A_1/(\delta h_1)$ and $\xi_2 = \alpha_2 A_2/(\delta h_2)$, z = $\gamma/\delta$ and $A_1(\alpha_1, \alpha_2)$ are the coefficients of the first quadratic form on the mid surface of the layer. The above functions are determined by using the following equations:

$$b_{kl}^{mn} = \frac{1}{h_\beta}\,\alpha_{kli\beta}\,\frac{\partial U_i^{mn}}{\partial \xi_\beta} + \alpha_{kli3}\frac{\partial U_i^{mn}}{\partial z} + \alpha_{klmn} \tag{4.43}$$

$$c_{kl}^{mn} = \frac{1}{h_\beta}\,\alpha_{kli\beta}\,\frac{\partial U_i^{mn}}{\partial \xi_\beta} + \alpha_{kli3}\frac{\partial V_i^{mn}}{\partial z} + z\alpha_{klmn} \tag{4.44}$$

The functions $U_i^{mn}(\xi_1,\xi_2,z)$ and $V_i^{mn}(\xi_1,\xi_2,z)$ are periodic invariable $\xi_1$ and $\xi_2$ with periods $A_1$ and $A_2$, respectively. The functions are determined in turn by using the local variables (I,j = 1,2,3 and $\lambda, \mu = 1,2$ ) :

$$\frac{1}{h_\beta}\frac{\partial b_{i\beta}^{\lambda\mu}}{\partial \xi_\beta} + \frac{\partial b_{i3}^{\lambda\mu}}{\partial z} = 0, \frac{1}{h_\beta} n_\beta^{\pm} b_{i\beta}^{\lambda\mu} + n_3^{\pm} b_{i3}^{\lambda\mu}\ at\ z = z^{\pm},$$

$$\frac{1}{h_\beta}\frac{\partial c_{i\beta}^{\lambda\mu}}{\partial \xi_\beta} + \frac{\partial c_{i3}^{\lambda\mu}}{\partial z} = 0, \quad \frac{1}{h_\beta} n_\beta^{\pm} c_{i\beta}^{\lambda\mu} + n_3^{\pm} c_{i3}^{\lambda\mu}\ at\ z = z^{\pm} \tag{4.45}$$

Where $n_i^{\pm}$ are components of the normal to the upper and lower surfaces of the unit cell. Then, we can calculate the effective stiffnesses using the same local problem formulation given as,

$$A_{11} = \delta\langle b_{11}^{11}\rangle, B_{11} = \delta\langle z b_{11}^{11}\rangle, D_{11} = \delta\langle z c_{11}^{11}\rangle$$

$$A_{12} = \delta\langle b_{11}^{22}\rangle, B_{11} = \delta\langle z b_{11}^{22}\rangle, D_{11} = \delta\langle z c_{11}^{22}\rangle$$

$$A_{16} = \delta\langle b_{11}^{12}\rangle, B_{11} = \delta\langle z b_{11}^{12}\rangle, D_{11} = \delta\langle z c_{11}^{12}\rangle$$

$$A_{11} = \delta\langle b_{22}^{22}\rangle, B_{11} = \delta\langle z b_{22}^{22}\rangle, D_{11} = \delta\langle z c_{22}^{22}\rangle$$

$$A_{26} = \delta\langle b_{22}^{12}\rangle, B_{11} = \delta\langle z b_{22}^{12}\rangle, D_{11} = \delta\langle z c_{22}^{12}\rangle$$

$$A_{66} = \delta\langle b_{12}^{12}\rangle, B_{11} = \delta\langle z b_{12}^{12}\rangle, D_{11} = \delta\langle z c_{12}^{12}\rangle \quad (4.46)$$

If there is higher density fiber placement, then it will result in a large amount of shear stresses in the matrix material. So this will induce torsional failure, which occurs at about a $V_f$ value of 0.6 or more. This causes delamination in the plies.

Finally, the general homogenization method is only used when the composite layers' thickness is relatively small compared to the other dimensions.

# CHAPTER 5 NUMERICAL FORMUATION

In this chapter, we will describe the mathematical equations used to calculate the effective properties of the composites. A myriad of composites with different structural orientations and materials are considered in this section. Each structure and material largely influence the effective coefficients, and so, the engineers use these according to their applications. The equations discussed in this section provide valuable data to the engineers to encourage the use of composites. The composites described are also shown in the form of figures with their structure and orientation explained briefly. The formulae follow the explanation along with abbreviations of parameters used in the set of equations. In the upcoming sections, these mathematical equations will be put into use with certain values being assigned for each parameter, and the effective property for each structure is computed from that. The mathematical representations give solutions to variable properties such as piezoelectric, elastic, thermal, and piezomagnetic coefficients, to name a few.

## 5.1 SANDWICH COMPOSITE SANDWICH SHELLS MADE OF GENERALLY ORTHOTROPIC MATERIALS

A micromechanical thermoelastic model for determining the effective properties was developed in [20]. The material used to develop this model was orthotropic in nature. Sandwich composites are discussed briefly in the section above.

### 5.1.1 SANDWICH STRUCTURE WITH HEXAGONAL-TRIANGULAR CORE AND STAR-HEXAGONAL CORE

A sandwich composite structure with a hexagonal core with a triangular cell is taken for analysis, and the basic angular architecture of $60^{o}$, $120^{o}$ is maintained. The effective properties of the structure can be tailored to any given application by use of the general homogenization model discussed in [20].

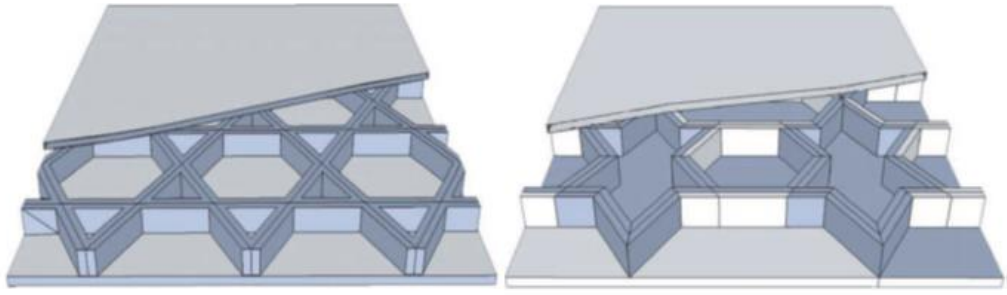

**Figure 5.1 Hexagonal sandwich cell and Star reinforced sandwich cell [20]**

The formulae used to calculate the effective thermoelastic properties of these structures are given as follows:

For hexagonal core,

$$\langle b_{11}^{11} \rangle = 16.6276 E_1 \upsilon_{21} Ht/(\nu_{12} a)$$

$$\langle b_{22}^{22} \rangle = 2.4250 E_2 Ht/a$$

$$\langle b_{22}^{11} \rangle = \langle b_{11}^{22} \rangle = 5.5424 E_1 \upsilon_{21} Ht/(\nu_{12} a)$$

$$\langle b_{22}^{11} \rangle = \langle b_{11}^{22} \rangle = 5.5424 E_1 \upsilon_{21} Ht/(\nu_{12} a)$$

$$\langle b_{12}^{12} \rangle = 5.5424 E_2 Ht/a$$

$$\langle z b_{11}^{*11} \rangle = 1.3856 E_1 \upsilon_{21} H^3 t/(\nu_{12} a)$$

$$\langle z b_{22}^{*22} \rangle = 0.2022 E_2 H^3 t/a$$

$$\langle z b_{22}^{*11} \rangle = \langle z b_{11}^{*22} \rangle = \frac{0.4620 E_1 \upsilon_{21} H^3 t}{\nu_{12} a}$$

$$\langle z b_{12}^{*12} \rangle = 0.4620 E_2 H^3 t/a$$

$$\langle\theta_{11}\rangle = \frac{1.155Ht}{a}\{(c_{11} - v_{12}c_{12} - 0.9v_{32}c_{13})\alpha_{11} + (c_{12} - v_{12}c_{22} - .9v_{32}c_{23})\alpha_{22} + (c_{13} - v_{12}c_{23} - 0.9v_{32}c_{33})\alpha_{33}\}$$

$$\langle\theta_{22}\rangle = \frac{0.0000196Ht}{a}\{(c_{12} - v_{12}c_{11} - 0.1v_{32}c_{13})\alpha_{11} + (c_{22} - v_{12}c_{12} - .1v_{32}c_{23})\alpha_{22} + (c_{23} - v_{12}c_{13} - 0.1v_{32}c_{33})\alpha_{33}\}$$

$$\langle z\theta_{11}^{*}\rangle = \frac{0.096H^3t}{a}\{(c_{11} - v_{12}c_{12} - 0.9v_{32}c_{13})\alpha_{11} + (c_{12} - v_{12}c_{22} - .9v_{32}c_{23})\alpha_{22} + (c_{13} - v_{12}c_{23} - 0.9v_{32}c_{33})\alpha_{33}\}$$

$$\langle z\theta_{22}^{*}\rangle = \frac{0.000016H^3t}{a}\{(c_{12} - v_{12}c_{11} - 0.1v_{32}c_{13})\alpha_{11} + (c_{22} - v_{12}c_{12} - .1v_{32}c_{23})\alpha_{22} + (c_{23} - v_{12}c_{13} - 0.1v_{32}c_{33})\alpha_{33}\}$$

For star core,

$$\langle b_{11}^{11}\rangle = 3.3366E_1v_{21}Ht/(v_{12}a)$$

$$\langle b_{22}^{22}\rangle = 2.3287E_2Ht/a$$

$$\langle b_{22}^{11}\rangle = \langle b_{11}^{22}\rangle = 1.1122E_1v_{21}Ht/(v_{12}a)$$

$$\langle b_{12}^{12}\rangle = 1.1122E_2Ht/a$$

$$\langle zb_{11}^{*11}\rangle = 0.2780E_1v_{21}H^3t/(v_{12}a)$$

$$\langle zb_{22}^{*22}\rangle = 0.1941E_2H^3t/a$$

$$\langle zb_{22}^{*11}\rangle = \langle zb_{11}^{*22}\rangle = 0.0927E_1v_{21}H^3t/(v_{12}a)$$

$$\langle zb_{12}^{*12}\rangle = 0.0927E_2H^3t/a$$

$$\langle\theta_{11}\rangle = \frac{1.1497Ht}{a}\{(c_{11} - \upsilon_{12}c_{12} - 0.69\nu_{32}c_{13})\alpha_{11} + (c_{12} - \nu_{12}c_{22} - .69\nu_{32}c_{23})\alpha_{22} + (c_{13} - \nu_{12}c_{23} - 0.69\nu_{32}c_{33})\alpha_{33}\}$$

$$\langle\theta_{22}\rangle = \frac{0.005Ht}{a}\{(c_{12} - \upsilon_{12}c_{11} - 0.31\nu_{32}c_{13})\alpha_{11} + (c_{22} - \nu_{12}c_{12} - .31\nu_{32}c_{23})\alpha_{22} + (c_{23} - \nu_{12}c_{13} - 0.31\nu_{32}c_{33})\alpha_{33}\}$$

$$\langle z\theta_{11}^{*}\rangle = \frac{0.0958H^3t}{a}\{(c_{11} - \upsilon_{12}c_{12} - 0.69\nu_{32}c_{13})\alpha_{11} + (c_{12} - \nu_{12}c_{22} - .69\nu_{32}c_{23})\alpha_{22} + (c_{13} - \nu_{12}c_{23} - 0.69\nu_{32}c_{33})\alpha_{33}\}$$

$$\langle z\theta_{22}^{*}\rangle = \frac{0.0004H^3t}{a}\{(c_{12} - \upsilon_{12}c_{11} - 0.31\nu_{32}c_{13})\alpha_{11} + (c_{22} - \nu_{12}c_{12} - .31\nu_{32}c_{23})\alpha_{22} + (c_{23} - \nu_{12}c_{13} - 0.31\nu_{32}c_{33})\alpha_{33}\}$$

The parameters $E_1, E_2, \upsilon_{ij}$, $\alpha_{ij}$ *and the* $c_{ij}$ terms represent the material properties constituting the composite structure. H, t, a is the dimensional parameters of the single unit cell under consideration.

## 5.2 GRID REINFORCED GENERALLY ORTHOTROPIC GRID-REINFORCED SHELLS

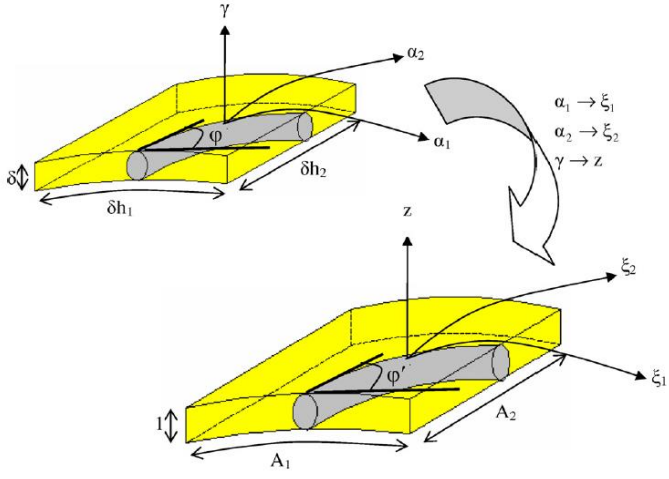


**Figure 5.2 Grid reinforced unit cells [21]**

The asymptotic homogenization method was derived for the thin composite shell consisting of generally orthotropic materials with parallel spaced reinforcements. The reinforcing elements are homogeneous and are typically taken in such a way that it is much stiffer than that of the matrix. So, in this analysis, the contribution of the matrix was neglected as its influence on the composite is negligent, see [21] for the detailed study conducted on this plate. The general equations for the calculation of effective properties of the composite shell are given as:

$$\langle b_{ij}^{\lambda\mu} \rangle = \frac{1}{|\Omega|} \int_{|\Omega|} b_{ij}^{\lambda\mu}\, dv = \frac{V}{h_1 h_2} b_{ij}^{\lambda\mu}$$

$$\langle z b_{ij}^{\lambda\mu} \rangle = \frac{1}{|\Omega|} \int_{|\Omega|} z b_{ij}^{\lambda\mu}\, dv = 0$$

$$\langle b_{ij}^{*\lambda\mu} \rangle = 0$$

$$\langle z b_{ij}^{*\lambda\mu} \rangle = \frac{V}{16 h_1 h_2} B_{ij}^{\lambda\mu}$$

where,

$$B_{11}^{\lambda\mu} = \frac{\Sigma_5\Sigma_6 - \Sigma_2\Sigma_3}{\Sigma_1\Sigma_2 - \Sigma_4\Sigma_5}, B_{22}^{\lambda\mu} = \frac{\Sigma_3\Sigma_4 - \Sigma_1\Sigma_6}{\Sigma_1\Sigma_2 - \Sigma_4\Sigma_5}, and\ B_{12}^{\lambda\mu} = \frac{A_2 tan\varphi}{A_1} B_{11}^{\lambda\mu} + \frac{A_1}{2A_2 tan\varphi} B_{22}^{\lambda\mu}$$

$$b_{11}^{\lambda\mu} = \frac{C_{12\lambda\mu}[\Lambda_4\Lambda_7 + \Lambda_8\Lambda_3] + C_{11\lambda\mu}[\Lambda_5\Lambda_7 - \Lambda_9\Lambda_3] + C_{22\lambda\mu}[\Lambda_6\Lambda_7] + C_{33\lambda\mu}\Lambda_3}{\Lambda_7\left[\frac{A_2 tan\varphi}{A_1}\Lambda_4 + \Lambda_5 + \frac{A_2^2 tan^2\varphi}{A_1^2}\Lambda_6\right] + \frac{A_2 tan\varphi}{A_1}[\Lambda_8\Lambda_3] - \Lambda_9\Lambda_3}$$

$$b_{22}^{\lambda\mu} = \frac{C_{12\lambda2}[\Lambda_4\Lambda_7 + \Lambda_8\Lambda_3] + C_{11\lambda1}[\Lambda_5\Lambda_7 - \Lambda_9\Lambda_3] + C_{22\lambda2}[\Lambda_6\Lambda_7] + C_{33\lambda3}\Lambda_3}{\Lambda_7\left[\frac{A_1}{A_2 tan\varphi}\Lambda_4 + \frac{A_1^2}{A_2^2 tan^2\varphi}\Lambda_5 + \Lambda_6\right] + \frac{A_1}{A_2 tan\varphi}[\Lambda_8\Lambda_3] - \frac{A_1^2}{A_2^2 tan^2\varphi}\Lambda_9\Lambda_3}$$

$$b_{12}^{\lambda\mu} = \frac{C_{12\lambda2}[\Lambda_4\Lambda_7 + \Lambda_8\Lambda_3] + C_{11\lambda1}[\Lambda_5\Lambda_7 - \Lambda_9\Lambda_3] + C_{22\lambda2}[\Lambda_6\Lambda_7] + C_{33\lambda3}\Lambda_3}{\Lambda_7\left[\Lambda_4 + \frac{A_1}{A_2 tan\varphi}\Lambda_5 + \frac{A_2 tan\varphi}{A_1}\Lambda_6\right] + [\Lambda_8\Lambda_3] - \frac{A_1}{A_2 tan\varphi}\Lambda_9\Lambda_3}$$

The remaining terms $b_{13}^{\lambda\mu} = b_{23}^{\lambda\mu} = b_{33}^{\lambda\mu} = 0$

The $C_{ij\lambda\mu}$ represents the material properties of the composite structure $h_{1,}h_2$ are dimensional parameters of the unit cell, and V is the volume of the unit cell. Also, it is taken that $A_1 = A_2 = 1$

## 5.3 SMART HONEYCOMB SANDWICH STRUCTURES

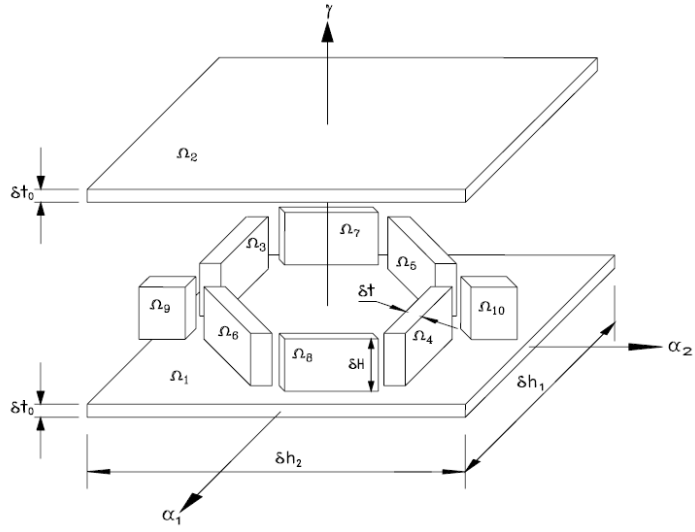


**Figure 5.3 Unit cell representation of smart honeycomb sandwich structure [29]**

In this type of structure, there is a need to consider the alignment and distribution of fibers and actuators as it largely influences the properties of the composite material on the macro scale. The modeling of this smart composite is performed using the general homogenization model for periodic structures by application of a modified asymptotic homogenization method based on a three-dimensional elastic problem, see [29]. As displayed in figure 5.3, $h_1$ and $h_2$ are the width and length of the structure considered. H is the thickness of the core, and $t_o$ is the thickness of the sandwich layer.

A three-layer structure reinforced with a hexagonal honeycomb structure is being developed in this formulation. The equations used to calculate the effective properties of this composite are given as follows.

For the honeycomb core, the effective properties are calculated using the equations

$$\langle b_{11}^{11} \rangle = \left( \frac{S^4/h_2^4}{\left( (C^2/h_1^2) + (S^2/h_2^2) \right)^2} \right) \sum_{i=3}^{10} E^{(i)} F_i$$

$$\langle b_{11}^{22} \rangle = \langle b_{11}^{11} \rangle = \langle b_{12}^{12} \rangle = \left( \frac{C^2 S^2/h_1^2 h_2^2}{\left( (C^2/h_1^2) + (S^2/h_2^2) \right)^2} \right) \sum_{i=3}^{10} E^{(i)} F_i$$

$$\langle b_{22}^{22} \rangle = \left( \frac{C^4/h_1^4}{\left( (C^2/h_1^2) + (S^2/h_2^2) \right)^2} \right) \sum_{i=3}^{10} E^{(i)} F_i$$

$$\langle b_{12}^{12} \rangle = \left( \frac{C^2 S^2/h_1^2 h_2^2}{\left( (C^2/h_1^2) + (S^2/h_2^2) \right)^2} \right) \sum_{i=3}^{10} E^{(i)} F_i$$

$$\langle zb_{11}^{*11} \rangle = \left( \frac{S^4/h_2^4}{\left( (C^2/h_1^2) + (S^2/h_2^2) \right)^2} \right) \sum_{i=3}^{10} E^{(i)} J_i$$

$$\langle zb_{11}^{*22} \rangle = \langle zb_{22}^{*11} \rangle = \left( \frac{C^2 S^2/h_1^2 h_2^2}{\left( (C^2/h_1^2) + (S^2/h_2^2) \right)^2} \right) \sum_{i=3}^{10} E^{(i)} J_i$$

$$\langle zb_{22}^{*22} \rangle = \left( \frac{C^4/h_1^4}{\left( (C^2/h_1^2) + (S^2/h_2^2) \right)^2} \right) \sum_{i=3}^{10} E^{(i)} F_i$$

$$\langle zb_{12}^{*12} \rangle = \left( \frac{C^2 S^2/h_1^2 h_2^2}{\left( (C^2/h_1^2) + (S^2/h_2^2) \right)^2} - \frac{8H}{3\pi^5 h_1} \sum_{n=1}^{\infty} \frac{\tanh\left[ \pi(2n-1) \left( \frac{t}{2H} \right) \right]}{(2n-1)^5} \right) \sum_{i=3}^{10} G_{12}^{(i)} J_i$$

The equations for the calculation of the effective properties of the sandwich material used in the top and bottom carrier faces are given as:

$$\langle b_{11}^{11} \rangle = \frac{E_1^{(1)} F_1}{1 - \nu_{12}^{(1)} \nu_{21}^{(1)}} + \frac{E_1^{(2)} F_2}{1 - \nu_{12}^{(2)} \nu_{21}^{(2)}}$$

$$\langle b_{11}^{22}\rangle = \langle b_{22}^{11}\rangle = \frac{\nu_{12}^{(1)}E_1^{(1)}F_1}{1-\nu_{12}^{(1)}\nu_{21}^{(1)}} + \frac{\nu_{12}^{(2)}E_1^{(2)}F_2}{1-\nu_{12}^{(2)}\nu_{21}^{(2)}}$$

$$\langle b_{22}^{22}\rangle = \frac{E_2^{(1)}F_1}{1-\nu_{12}^{(1)}\nu_{21}^{(1)}} + \frac{E_2^{(2)}F_2}{1-\nu_{12}^{(2)}\nu_{21}^{(2)}}$$

$$\langle b_{12}^{12}\rangle = G_{12}^{(1)}F_1 + G_{12}^{(2)}F_2$$

$$\langle zb_{11}^{*11}\rangle = \frac{E_1^{(1)}J_1}{12\left(1-\nu_{12}^{(1)}\nu_{21}^{(1)}\right)} + \frac{E_1^{(2)}J_2}{12\left(1-\nu_{12}^{(2)}\nu_{21}^{(2)}\right)}$$

$$\langle zb_{11}^{*22}\rangle = \langle zb_{22}^{*11}\rangle = \frac{\nu_{12}^{(1)}E_1^{(1)}F_1}{12\left(1-\nu_{12}^{(1)}\nu_{21}^{(1)}\right)} + \frac{\nu_{12}^{(2)}E_1^{(2)}F_2}{12\left(1-\nu_{12}^{(2)}\nu_{21}^{(2)}\right)}$$

$$\langle zb_{22}^{*22}\rangle = \frac{E_2^{(1)}J_1}{12\left(1-\nu_{12}^{(1)}\nu_{21}^{(1)}\right)} + \frac{E_2^{(2)}J_2}{12\left(1-\nu_{12}^{(2)}\nu_{21}^{(2)}\right)}$$

$$\langle zb_{12}^{*12}\rangle = \frac{G_{12}^{(1)}J_1}{12} + \frac{G_{12}^{(2)}J_2}{12}$$

The effective piezoelectric coefficients are given as:

$$\delta\langle d_{11}^{3}\rangle = \frac{\left(E_1^{(1)}d_{31}^{(r)(1)} + E_1^{(1)}\nu_{21}^{(1)}d_{32}^{(r)(1)}\right)F_1}{1-\nu_{12}^{(1)}\nu_{21}^{(1)}} + \frac{\left(E_1^{(2)}d_{31}^{(r)(2)} + E_1^{(2)}\nu_{21}^{(2)}d_{32}^{(r)(2)}\right)F_2}{1-\nu_{12}^{(2)}\nu_{21}^{(2)}}$$

$$\delta\langle d_{22}^{3}\rangle = \frac{\left(E_2^{(1)}d_{32}^{(r)(1)} + E_2^{(1)}\nu_{12}^{(1)}d_{31}^{(r)(1)}\right)F_1}{1-\nu_{12}^{(1)}\nu_{21}^{(1)}} + \frac{\left(E_2^{(2)}d_{32}^{(r)(2)} + E_2^{(2)}\nu_{12}^{(2)}d_{31}^{(r)(2)}\right)F_2}{1-\nu_{12}^{(2)}\nu_{21}^{(2)}}$$

$$\delta\langle zd_{11}^{*3}\rangle = \frac{\left(E_1^{(1)}d_{31}^{(r)(1)} + E_1^{(1)}\nu_{21}^{(1)}d_{32}^{(r)(1)}\right)J_1}{12\left(1-\nu_{12}^{(1)}\nu_{21}^{(1)}\right)} + \frac{\left(E_1^{(2)}d_{31}^{(r)(2)} + E_1^{(2)}\nu_{21}^{(2)}d_{32}^{(r)(2)}\right)J_2}{12\left(1-\nu_{12}^{(2)}\nu_{21}^{(2)}\right)}$$

$$\delta\langle zd_{22}^{*3}\rangle = \frac{\left(E_2^{(1)}d_{32}^{(r)(1)} + E_2^{(1)}\nu_{12}^{(1)}d_{31}^{(r)(1)}\right)J_1}{12\left(1-\nu_{12}^{(1)}\nu_{21}^{(1)}\right)} + \frac{\left(E_1^{(2)}d_{32}^{(r)(2)} + E_2^{(2)}\nu_{12}^{(2)}d_{31}^{(r)(2)}\right)J_2}{12\left(1-\nu_{12}^{(2)}\nu_{21}^{(2)}\right)}$$

Note that $F_i$ is the cross-sectional area, and $J_i$ is the moment of inertia of the cross-section of the unit cells. $E_1^{(1)}, E_2^{(1)}, d_{32}^{(r)(1)}, d_{31}^{(r)(1)}, G_{12}^{(1)}, \nu_{12}^{(1)}, and\ \nu_{21}^{(1)}$ are all material properties of the material used for the construction of the composite under analysis. *C* is cos$\varphi$, and *S* is sin$\varphi$ with $\varphi$ being the angle of alignment of the reinforcing element. $h_1\ and\ h_2$ are the dimensional parameters of the unit cell being used.

## 5.4 SMART COMPOSITE SANDWICH SHELLS MADE OF GENERALLY ORTHOTROPIC SHELLS

### 5.4.1 COMPOSITE SANDWICH SHELL REINFORCED WITH HEXAGONAL HONEYCOMB CORE

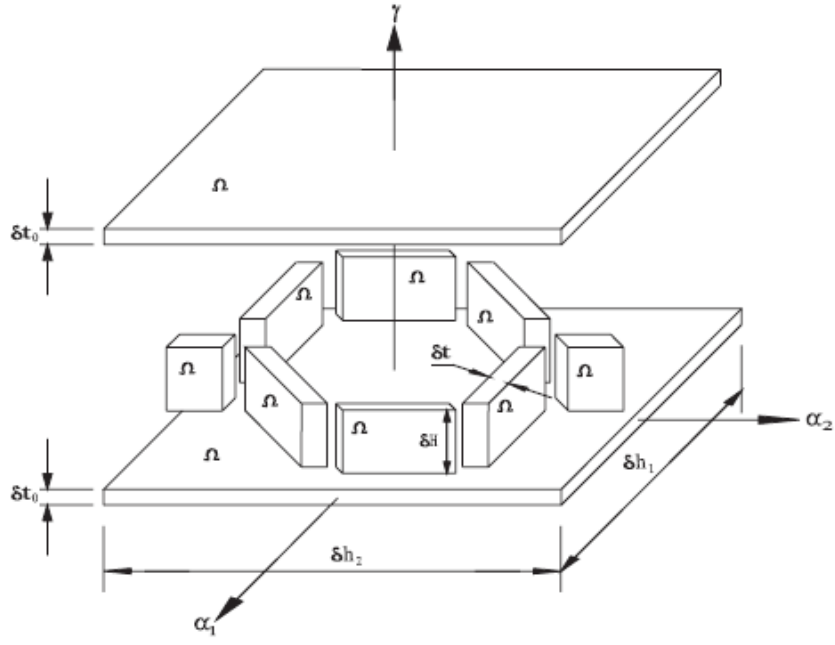


**Figure 5.4 Sandwich shell reinforced with honeycomb filler [30]**

A three-layer smart composite structure is considered here as a smart composite along with a hexagon-shaped honeycomb center layer. The material used in the core and carrier faces may exhibit piezoelectric behavior in certain conditions, so the composite is

considered a smart structure. As shown in figure 5.4, $h_1$ and $h_2$ are the width and length of the structure considered. H is the thickness of the core, and $t_o$ is the thickness of the sandwich layer. It is also assumed to derive the effective properties that the thickness of the elements in the unit cell is considered very small compared to the other dimensions.

The effective elastic and piezoelectric properties for the smart composite shell with a hexagonal honeycomb core made of orthotropic material are readily determined using the asymptotic homogenization method and are given in the form of equations as depicted below:

$$\langle b_{11}^{11} \rangle = \frac{2E_1 t_0}{1 - \nu_{12}\nu_{21}} + 1.1732 \frac{E_1 \nu_{21} Ht}{\nu_{12} a}$$

$$\langle b_{22}^{22} \rangle = \frac{2E_2 t_0}{1 - \nu_{12}\nu_{21}} + 0.5152 \frac{E_2 Ht}{a}$$

$$\langle b_{11}^{22} \rangle = \langle b_{22}^{11} \rangle = \frac{2\nu_{12} E_1 t_0}{1 - \nu_{12}\nu_{21}} + 0.3908 \frac{E_1 \nu_{21} Ht}{\nu_{12} a}$$

$$\langle b_{12}^{12} \rangle = 2G_{12} t_0 + 0.3908 \frac{E_2 Ht}{a}$$

$$\langle z b_{11}^{*11} \rangle = \frac{2E_1 t_0}{36(1 - \nu_{12}\nu_{21})} \left( \frac{3H^2}{4} + \frac{3Ht_0}{2} + t_0^2 \right) + 0.0976 \frac{E_1 \nu_{21} H^3 t}{\nu_{12} a}$$

$$\langle z b_{22}^{*22} \rangle = \frac{2E_2 t_0}{36(1 - \nu_{12}\nu_{21})} \left( \frac{3H^2}{4} + \frac{3Ht_0}{2} + t_0^2 \right) + 0.0429336 \frac{E_2 H^3 t}{a}$$

$$\langle z b_{11}^{*22} \rangle = \langle z b_{22}^{*11} \rangle = \frac{2\nu_{12} E_1 t_0}{36(1 - \nu_{12}\nu_{21})} \left( \frac{3H^2}{4} + \frac{3Ht_0}{2} + t_0^2 \right) + 0.03256 \frac{E_1 \nu_{21} H^3 t}{\nu_{12} a}$$

$$\langle z b_{12}^{*12} \rangle = \frac{2G_{12} t_0}{36} \left( \frac{3H^2}{4} + \frac{3Ht_0}{2} + t_0^2 \right) + 0.03256 \frac{E_2 H^3 t}{a}$$

$$\delta\langle d_{11}^{3}\rangle = \frac{2t_0(E_1 d_{31}^{(r)} + \nu_{21} E_1 d_{32}^{(r)})}{1-\nu_{12}\nu_{21}} + 0.77\Big\{(c_{11} - \nu_{12}c_{12} - 0.9\nu_{32}c_{13})d_{31}^{(r)} + (c_{12} - \nu_{12}c_{22} - 0.9\nu_{32}c_{23})d_{32}^{(r)} + (c_{13} - \nu_{12}c_{23} - 0.9\nu_{32}c_{33})d_{33}^{(r)}\Big\}\frac{Ht}{a}$$

$$\delta\langle d_{22}^{3}\rangle = \frac{2t_0(E_2 d_{32}^{(r)} + \nu_{12} E_2 d_{31}^{(r)})}{1-\nu_{12}\nu_{21}} + 0.000013\Big\{(c_{12} - \nu_{12}c_{11} - 0.1\nu_{32}c_{13})d_{31}^{(r)} + (c_{22} - \nu_{12}c_{12} - 0.1\nu_{32}c_{23})d_{32}^{(r)} + (c_{23} - \nu_{12}c_{13} - 0.1\nu_{32}c_{33})d_{33}^{(r)}\Big\}\frac{Ht}{a}$$

$$\delta\langle z d_{11}^{*3}\rangle = \frac{2t_0(E_1 d_{31}^{(r)} + \nu_{21} E_1 d_{32}^{(r)})}{1-\nu_{12}\nu_{21}}\left(\frac{3H^2}{4} + \frac{3Ht_0}{2} + t_0^2\right) + 0.06415\Big\{(c_{11} - \nu_{12}c_{12} - 0.9\nu_{32}c_{13})d_{31}^{(r)} + (c_{12} - \nu_{12}c_{22} - 0.9\nu_{32}c_{23})d_{32}^{(r)} + (c_{13} - \nu_{12}c_{23} - 0.9\nu_{32}c_{33})d_{33}^{(r)}\Big\}\frac{H^3 t}{a}$$

$$\delta\langle z d_{22}^{*3}\rangle = \frac{2t_0(E_2 d_{32}^{(r)} + \nu_{12} E_2 d_{31}^{(r)})}{1-\nu_{12}\nu_{21}}\left(\frac{3H^2}{4} + \frac{3Ht_0}{2} + t_0^2\right) + 0.0000011\Big\{(c_{12} - \nu_{12}c_{11} - 0.1\nu_{32}c_{13})d_{31}^{(r)} + (c_{22} - \nu_{12}c_{12} - 0.1\nu_{32}c_{23})d_{32}^{(r)} + (c_{23} - \nu_{12}c_{13} - 0.1\nu_{32}c_{33})d_{33}^{(r)}\Big\}\frac{H^3 t}{a}$$

### 5.4.2 COMPOSITE SANDWICH SHELL REINFORCED WITH MIXED HEXAGONAL-TRIANGULAR CORE

The following equations are used to provide the effective properties of a mixed hexagonal-triangular cored sandwich composite structure. The procedure used to derive these formulae are shown in [30].

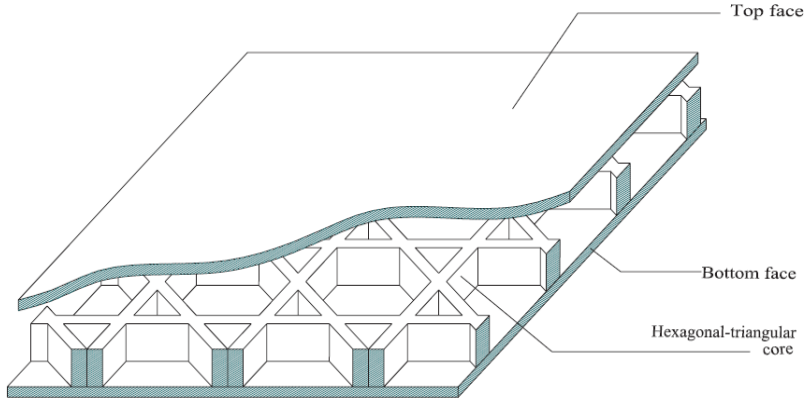


**Figure 5.5 Sandwich shell reinforced with mixed hexagonal-triangular core [30]**

$$\langle b_{11}^{11}\rangle = \frac{2E_1 t_0}{1-\nu_{12}\nu_{21}} + 16.6276\frac{E_1\nu_{21}Ht}{\nu_{12}a}$$

$$\langle b_{22}^{22}\rangle = \frac{2E_2 t_0}{1-\nu_{12}\nu_{21}} + 2.4250\frac{E_2 Ht}{a}$$

$$\langle b_{11}^{22}\rangle = \langle b_{22}^{11}\rangle = \frac{2\nu_{12}E_1 t_0}{1-\nu_{12}\nu_{21}} + 5.5424\frac{E_1\nu_{21}Ht}{\nu_{12}a}$$

$$\langle b_{12}^{12}\rangle = 2G_{12}t_0 + 5.5424\frac{E_2 Ht}{a}$$

$$\langle zb_{11}^{*11}\rangle = \frac{2E_1 t_0}{36(1-\nu_{12}\nu_{21})}\left(\frac{3H^2}{4}+\frac{3Ht_0}{2}+t_0^2\right) + 1.3856\frac{E_1\nu_{21}H^3 t}{\nu_{12}a}$$

$$\langle zb_{22}^{*22}\rangle = \frac{2E_2 t_0}{36(1-\nu_{12}\nu_{21})}\left(\frac{3H^2}{4}+\frac{3Ht_0}{2}+t_0^2\right) + 0.2022\frac{E_2 H^3 t}{a}$$

$$\langle zb_{11}^{*22}\rangle = \langle zb_{22}^{*11}\rangle = \frac{2\nu_{12}E_1 t_0}{36(1-\nu_{12}\nu_{21})}\left(\frac{3H^2}{4}+\frac{3Ht_0}{2}+t_0^2\right) + 0.4620\frac{E_1\nu_{21}H^3 t}{\nu_{12}a}$$

$$\langle zb_{12}^{*12}\rangle = \frac{2G_{12}t_0}{36}\left(\frac{3H^2}{4}+\frac{3Ht_0}{2}+t_0^2\right) + 0.4620\frac{E_2 H^3 t}{a}$$

$$\delta\langle d_{11}^3\rangle = \frac{2t_0(E_1 d_{31}^{(r)}+\nu_{21}E_1 d_{32}^{(r)})}{1-\nu_{12}\nu_{21}} + 1.155\Big\{(c_{11}-\nu_{12}c_{12}-0.9\nu_{32}c_{13})d_{31}^{(r)} + (c_{12}-\nu_{12}c_{22}-$$

$$0.9\nu_{32}c_{23})d_{32}^{(r)} + (c_{13}-\nu_{12}c_{23}-0.9\nu_{32}c_{33})d_{33}^{(r)}\Big\}\frac{Ht}{a}$$

$$\delta\langle d_{22}^3\rangle = \frac{2t_0(E_2 d_{32}^{(r)}+\nu_{12}E_2 d_{31}^{(r)})}{1-\nu_{12}\nu_{21}} + 0.0000196\Big\{(c_{12}-\nu_{12}c_{11}-0.1\nu_{32}c_{13})d_{31}^{(r)} +$$

$$(c_{22}-\nu_{12}c_{12}-0.1\nu_{32}c_{23})d_{32}^{(r)} + (c_{23}-\nu_{12}c_{13}-0.1\nu_{32}c_{33})d_{33}^{(r)}\Big\}\frac{Ht}{a}$$

$$\delta\langle zd_{11}^{*3}\rangle = \frac{2t_0(E_1 d_{31}^{(r)} + \nu_{21} E_1 d_{32}^{(r)})}{1-\nu_{12}\nu_{21}}\left(\frac{3H^2}{4} + \frac{3Ht_0}{2} + t_0^2\right) + 0.096\Big\{(c_{11} - \nu_{12}c_{12} -$$

$$0.9\nu_{32}c_{13})d_{31}^{(r)} + (c_{12} - \nu_{12}c_{22} - 0.9\nu_{32}c_{23})d_{32}^{(r)} + (c_{13} - \nu_{12}c_{23} - 0.9\nu_{32}c_{33})d_{33}^{(r)}\Big\}\frac{H^3 t}{a}$$

$$\delta\langle zd_{22}^{*3}\rangle = \frac{2t_0(E_2 d_{32}^{(r)} + \nu_{12} E_2 d_{31}^{(r)})}{1-\nu_{12}\nu_{21}}\left(\frac{3H^2}{4} + \frac{3Ht_0}{2} + t_0^2\right) + 0.0000016\Big\{(c_{12} - \nu_{12}c_{11} -$$

$$0.1\nu_{32}c_{13})d_{31}^{(r)} + (c_{22} - \nu_{12}c_{12} - 0.1\nu_{32}c_{23})d_{32}^{(r)} + (c_{23} - \nu_{12}c_{13} - 0.1\nu_{32}c_{33})d_{33}^{(r)}\Big\}\frac{H^3 t}{a}$$

In the equations in section 5.4, the terms E, $c_{ij}$, $d_{ij}$, $\nu_{ij}$ refer to the elastic modulus, properties of a single layer, piezoelectric properties, and Poisson ratio of the material used, respectively. $t_0$ is the thickness of the unit cell, with H being the dimensional parameter of the same unit cell.

## 5.5 THIN COMPOSITE NETWORK STRUCTURES

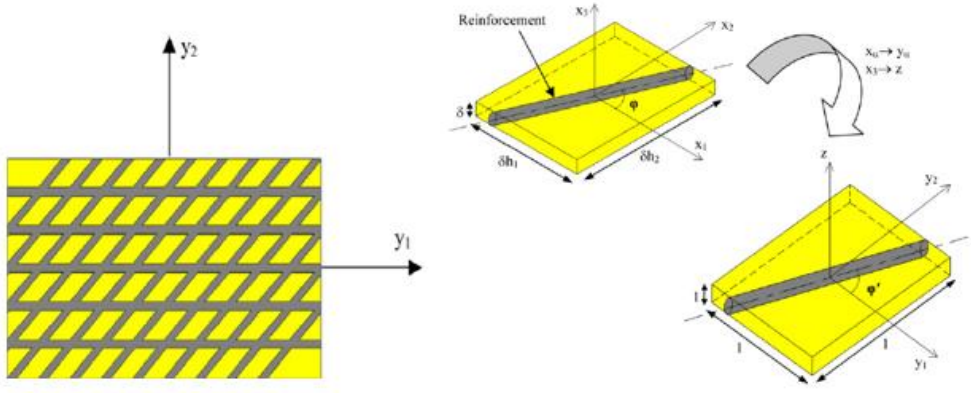


**Figure 5.6 Composite with thin bar reinforcement and unit cell representation [45]**

A thin composite smart plate that has been reinforced by a myriad of reinforcing bars in an orientation that is mutually parallel to each other is considered in this variant, see Figure 5.6. Some assumptions are being made in order to obtain an efficient model. The stiffness of the reinforcing orthotropic bars is deemed to be notable larger than the matrix. This, in turn, allows us to neglect the contribution of the matrix. The materials used for the reinforcing bar are assumed to be homogenous orthotropic material. Each set

of reinforcing bars makes a unique angle in accordance with the $y_1$ axis, and thus a single reinforcement unit cell has been taken into consideration. The solution to this is obtained at the preliminary stage and superpositioned to obtain the more general effective properties applying to the whole structure. The calculated properties are given in the form below.

$$\langle b_{ij}^{\lambda\mu} \rangle = \frac{1}{|\Omega|} \int_{|\Omega|} b_{ij}^{\lambda\mu}\, dv = \frac{V}{h_1 h_2} b_{ij}^{\lambda\mu}$$

$$\langle z b_{ij}^{\lambda\mu} \rangle = \frac{1}{|\Omega|} \int_{|\Omega|} z b_{ij}^{\lambda\mu}\, dv = 0$$

$$\langle b_{ij}^{*\lambda\mu} \rangle = 0$$

$$\langle z b_{ij}^{*\lambda\mu} \rangle = \frac{V}{16 h_1 h_2} B_{ij}^{\lambda\mu}$$

Where,

$$B_{11}^{\lambda\mu} = \frac{\Lambda_5\Lambda_6 - \Lambda_2\Lambda_3}{\Lambda_1\Lambda_2 - \Lambda_4\Lambda_5}, B_{22}^{\lambda\mu} = \frac{\Lambda_3\Lambda_4 - \Lambda_1\Lambda_6}{\Lambda_1\Lambda_2 - \Lambda_4\Lambda_5}, and\ B_{12}^{\lambda\mu} = \frac{s h_2}{2 c h_1} B_{11}^{\lambda\mu} + \frac{c h_1}{2 s h_2} B_{22}^{\lambda\mu}$$

$$b_{11}^{\lambda\mu} = \frac{C_{12\lambda\mu}[\sum_4\sum_7 + \sum_8\sum_3] + C_{11\lambda\mu}[\sum_5\sum_7 - \sum_9\sum_3] + C_{22\lambda\mu}[\sum_6\sum_7] + C_{33\lambda\mu}\sum_3}{\sum_7\left[\frac{h_2 s}{h_{1c}}\sum_4 + \sum_5 + \frac{h_2^2 s^2}{h_1^2 c^2}\sum_6\right] + \frac{h_2 s}{h_1 c}[\sum_8\sum_3] - \sum_9\sum_3}$$

$$b_{22}^{\lambda\mu} = \frac{C_{12\lambda\mu}[\sum_4\sum_7 + \sum_8\sum_3] + C_{11\lambda\mu}[\sum_5\sum_7 - \sum_9\sum_3] + C_{22\lambda\mu}[\sum_6\sum_7] + C_{33\lambda\mu}\sum_3}{\sum_7\left[\frac{h_{1c}}{h_2 s}\sum_4 + \frac{h_1^2 c^2}{h_2^2 s^2}\sum_5 + \sum_6\right] + \frac{h_1 c}{h_2 s}[\sum_8\sum_3] - \frac{h_1^2 c^2}{h_2^2 s^2}\sum_9\sum_3}$$

$$b_{12}^{\lambda\mu} = \frac{C_{12\lambda\mu}[\sum_4\sum_7 + \sum_8\sum_3] + C_{11\lambda\mu}[\sum_5\sum_7 - \sum_9\sum_3] + C_{22\lambda\mu}[\sum_6\sum_7] + C_{33\lambda\mu}\sum_3}{\sum_7\left[\frac{h_{1c}}{h_2 s}\sum_4 + \frac{h_{1c}}{h_2 s}\sum_5 + \frac{h_2 s}{h_1 c}\sum_6\right] + [\sum_8\sum_3] - \frac{h_{1c}}{h_2 s}\sum_9\sum_3}$$

The remaining terms $b_{13}^{\lambda\mu} = b_{23}^{\lambda\mu} = b_{33}^{\lambda\mu} = 0$

$C_{ij\lambda\mu}$ represents the properties of a single layer of composite material being used. Also, the 'c' and 's' stand for cos$\varphi$` and sin$\varphi$` respectively. $h_1$ and $h_2$ stand for the length and width of the plate being used, and V is the volume of the single bar of reinforcement.

## 5.6 SMART COMPOSITE REINFORCED AND SANDWICH SHELLS

### 5.6.1 RECTANGULAR WAFER REINFORCED COMPOSITE STRUCTURE

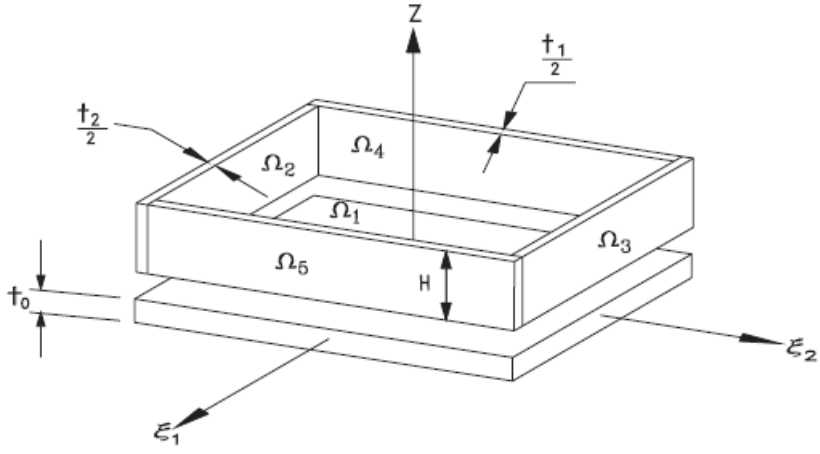


**Figure 5.7 Unit cell of rectangular wafer structure [44]**

The effective coefficients of the structure are given as

$$\langle b_{11}^{11}\rangle = \langle b_{22}^{22}\rangle = \frac{E_0 t_0}{5(1-\nu_0^2)} + \frac{3\sqrt{3}EHt}{20a}$$

$$\langle b_{22}^{11}\rangle = \langle b_{11}^{22}\rangle = \frac{4\nu_0 E_0 t_0}{5(1-\nu_0^2)} + \frac{\sqrt{3}EHt}{20a}$$

$$\langle b_{12}^{12}\rangle = \frac{2E_0 t_0}{5(1+\nu_0)} + \frac{\sqrt{3}EHt}{20a}$$

$$\langle zb_{11}^{*11}\rangle = \langle zb_{22}^{*22}\rangle = \frac{E_0 t_0^3}{180(1-\nu_0^2)} + \frac{3\sqrt{3}EH^3 t}{40a}\left(\frac{Ht_0^2}{2} + H^2 t_0 + \frac{2H^3}{3}\right)$$

$$\langle zb_{22}^{*11}\rangle = \langle zb_{11}^{*22}\rangle = \frac{\nu_0 E_0 t_0^3}{180(1-\nu_0^2)} + \frac{\sqrt{3}EH^3 t}{40a}\left(\frac{Ht_0^2}{2} + H^2 t_0 + \frac{2H^3}{3}\right)$$

$$\langle zb_{12}^{*12}\rangle = \frac{E_0 t_0^3}{30(1+\nu_0)} + \frac{\sqrt{3}Et}{12a(1+\nu)}\left(\frac{Ht_0^2}{2} + H^2 t_0 + \frac{2H^3}{3}\right) \times \left(\frac{1}{5}\frac{32H}{9\pi^5 h_1}\sum_{n=1}^{\infty}\frac{\tanh\left[\pi(2n-1)\left(\frac{t}{2H}\right)\right]}{(2n-1)^5}\right)$$

$$\delta\langle d_{11}^3\rangle = \delta\langle d_{11}^3\rangle = \frac{4t_0(E_0 d_{31}^{(r)} + \nu_0 E_0 d_{32}^{(r)})}{5(1-\upsilon_0^2)}$$

$$\delta\langle zd_{11}^{*3}\rangle = \delta\langle zd_{11}^{*3}\rangle = \frac{t_0^3(E_0 d_{31}^{(r)} + \nu_0 E_0 d_{32}^{(r)})}{180(1-\upsilon_0^2)}$$

### 5.6.2 HEXAGONAL HONEYCOMB CORE COMPOSITE SANDWICH STRUCTURE

Certain assumptions are made in this analysis which is that the constituents of the honeycomb layer are made of an isotropic material while the sandwich faces are made of orthotropic materials, which may exhibit piezoelectric behavior in certain conditions.

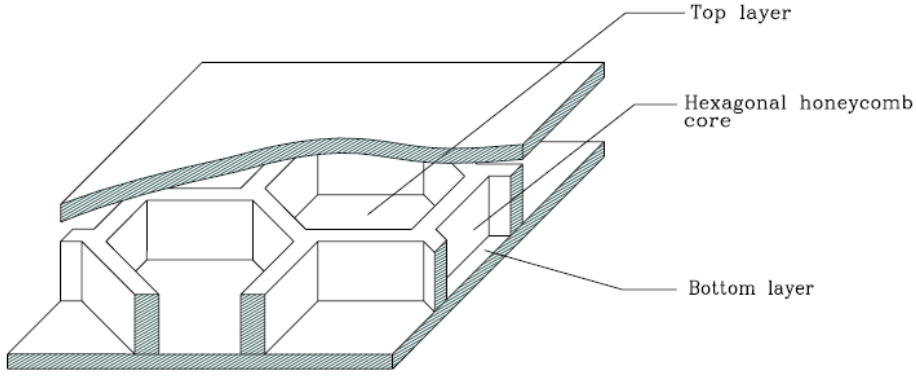


**Figure 5.8 Hexagonal honeycomb structure [44]**

The effective properties of this structure take the form of the below-given equations.

$$\langle b_{11}^{11}\rangle = \langle b_{22}^{22}\rangle = \frac{2E_0 t_0}{1-\nu_0^2} + \frac{\sqrt{3}EHt}{4a}$$

$$\langle b_{22}^{11}\rangle = \langle b_{11}^{22}\rangle = \frac{2\nu_0 E_0 t_0}{1-\nu_0^2} + \frac{\sqrt{3}EHt}{12a}$$

$$\langle b_{12}^{12}\rangle = \frac{E_0 t_0}{1+\nu_0} + \frac{\sqrt{3}EHt}{12a}$$

$$\langle zb_{11}^{*11}\rangle = \langle zb_{22}^{*22}\rangle = \frac{E_0}{12(1-\nu_0^2)}\left(\frac{H^2 t_0}{2} + Ht_0^2 + \frac{2t_0^3}{3}\right) + \frac{\sqrt{3}EH^3 t}{48a}$$

$$\langle zb_{22}^{*11}\rangle = \langle zb_{11}^{*22}\rangle = \frac{\nu_0 E_0}{12(1-\nu_0^2)}\left(\frac{H^2 t_0}{2} + Ht_0^2 + \frac{2t_0^3}{3}\right) + \frac{\sqrt{3}EH^3 t}{144a}$$

$$\langle zb_{12}^{*12}\rangle = \frac{E_0}{2(1-\nu_0)}\left(\frac{H^2 t_0}{2} + Ht_0^2 + \frac{2t_0^3}{3}\right) + \frac{EH^3 t}{12a(1+\nu)} \times \left(\frac{1}{\sqrt{3}}\frac{128H}{\sqrt{3\pi^5}}\sum_{n=1}^{\infty}\frac{\tanh\left[\pi(2n-1)\left(\frac{t}{2H}\right)\right]}{(2n-1)^5}\right)$$

$$\delta\langle d_{11}^{3}\rangle = \delta\langle d_{11}^{3}\rangle = \frac{2t_0(E_0 d_{31}^{(r)} + \nu_0 E_0 d_{32}^{(r)})}{1-\upsilon_0^2}$$

$$\delta\langle zd_{11}^{*3}\rangle = \delta\langle zd_{11}^{*3}\rangle = \frac{t_0(E_0 d_{31}^{(r)} + \nu_0 E_0 d_{32}^{(r)})}{18(1-\upsilon_0^2)} \times \left(\frac{3H^2}{4} + \frac{3Ht_0}{2} + t_0^2\right)$$

### 5.6.3 SMART THIN WAFER COMPOSITE STRUCTURE WITH TRIANGULAR REINFORCEMENTS

The nonzero effective properties and piezoelectric properties of a thin wafer element are given in this section by considering the unit cells.

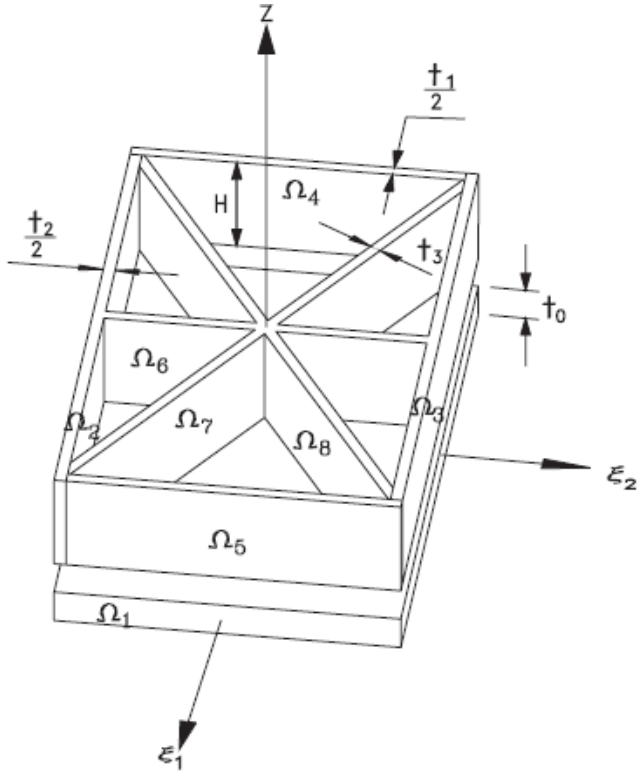


**Figure 5.9 Triangular wafer reinforced structure unit cell [44]**

$$\langle b_{11}^{11}\rangle = \langle b_{22}^{22}\rangle = \frac{E_0 t_0}{1-\nu_0^2} + \left(\frac{9(1+2\sqrt{3}}{32}\right)\frac{EHt}{a}$$

$$\langle b_{22}^{11}\rangle = \langle b_{11}^{22}\rangle = \frac{E_0 \nu_0 t_0}{1-\nu_0^2} + \left(\frac{3(1+2\sqrt{3}}{32}\right)\frac{EHt}{a}$$

$$\langle b_{12}^{12}\rangle = \frac{E_0 t_0}{2(1+\nu_0)} + \left(\frac{3(1+2\sqrt{3}}{32}\right)\frac{EHt}{a}$$

$$\langle zb_{11}^{*11}\rangle = \langle zb_{22}^{*22}\rangle = \frac{E_0 t_0^3}{144(1-\nu_0^2)} + \left(\frac{9(1+2\sqrt{3}}{64}\right)\frac{Et}{a} \times \left(\frac{Ht_0^2}{2} + H^2 t_0 + \frac{2H^3}{3}\right)$$

$$\langle zb_{22}^{*11}\rangle = \langle zb_{11}^{*22}\rangle = \frac{\nu_0 E_0 t_0^3}{144(1-\nu_0^2)} + \left(\frac{3(1+2\sqrt{3})}{32}\right)\frac{Et}{a} \times \left(\frac{Ht_0^2}{2} + H^2 t_0 + \frac{2H^3}{3}\right)$$

$$\langle zb_{12}^{*12}\rangle = \frac{E_0 t_0^3}{288(1+\nu_0)} + \frac{(1+2\sqrt{3})}{8}\frac{Et}{a(1+\nu)} \times \left(\frac{H^2 t_0}{2} + Ht_0^2 + \frac{2t_0^3}{3}\right) \times \left(\frac{3}{16} - \frac{8H}{3\pi^5 h_1}\sum_{n=1}^{\infty}\frac{\tanh\left[\pi(2n-1)\left(\frac{t}{2H}\right)\right]}{(2n-1)^5}\right)$$

$$\delta\langle d_{11}^3\rangle = \delta\langle d_{11}^3\rangle = \frac{t_0(E_0 d_{31}^{(r)} + \nu_0 E_0 d_{32}^{(r)})}{1-\upsilon_0^2}$$

$$\delta\langle zd_{11}^{*3}\rangle = \delta\langle zd_{11}^{*3}\rangle = \frac{t_0^3(E_0 d_{31}^{(r)} + \nu_0 E_0 d_{32}^{(r)})}{144(1-\upsilon_0^2)}$$

### 5.6.4 SMART DIAGONALLY RESTRAINED WAFER STRUCTURE

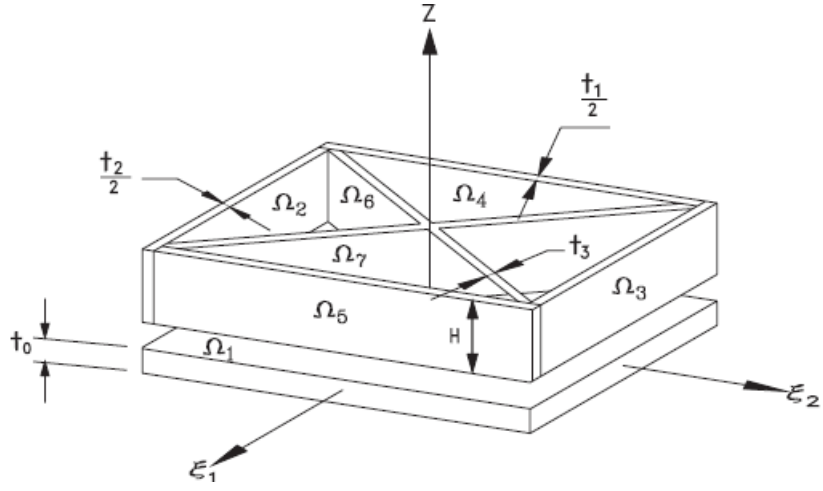


**Figure 5.10 Smart thin wafer structure unit cell [44]**

The smart diagonally restrained wafer structure has the following non-zero properties.

$$\langle b_{11}^{11}\rangle = \langle b_{22}^{22}\rangle = \frac{4E_0 t_0}{5(1-\nu_0^2)} + \left(\frac{3\sqrt{3}}{20} + \frac{9\sqrt{34}}{100\sqrt{26}} + \frac{9}{10}\right)\frac{EHt}{a}$$

$$\langle b_{22}^{11}\rangle = \langle b_{11}^{22}\rangle = \frac{4\nu_0 E_0 t_0}{5(1-\nu_0^2)} + \left(\frac{3\sqrt{3}}{20} + \frac{9\sqrt{34}}{100\sqrt{26}} + \frac{9}{10}\right)\frac{EHt}{a}$$

$$\langle b_{12}^{12}\rangle = \frac{2E_0 t_0}{5(1+\nu_0)} + \left(\frac{3\sqrt{3}}{20} + \frac{9\sqrt{34}}{100\sqrt{26}} + \frac{9}{10}\right)\frac{EHt}{a}$$

$$\langle zb_{11}^{*11}\rangle = \langle zb_{22}^{*22}\rangle = \frac{E_0 t_0^3}{180(1-\nu_0^2)} + \left(\frac{3\sqrt{3}}{40} + \frac{9\sqrt{34}}{200\sqrt{26}}\right) \times \frac{Ht}{a}\left(\frac{Ht_0^2}{2} + H^2 t_0 + \frac{2H^3}{3}\right)$$

$$\langle zb_{22}^{*11}\rangle = \langle zb_{11}^{*22}\rangle = \frac{\nu_0 E_0 t_0^3}{180(1-\nu_0^2)} + \left(\frac{3\sqrt{3}}{40} + \frac{9\sqrt{34}}{200\sqrt{26}}\right) \times \frac{Ht}{a}\left(\frac{Ht_0^2}{2} + H^2 t_0 + \frac{2H^3}{3}\right)$$

$$\langle zb_{12}^{*12}\rangle = \frac{E_0 t_0^3}{360(1+\nu_0)} + \frac{Et}{a(1+\nu)}\left(\frac{H^2 t_0}{2} + Ht_0^2 + \frac{2t_0^3}{3}\right) \times \left(\left(\frac{\sqrt{3}}{5} + \frac{\sqrt{34}}{50\sqrt{26}}\right)\left(\frac{120H}{9\pi^5 h_1}\sum_{n=1}^{\infty}\frac{\tanh\left[\pi(2n-1)\left(\frac{t}{2H}\right)\right]}{(2n-1)^5}\right)\right)$$

$$\delta\langle d_{11}^3\rangle = \delta\langle d_{11}^3\rangle = \frac{4t_0(E_0 d_{31}^{(r)} + \nu_0 E_0 d_{32}^{(r)})}{5(1-\upsilon_0^2)}$$

$$\delta\langle zd_{11}^{*3}\rangle = \delta\langle zd_{11}^{*3}\rangle = \frac{t_0^3(E_0 d_{31}^{(r)} + \nu_0 E_0 d_{32}^{(r)})}{180(1-\upsilon_0^2)}$$

The abbreviations for the terms used in section 5.6.1 - 5.6.4 are taken as the following. $t_0$ and H is the thickness of the sandwich layer and the wafer core, respectively. n is the number of layers. $E_0$ and $\nu_0$ denote the material properties of the constituents being used. H, t, and a are geometric parameters that highly influence the effective properties of the composite structure. One can influence the effective properties by varying these parameters.

## 5.7 SMART COMPOSITE PLATES WITH EMBEDDED ACTUATORS AND RAPIDLY VARYING THICKNESS

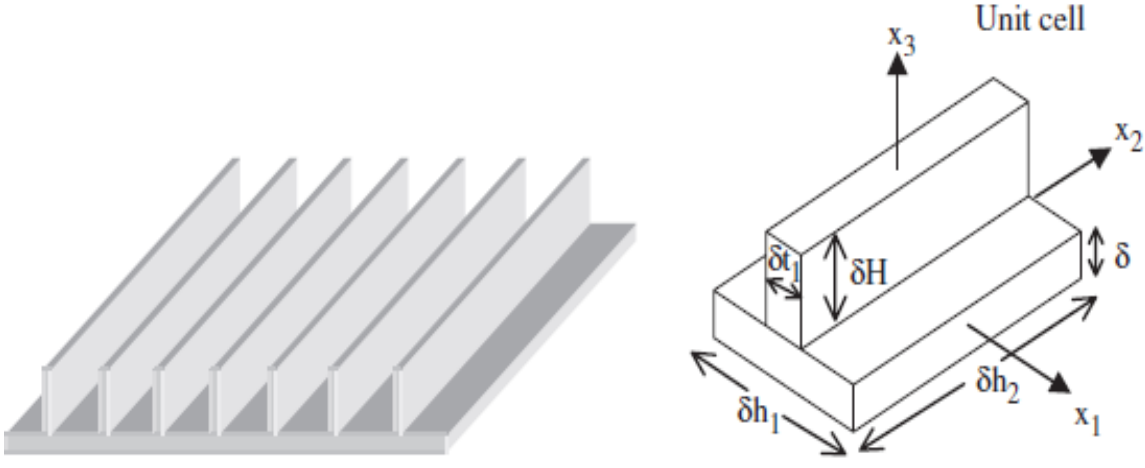


**Figure 5.11 Rib-reinforced composite and unit cell [46]**

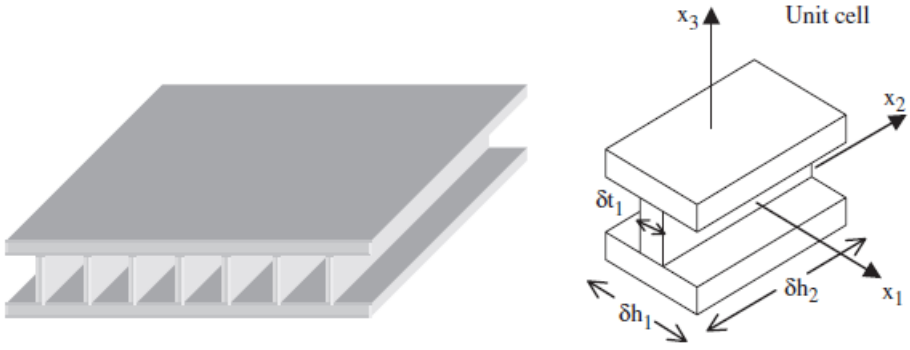


**Figure 5.12 Rib-reinforced sandwich composite and unit cell [46]**

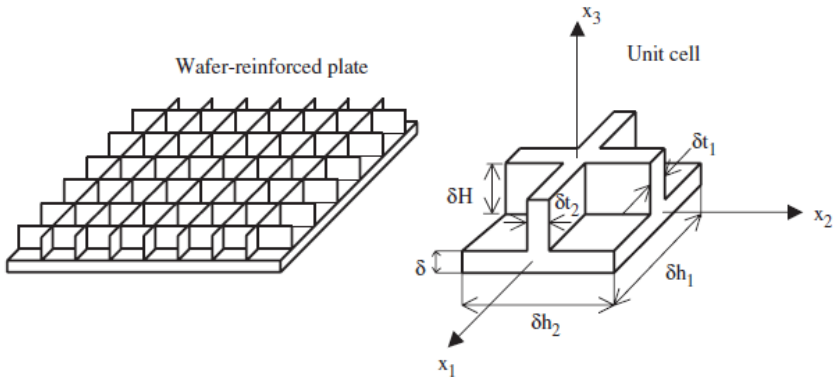


**Figure 5.13 Wafer-reinforced smart composite and unit cell [46]**

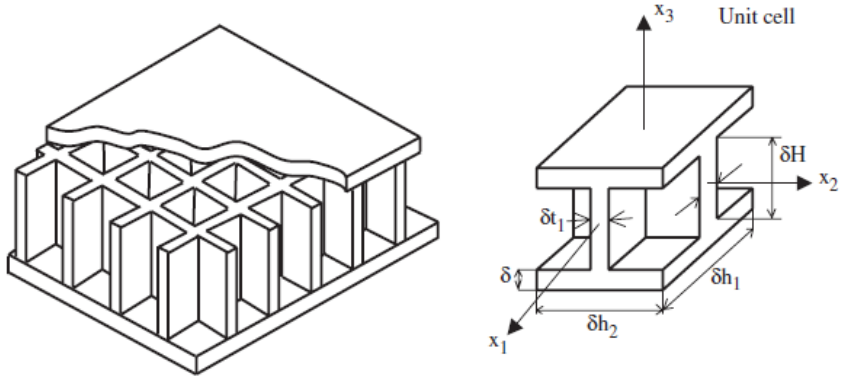


**Figure 5.14 Wafer-reinforced sandwich composite and unit cell [46]**

The effective properties can be obtained for this geometry considering that the thickness of the cell is a very small parameter compared to the other dimensions of the unit cell, depicted in the form of t1 << h2, t2 << h1, and H ~ h1, h2. Further, the local problems are solved, and the pertinent effective coefficients are obtained. The material

used is assumed to be orthotropic, which may also exhibit piezoelectric characteristics. The properties for all the fours structures shown in Figure 5.11 - 5.14 are given in the form of a general set of equations as:

$$\delta\langle\Theta_{11}\rangle = \frac{E_1^{(3)}\alpha_1^{(\theta)(3)} + E_1^{(3)}\nu_{21}^{(3)}\alpha_2^{(\theta)(3)}}{1-\nu_{12}^{(3)}\nu_{21}^{(3)}}, \delta\langle z\Theta_{11}\rangle = \delta\langle\Theta_{11}^{*}\rangle = 0$$

$$\delta\langle\Theta_{22}\rangle = E_2^{(1)}\alpha_2^{(\theta)(1)}F_1^{(w)} + \frac{E_2^{(3)}\alpha_2^{(\theta)(3)} + E_2^{(3)}\nu_{12}^{(3)}\alpha_1^{(\theta)(3)}}{1-\nu_{12}^{(3)}\nu_{21}^{(3)}}, \delta\langle z\Theta_{22}\rangle = E_2^{(1)}\alpha_2^{(\theta)(1)}S_1^{(w)}$$

$$\delta\langle \mathrm{z}\Theta_{11}^{*}\rangle = \frac{E_1^{(3)}\alpha_1^{(\theta)(3)} + E_1^{(3)}\nu_{21}^{(3)}\alpha_2^{(\theta)(3)}}{12(1-\nu_{12}^{(3)}\nu_{21}^{(3)})}$$

$$\delta\langle z\Theta_{22}^{*}\rangle = E_2^{(1)}\alpha_2^{(\theta)(1)}J_1^{(w)} + \frac{E_2^{(3)}\alpha_2^{(\theta)(3)} + E_2^{(3)}\nu_{12}^{(3)}\alpha_1^{(\theta)(3)}}{12(1-\nu_{12}^{(3)}\nu_{21}^{(3)})}$$

$$\delta\langle \mathrm{d}_{11}^{3}\rangle = E_1^{(2)}d_{31}^{(r)(2)}F_2^{(w)} + \frac{E_1^{(3)}d_{31}^{(r)(3)} + E_1^{(3)}\nu_{21}^{(3)}d_{32}^{(r)(3)}}{1-\nu_{12}^{(3)}\nu_{21}^{(3)}}$$

$$\delta\langle \mathrm{d}_{22}^{3}\rangle = E_2^{(1)}d_{32}^{(r)(1)}F_1^{(w)} + \frac{E_2^{(3)}d_{32}^{(r)(3)} + E_2^{(3)}\nu_{12}^{(3)}d_{31}^{(r)(3)}}{1-\nu_{12}^{(3)}\nu_{21}^{(3)}}$$

$$\delta\langle \mathrm{zd}_{11}^{3}\rangle = \delta\langle \mathrm{d}_{11}^{*3}\rangle = E_1^{(2)}d_{31}^{(r)(2)}S_2^{(w)}$$

$$\delta\langle \mathrm{zd}_{22}^{3}\rangle = \delta\langle \mathrm{d}_{22}^{*3}\rangle = E_2^{(1)}d_{32}^{(r)(1)}S_1^{(w)}$$

$$\delta\langle \mathrm{zd}_{11}^{*3}\rangle = E_1^{(2)}d_{31}^{(r)(2)}J_2^{(w)} + \frac{E_1^{(3)}d_{31}^{(r)(3)} + E_1^{(3)}\nu_{21}^{(3)}d_{32}^{(r)(3)}}{12(1-\nu_{12}^{(3)}\nu_{21}^{(3)})}$$

$$\delta\langle z\mathrm{d}_{22}^{*3}\rangle = E_2^{(1)}d_{32}^{(r)(1)}J_1^{(w)} + \frac{E_2^{(3)}d_{32}^{(r)(3)} + E_2^{(3)}\nu_{12}^{(3)}d_{31}^{(r)(3)}}{12(1-\nu_{12}^{(3)}\nu_{21}^{(3)})}$$

In these set of equations, the parameters $E_1$, $E_2$, $\nu_{12}, \nu_{21}$ define the material properties used in the composite manufacture. $d_{31}, d_{32}$, $\alpha_1, \alpha_2$ are also the material properties but specific to those exhibiting piezoelectric behavior. $F_i^{(w)}, J_i^{(w)}, S_i^{(w)} W$here i=1,2 is the cross-sectional area, moment of inertia of the rib in reference to the plate, and first moment of inertia, respectively.

## 5.8 PRISMATIC SMART COMPOSITE STRUCTURES

We consider the material PZT-5A to be exhibiting the piezoelectric properties in order to skim the representative equations of the effective piezoelectric coefficients. It is also assumed that all the reinforcements are made of the same orthotropic material.

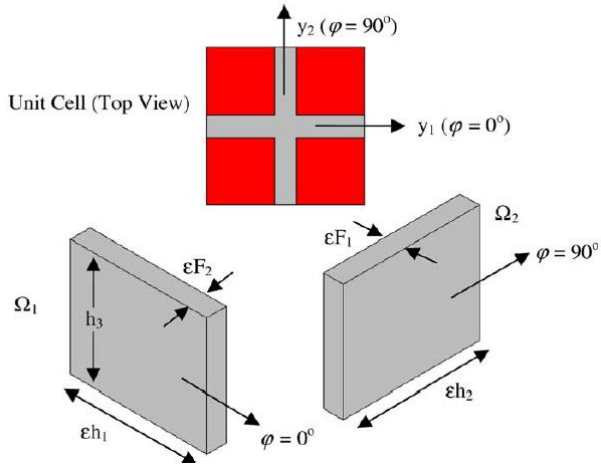


**Figure 5.15 Smart Structure with Unit cell 0° and 90° [31]**

The elastic properties of the above structure with two unit cells and reinforcements in 0 and 90 degrees orientation are given to be:

$$\langle C_{ijkl} \rangle = \frac{F_2}{h_2} b_{ij}^{kl}(\text{for } \Omega_1) + \frac{F_1}{h_1} b_{ij}^{kl}(\text{for } \Omega_2)$$

Where for element $\Omega_1 = 0^o$

$$b_{11}^{11} = C_{11} - \frac{C_{12}^2}{C_{22}},\ b_{33}^{11} = C_{13} - \frac{C_{23}C_{12}}{C_{22}}, b_{33}^{33} = C_{33} - \frac{C_{23}^2}{C_{22}}, b_{13}^{13} = C_{55}$$

For element $\Omega_2$ =90°

$$b_{22}^{22} = C_{22} - \frac{C_{12}^2}{C_{11}},\ b_{33}^{22} = C_{23} - \frac{C_{13}C_{12}}{C_{11}}, b_{33}^{33} = C_{33} - \frac{C_{13}^2}{C_{11}}, b_{23}^{23} = C_{44}$$

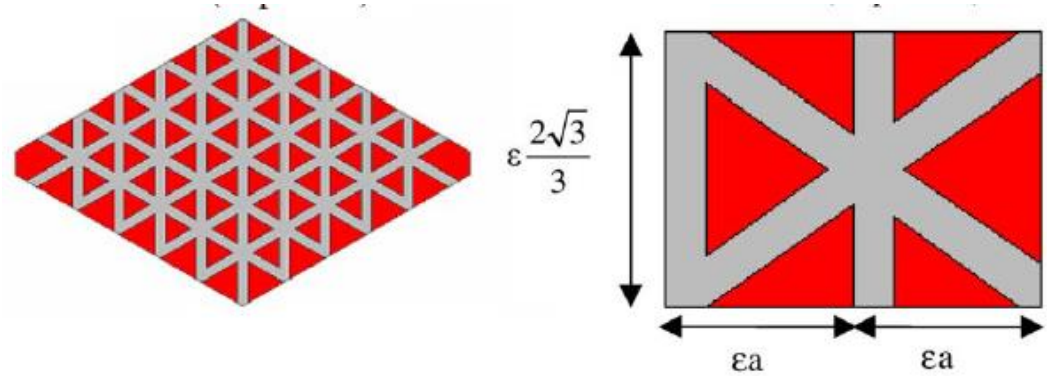


**Figure 5.16 Smart prismatic structure [31]**

The effective piezoelectric coefficient for the structure is given as

$$\langle P_{13} \rangle = -1.6 * 10^{-6} \left( \frac{F_1}{a} + \frac{F_2}{a} \right), \langle P_{23} \rangle = -5.5 * 10^{-7} \left( \frac{F_1}{a} + \frac{F_2}{a} \right)$$

$$\langle P_{63} \rangle = -9.4 * 10^{-7} \left( \frac{F_1}{a} + \frac{F_2}{a} \right), \langle P_{51} \rangle = -1.8 * 10^{-5} \left( \frac{F_1}{a} + \frac{F_2}{a} \right)$$

$$\langle P_{42} \rangle = 6.1 * 10^{-6} \left( \frac{F_1}{a} + \frac{F_2}{a} \right) + 2.5 * 10^{-5} \frac{F_3}{a}$$

$$\langle P_{33} \rangle = 1.8 * 10^{-5} \left( \frac{F_1}{a} + \frac{F_2}{a} \right) + 1.9 * 10^{-5} \frac{F_3}{a}$$

Assuming all reinforcements are made of E-glass/epoxy, the thermal expansion coefficients can be given as

$$\langle K_1 \rangle = \frac{0.14F_1}{a} + \frac{0.14F_2}{a}, \langle K_2 \rangle = \frac{0.23F_1}{a} + \frac{0.23F_2}{a} + \frac{0.33F_3}{a}$$

$$\langle K_6 \rangle = \frac{0.08F_1}{a} - \frac{0.08F_2}{a}, \langle K_3 \rangle = \frac{0.19F_1}{a} + \frac{0.19F_2}{a} + \frac{0.20F_3}{a}$$

Here, all the $C_{ij}$ represents the material properties. $F_i$ where i=1,2,3 is a depiction of the thickness of the elements, as shown in figure 5.15. a is the dimensional parameter controlling the properties of the material along with other factors.

## 5.9 SMART COMPOSITE PLATES WITH GENERALLY ORTHOTROPIC REINFORCING NETWORKS

The effective coefficients for a composite with networks of reinforcing elements and actuators for a smart thin composite are given in this section. These reinforcements are made of orthotropic materials. After calculations and using the general homogenization method for smart composites that are too lengthy to be reproduced here, further details refer [47]. The effective coefficients are given in the form of the following set of equations.

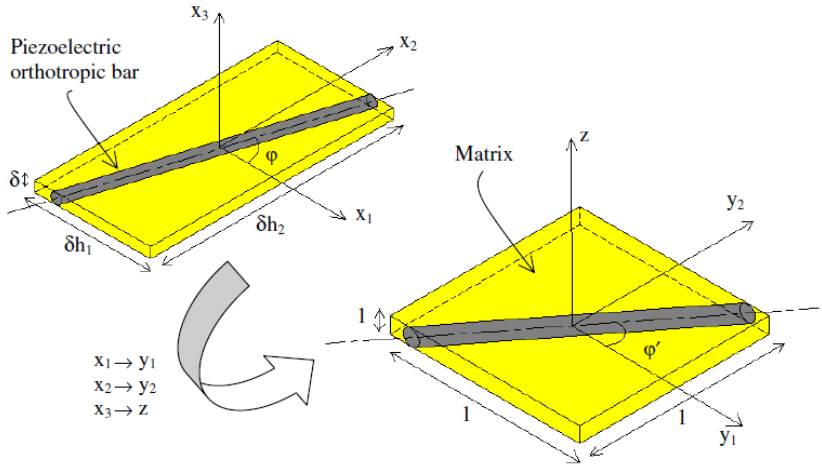


**Figure 5.17 Unit cell of a single bar reinforced composite [47]**

The effective piezoelectric coefficients are given as

$$\langle d_{ij}^k \rangle = \frac{1}{|Y|}\int_{|Y|} d_{ij}^k \, dv = \frac{V}{h_1 h_2} d_{ij}^k$$

$$\langle z d_{ij}^k \rangle = \langle d_{ij}^{*k} \rangle = 0$$

$$\langle z d_{ij}^{*k} \rangle = \frac{V}{16 h_1 h_2} D_{ij}^k$$

where,

$$D_{11}^{k} = \frac{\Delta_5\Delta_6 - \Delta_2\Delta_3}{\Delta_1\Delta_2 - \Delta_4\Delta_5}, D_{22}^{k} = \frac{\Delta_3\Delta_4 - \Delta_1\Delta_6}{\Delta_1\Delta_2 - \Delta_4\Delta_5}, D_{12}^{k} = \frac{sh_2}{2ch_1} D_{11}^{k} + \frac{ch_1}{2sh_2}\ D_{22}^{k}$$

And,

$$d_{11}^{k} = \{P_{12k}[\alpha_4\alpha_7 + \alpha_8\alpha_3] + P_{11k}[\alpha_5\alpha_7 + \alpha_9\alpha_3] + P_{22k}[\alpha_6\alpha_7] + P_{33k}\alpha_3\}\left\{\alpha_7\left[\frac{h_2 s}{h_1 c}\alpha_4 + \alpha_5 + \frac{h_2^2 s^2}{h_1^2 c^2}\alpha_6\right] + \frac{h_2 s}{h_1 c}[\alpha_8\alpha_3] + \alpha_9\alpha_3\right\}^{-1}$$

$$d_{22}^{k} = \{P_{12k}[\alpha_4\alpha_7 + \alpha_8\alpha_3] + P_{11k}[\alpha_5\alpha_7 + \alpha_9\alpha_3] + P_{22k}[\alpha_6\alpha_7] + P_{33k}\alpha_3\}\left\{\alpha_7\left[\frac{h_1 c}{h_2 s}\alpha_4 + \alpha_5 + \frac{h_1^2 c^2}{h_2^2 s^2}\alpha_6\right] + \frac{h_1 c}{h_2 s}[\alpha_8\alpha_3] + \frac{h_1^2 c^2}{h_2^2 s^2}\alpha_9\alpha_3\right\}^{-1}$$

$$d_{12}^{k} = \{P_{12k}[\alpha_4\alpha_7 + \alpha_8\alpha_3] + P_{11k}[\alpha_5\alpha_7 + \alpha_9\alpha_3] + P_{22k}[\alpha_6\alpha_7] + P_{33k}\alpha_3\}\left\{\alpha_7\left[\alpha_4 + \frac{h_1 c}{h_2 s}\alpha_5 + \frac{h_2 s}{h_1 c}\alpha_6\right] + [\alpha_8\alpha_3] + \frac{h_1 c}{h_2 s}\alpha_9\alpha_3\right\}^{-1}$$

$$d_{13}^{k} = d_{23}^{k} = d_{33}^{k} = 0$$

The thermal expansion coefficients are

$$\langle\Theta_{ij}\rangle = \frac{1}{|\mathrm{Y}|}\int_{|\mathrm{Y}|}\Theta_{ij}\, dv = \frac{V}{h_1 h_2}\Theta_{ij}$$

$$\langle z\Theta_{ij}\rangle = \langle\Theta_{ij}^{*}\rangle = 0$$

$$\langle z\Theta_{ij}^{*}\rangle = \frac{V}{16h_1 h_2}T_{ij}$$

Where,

$$\Theta_{11} = \{K_{12}[\alpha_4\alpha_7 + \alpha_8\alpha_3] + K_{11}[\alpha_5\alpha_7 + \alpha_9\alpha_3] + K_{22}[\alpha_6\alpha_7] + K_{33}\alpha_3\}\left\{\alpha_7\left[\frac{h_2 s}{h_1 c}\alpha_4 + \alpha_5 + \frac{h_2^2 s^2}{h_1^2 c^2}\alpha_6\right] + \frac{h_2 s}{h_1 c}[\alpha_8\alpha_3] + \alpha_9\alpha_3\right\}^{-1}$$

$$\Theta_{22} = \{K_{12}[\alpha_4\alpha_7 + \alpha_8\alpha_3] + K_{11}[\alpha_5\alpha_7 + \alpha_9\alpha_3] + K_{22}[\alpha_6\alpha_7] + K_{33}\alpha_3\}\left\{\alpha_7\left[\frac{h_1 c}{h_2 s}\alpha_4 + \frac{h_1^2 c^2}{h_2^2 s^2}\alpha_5 + \alpha_6\right] + \frac{h_1 c}{h_2 s}[\alpha_8\alpha_3] + \frac{h_1^2 c^2}{h_2^2 s^2}\alpha_9\alpha_3\right\}^{-1}$$

$$\Theta_{12} = \{K_{12}[\alpha_4\alpha_7 + \alpha_8\alpha_3] + K_{11}[\alpha_5\alpha_7 + \alpha_9\alpha_3] + K_{22}[\alpha_6\alpha_7] + K_{33}\alpha_3\}\left\{\alpha_7\left[\alpha_4 + \frac{h_1 c}{h_2 s}\alpha_5 + \frac{h_2 s}{h_1 c}\alpha_6\right] + [\alpha_8\alpha_3] + \frac{h_1 c}{h_2 s}\alpha_9\alpha_3\right\}^{-1}$$

$$\Theta_{13} = \Theta_{23} = \Theta_{33} = 0$$

and

$$T_{11} = \frac{\Lambda_5\Lambda_6 - \Lambda_2\Lambda_3}{\Lambda_1\Lambda_2 - \Lambda_4\Lambda_5}, T_{22} = \frac{\Lambda_3\Lambda_4 - \Lambda_1\Lambda_6}{\Lambda_1\Lambda_2 - \Lambda_4\Lambda_5}, T_{12} = \frac{sh_2}{2ch_1}T_{11} + \frac{ch_1}{2sh_2}\ T_{22}$$

Here c and s are cos$\varphi$ and sin$\varphi$ respectively, with $\varphi$ being the angle of the reinforcing element. V is the volume of the reinforcing bar in the unit cell, and $h_1$, $h_2$ is the dimensional parameters for the unit cell. $K_{ij}$ and $P_{ij}$ are thermal and piezoelectric constants, respectively.

## 5.10 WAFER REINFORCED PIEZOELECTRIC PLATE

In the previous section, we considered a wafer-reinforced smart plate with actuators. Here a wafer-reinforced piezoelectric plate is in consideration. We will also assume that the reinforcements are exhibiting piezoelectric properties. Also, the thickness of the plate is considered to be very small compared to the other dimensions of the composite plate.

The effective thermal expansion coefficients are given by

$$\delta\langle\Theta_{11}\rangle = E_1^{(2)}\alpha_1^{(\theta)(2)}F_2^{(w)} + \frac{E_1^{(3)}\alpha_1^{(\theta)(3)} + E_1^{(3)}\alpha_2^{(\theta)(3)}\upsilon_{21}^{(3)}}{1 - \upsilon_{12}^{(3)}\upsilon_{21}^{(3)}}$$

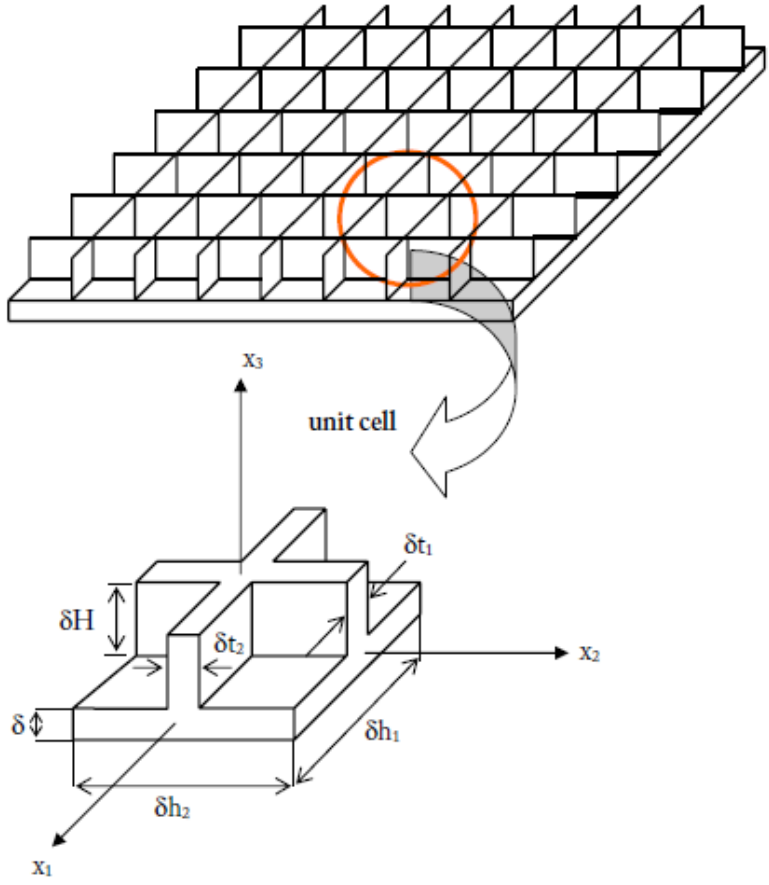


**Figure 5.18 Wafer reinforced composite and its unit cell [48]**

$$\delta\langle\Theta_{22}\rangle = E_2^{(1)}\alpha_2^{(\theta)(1)}F_1^{(w)} + \frac{E_2^{(3)}\alpha_2^{(\theta)(3)} + E_2^{(3)}\alpha_1^{(\theta)(3)}\upsilon_{12}^{(3)}}{1-\upsilon_{12}^{(3)}\upsilon_{21}^{(3)}}$$

$$\delta\langle z\Theta_{11}\rangle = \delta\langle z\Theta_{11}^{*}\rangle = E_1^{(2)}\alpha_1^{(\theta)(2)}S_2^{(w)}, \delta\langle z\Theta_{22}\rangle = \delta\langle z\Theta_{22}^{*}\rangle = E_2^{(1)}\alpha_2^{(\theta)(1)}S_1^{(w)}$$

$$\delta\langle z\Theta_{11}^{*}\rangle = E_1^{(2)}\alpha_1^{(\theta)(2)}J_2^{(w)} + \frac{E_1^{(3)}\alpha_1^{(\theta)(3)} + E_1^{(3)}\alpha_2^{(\theta)(3)}\upsilon_{21}^{(3)}}{12(1-\upsilon_{12}^{(3)}\upsilon_{21}^{(3)})}$$

$$\delta\langle z\Theta_{22}^{*}\rangle = E_2^{(1)}\alpha_2^{(\theta)(1)}J_1^{(w)} + \frac{E_2^{(3)}\alpha_2^{(\theta)(3)} + E_2^{(3)}\alpha_1^{(\theta)(3)}\upsilon_{12}^{(3)}}{12(1-\upsilon_{12}^{(3)}\upsilon_{21}^{(3)})}$$

With similar unit cell problems, the hygroscopic expansion coefficients take a similar form as the thermal coefficients. These set of equations are given as

$$\delta\langle\Lambda_{11}\rangle = E_1^{(2)}\beta_1^{(c)(2)}F_2^{(w)} + \frac{E_1^{(3)}\beta_1^{(c)(3)} + E_1^{(3)}\beta_2^{(c)(3)}\upsilon_{21}^{(3)}}{1-\upsilon_{12}^{(3)}\upsilon_{21}^{(3)}}$$

$$\delta\langle\Lambda_{22}\rangle = E_2^{(1)}\beta_2^{(c)(1)}F_1^{(w)} + \frac{E_2^{(3)}\beta_2^{(c)(3)} + E_2^{(3)}\beta_1^{(c)(3)}\upsilon_{12}^{(3)}}{1-\upsilon_{12}^{(3)}\upsilon_{21}^{(3)}}$$

$$\delta\langle z\Lambda_{11}\rangle = \delta\langle\Lambda_{11}^{*}\rangle = E_1^{(2)}\beta_1^{(c)(2)}S_2^{(w)}, \delta\langle z\Lambda_{22}\rangle = \delta\langle\Lambda_{22}^{*}\rangle = E_2^{(1)}\beta_2^{(c)(1)}S_1^{(w)}$$

$$\delta\langle z\Lambda_{11}^{*}\rangle = E_1^{(2)}\beta_1^{(c)(2)}J_2^{(w)} + \frac{E_1^{(3)}\beta_1^{(c)(3)} + E_1^{(3)}\beta_2^{(c)(3)}\upsilon_{21}^{(3)}}{12(1-\upsilon_{12}^{(3)}\upsilon_{21}^{(3)})}$$

$$\delta\langle z\Lambda_{22}^{*}\rangle = E_2^{(1)}\beta_2^{(c)(1)}J_1^{(w)} + \frac{E_2^{(3)}\beta_2^{(c)(3)} + E_2^{(3)}\beta_1^{(c)(3)}\upsilon_{12}^{(3)}}{12(1-\upsilon_{12}^{(3)}\upsilon_{21}^{(3)})}$$

Effective piezoelectric coefficients are given as

$$\delta\langle d_{11}^{3}\rangle = E_1^{(2)}d_{31}^{(r)(2)}F_2^{(w)} + \frac{E_1^{(3)}d_{31}^{(r)(3)} + E_1^{(3)}d_{32}^{(r)(3)}\upsilon_{21}^{(3)}}{1-\upsilon_{12}^{(3)}\upsilon_{21}^{(3)}}$$

$$\delta\langle d_{22}^{3}\rangle = E_2^{(1)}d_{32}^{(r)(1)}F_1^{(w)} + \frac{E_2^{(3)}d_{32}^{(r)(3)} + E_2^{(3)}d_{31}^{(r)(3)}\upsilon_{12}^{(3)}}{1-\upsilon_{12}^{(3)}\upsilon_{21}^{(3)}}$$

$$\delta\langle zd_{11}^{3}\rangle = \delta\langle zd_{11}^{*3}\rangle = E_1^{(2)}d_{31}^{(r)(2)}S_2^{(w)}, \delta\langle zd_{22}^{3}\rangle = \delta\langle d_{22}^{*3}\rangle = E_2^{(1)}d_{32}^{(r)(1)}S_1^{(w)}$$

$$\delta\langle zd_{11}^{*3}\rangle = E_1^{(2)}d_{31}^{(r)(2)}J_2^{(w)} + \frac{E_1^{(3)}d_{31}^{(r)(3)} + E_1^{(3)}d_{32}^{(r)(3)}\upsilon_{21}^{(3)}}{12(1-\upsilon_{12}^{(3)}\upsilon_{21}^{(3)})}$$

$$\delta\langle zd_{22}^{*3}\rangle = E_2^{(1)}d_{32}^{(r)(1)}J_1^{(w)} + \frac{E_2^{(3)}d_{32}^{(r)(3)} + E_2^{(3)}d_{31}^{(r)(3)}\upsilon_{12}^{(3)}}{12(1-\upsilon_{12}^{(3)}\upsilon_{21}^{(3)})}$$

$$\langle b_{11}^{11}\rangle = \frac{E_1^{(3)}}{1-\nu_{12}^{(3)}\nu_{21}^{(3)}} + E_1^{(2)}F_2^{(w)}, \langle b_{22}^{22}\rangle = \frac{E_2^{(3)}}{1-\nu_{12}^{(3)}\nu_{21}^{(3)}} + E_2^{(1)}F_1^{(w)}, \langle b_{22}^{11}\rangle = \frac{\nu_{21}^{(3)}E_2^{(3)}}{1-\nu_{12}^{(3)}\nu_{21}^{(3)}},$$

$$\langle b_{12}^{12}\rangle = G_{12}^{(3)}, \langle zb_{11}^{11}\rangle = \langle b_{11}^{*11}\rangle = E_1^{(2)}S_2^{(w)}, \langle zb_{22}^{22}\rangle = \langle b_{22}^{*22}\rangle = E_2^{(1)}S_1^{(w)}$$

$$\langle zb_{11}^{*11}\rangle = \frac{E_1^{(3)}}{12(1-\nu_{12}^{(3)}\nu_{21}^{(3)})} + E_1^{(2)}J_2^{(w)}, \langle zb_{22}^{*22}\rangle = \frac{E_2^{(3)}}{12(1-\nu_{12}^{(3)}\nu_{21}^{(3)})} + E_2^{(1)}J_1^{(w)}$$

$$\langle zb_{22}^{*11}\rangle = \frac{\nu_{21}^{(3)}E_1^{(3)}}{12(1-\nu_{12}^{(3)}\nu_{21}^{(3)})}, \langle zb_{12}^{*12}\rangle = \frac{G_{12}^{(3)}}{12} + \frac{G_{12}^{(1)}}{12}\left(\frac{H^3t_1}{h_1} - K_1\right) + \frac{G_{12}^{(2)}}{12}\left(\frac{H^3t_2}{h_2} - K_2\right)$$

where,

$$K_1 = \frac{96H^4}{\pi^5 h_1}\sqrt{\frac{G_{12}^{(1)}}{G_{23}^{(1)}}}\sum_{n=1}^{\infty}\frac{[1-(-1)^n]}{n^5}tanh\left(\sqrt{\frac{G_{23}^{(1)}}{G_{12}^{(1)}}}\frac{n\pi t_1}{2H}\right)$$

$$K_2 = \frac{96H^4}{\pi^5 h_2}\sqrt{\frac{G_{12}^{(2)}}{G_{13}^{(2)}}}\sum_{n=1}^{\infty}\frac{[1-(-1)^n]}{n^5}tanh\left(\sqrt{\frac{G_{13}^{(2)}}{G_{12}^{(2)}}}\frac{n\pi t_2}{2H}\right)$$

In all the above equations, the values are given by

$$\langle 1\rangle_{\Omega_a} = |\Omega_\alpha|^{-1}\int_{\Omega_a} 1dy_1dy_2dz = \frac{Ht_\alpha}{h_\alpha} = F_a^{(w)}, \langle 1\rangle_{\Omega_3} = 1$$

$$\langle z\rangle_{\Omega_a} = |\Omega_\alpha|^{-1}\int_{\Omega_a} zdy_1dy_2dz = \frac{(H^2+H)t_\alpha}{2h_\alpha} = S_a^{(w)}, \langle z\rangle_{\Omega_3} = 1$$

$$\langle z^2\rangle_{\Omega_a} = |\Omega_\alpha|^{-1}\int_{\Omega_a} z^2dy_1dy_2dz = \frac{(4H^3+6H^2+H)t_\alpha}{2h_\alpha} = J_a^{(w)}, \langle z^2\rangle_{\Omega_3} = 1/12$$

Here $h_1, h_2, H, t_1, t_2$ are all dimensional parameters of the composite plate and largely influence the properties of the composite structure. $E_1^{(i)}, E_2^{(i)}, G_{12}^{(i)}, d_{31}^{(r)(3)}, d_{32}^{(r)(3)}$ represents the material properties used in the respective

regions. $F_a^{(w)}, S_a^{(w)}, and\ J_a^{(w)}$ are cross-sectional areas, first moments, and moments of inertia of the cross-sections, respectively.

## 5.11 GRID REINFORCED COMPOSITE SHELL WITH A NETWORK OF REINFORCEMENTS/ACTUATORS

A thin smart composite shell with several parallel reinforcements is considered in this section. These reinforcing elements can be taken as a material that may exhibit piezoelectric behavior. They are made of generally orthotropic material and are homogeneous in nature. The reinforcements are generally assumed to be much stiffer than the enclosing matrix, which creates the path for us to neglect the contribution of the matrix in the analysis. It is known that the matrix is highly influential in the other directions, but the analysis mainly involves the contribution of the reinforcements or actuators. The analysis is conducted using the unit cell with a single bar reinforcement from the figure shown in Figure 5.20. The mathematical framework of the derivation of the following equations is given in [49].

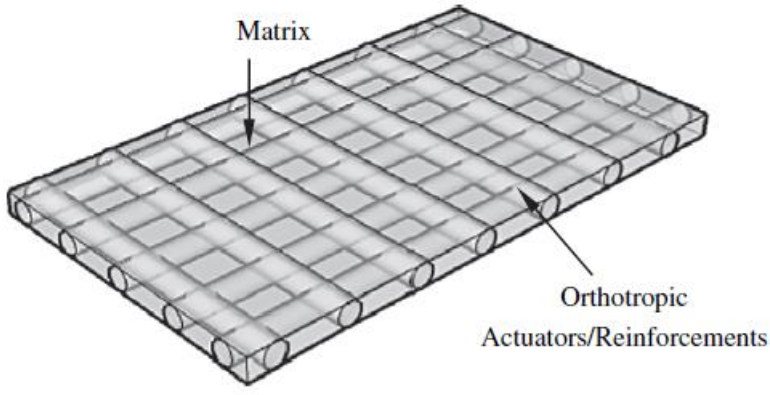


**Figure 5.19 Grid reinforced composite with orthotropic reinforcements [5]**

The effective piezoelectric coefficients are

$$\langle d_{ij}^k \rangle = \frac{1}{|\Omega|}\int_{|\Omega|} d_{ij}^k\, dv = \frac{V}{h_1 h_2} d_{ij}^k$$

$$\langle zd_{ij}^{k}\rangle = \frac{1}{|\Omega|}\int_{|\Omega|} zd_{ij}^{k}\, dv = 0$$

$$\langle d_{ij}^{*k}\rangle = 0$$

$$\langle zd_{ij}^{*k}\rangle = \frac{V}{16h_1h_2} D_{ij}^{\lambda\mu}$$

where,

$$D_{11}^{k} = \frac{\Sigma_5\Sigma_6 - \Sigma_2\Sigma_3}{\Sigma_1\Sigma_2 - \Sigma_4\Sigma_5}, D_{22}^{k} = \frac{\Sigma_3\Sigma_4 - \Sigma_1\Sigma_6}{\Sigma_1\Sigma_2 - \Sigma_4\Sigma_5}, and\ D_{12}^{k} = \frac{A_2 tan\varphi}{A_1} D_{11}^{k} + \frac{A_1}{2A_2 tan\varphi} D_{22}^{k}$$

$$d_{11}^{k} = \frac{P_{12k}[\Lambda_4\Lambda_7 + \Lambda_8\Lambda_3] + P_{11k}[\Lambda_5\Lambda_7 - \Lambda_9\Lambda_3] + P_{22k}[\Lambda_6\Lambda_7] + P_{33k}\Lambda_3}{\Lambda_7\left[\frac{A_2 tan\varphi}{A_1}\Lambda_4 + \Lambda_5 + \frac{A_2^2 tan^2\varphi}{A_1^2}\Lambda_6\right] + \frac{A_2 tan\varphi}{A_1}[\Lambda_8\Lambda_3] - \Lambda_9\Lambda_3}$$

$$d_{22}^{k} = \frac{P_{12k}[\Lambda_4\Lambda_7 + \Lambda_8\Lambda_3] + P_{11k}[\Lambda_5\Lambda_7 - \Lambda_9\Lambda_3] + P_{22k}[\Lambda_6\Lambda_7] + P_{33k}\Lambda_3}{\Lambda_7\left[\frac{A_1}{A_2 tan\varphi}\Lambda_4 + \frac{A_1^2}{A_2^2 tan^2\varphi}\Lambda_5 + \Lambda_6\right] + \frac{A_1}{A_2 tan\varphi}[\Lambda_8\Lambda_3] - \frac{A_1^2}{A_2^2 tan^2\varphi}\Lambda_9\Lambda_3}$$

$$d_{12}^{k} = \frac{P_{12k}[\Lambda_4\Lambda_7 + \Lambda_8\Lambda_3] + P_{11k}[\Lambda_5\Lambda_7 - \Lambda_9\Lambda_3] + P_{22k}[\Lambda_6\Lambda_7] + P_{33k}\Lambda_3}{\Lambda_7\left[\Lambda_4 + \frac{A_1}{A_2 tan\varphi}\Lambda_5 + \frac{A_2 tan\varphi}{A_1}\Lambda_6\right] + [\Lambda_8\Lambda_3] - \frac{A_1}{A_2 tan\varphi}\Lambda_9\Lambda_3}$$

The remaining terms $d_{13}^{k} = d_{23}^{k} = d_{33}^{k} = 0$

The effective thermal expansion coefficients are

$$\langle\theta_{ij}\rangle = \frac{1}{|\Omega|}\int_{|\Omega|}\theta_{ij}\, dv = \frac{V}{h_1h_2}\theta_{ij}$$

$$\langle z\theta_{ij}\rangle = \langle\theta_{ij}^{*}\rangle = 0$$

$$\langle z\theta_{ij}^{*}\rangle = \frac{V}{16h_1h_2} T_{ij}$$

where,

$$T_{11} = \frac{\Sigma_5\Sigma_6 - \Sigma_2\Sigma_3}{\Sigma_1\Sigma_2 - \Sigma_4\Sigma_5}, T_{22} = \frac{\Sigma_3\Sigma_4 - \Sigma_1\Sigma_6}{\Sigma_1\Sigma_2 - \Sigma_4\Sigma_5}, and\ T_{12} = \frac{A_2 tan\varphi}{A_1} T_{11} + \frac{A_1}{2A_2 tan\varphi} T_{22}$$

$$\theta_{11} = \frac{K_{12}[\Lambda_4\Lambda_7 + \Lambda_8\Lambda_3] + K_{11}[\Lambda_5\Lambda_7 - \Lambda_9\Lambda_3] + K_{22}[\Lambda_6\Lambda_7] + K_{33}\Lambda_3}{\Lambda_7\left[\frac{A_2 tan\varphi}{A_1}\Lambda_4 + \Lambda_5 + \frac{A_2^2 tan^2\varphi}{A_1^2}\Lambda_6\right] + \frac{A_2 tan\varphi}{A_1}[\Lambda_8\Lambda_3] - \Lambda_9\Lambda_3}$$

$$\theta_{22} = \frac{K_{12}[\Lambda_4\Lambda_7 + \Lambda_8\Lambda_3] + K_{11}[\Lambda_5\Lambda_7 - \Lambda_9\Lambda_3] + K_{22}[\Lambda_6\Lambda_7] + K_{33}\Lambda_3}{\Lambda_7\left[\frac{A_1}{A_2 tan\varphi}\Lambda_4 + \frac{A_1^2}{A_2^2 tan^2\varphi}\Lambda_5 + \Lambda_6\right] + \frac{A_1}{A_2 tan\varphi}[\Lambda_8\Lambda_3] - \frac{A_1^2}{A_2^2 tan^2\varphi}\Lambda_9\Lambda_3}$$

$$\theta_{12} = \frac{K_{12}[\Lambda_4\Lambda_7 + \Lambda_8\Lambda_3] + K_{11}[\Lambda_5\Lambda_7 - \Lambda_9\Lambda_3] + K_{22}[\Lambda_6\Lambda_7] + K_{33}\Lambda_3}{\Lambda_7\left[\Lambda_4 + \frac{A_1}{A_2 tan\varphi}\Lambda_5 + \frac{A_2 tan\varphi}{A_1}\Lambda_6\right] + [\Lambda_8\Lambda_3] - \frac{A_1}{A_2 tan\varphi}\Lambda_9\Lambda_3}$$

$h_1, h_2$ are all dimensional parameters of the composite plate and can be modified according to the properties required. V is the volume of the unit cell and the values for $A_1$ $and$ $A_2$ is taken as 1. The terms $P_{ijk}$ and $K_{ij}$ where i, j, k=1,2 are the piezoelectric and thermal constants for the material being used.

# CHAPTER 6 PARAMETRIC ANALYSIS

The parametric analysis of various composite structures with different types of reinforcing elements is conducted in this chapter. The parametric analysis is considered by considering some materials suitable for the application and assuming realistic dimensions to the composite plate or shell. The aim is to calculate the effective properties of coefficients for a wide range of composites and provide valuable real-life usage data. These coefficients are calculated by use of the equations discussed in the previous section. The thickness or any other required dimension of the composite structure is varied for the same material properties, and the effective coefficients are calculated for each of the varying dimensions. This provides huge amounts of data and statistics to encourage the use of composites in more layman applications instead of them already being used in high-tech applications. The results are represented graphically and discussed in terms of the dimensional changes and material property variation. Optimization of the results is also carried out by tweaking the input parameters to obtain the best possible combination of properties from these composite structures.

## 6.1 SANDWICH COMPOSITE SANDWICH SHELLS MADE OF GENERALLY ORTHOTROPIC MATERIALS

In this section, we are conducting the parametric analysis of two types of composite shells, namely a hexagonal star core and a hexagonal triangular core. The formulation for the analysis is discussed in Section 5.1. For the sake of analysis, we vary the thickness H from 8 to 20 and keep t = a = 2.5 throughout the analysis.

The material considered for the construction of the shell is unidirectional AS/3501 graphite/epoxy laminate. The material properties of this material are $E_1 = 140\ Gpa, E_2 = 10\ Gpa, \upsilon_{12} = 0.3\ and\ \upsilon_{21} = 0.0196$. All of these terms can, of course,

be varied according to the many applications and materials one may wish to use. The equations described in the previous chapter can be used to tailor the effective coefficients of the smart composite structures. The following graphs in Fig 6.1 show the variation of $\delta\langle b_{11}^{11}\rangle$ and $\delta\langle b_{22}^{22}\rangle$ versus the thickness H for the hexagonal-triangular core smart sandwich shells. The extensional stiffness in the $\delta\langle b_{22}^{22}\rangle$ direction is significantly smaller than the stiffness in the $\delta\langle b_{11}^{11}\rangle$ direction. It is a highly pertinent coefficient as the $\delta\langle b_{11}^{11}\rangle$ is independent of the effect of Poisson's ratio and influenced largely by the reinforcing elements in the $\alpha_1$ coordinate.

Figure 6.2 shows the variation of $\delta\langle b_{11}^{22}\rangle, \delta\langle b_{22}^{11}\rangle$ *and* $\delta\langle b_{12}^{12}\rangle$ with H. It is noteworthy that the coefficients being obtained in all these directions are exactly similar to each other in variation and values. The coefficients are as expected and are comparable to the coefficients obtained for the $\delta\langle b_{22}^{22}\rangle$ direction.

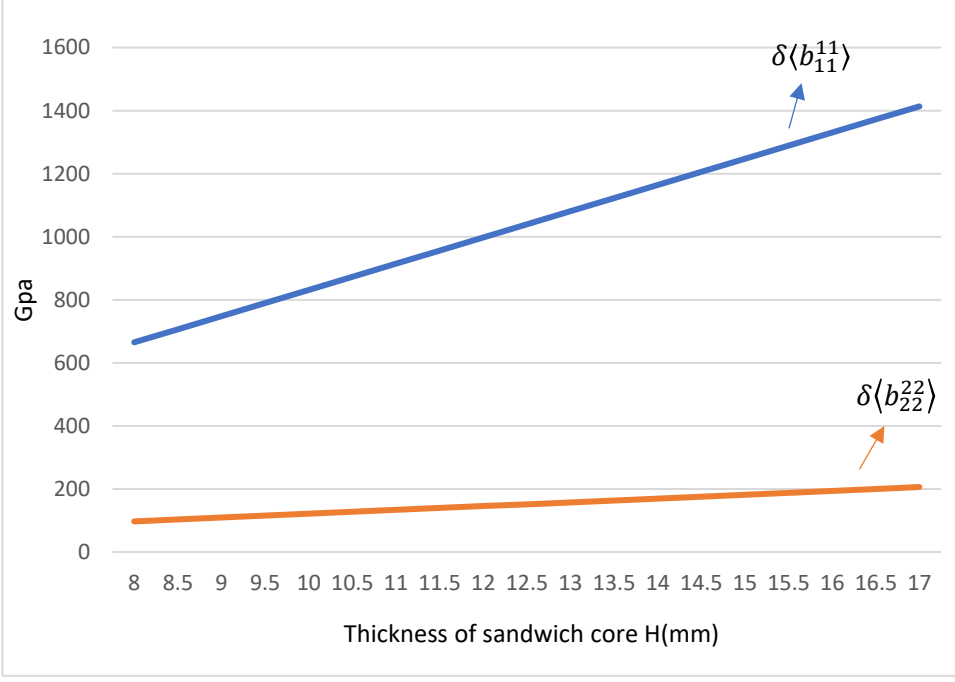


**Figure 6.1 Effective coefficients $\delta\langle b_{11}^{11}\rangle$ and $\delta\langle b_{22}^{22}\rangle$ of hexagonal-triangular sandwich core**

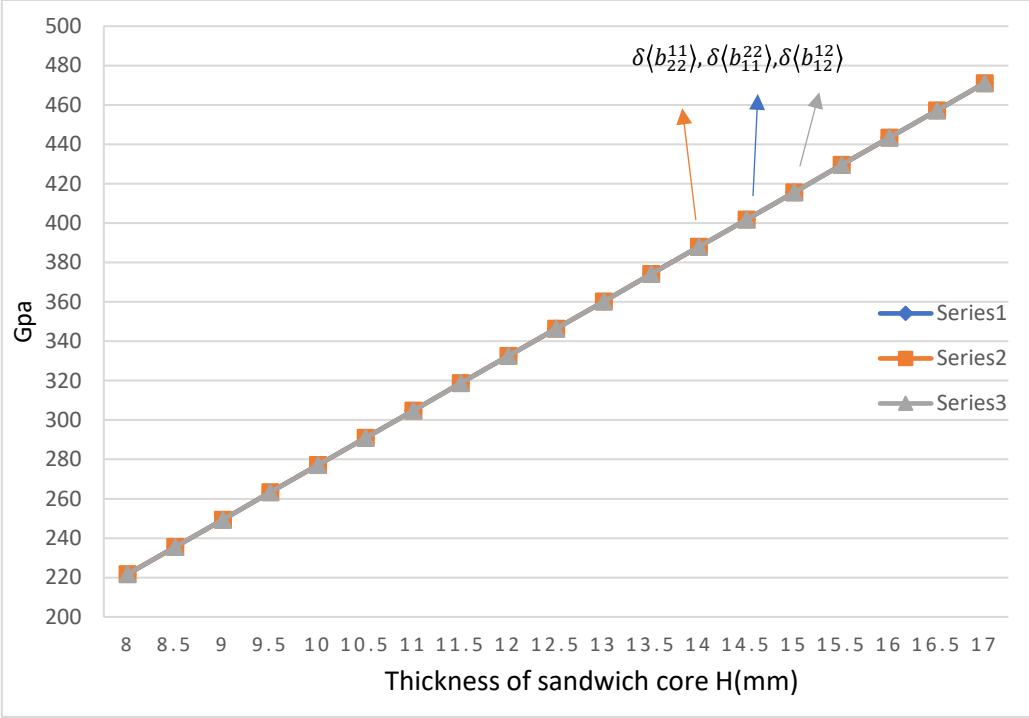


**Figure 6.2 Effective coefficients $\delta\langle b_{11}^{22}\rangle, \delta\langle b_{22}^{11}\rangle$ *and* $\delta\langle b_{12}^{12}\rangle$ of hexagonal-triangular sandwich core**

The following graph in Fig 6.3 show the variation of $\delta\langle b_{11}^{11}\rangle$ and $\delta\langle b_{22}^{22}\rangle$ versus the thickness H for the hexagonal-star core smart sandwich shells. The extensional stiffness in the $\delta\langle b_{22}^{22}\rangle$ direction is slightly smaller than the stiffness in the $\delta\langle b_{11}^{11}\rangle$ direction. The stiffness in the $\delta\langle b_{22}^{22}\rangle$ for the hexagonal-star core is similar to the hexagonal-triangular core but the stiffness in the $\delta\langle b_{11}^{11}\rangle$ direction has reduced a large deal from the hexagonal-triangular core. This suggests that if there is loading predominantly in the $\delta\langle b_{11}^{11}\rangle$ direction, it is better to use the hexagonal-triangular core as it offers better properties in that direction.

Figure 6.4 shows the variation of $\delta\langle b_{11}^{22}\rangle, \delta\langle b_{22}^{11}\rangle$ *and* $\delta\langle b_{12}^{12}\rangle$ with H of the hexagonal-star core sandwich cell. The coefficients in this structure are as expected. Also, as previously noted in the hexagonal-triangular structure, these properties vary linearly with the thickness of the shell, and the properties in all three directions are the

same. In comparison with the hexagonal-triangular core structure, it is still inferior in these three directions and also in the overall extensional stiffness properties.


**Figure 6.3 Effective coefficients $\delta\langle b_{11}^{11}\rangle$ *and* $\delta\langle b_{22}^{22}\rangle$ of hexagonal-star sandwich core**

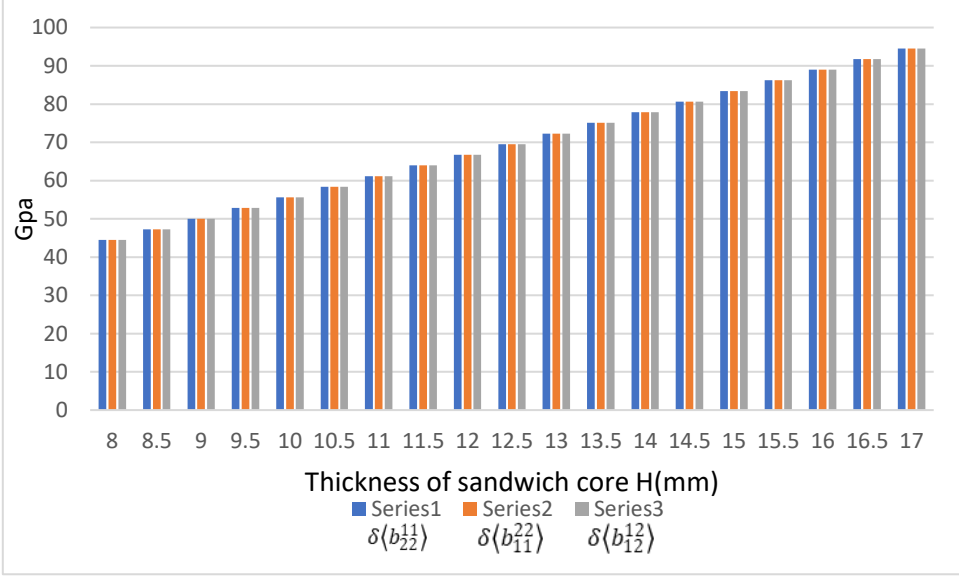


**Figure 6.4 Effective coefficients $\delta\langle b_{11}^{22}\rangle$, $\delta\langle b_{22}^{11}\rangle$ *and* $\delta\langle b_{12}^{12}\rangle$ of hexagonal-star sandwich core**

The terms similar to $\delta\langle zb_{11}^{*11}\rangle$ represent the torsional stiffness coefficients or the coupling stiffness coefficients of the composite structure. Figure 6.5 represents the coefficients $\delta\langle zb_{11}^{*11}\rangle, \delta\langle zb_{22}^{*22}\rangle$. The properties in the $\delta\langle zb_{11}^{*11}\rangle$ direction for the

hexagonal-triangular core offers the most superior stiffness value of all the other coefficients in this section. The $\delta\langle zb_{11}^{*11}\rangle$ direction offers higher stiffness values than the $\delta\langle zb_{22}^{*22}\rangle$ direction. The coefficients are as expected as the structural elements in the triangular-hexagonal shell are suited to offer a higher overall stiffness.

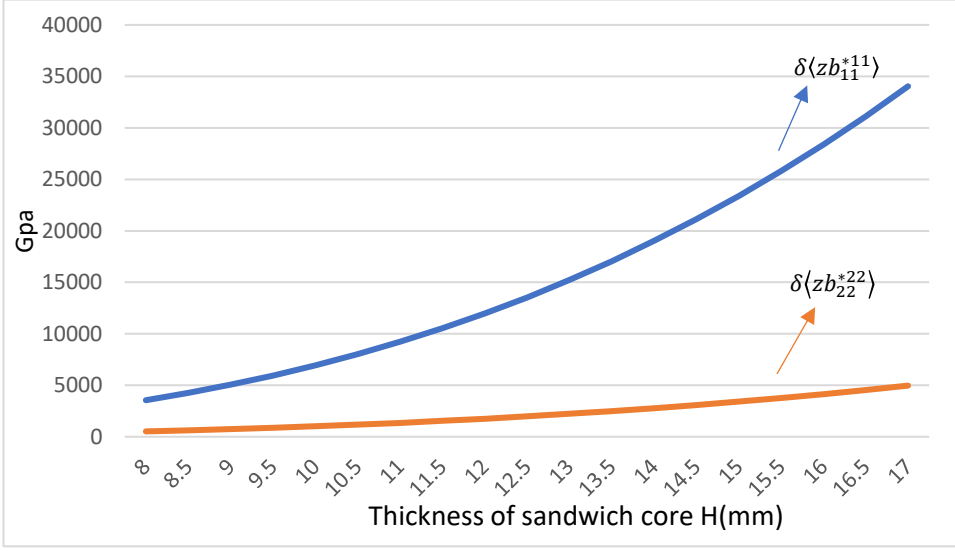


**Figure 6.5 Effective coefficients $\delta\langle zb_{11}^{*11}\rangle$ *and* $\delta\langle zb_{22}^{*22}\rangle$ of hexagonal-triangular sandwich core**

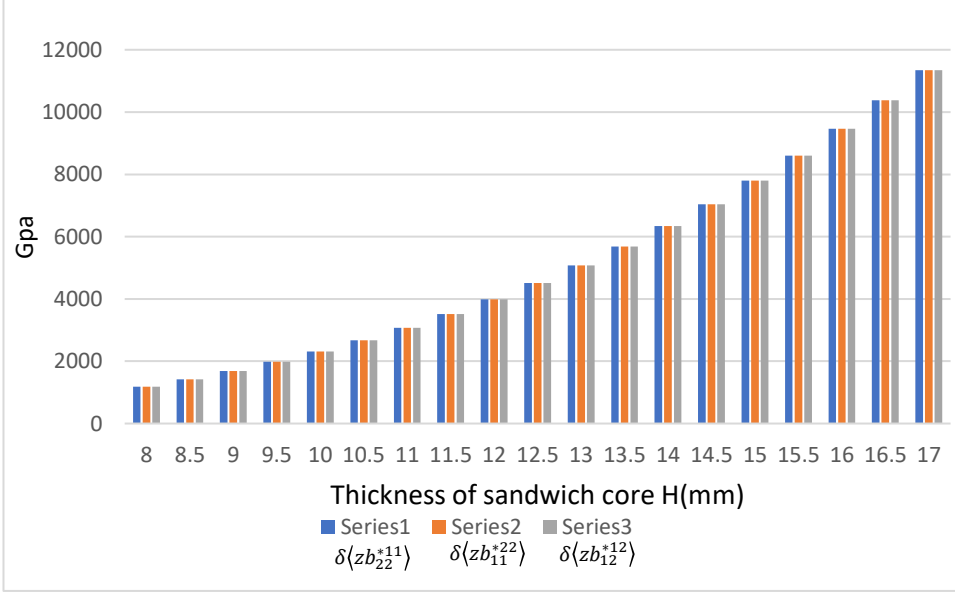


**Figure 6.6 Effective coefficients $\delta\langle zb_{22}^{*11}\rangle$, $\delta\langle zb_{12}^{*12}\rangle$ *and* $\delta\langle zb_{11}^{*22}\rangle$ of hexagonal-triangular sandwich core**

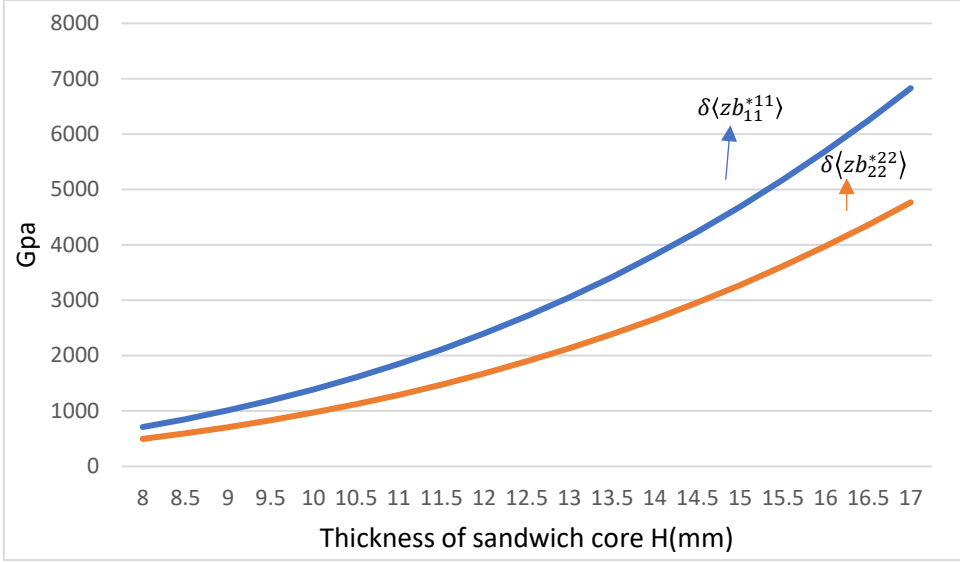


**Figure 6.7 Effective coefficients $\delta\langle zb_{11}^{*11}\rangle$ *and* $\delta\langle zb_{22}^{*22}\rangle$ of hexagonal-star sandwich core**

Figure 6.6, 6.7 and 6.8 represents the torsional stiffness values of the triangular-hexagonal and star-hexagonal, respectively. The torsional stiffness values in $\delta\langle zb_{22}^{*11}\rangle$, $\delta\langle zb_{12}^{*12}\rangle$, *and* $\delta\langle zb_{11}^{*22}\rangle$ are larger and gives a linear variation like any other coefficient in the hexagonal-triangular core.

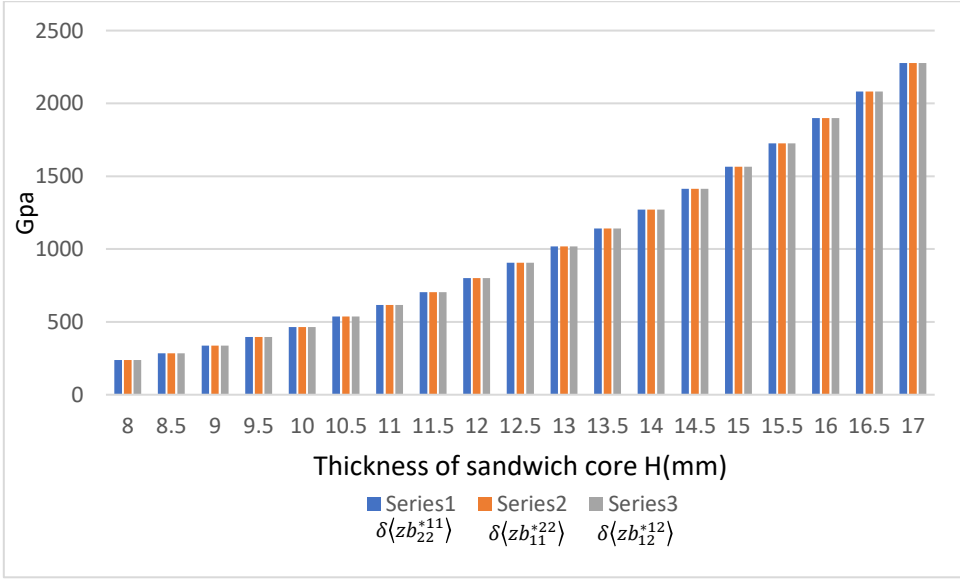


**Figure 6.8 Effective coefficients $\delta\langle zb_{22}^{*11}\rangle$, $\delta\langle zb_{12}^{*12}\rangle$ *and* $\delta\langle zb_{11}^{*22}\rangle$ of hexagonal-star sandwich core**

Variations with thickness H is similar in both structures, but the stiffness is less in the star-cored shell. We could conclude that the hexagonal-triangular cored shell is able to offer far better superior stiffness properties in all directions. The dominance in offering this property is expected as the structural elements in the triangular core are very much suited to offer a good stiffness in all directions. Considering all other factors like the cost of manufacture, material accumulation, and ease of design, it is suggested that the use of the hexagonal-triangular core is better suited if both structures do not offer much difference in the factors mentioned.

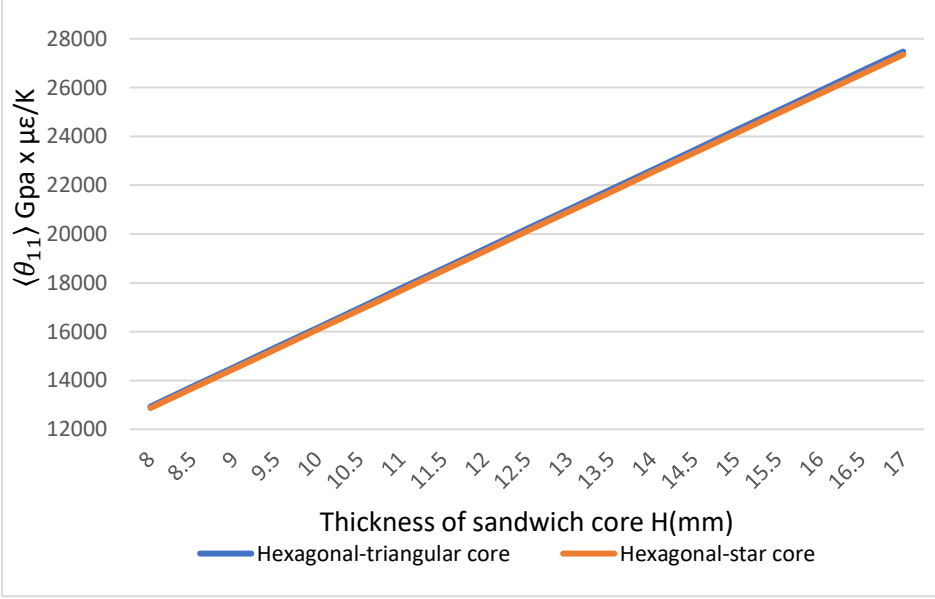


**Figure 6.9 Effective thermoelastic coefficient $\langle\theta_{11}\rangle$ of sandwich unit cell**

Now, we move forward with the thermoelastic properties of these shells. These coefficients are represented by $\theta$ with respective numbers depicting the directions. Figure 6.9 represents the variation of $\langle\theta_{11}\rangle$ with the thickness for both the hexagonal star and hexagonal-triangular core. It offers relatively high thermoelastic properties in this direction, and it must also be noted that both offer similar properties even with the variation of H. Figure 6.10 represent $\langle z\theta_{11}^{*}\rangle$ with respect to the thickness and as

expected, the shells with both the differing cores offer nearly similar properties that do not separate them much in terms of superiority. But the $\langle z\theta_{11}^{*} \rangle$ direction offers much higher values than the coefficients in $\langle \theta_{11} \rangle$ direction.

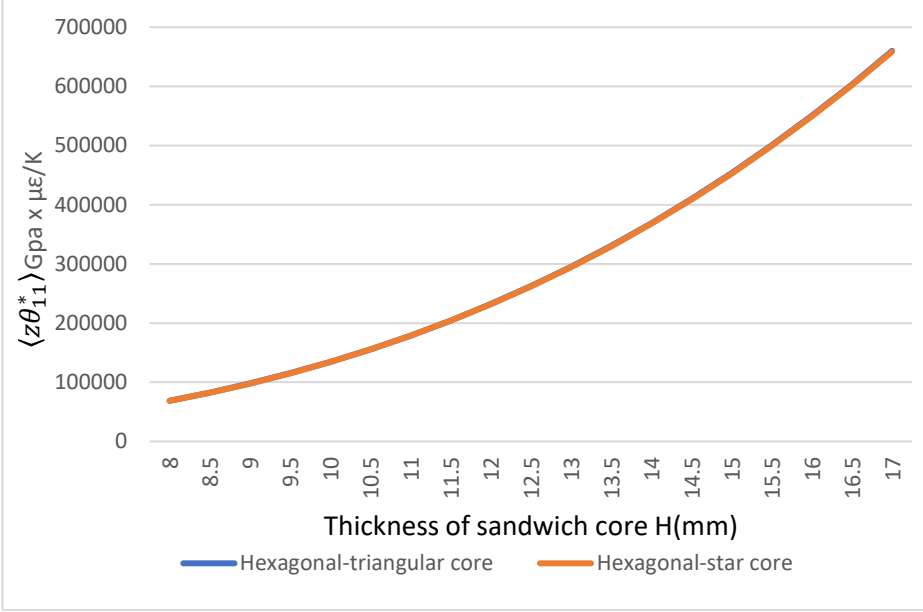


**Figure 6.10 Effective thermoelastic coefficient $\langle z\theta_{11}^{*} \rangle$ of sandwich shell**

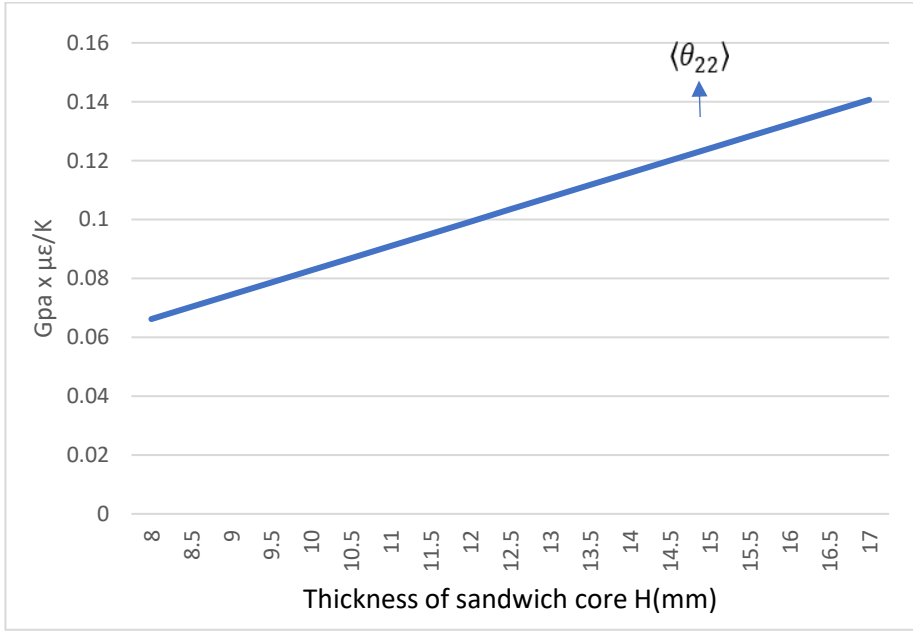


**Figure 6.11 Effective thermoelastic coefficient $\langle \theta_{22} \rangle$ of hexagonal-triangular sandwich shell**

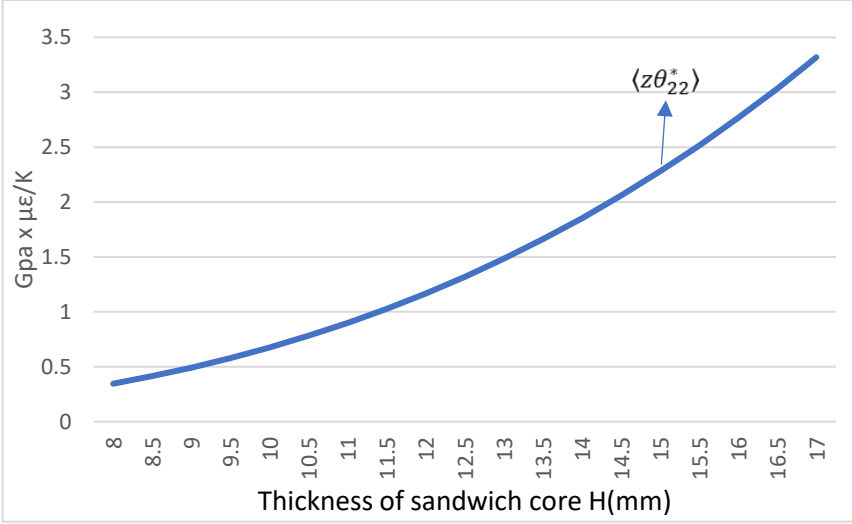


**Figure 6.12 Effective thermoelastic coefficient$\langle z\theta_{22}^{*}\rangle$ of hexagonal-triangular sandwich shell**

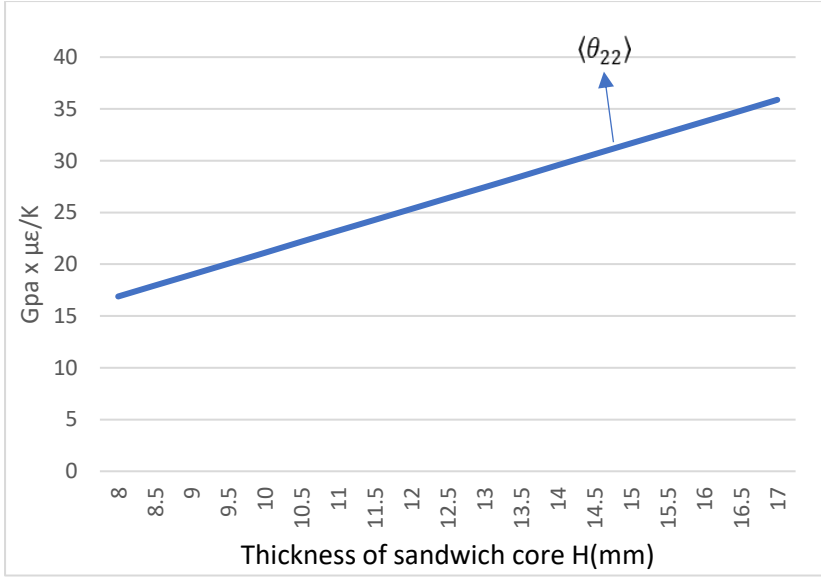


**Figure 6.13 Effective thermoelastic coefficient $\langle\theta_{22}\rangle$ of hexagonal-star sandwich shell**

Figure 6.11-6.14 is a depiction of the properties in the $\langle\theta_{22}\rangle$ *and* $\langle z\theta_{22}^{*}\rangle$ direction for the hexagonal-triangular and hexagonal-star core, respectively. Here the properties are highly differing for both these cores as opposed to the similar properties obtained in the previous figures. The thermoelastic properties in both the $\langle\theta_{22}\rangle$ *and* $\langle z\theta_{22}^{*}\rangle$ direction is very weak for the hexagonal-triangular sandwich shell. At

the same time, the latter star cored shell is able to offer significantly high properties with both varying linearly in an increasing manner along with the thickness of the composite shell. In the thermoelastic consideration of coefficients, the star-core has turned out to be far more superior in $\langle \theta_{22} \rangle \, and \, \langle z\theta_{22}^{*} \rangle$ directions than the hexagonal-triangular cored shell.

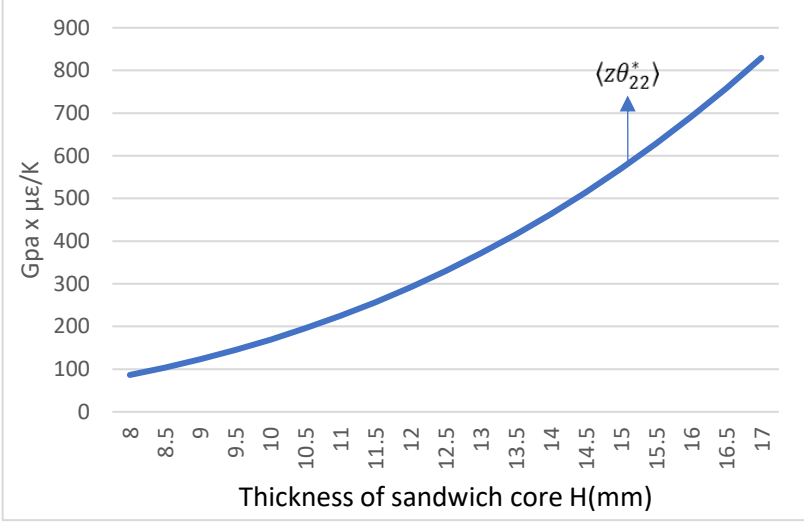


**Figure 6.14 Effective thermoelastic coefficient $\langle z\theta_{22}^{*} \rangle$ of hexagonal-star sandwich shell**

Sandwich composites generally have a very lightweight core. The cores we have seen are hexagonal-triangular and hexagonal-star shaped, which is one of many designs used currently. These structures are often used in the aerospace industry and mostly for layered thin-framed panels. The design is drawn in such a way that the encoring materials are able to take the loads, bending stresses, and shear stresses while the core is focused on withstanding the flexural stresses. It can be used in the roofs of a train, as reported in [61]. The thermoelastic properties we displayed in the previous graphs align with the requirements and are typical values for a sandwich composite plate used in general applications. In composite materials used in various industries, the coefficient of thermal expansion typically for an aerospace-grade graphite material is from -1E-6 to

1E-6 in-in/F [73]. This was used for applications like drive shafts for high-performance vehicles, structural members in aircraft, etc. For the units used in this analysis for the material properties, the coefficients obtained are tandem with the above values. When compared with the analysis performed in [61], these thermoelastic properties can withstand the stresses in the aforementioned application.

Other applications also include protective shields for vehicles and spacecraft, soundproofing of auditoriums, etc. The general industry requirement is that the materials used must handle the impacts and loads and offer thermal stability. So, proper use of materials is warranted, and therefore, phenolic resins can be used to replace the epoxy resin in this analysis. Phenolic resins offer excellent fire resistance are almost incapable of burning. In view of the applications we saw, it gives fire resistance in the roofs and soundproofing of auditoriums which will provide excellent safety features for the people. While it is true that the phenolic resin is not able to offer superior properties to the epoxy resin, it will still be able to satisfy the application. We also see that the elastic coefficients in the transverse direction are also not that favorable. Naturally, sandwich structures have the problem of debonding due to the heterogeneous nature of the core and its encompassing material. The properties obtained also confirm this phenomenon. So, external recuperation of these plates and shells is also suggested.

For example, when used for an application that requires more transverse strength, the star-cored shell can be preferred over the hexagonal shell. It is able to offer more stability as a result of more reinforcing elements being used in the core. There are also new design ideas where the traditional honeycomb, hexagonal and star-cored shells are modified and reinforced with smaller elements that can offer more superior elastic coefficients than the traditional ones.

## 6.2 GRID REINFORCED GENERALLY ORTHOTROPIC GRID-REINFORCED SHELL

In this section, an orthotropic composite shell, as discussed in the previous section 6.1, is taken into consideration. The reinforcing elements are made of orthotropic homogenous material, which is, in practicality, much stiffer than the matrix being used. So, there is not much of a contribution from the matrix to this structure. The properties assumed for this analysis are that of carbon and composite single-walled nanotubes. It has a much higher Young's Modulus value than other tubes and will give us good effective properties. The graphs show the variation of the elastic coefficients of the composite along with the variation of the volume fraction of the structure. The volume fraction is described as $R = V/h_1h_2$ which is the ratio of volume of the structure to its geometrical dimensions.

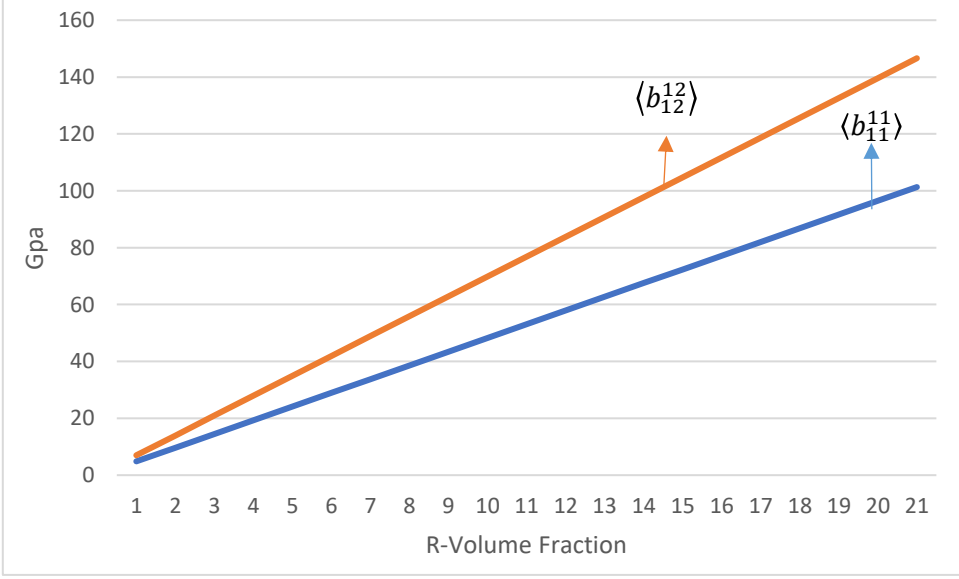


**Figure 6.15 Effective coefficients $\delta\langle b_{11}^{11} \rangle$ *and* $\delta\langle b_{12}^{12} \rangle$ of grid-reinforced shell**

The elastic coefficients $\delta\langle b_{11}^{11} \rangle$ *and* $\delta\langle b_{22}^{22} \rangle$ are illustrated by the graph in Figure 6.15. We are getting a decent set of values in these two directions. Even though not very much suited for high-tech applications, these properties have high applicability in mid-

stiffness usage. It is noted that we are not able to obtain very good properties as the other structures being analyzed in this chapter, it is justified that we get these set of properties because of the alignment of the reinforcement and design of the shell. It is also interesting that the set of properties we used for this analysis is able to give superiority of properties in the $\delta\langle b_{12}^{12}\rangle$ direction than the $\delta\langle b_{11}^{11}\rangle$ direction. This becomes an important factor because most of the other structures in a predictable nature offer advantageous properties in the $\delta\langle b_{11}^{11}\rangle$ direction. The properties vary linearly through the difference in volume fraction, meaning the higher the thickness, the higher the coefficient. Since most applications demand shells and plates with advanced properties in the thinnest forms, it might not be suited to use much thickness. Thus, it is required to optimize the properties and dimensions in the best manner possible.

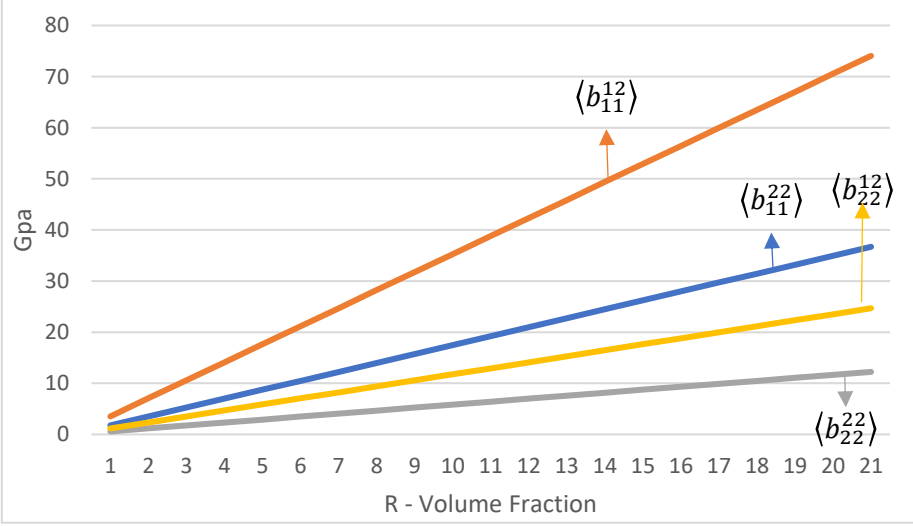


**Figure 6.16 Effective elastic coefficients $\delta\langle b_{11}^{12}\rangle$, $\delta\langle b_{11}^{22}\rangle$ , $\delta\langle b_{22}^{12}\rangle$ *and* $\delta\langle b_{22}^{22}\rangle$ of grid-reinforced shell**

Figure 6.16 represents the remaining coefficients that complete the extensional stiffness matrix. Here, the properties in the $\delta\langle b_{11}^{12}\rangle$ direction is good and can offer comparable properties to the $\delta\langle b_{11}^{11}\rangle$ direction, which is very efficient. It is advisable to check the loading in the $\delta\langle b_{22}^{22}\rangle$ direction as the coefficients there are the lowest among

all directions. So, the load dissipation in the direction must be handled well for optimal usage of this structure.

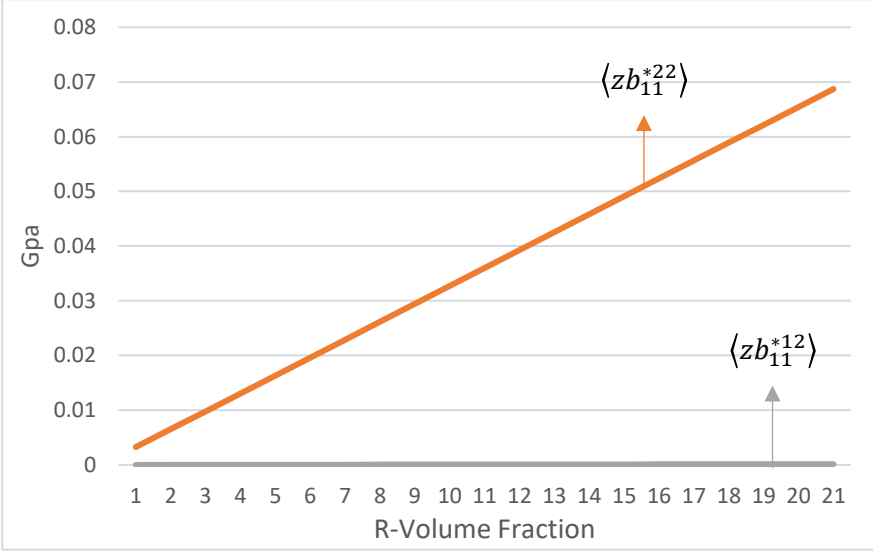


**Figure 6.17 Effective coefficients $\delta\langle zb_{11}^{*11} \rangle$ *and* $\langle zb_{11}^{*12} \rangle$ of grid-reinforced shell**

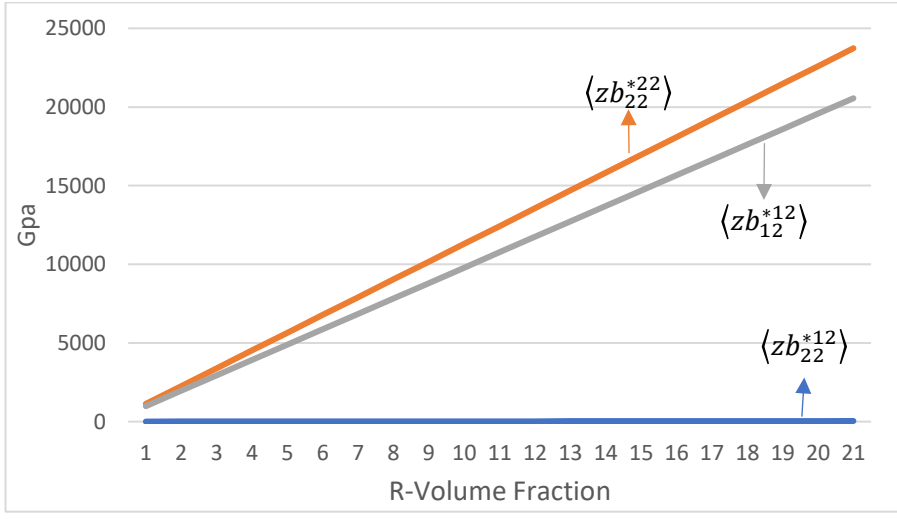


**Figure 6.18 Effective coefficients $\delta\langle zb_{22}^{*22} \rangle, \langle zb_{12}^{*12} \rangle$ *and* $\delta\langle zb_{22}^{*12} \rangle$ of grid-reinforced shell**

Figures 6.17 and 6.18 represent the torsional stiffness coefficients of the grid reinforced shell. The coefficients in the $\delta\langle zb_{11}^{*11} \rangle$ direction is on the negative side. We can obtain the best properties in the $\delta\langle zb_{22}^{*22} \rangle$ and $\delta\langle zb_{12}^{*12} \rangle$ direction. These are higher than any other properties in this analysis, but concentrating the torque solely in these

directions will be a challenge in any situation. These properties are also not well balanced in all directions because the coefficients in $\delta\langle zb_{22}^{*12}\rangle, \delta\langle zb_{11}^{*22}\rangle \; and \; \langle zb_{11}^{*12}\rangle$ direction, as we can see, is very low as compared to the other directions.

Grid reinforced composites are finding their functions mostly in the civil engineering industry. It did not require much research and was also a straightforward way of reinforcing materials to increase their strength or load-bearing capabilities and other mechanical properties. Grid reinforced shells are being used extensively in buildings (pillars, beams, ceilings, etc.) and more structural elements like pavements, insulation panels, etc. In the analysis, carbon nanotubes were used as the reinforcement, and the properties were calculated accordingly. There are several other materials readily available for use in these structures. Steel fiber reinforced pavement with CFRP reinforcements can replace the traditional way of laying the pavement using concrete. This creates better resistance to wear and gives longer life. The concrete also tends to wear off in corners, and the structural integrity is lost due to effects from various external factors. These structures can give excellent mechanical properties such as high bending stiffness, fatigue resistance, corrosion resistance, etc. [68]. These are some of the properties where a standard steel-reinforced concrete structure is not able to provide. The grids are an extensive part of the construction of beams. A geo-grid structured concrete beam was developed in [69] to provide better mechanical characteristics than conventional beams. The geo-grid was designed in tubular form with polyester material in similarity to the carbon nanotubes used in the analysis. This material is able to improve the strain characteristics of the composite. The failure of the beams is extended to a higher load when the stiffness and strength are comparable to the conventional beams. Another application is the replacing of conventional insulation panels by use of

grid reinforced panels. A grid reinforcement typically made of glass fiber material is arranged on the surface of the insulation. This reinforcement is provided on the outer surface of the thermal insulation panel but given a protective coating (e.g., plaster, mortar) and thus increases the panel's durability and acts as a protective layer for the grid being used. It improves the corrosion resistance and reduces moisture absorption of the grid, and ensures longer life.

Fiberglass also is dominantly being used in boat building, medical and recreation equipment manufacturing. Stiffness coefficients for a fiberglass and polyester material used in boat structures are around 8 Gpa. In almost all directions, the grid reinforced composite we analyzed can give coefficients matching that or larger to that. Resins available for fire insulation purposes can be used to provide those properties, and the properties obtained were in agreement with ASTM and UL standards [73]. Design considerations can be made up to n number of layers according to the application and mechanical properties required. Sandwich structures might be preferred design-wise to obtain a lighter weight and high stiffness plate if required. Overall, these insulation panels' has improved properties, such as superior tensile strength and bending strength. It also has high fracture toughness and is not brittle. So, we can conclude that this grid reinforced composite shell with carbon nanotube material is suited for highly specific applications. It can offer similar mechanical properties as discussed above.

## 6.3 SMART HONEYCOMB SANDWICH STRUCTURES

In this section, the analysis of a smart honeycomb cored sandwich shell is carried out. We calculate the properties of the honeycomb core and the top and bottom faces individually and make a representation by means of graphs. As in the other sections, the variation of these properties along the thickness H of the composite is

captured. The materials used in this analysis will be Graphite epoxy which is stiffer in nature and has the following properties: $E_1$=180 Gpa, $E_2$=20 Gpa $\upsilon_{12} = 0.28$ and $\upsilon_{12} = 0.03$ [50]. For the face carriers and we will be using an E-glass epoxy material with properties $E_1$ = 38.26 Gpa, $E_2$ = 8.27 Gpa, $\upsilon_{12} = 0.26$ and $\upsilon_{12} = 0.055$ [50] for the core, which is naturally meant to be softer in nature. We keep t = 2.5mm and a = 1.5mm throughout the analysis and vary H from 10 to 20 mm. The following figures are unique to the properties illustrated by the core material used in this structure. The predictability criteria are in sync with the results obtained because we are able to attain enhanced properties in the $\delta\langle b_{11}^{11}\rangle$ direction. Similarly, it is also noted that the properties exhibited in the $\delta\langle b_{11}^{22}\rangle, \delta\langle b_{22}^{11}\rangle \; and \; \delta\langle b_{12}^{12}\rangle$ are equal in values and variation with the overall thickness. These coefficients are not lacking in stiffness from the $\delta\langle b_{11}^{11}\rangle$ direction and are able to provide good support. The properties in the perpendicular $\delta\langle b_{22}^{22}\rangle$ direction is the lowest of all in this structure but can satisfy the requirements of most applications. It must also be considered that the properties do not give a huger variation when we increase the thickness, with them being doubled at most when the thickness is doubled. These properties make up the extensional stiffness matrix of the composite sandwich structure, with the values not being mentioned here being zero.

The torsional stiffness coefficients offered by this structure are far higher than many others. The $\delta\langle z b_{11}^{*11}\rangle$ coefficient, as usual, is the highest among the other directions. It also gives a very high differential as much as ten times with the increase of thickness. This will enable us to keep the variation in thickness minimal and obtain higher properties in minimal thickness, thereby saving on material cost and give us the option to use it as thin panels in aircraft. Reducing the thickness of the core is a huge

influencing factor on the overall thickness of the composite. These properties are well supported by the other stiffness coefficients in the other directions. While all directions are superior in nature, it is noticeable that the $\delta\langle zb_{12}^{*12}\rangle$ direction is very small and disadvantageous to the overall core structure.

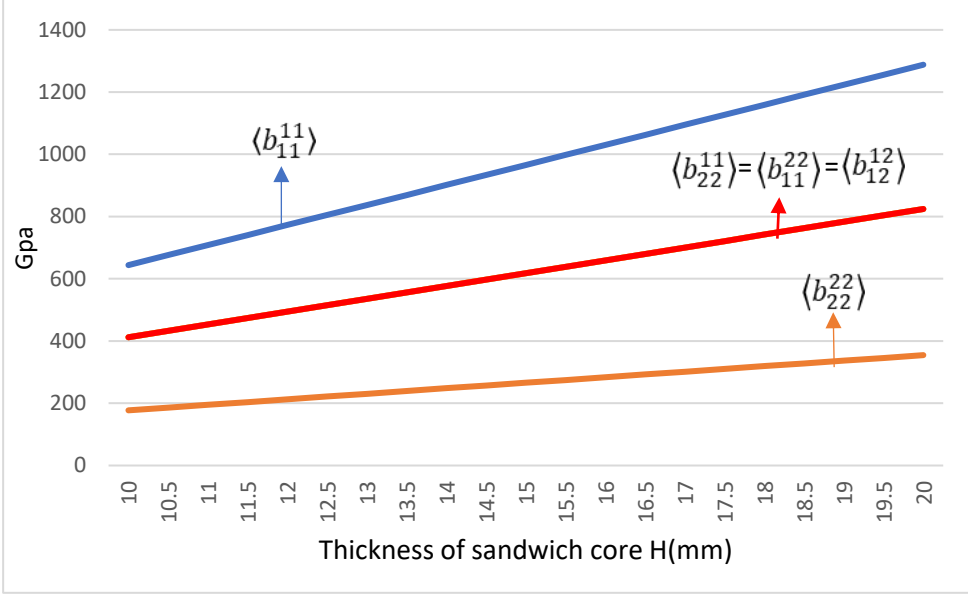


**Figure 6.19 Effective coefficients of hexagonal-honeycomb sandwich core**

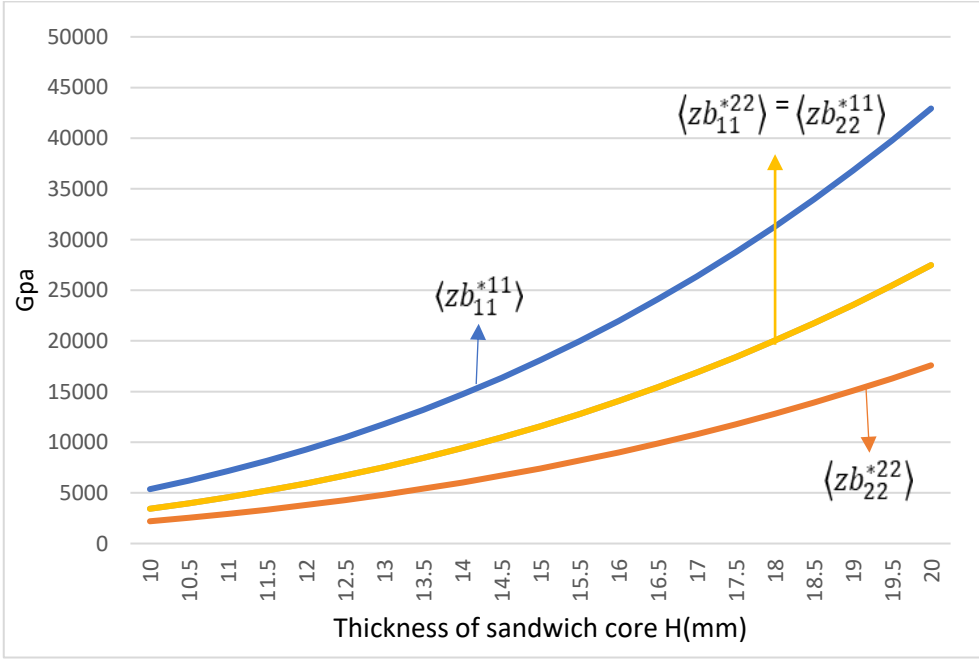


**Figure 6.20 Effective torsional coefficients of hexagonal-honeycomb sandwich core**

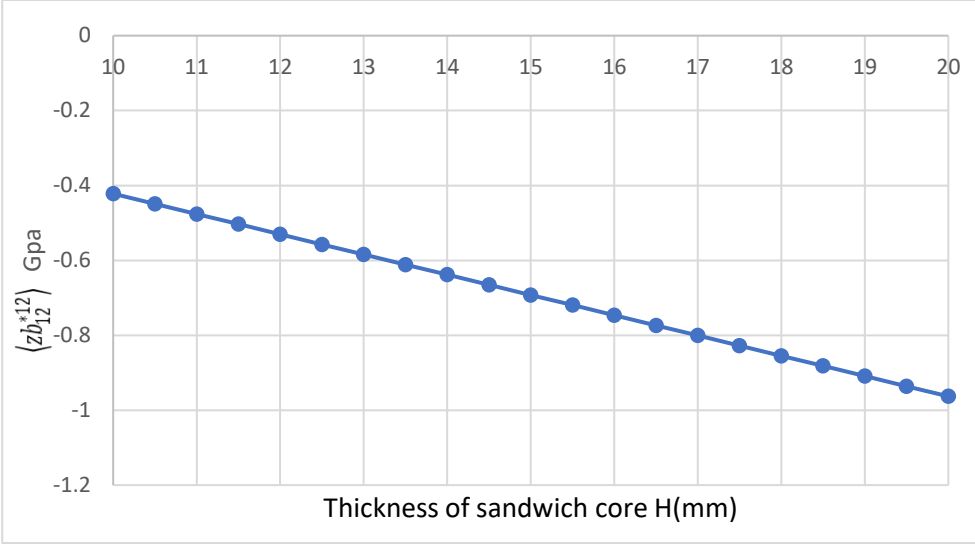


**Figure 6.21 Effective coefficient $\delta\langle zb_{12}^{*12}\rangle$of hexagonal-honeycomb sandwich core**

The following figures are the representation of properties of the sandwich panels used in the top and bottom of the core. The values are expected to be lower than that of the core as these panels do not have the structural configuration and stress dissipation capable of the core. Overall, coefficients of direction $\delta\langle b_{11}^{11}\rangle$ can shadow the other directions and are very potent in multiple applications.

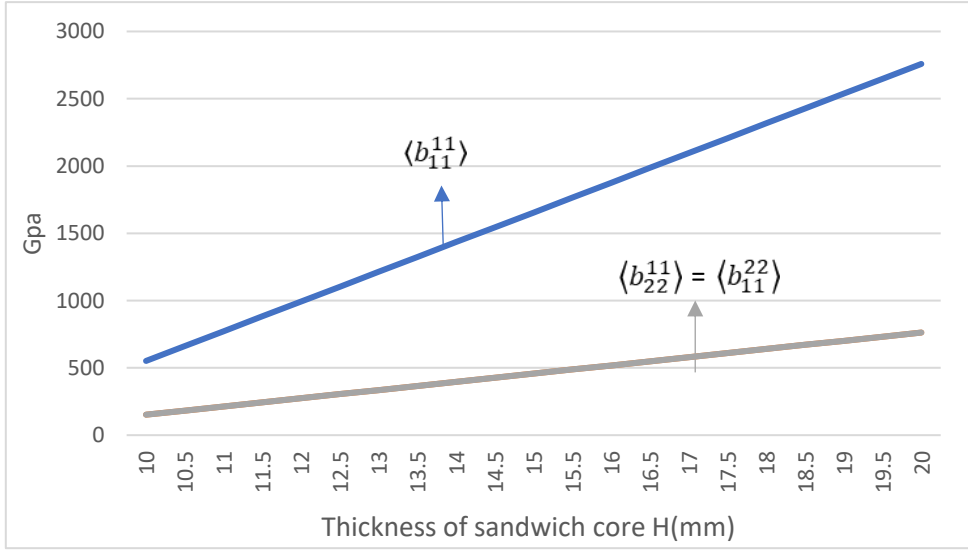


**Figure 6.22 Effective coefficients $\delta\langle b_{11}^{11}\rangle, \delta\langle b_{11}^{22}\rangle$ $and$ $\delta\langle b_{22}^{11}\rangle$ of hexagonal-honeycomb sandwich plates**

The coefficients in $\delta\langle b_{22}^{11}\rangle$ and $\delta\langle b_{11}^{22}\rangle$ direction is similar. The $\delta\langle b_{12}^{12}\rangle$ coefficient is again the lower of all directions as being exhibited through this analysis. The core and properties exhibited by the face carriers give way to this structure being capable of handling high-end applications requiring high stiffness. These features are also offered in a minimized thickness compared to other sandwich structures with different materials and orientations.

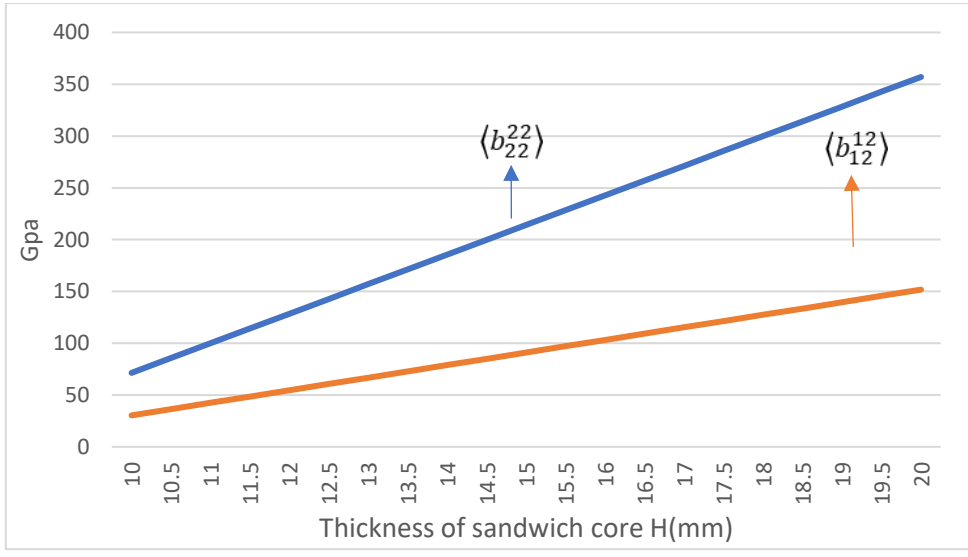


**Figure 6.23 Effective coefficients $\delta\langle b_{22}^{22}\rangle$ *and* $\delta\langle b_{12}^{12}\rangle$ of hexagonal-honeycomb sandwich plates**

The variation of the torsional coefficients is similar to the core's, but the core is still able to offer enhanced coefficients than the face carriers in the $\delta\langle zb_{11}^{*11}\rangle$ direction. These are shown in the following Figures 6.24 and 6.25. In other directions, the core is stiffer in nature, but combined properties are very good due to the structural orientation and the material used highly influencing these enhanced properties. The coefficients in the $\delta\langle zb_{11}^{*11}\rangle$ direction, as illustrated in the graph, is the largest of all the torsional properties. But again, even on the torsional side, the $\delta\langle b_{12}^{12}\rangle$ coefficient offers less versatility and has the lowest stiffness amongst the others.

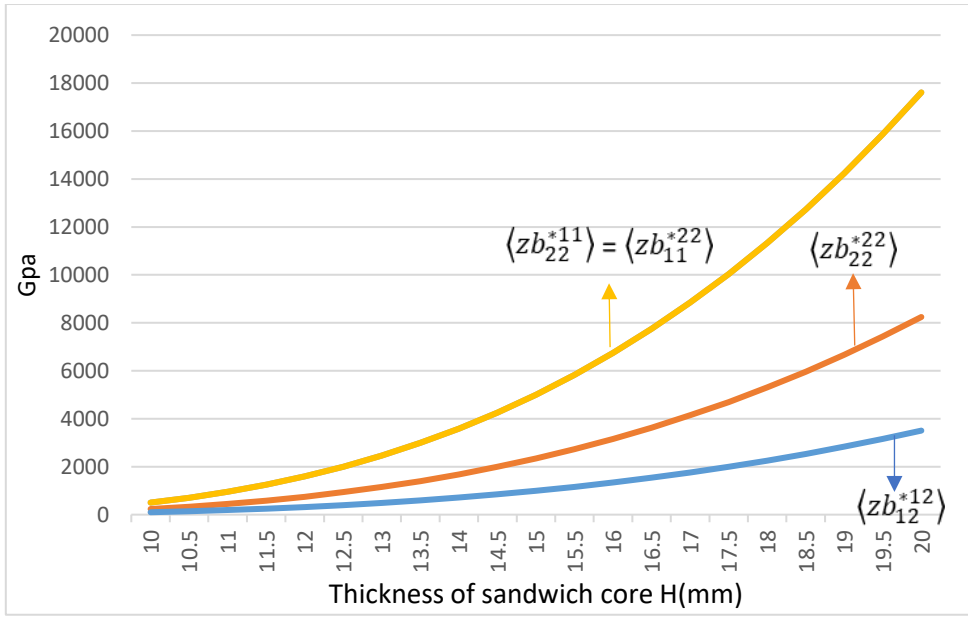


**Figure 6.24 Effective torsional coefficients of hexagonal-honeycomb sandwich plates**

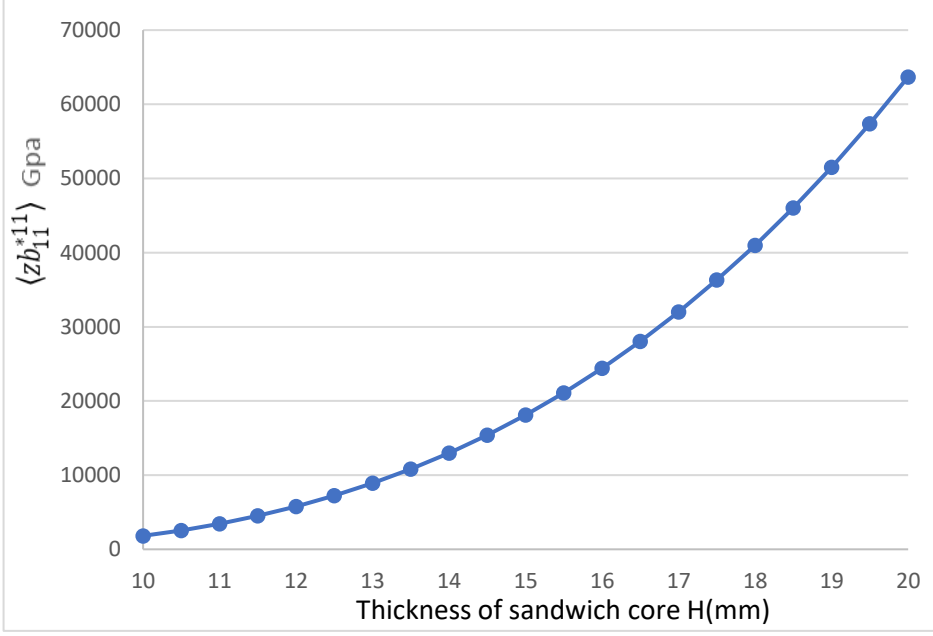


**Figure 6.25 Effective torsional coefficient $\delta\langle zb_{11}^{*11}\rangle$of hexagonal-honeycomb sandwich plates**

The kinds of plates having a honeycomb core being discussed above is pretty similar to the plates discussed in Section 5.1. The honeycomb cores largely find their use in aerospace and automobile applications, with civil engineering applications being their

next mode of usage. Some practical engineering applications include them being used as shields for protection of debris on spacecraft, protection from thermal loads of spacecraft and energy absorption devices, etc. A thermal protection system was considered in Japan for space vehicles in a planet exploration project. They used a sandwich structure with a honeycomb core with carbon composite skin, insulation with thermal protection, the resistance of heat, and structural integrity and strength [62]. It is a generally known fact that the most disadvantageous feature in the use of these honeycomb core sandwich structures in the applications as mentioned above is the environmental effect on these panels. The cores are mainly prone to damage from ecological effects, with some of the factors being heat, fire, and moisture. With these panels being used in aerospace applications, it is a given that it must be sustainable to these three factors.

In the comparison of Figures 6.19, 6.22, and 6.23, it is very much typical that the sandwich encoring material can provide better elastic coefficients for the plate than the core itself. The material used for our analysis is E- glass epoxy and Graphite epoxy, which is not very sustainable for these three factors. When the sandwich plates are capable of giving good properties, the resin is disadvantageous to be used in these applications. So, the phenolic resin can be used in place of epoxy, which has more sustainability considering environmental factors. A sandwich panel with excellent fire resistance was created using phenolic resin and phenolic foam, currently used in various structures. For this heat resistance, the thickness of the core must be higher than what we are using, as it is seen that the minimum thickness requirement is 16 mm when using a phenolic-filled foam core. This minimum thickness increases up to 100 mm when using different cores compared to a thickness of 3mm, which we used in this analysis [63]. A phenolic coating is also capable of giving resistance to these factors. This is an important

design challenge and material selection to consider. Delamination is also an important defect to consider during the research stages of these types of composites. This defect occurs due to the mismatch in properties between the core and the sandwich plates.

Comparing the properties attained through our analysis, we can make a comparison to another type of plate. A tilted sandwich honeycomb plate considered and has the following properties for the reinforcement $E_1$= 210 Gpa, $E_2$= 16.4 Gpa, and $\upsilon_{12} = 0.3$. For the core, H100 cores were analyzed with the properties being $E_1$=13 Gpa, $E_2$=3.54 Gpa, and $\upsilon_{12} = 0.32$. These plates were able to reach a displacement of 0.8mm before fracturing with a load of up to 1.4 KN. The mechanical properties used for the core are lesser than what we used in our analysis. The core material we used is expected to increase the load-bearing capacity of the sandwich plate. The fracture was mostly observed between the face and the resin in the face-core areas, as expected [64]. We also obtained the piezoelectric properties for this structure which translates to us using smart composite plates for the analysis in layman terms. These types of materials are actively being used these days for some very important applications. Vibration damping is one of them where these piezoelectric properties are controlled in efforts to produce active damping of natural and unnatural vibrations of sandwich plates, shells, etc. The use of piezoelectric materials is also problematic because of the huge variation of properties between the other materials used to manufacture the plate. The values of these piezoelectric coefficients we obtained are positive and more suitable in a higher impact loading system. These coefficients suggest that the plate can produce a higher range of damping applications that can be used for impact loading, larger loads that will involve more compression than tensile loads.

## 6.4 SMART COMPOSITE SANDWICH SHELLS MADE OF GENERALLY ORTHOTROPIC SHELLS

The following section is a depiction of parametric analysis for a hexagonal honeycomb cored three-layered sandwich shell in comparison with a mixed hexagonal-triangular cored shell. The preliminary set of equations in (5.15) and (5.16) represents the contribution of the face carriers, while the forthcoming equations represent the contribution of the sandwich core. The effective properties can be modified according to the application required by engineers by varying a large set of incoming parameters such as the length, area, thickness of core and face-carriers, height of core, and the angles in which the material is oriented. Also, the material itself can be changed according to a higher or lower requirement.

**Table 1 Material properties of graphite epoxy, PVDF, and PZT-5A**

| Property | $0^0$ graphite-epoxy | $0^0$ PVDF | PZT-5A |
|---|---|---|---|
| $c_{11}$ (GPa) | 183.44 | 238.24 | 99.20 |
| $c_{12}$ (GPa) | 4.36 | 3.98 | 54.02 |
| $c_{13}$ (GPa) | 4.36 | 2.19 | 50.78 |
| $c_{22}$ (GPa) | 11.66 | 23.60 | 99.20 |
| $c_{23}$ (GPa) | 3.92 | 1.92 | 50.78 |
| $c_{33}$ (GPa) | 11.66 | 10.64 | 86.86 |
| $c_{44}$ (GPa) | 2.87 | 2.15 | 21.10 |
| $c_{55}$ (GPa) | 7.17 | 4.40 | 21.10 |
| $c_{66}$ (GPa) | 7.17 | 6.43 | 22.59 |
| $\upsilon_{12}$ | 0.016 | 0.015 | 0.350 |
| $\upsilon_{21}$ | 0.280 | 0.154 | 0.350 |
| $\upsilon_{32}$ | 0.330 | 0.177 | 0.380 |
| $d_{31}$ (C m$^{-2}$) | 0 | −0.135 | 12.322 |
| $d_{32}$ (C m$^{-2}$) | 0 | −0.009 | 12.322 |
| $d_{33}$ (C m$^{-2}$) | 0 | −0.276 | 15.118 |
| $d_{24}$ (C m$^{-2}$) | 0 | −0.145 | −7.209 |
| $d_{15}$ (C m$^{-2}$) | 0 | −0.130 | −7.209 |

The formulation for the analysis is discussed in Section 5.4. For the sake of analysis, we vary the thickness H from 8 to 20 and keep t = a = 2.5 throughout the analysis. The material considered for the construction of the shell is unidirectional AS/3501 graphite/epoxy laminate. The material properties of this material are $E_1 = 140\ Gpa, E_2 = 10\ Gpa, \upsilon_{12} = 0.3\ and\ \upsilon_{21} = 0.0196$. The core may also relay some

piezoelectric properties if desired. The material used for the representation of piezoelectric properties is PZT-5A and $0^0$ PVDF.

### 6.4.1 COMPOSITE SANDWICH SHELL REINFORCED WITH HEXAGONAL HONEYCOMB CORE

A hexagonal honeycomb core sandwich shell is considered in this section for analysis. The relevant results are discussed and represented by means of graphs. Figure 6.25 and 6.26 makes up the coefficients for the extensional stiffness matrix of the composite shell. The variation according to expectation is increasing along with the thickness. The stiffness coefficients in the $\delta\langle b_{22}^{11}\rangle$ *and* $\delta\langle b_{11}^{22}\rangle$ direction is equal to each other. The stiffness in $\delta\langle b_{11}^{11}\rangle$ direction is significantly higher by three times in any given thickness.

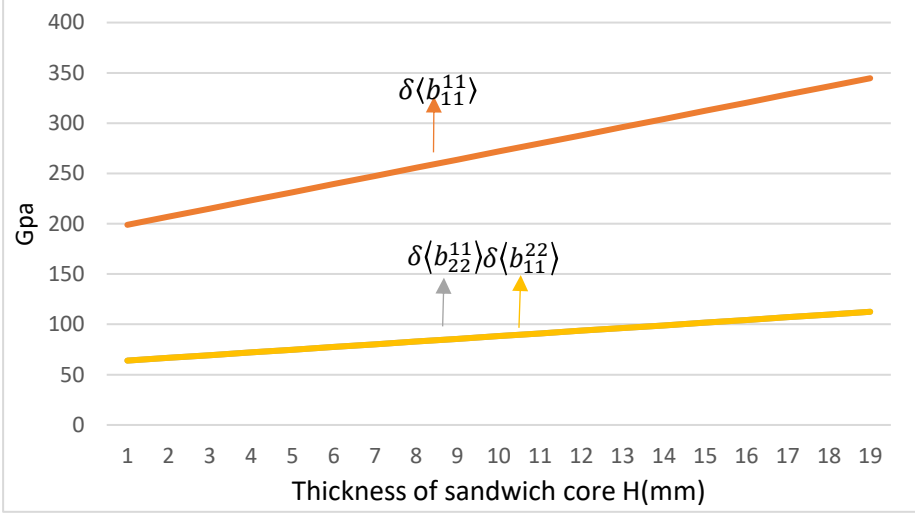


**Figure 6.26 Effective coefficients $\delta\langle b_{11}^{11}\rangle, \delta\langle b_{22}^{11}\rangle$ *and* $\delta\langle b_{11}^{22}\rangle$ of hexagonal-honeycomb sandwich core**

The effective coefficients in the $\delta\langle b_{22}^{22}\rangle$ *and* $\delta\langle b_{12}^{12}\rangle$ direction in this current structure is not up to mark and offers very weak stiffness in these directions. It is suggested to use alternative structures similar to the previous section in loading or applications which require high stiffness in the $\delta\langle b_{22}^{22}\rangle$ *and* $\delta\langle b_{12}^{12}\rangle$ direction. The overall

increment, along with the variation of thickness, is also just above 5 Gpa, which is very less to justify its value for money in using it in different applications.

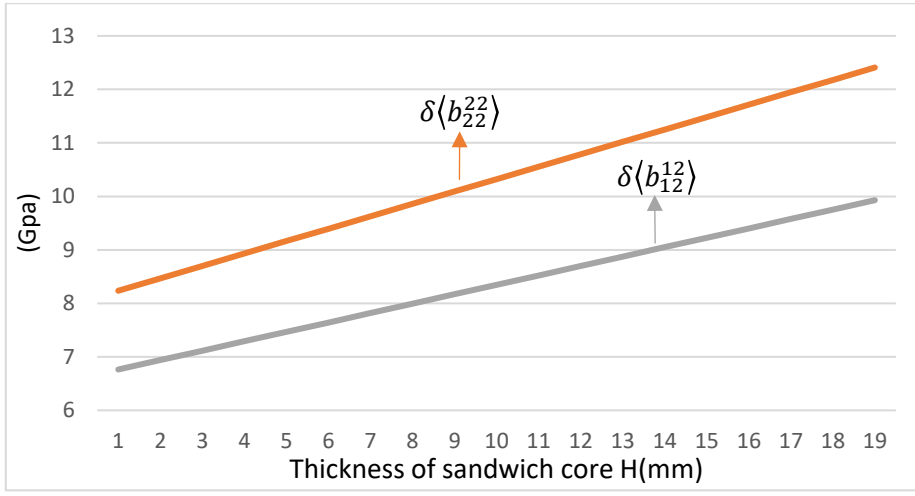


**Figure 6.27 Effective coefficients $\delta\langle b_{22}^{22}\rangle$ *and* $\delta\langle b_{12}^{12}\rangle$of hexagonal-honeycomb sandwich core**

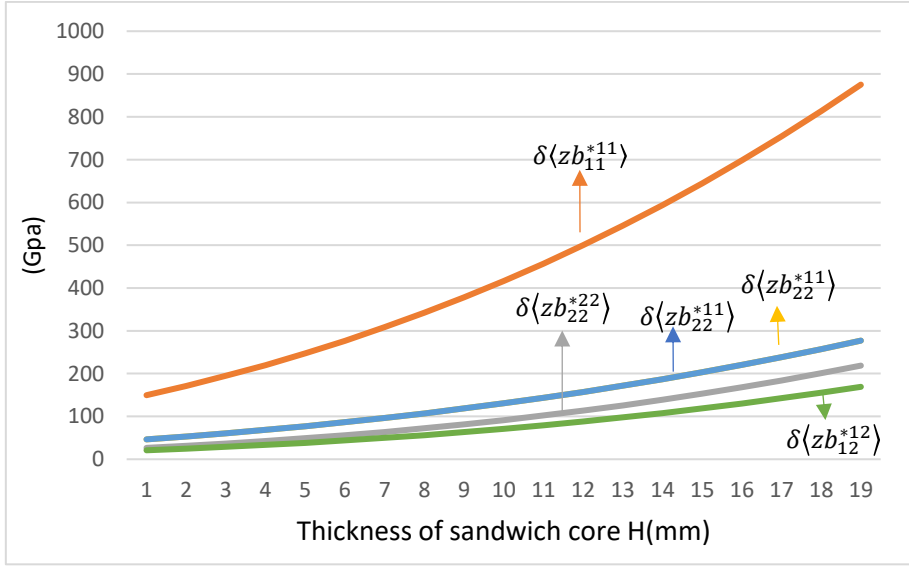


**Figure 6.28 Effective torsional stiffness coefficients of hexagonal-honeycomb sandwich core**

Figure 6.27 is a representation of the effective torsional stiffness coefficients of the hexagonal-honeycomb sandwich shell. The coefficients normally anticipated in the $\delta\langle zb_{11}^{*11}\rangle$ direction is substantially higher than the properties in the other directions. The properties in the $\delta\langle zb_{22}^{*11}\rangle$ *and* $\delta\langle zb_{11}^{*22}\rangle$ direction is equal, and all the values offer decent

stiffness in comparison with Figure 6.26. It is also noted that all the coefficients obtained are higher than the $\delta\langle zb_{12}^{*12}\rangle$ direction.

### 6.4.2 COMPOSITE SANDWICH SHELL REINFORCED WITH MIXED HEXAGONAL-TRIANGULAR CORE

A mixed hexagonal-triangular honeycomb core sandwich shell is considered in this section for analysis. The relevant results are discussed and represented by means of graphs. Figure 6.29 and 6.30 makes up the coefficients for the extensional stiffness matrix of the composite shell and Figure 6.21 for torsional coefficients.

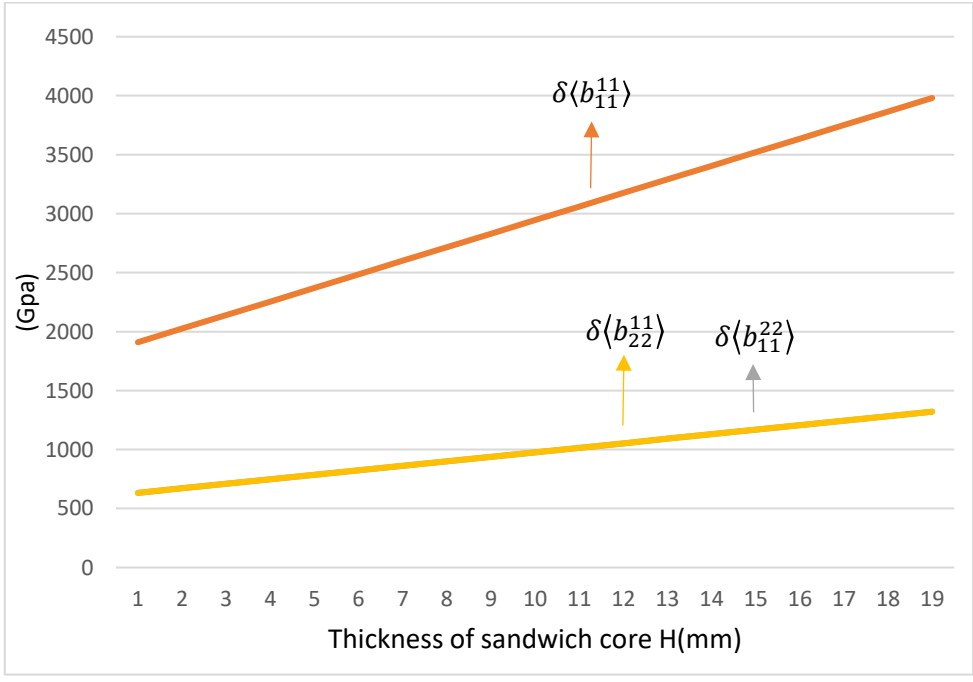


**Figure 6.29 Effective coefficients $\delta\langle b_{11}^{11}\rangle, \delta\langle b_{22}^{11}\rangle$ *and* $\delta\langle b_{11}^{22}\rangle$ of hexagonal-triangular sandwich core**

The variants offered by this structure along the thickness in all directions are similar to the hexagonal honeycomb shell. It is worth noting that this structure offers far superior properties as the number of structural elements is higher and, therefore, the stiffness being higher.

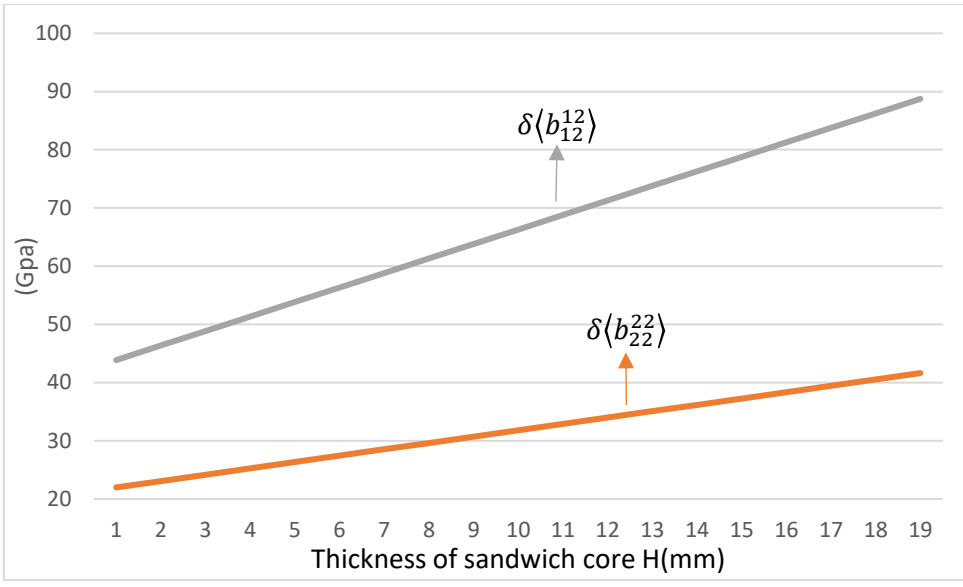


**Figure 6.30 Effective coefficients $\delta\langle b_{22}^{22}\rangle$ *and* $\delta\langle b_{12}^{12}\rangle$of hexagonal-triangular sandwich core**

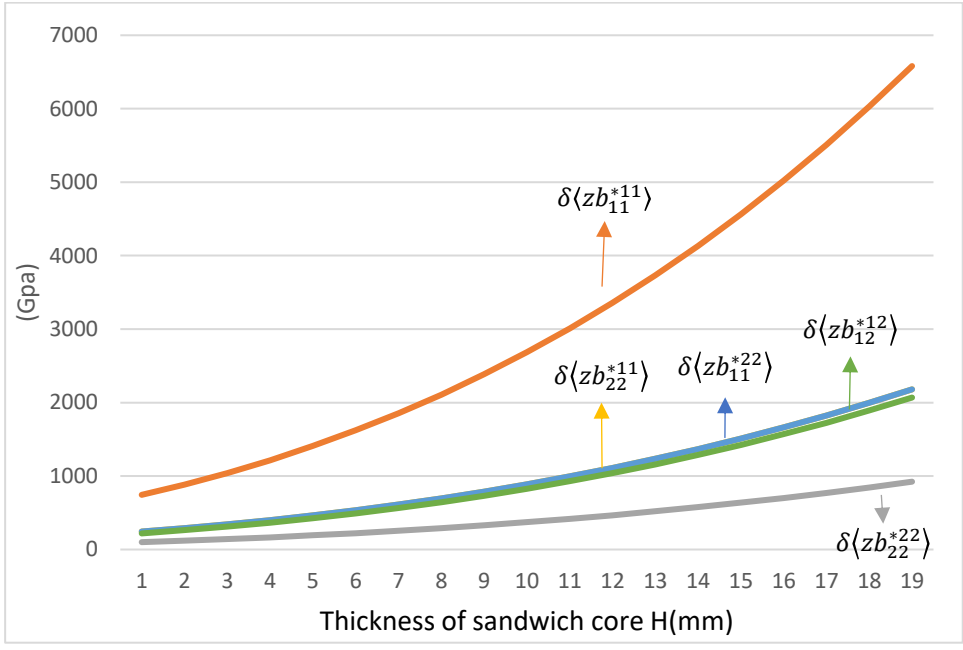


**Figure 6.31 Effective torsional stiffness coefficients of hexagonal-triangular sandwich core**

The following graphs represent the piezoelectric properties of both the structures in sections 6.4.1 and 6.4.2. The material used is $0^0$ PVDF, and PZT-5A and the coefficients are shown in Table 2. The formulae used for this analysis are also discussed briefly in Section 5.4.

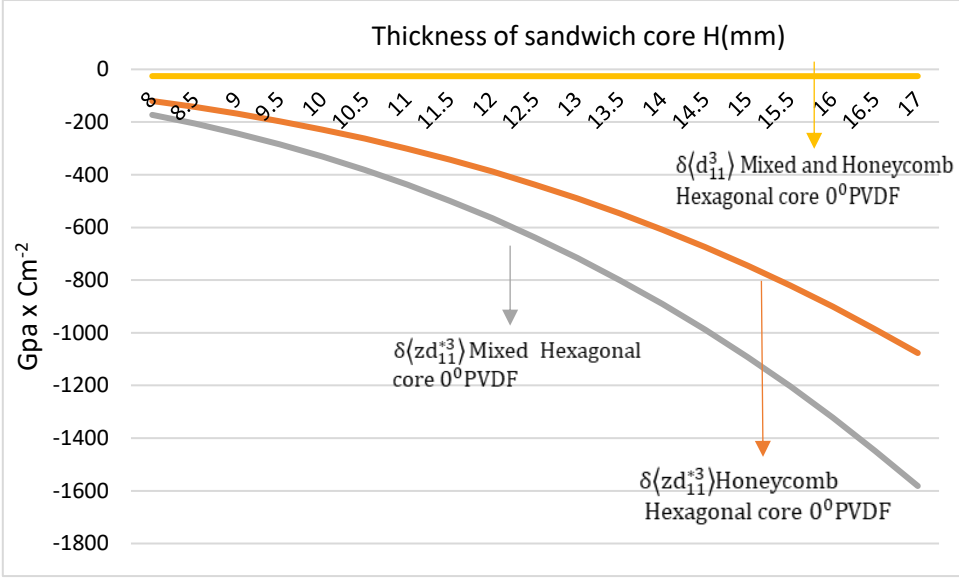


**Figure 6.32 Piezoelectric coefficients $\delta\langle d_{11}^3\rangle$ *and* $\delta\langle zb_{11}^{*3}\rangle$ of mixed hexagonal and honeycomb sandwich shells**

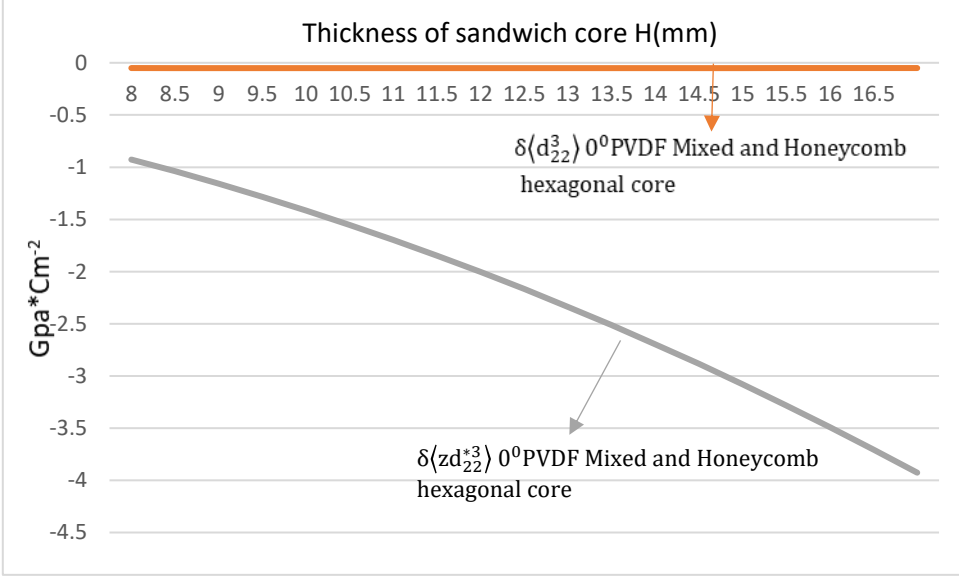


**Figure 6.33 Piezoelectric coefficients $\delta\langle d_{22}^3\rangle$ *and* $\delta\langle zb_{22}^{*3}\rangle$of mixed hexagonal and honeycomb sandwich shells**

Figure 6.32 and 6.33 represents the piezoelectric coefficients of mixed hexagonal and honeycomb sandwich shell structures. These two structures offer almost similar piezoelectric properties in all directions of the composite shell. While it is accepted that the values are slightly higher for the mixed hexagonal core in the

$\delta\langle d_{11}^3\rangle, \delta\langle d_{22}^3\rangle$ *and* $\delta\langle zb_{22}^{*3}\rangle$ directions, the coefficients show a significantly higher value in the $\delta\langle zb_{11}^{*3}\rangle$ direction. This is predictable because of the larger number of structural elements and reinforcements existing because of the hexagonal-triangular mixed composite shell arrangement.

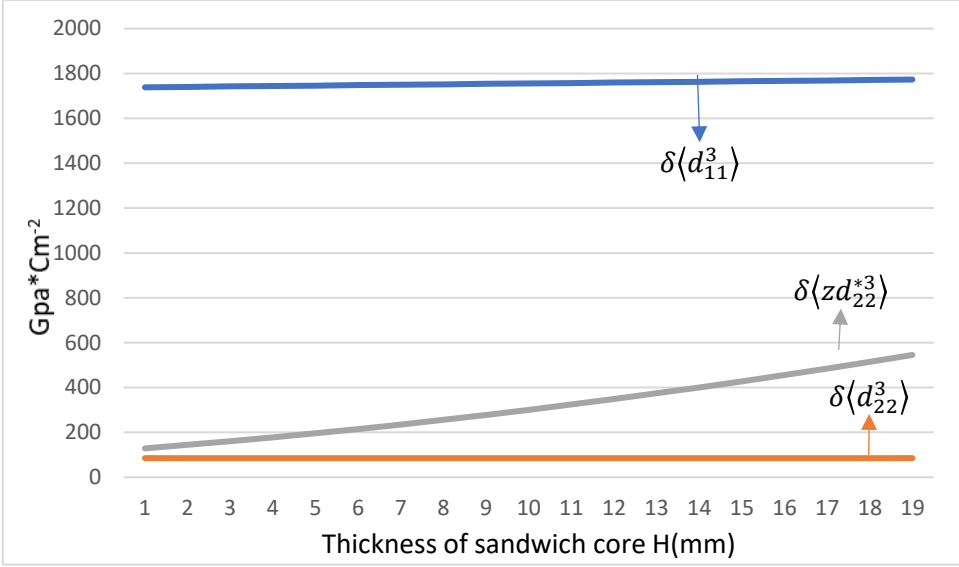


**Figure 6.34 Piezoelectric coefficients $\delta\langle d_{11}^3\rangle, \delta\langle d_{22}^3\rangle$ *and* $\delta\langle zb_{22}^{*3}\rangle$ of hexagonal honeycomb sandwich shells**

In Figures 6.34 and 6.35, we use a PZT-5A which is a piezoelectric material. These figures represent the piezoelectric properties of the hexagonal-triangular and honeycomb sandwich cored shell. In the $\delta\langle d_{11}^3\rangle, \delta\langle d_{22}^3\rangle$ *and* $\delta\langle zb_{22}^{*3}\rangle$ directions, both the cores used do not make a significant difference in the piezoelectric properties. The coefficients as predictable in the $\delta\langle d_{11}^3\rangle$ are significantly higher than its counterparts.

When compared, the hexagonal-triangular structure can offer advanced piezoelectric properties in all directions. While the difference is not much in the $\delta\langle d_{11}^3\rangle, \delta\langle d_{22}^3\rangle$ *and* $\delta\langle zb_{22}^{*3}\rangle$ directions, a noticeable difference, and superiority is being offered by the mixed hexagonal-triangular cored structure in the $\delta\langle zd_{11}^{*3}\rangle$ direction. This

is also predictable, knowing that the hexagonal-triangular core requires more structural elements than the honeycomb core.

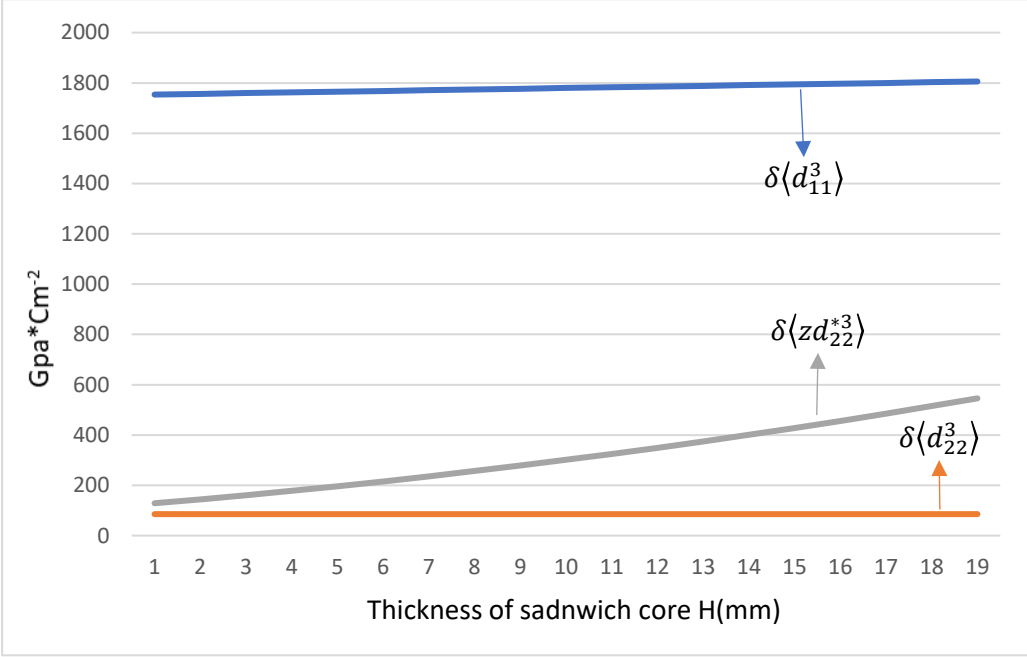


**Figure 6.35 Piezoelectric coefficients $\delta\langle d_{11}^3\rangle$, $\delta\langle d_{22}^3\rangle$ *and* $\delta\langle zb_{22}^{*3}\rangle$ of mixed hexagonal-triangular sandwich shells**

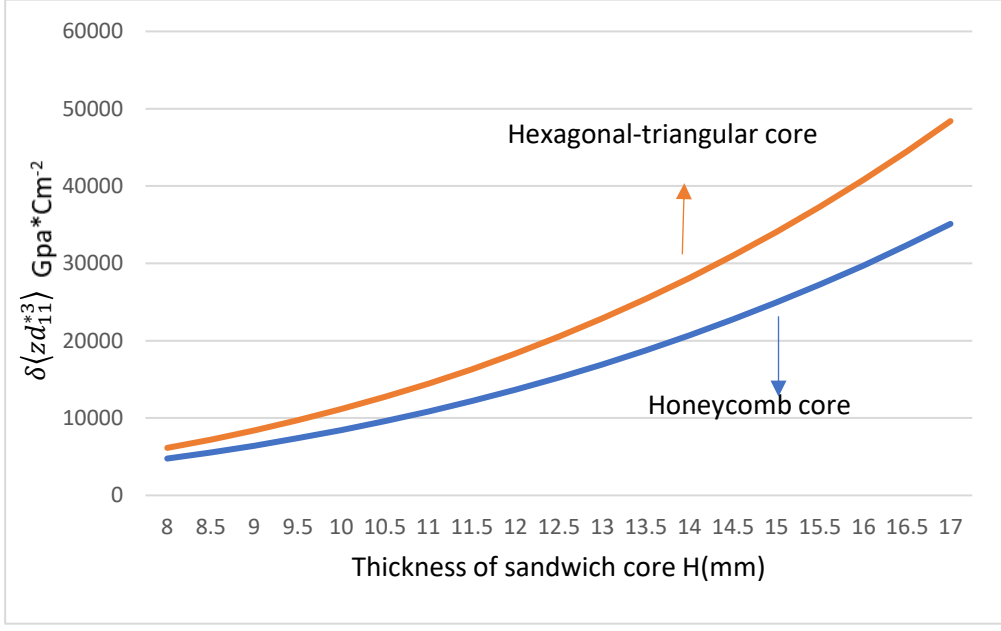


**Figure 6.36 Piezoelectric coefficients $\delta\langle zd_{11}^{*3}\rangle$ of mixed hexagonal-triangular and honeycomb sandwich shells**

The materials $0^0$PVDF and PZT-5A can both be used to exhibit piezoelectric properties. In comparison, the PZT-5A can offer far larger values for the piezoelectric constants. This is the case for both the hexagonal sandwich structures. The values of the piezoelectric strain constants in the material PVDF are much bigger than those of PZT-5A, which hinders its ability to provide larger coefficients which are evidently visible in all the directions of the composite shell.

Section 6.4.1 and Section 6.4.2 investigates very similar structures to what was seen previously in this chapter with varied dimensional parameters and material properties. Sandwich shells with honeycomb core and mixed hexagonal-triangular core were analyzed in this section. These sandwich shells are an integral part of the industry such that it is a widely used entity in a myriad of applications. Overall, in this case, the comparison leads to the point that the composite structure with more reinforcing elements can offer better elastic coefficients. This is because the mixed-hexagonal triangular cores have a higher number of structural elements in their design than the normal honeycomb core. There is also the capability to replace the conventional honeycomb and hexagonal cored using auxetic cores with a change in mechanical properties, specifically with a negative Poisson's ratio [62]. It creates the scope of having potentially higher flexural stiffness and can be more durable in tough conditions. In applications relating to the automobile industry, the sandwich shells can replace the roof, walls, fenders, and other parts that do not involve much loading. These parts require higher flexural stiffness and durability, as mentioned above. Typical stiffness properties for a steel plate are around 200 Gpa, and the composite plate used for analysis can provide superiority in most directions, and the torsional stiffness coefficients are also very high. The material cost for the composite is higher than these materials, and it is

justified to use this only if the properties given are put to full use. The sandwich shells can also be used in underwater applications, which require resistance to moisture, waterproofing, and impact resistance. The soft cores being used in the sandwich shells can be a good source to reduce the impact resistance of water vehicles. It is also very much beneficial because of its lightweight, which in turn offers buoyancy. It is also shown that the mechanical properties are also capable of reducing deformation in underwater structures. There are various challenging design issues to solve because of the nature of this composite shell. The fatigue characteristics of this shell underwater are not that promising for extensive use and higher loading conditions [64]. There is also delamination of the composite sandwich shell, which is most common among all the sandwich structures analyzed in this chapter. There are ways to detect this defect by means of wave propagation, as explained in [66], but since these planes are so prone to delamination defects, it is important to ensure the use of proper resin to achieve proper bonding of the structures. Sandwich shells with higher and suitable mechanical properties also lose their strength when constantly being exposed to moisture. When testing was conducted with a sandwich shell with foam core with the structure being exposed to 95 % humidity conditions, there is a significant depreciation in the mechanical properties of the sandwich shell. It is also observed that the top and bottom carrier faces are prone to more degradation in properties like the strength of laminates and the flexural stiffness of the laminate. Comparatively, there is relatively less damage to properties such as stiffness and tensile strength to the foam core used in this analysis. Further, it is also observed that prolonged exposure leads to visible cracks and degradation of the plate through the human eye [67].

Most importantly, proper use of materials is warranted for these sandwich shells and is an integral part of what or where it is suitable to be used. These applications range very widely, with usage only being more and more in the future. The properties we have attained are adept at satisfying most of these applications in terms of elastic coefficients, but the materials we analyzed might not suit all these applications. The resins and fibers and the core material are the important factors to consider before deciding the application in which these shells are being used.

## 6.5 THIN COMPOSITE NETWORK STRUCTURES

The following section is a depiction of parametric analysis for composites which are comprised of composites with thin reinforcing elements through it. The effective properties can be tailored according to the uses required by several industries by varying the set of incoming parameters such as the length, area, thicknesses, height, and the angles in which the material is oriented. Also, the material itself can be changed according to a higher or lower requirement. We consider this structure with a reinforcing element oriented in 45 degrees, as shown in Figure 4.6 in the previous section. We assume the material properties of this structure as referenced in [49]. For this structure, the values of the elastic coefficients are presented with the variation of the volume fraction of the structure defined as $R = V/h_1h_2$.

Figure 6.37 is a representation of the effective elastic properties of the thin network reinforced structure. The $\delta\langle b_{11}^{11}\rangle$ direction can offer supreme properties for this structure. This is not uncommon, as is the case for many of the other structures analyzed in this section. The main concentration of loads and stresses will be oriented in such a way that it will be dissipated through the $\delta\langle b_{11}^{11}\rangle$ direction mainly. This explains why we need better properties in this direction over all the other directions. This is followed up

by the directions through $\delta\langle b_{22}^{12}\rangle$ and $\delta\langle b_{11}^{22}\rangle$ which has equal properties through the variation of the volume fraction of the structure. The three directions discussed until now can offer very good properties and will be able to satisfy most of the required applications. Then, we have a look at the directions $\delta\langle b_{11}^{12}\rangle, \delta\langle b_{12}^{12}\rangle$ and $\delta\langle b_{22}^{22}\rangle$ which also have equal properties when compared to each other. It is noticeable that the properties given by these directions are for the negative direction when seen in the coordinate axis of a 3D structure. So, it is required to recalibrate the load distribution according to these properties through the composite.

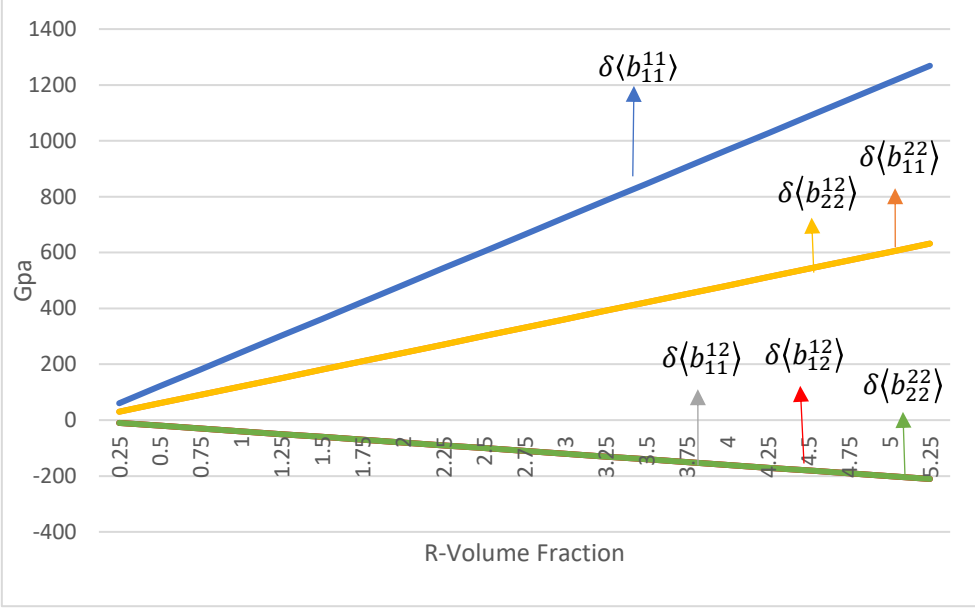


**Figure 6.37 Effective elastic coefficients of thin network 45 degrees reinforced structure**

Figures 6.38 and 6.39 depict the torsional stiffness coefficients of the same structure being discussed until now. These properties are only offering limited capability in real-life usage, thereby reducing many applications involving twisting forces. While it is true that the structure will still withstand very minimal forces, compared to other structures, it cannot give us superiority. We can obtain good properties in the negative

direction in the $\delta\langle zb_{22}^{*12}\rangle$ *and* $\delta\langle zb_{12}^{*12}\rangle$ directions, but these will be well suited in very rare functions and not up to the mark for all applications.

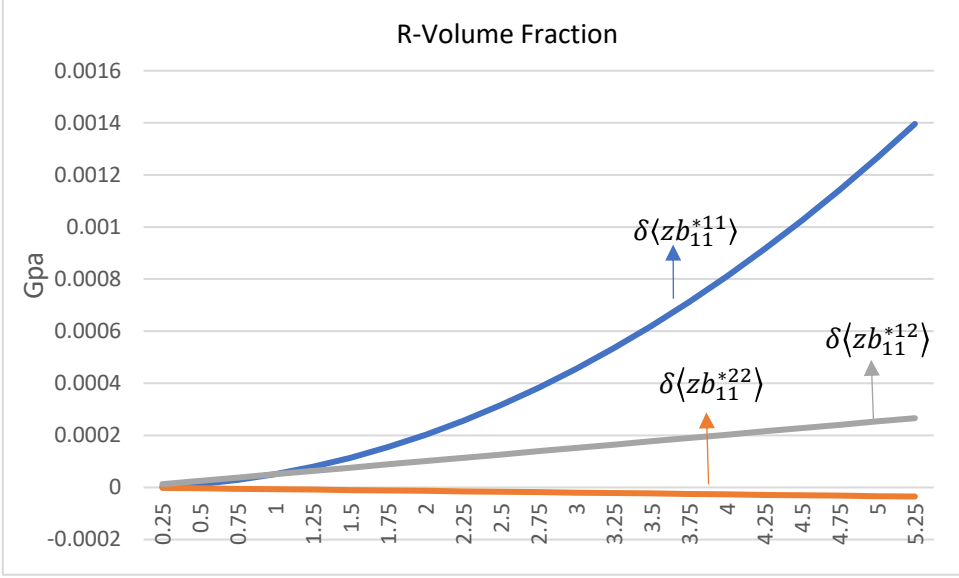


**Figure 6.38 Effective torsional elastic coefficients of thin network 45-degree reinforced structure**

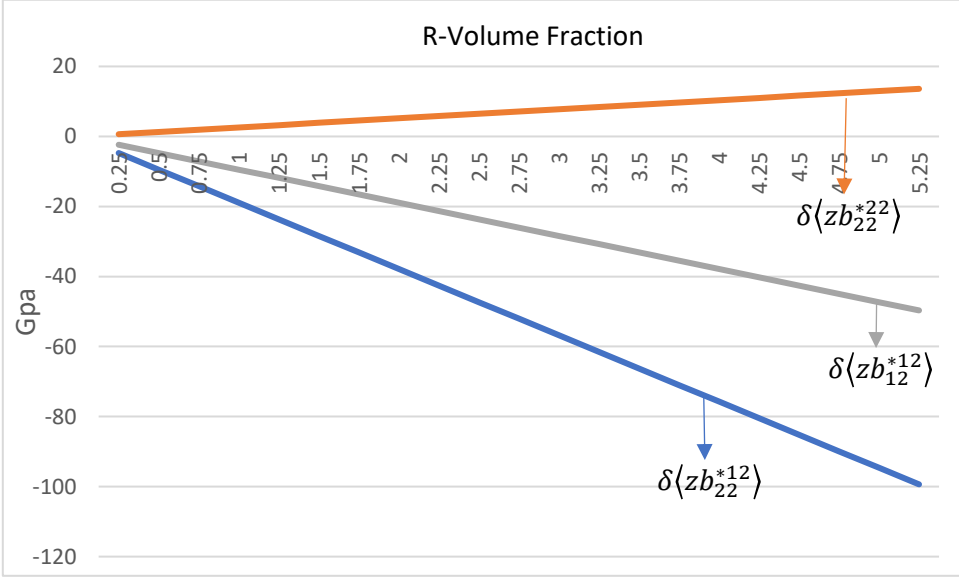


**Figure 6.39 Effective torsional elastic coefficients of thin network 45-degree reinforced structure**

We move forward with our analysis by modifying the structure and obtaining the properties for those structures. The material properties and dimensions are assumed

to be the same for these structures, but the angular orientation is varied. We have a look at three different structures. The first will be referred to as S1 for simplicity and is a thin network structure with rectangularly arranged reinforcing elements with elements being oriented in the 0- and 90-degree alignment. The second referred to as S2, is the same structure with the triangular arrangement and the orientation in the 30-, 90- and 150-degree angles. S3, which is the third and final structure, has the reinforcements aligned in a rhombic manner which leads to it being oriented in the 30- and 150-degree angles.

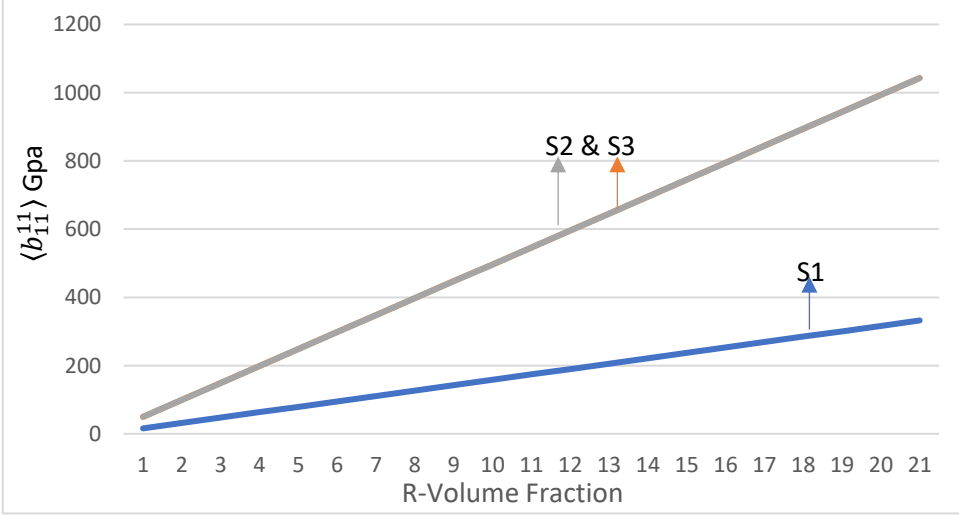


**Figure 6.40: Effective elastic coefficient $\delta\langle b_{11}^{11} \rangle$ for structures S1, S2 and S3**

In similarity with the structure with a 45-degree reinforcement, the structures S1, S2 and S3 are also able to offer higher coefficients in the $\delta\langle b_{11}^{11} \rangle$ direction. The rectangular reinforced structure falls back in this direction while the other two orientations offer similar properties with far higher values similar to the 45-degree reinforced thin network structure. These improved properties in S2 & S3 are due to more complex reinforcing elements and increment in reinforcements than S1.

Figures 6.41 and 6.42 represent the remaining elastic properties of the three structures. Again, the properties obtained from S2 & S3 in the $\delta\langle b_{11}^{22} \rangle$ and $\delta\langle b_{11}^{12} \rangle$ are

equal and also give higher stiffness in comparison with S1. The structure S1 gives a variation of properties in these two directions with the $\delta\langle b_{11}^{22}\rangle$ direction being higher in stiffness. In the $\delta\langle b_{22}^{22}\rangle$ direction, the structure S1 offers more superiority and is better than its counterparts. Overall, the properties for stiffness provided by these sets of structures are very flexible and, with minor modifications, can give hope to a wide variety of applications in the real world.

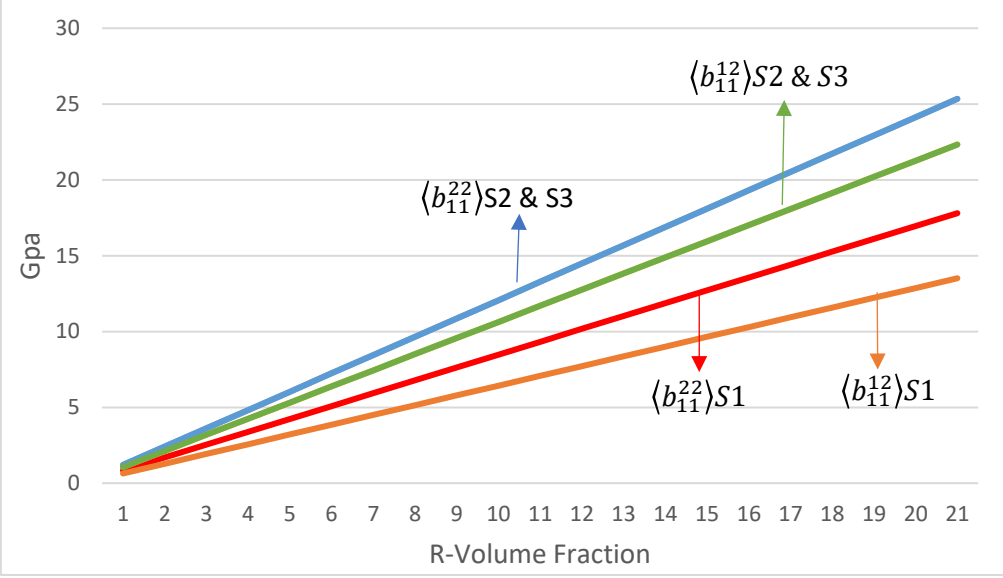


**Figure 6.41 Elastic coefficient $\delta\langle b_{11}^{22}\rangle$ and $\delta\langle b_{11}^{12}\rangle$ for structures S1, S2 and S3**

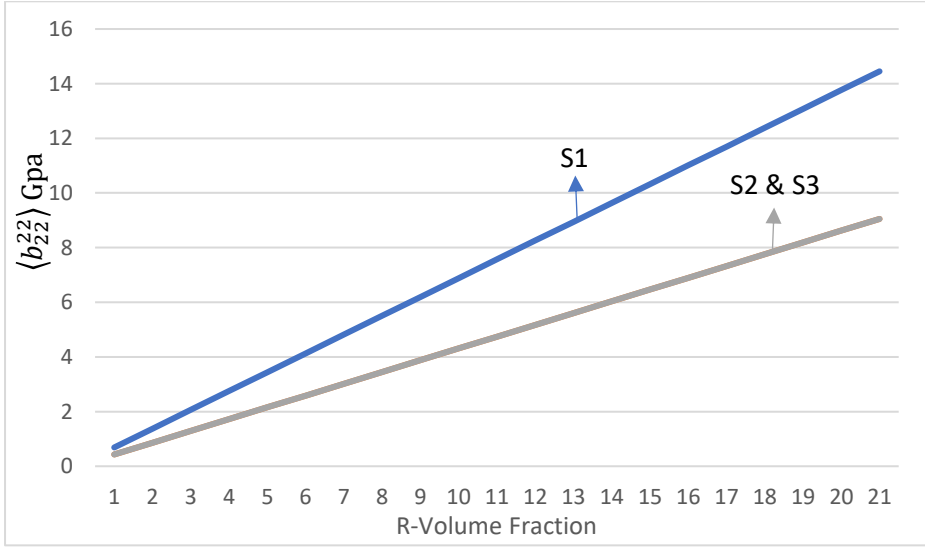


**Figure 6.42 Effective elastic coefficient $\delta\langle b_{22}^{22}\rangle$ for structures S1, S2 and S3**

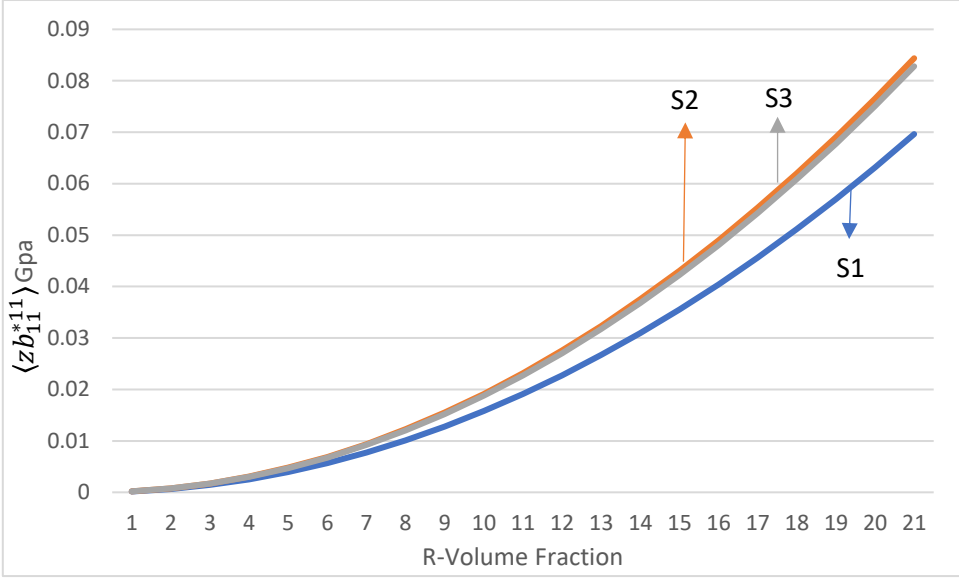


**Figure 6.43 Effective torsional elastic coefficient $\delta\langle zb_{11}^{*11}\rangle$ for structures S1, S2 and S3**

The composite structures analyzed in this section are comparable to a grid reinforced composite structure due to the nature of its design. But usually, grid reinforced structures have a thick set of reinforcements that will drastically increase the composite structure's mechanical properties and are used in highly rigid structures. Here, a thinner set of orthotropic bars are used as the reinforcements. This will ensure it can be used in smaller structures than the grid-reinforced structures used in pillars, beams, etc. This type of thin network construction can be used as holding containers in chemical industries or water tankers. The thin construction helps with this kind of application. It can offer superior properties through corrosion resistance, reduced maintenance, good strain bearing capability, and metallic tankers or containers being sued currently. There are also problems regarding the resins' chemical reactivity, which will be the outer layer when these tankers are used to store chemicals. C-glass, a modified glass fiber lamina, can offer chemical resistance along with epoxy or vinyl ester resins for the matrix layer. Initially, the cost might be higher than with metallic or alloy tanks, but there will be

minimal maintenance with this investment. Aluminum sheets are also used in this application with a stiffness value of 70 Gpa. Vinyl ester resins provide hydraulic stability, excellent impact, and fatigue resistance but have more shrinkage than epoxy resin. The rhombic arrangement and triangular network arrangement offer similar design elements and offer good elastic properties with the 0/90 rectangular reinforcement. The former design may offer more structural integrity to the application due to the presence of more reinforcing elements. The thin network structure composites were used as a film to satisfy the application of nanofiltration membrane. The membranes were compared to a traditional filtration membrane and were found to offer better hydrophilicity and antifouling and, because of this property, avoided the absorption of protein [70]. This can also be used for certain automobile fenders replacing carbon fibers and glass fibers because of fewer material consumptions. Carbon fiber is a costly material, and the construction of the laminates for fenders requires more raw material. Even though glass fiber is more readily available and affordable by cost, the method of construction of this thin network structure is more suitable for on-road automobiles, whereas glass fiber can be used more for water-based automobiles.

## 6.6 SMART COMPOSITE REINFORCED AND SANDWICH SHELLS

In this section, we consider a smart composite sandwich structure with various cores and reinforcements. We consider four different structures starting with the traditional hexagonal honeycomb core structure, sandwich panel with thin rectangular and triangular reinforcements, and a diagonally restrained thin wafer structure. The materials used in these structures are made to exhibit piezoelectric properties, and thus, these become smart structures. It is also assumed that the face carriers are made of orthotropic material, and the core is made of isotropic material. The properties exhibit

the mechanical behavior of the core and its encompassing panels. Historically, the core is a softer material than the encompassing materials, and therefore, the properties of the core will be lesser than that of the face carriers. It is possible to make these properties similar for our required application or even make the core properties superior to the face carriers by appropriately differing some material properties and dimensional parameters in the form of E, H, t, $t_0$, etc. In our analysis, we differ the value of H where required from 10 to 30 mm, and we also differ $t_0$ appropriately due to its large influence on the final properties of the sandwich structures. Here E represents the material properties being used, H is the thickness of the core, t is the thickness of the reinforcements in the core, and $t_0$ is the thickness of the face carriers. The material properties used are shown using the table below.

**Table 2 Material properties for the sandwich structures**

| Material | $E_0$ (GPa) | $E$ (GPa) | $\nu_0$ | $\nu$ | $d_{31}$ ($10^{-10}$ C/N) | $d_{32}$ ($10^{-10}$ C/N) |
|---|---|---|---|---|---|---|
| H130 | | 0.13 | | 0.320 | | |
| PZT4 | 81.23 | | 0.327 | | −1.24 | −1.24 |

The terms $d_{31}$ and $d_{32}$ are the piezoelectric coefficients used to calculate the piezoelectric properties of the structure. $\nu$ and $\nu_0$ is the Poisson's ratio for the face carrier material, and the piezoelectric material is used, respectively.

### 6.6.1 SMART HEXAGONAL SANDWICH STRUCTURE

In this section, the most common sandwich structure in the industry is being analyzed. The hexagonal honeycomb sandwich structure was also discussed numerous times in this chapter and the previous chapters. The elastic coefficients of the hexagonal honeycomb structure obtained by assuming material properties, as seen in Table 2, are discussed in this section. Figures 6.44 and 6.45 illustrate the values of the elastic

coefficients and the torsional elastic coefficients, respectively, when capturing its variation with the thickness of the core H. Here, the properties obtained in the $\delta\langle b_{11}^{11}\rangle$ and $\delta\langle b_{22}^{22}\rangle$ direction are equal to each other. In this direction, the discrepancy is also hyped when compared to the other directions. These are the main two directions that dominate the composite structure's properties and how it behaves in reality. The values seen are historically accepted for this type of structure. The remaining elastic coefficients $\delta\langle b_{22}^{11}\rangle, \delta\langle b_{11}^{22}\rangle$ and $\delta\langle b_{12}^{12}\rangle$ are also equal. The coefficients obtained are inferior to the preliminary two directions but still suitable for a myriad of applications.

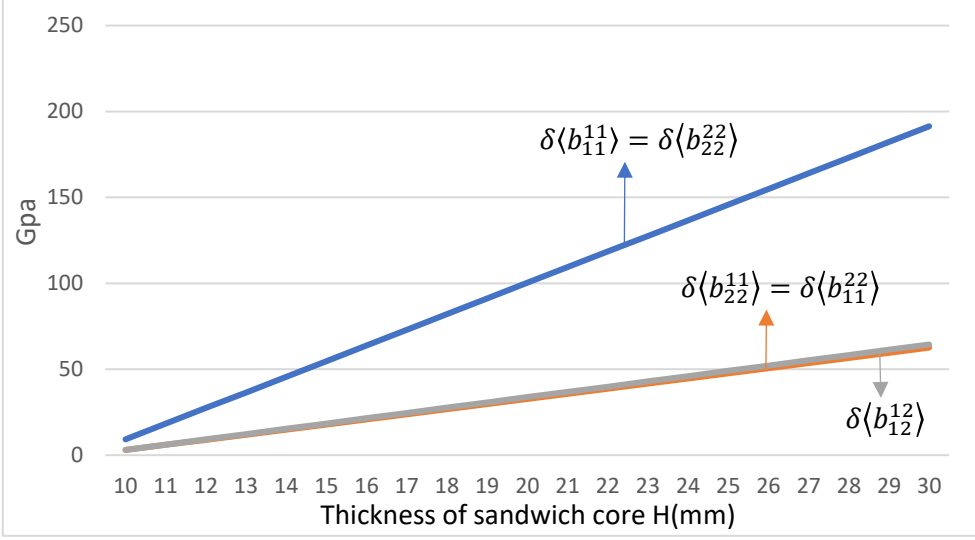


**Figure 6.44 Effective elastic coefficients of hexagonal honeycomb structure**

The coupling coefficients follow the same pattern as the stiffness coefficients and are equal to each other in all the directions in which the stiffness coefficients are. The coefficients obtained in the $\delta^3\langle zb_{22}^{*11}\rangle$ and $\delta^3\langle zb_{11}^{*22}\rangle$ direction is comparable in values to the ones obtained in the $\delta\langle b_{11}^{11}\rangle$ and $\delta\langle b_{22}^{22}\rangle$ direction. But, in the $\delta^3\langle zb_{22}^{*11}\rangle$ and $\delta^3\langle zb_{11}^{*22}\rangle$ direction, the values are more on the higher range than any other directions. It also gives a steep variation from the H=20 mm to 30 mm range while the variation is steady across the thickness in the other remaining direction.

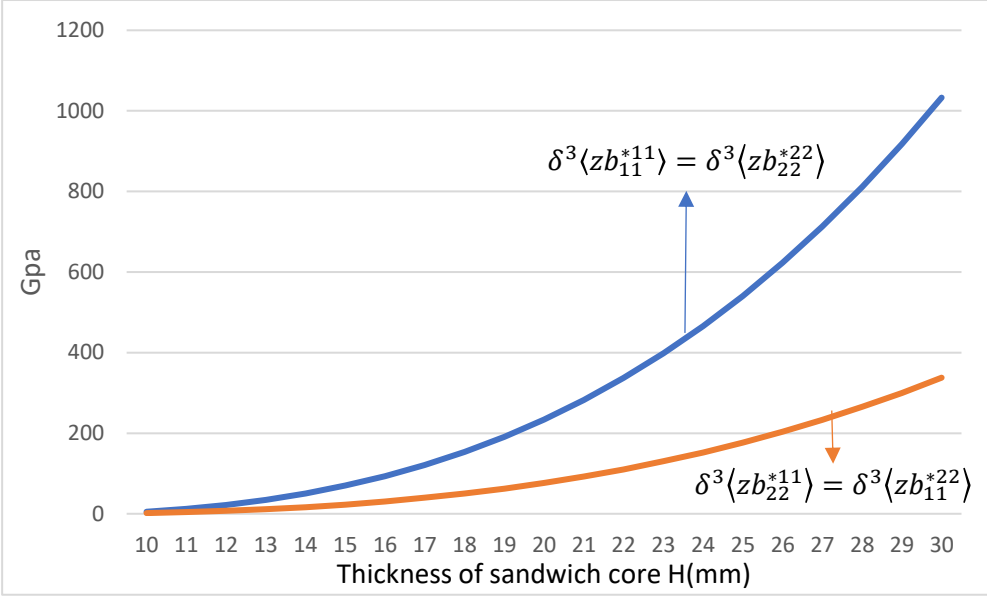


**Figure 6.45 Effective torsional elastic coefficients of hexagonal honeycomb structure**

### 6.6.2 SMART THIN SANDWICH STRUCTURE WITH RECTANGULAR CORE

In this section, the hexagonal honeycomb sandwich structure is supplanted by a smart thin sandwich structure with the core having rectangular-shaped reinforcements. Figure 6.46 represents the variation of the elastic coupling and stiffness coefficients, with the H being varied in millimeters. The material properties considered for this structure are the same as hexagonal honeycomb sandwich structure. As the standard result among most structures, the stiffness coefficients in the $\delta\langle b_{11}^{11}\rangle$ and $\delta\langle b_{22}^{22}\rangle$ direction are similar to each other and is the most superior of the analyzed values. It is followed up by the coefficients in $\delta\langle b_{12}^{12}\rangle$ direction. It must be noted that this direction is varied from $\delta\langle b_{22}^{11}\rangle$ and $\delta\langle b_{22}^{11}\rangle$ direction as opposed to what was seen in the previous section. The stiffness values generally obtained for this structure are very less than the traditional hexagonal honeycomb structure. This reduction in stiffness properties can be attributed to the 0/90 orientation of the rectangular core, which is not capable of supporting the panels effectively. Through its arrangement of the reinforcing material, the honeycomb core can

give better reinforcement and, therefore, increase the composite's overall stiffness and flexural strength. The coupling coefficients in this structure is inferior in all directions to the extensional stiffness coefficients, while the extensional coefficients in the $\delta\langle b_{22}^{11}\rangle$ and $\delta\langle b_{22}^{11}\rangle$ direction acts as the median for these coefficients in the other directions.

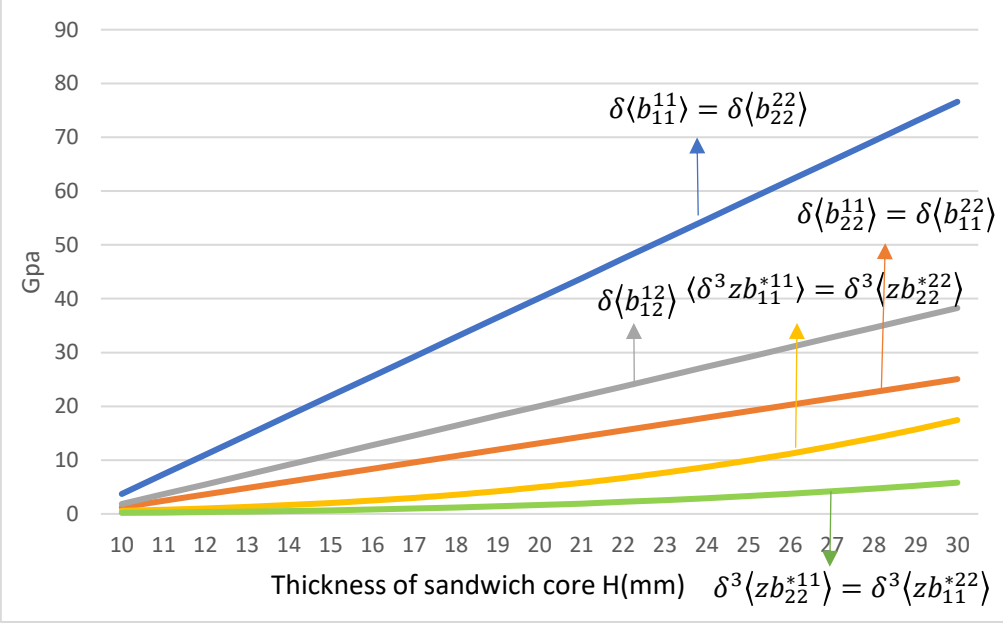


**Figure 6.46 Effective elastic coefficients of smart thin wafer structure with rectangular reinforcements**

### 6.6.3 SMART DIAGONALLY RESTRAINED THIN WAFER STRUCTURE

Smart diagonally restrained thin wafer structure is analyzed in this section, and the extensional and coupling coefficients are compared and illustrated by means of Figure 6.47. In general, the diagonally restrained wafer structure has a complex design with reinforcements requiring to be aligned in different directions. The design is similar to the structure considered in section 6.6.2, with diagonals of the rectangle being added to the structural reinforcement. The extensional and coupling coefficients for this structure are exactly similar with respect to the previous structure, with a minor variation in the slope in the coefficients plotted in the $\delta^3\langle z b_{22}^{*11}\rangle$ and $\delta^3\langle z b_{11}^{*22}\rangle$ direction. The

other values remain the same, and the comparison between the values remains the same, as discussed in the previous section. It is very intriguing to see this observation because the addition of reinforcing elements to the structure in the form of diagonals to the rectangular structure is expected to give better stiffness properties due to the presence of a higher number of reinforcing elements to the sandwich structure. This exemplifies the minor influence the core has in the sandwich structure. Design changes can be made to the core to increase its efficacy in the sandwich structure by means of varying the dimensional parameters. The core can provide better flexural strength, and some cores can increase the bonding and correct some errors in the form of delamination. But overall, the elastic coefficients calculated here remain unaffected by this structural change.

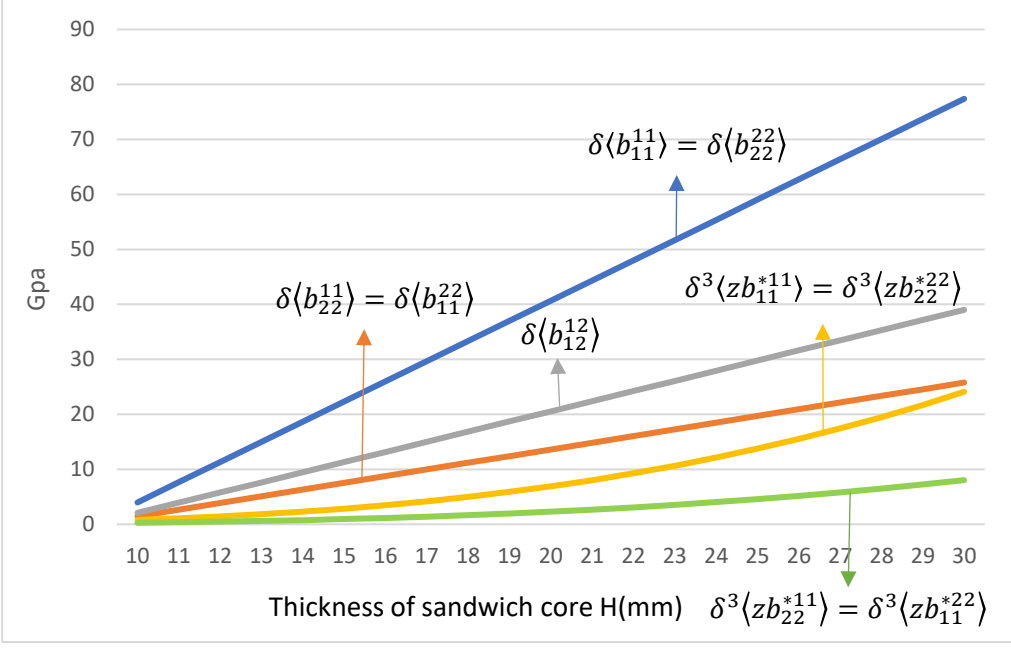


**Figure 6.47 Effective elastic coefficients of smart diagonally restrained wafer structure**

### 6.6.4 SMART THIN SANDWICH STRUCTURE WITH TRIANGULAR CORE

This section analyses the effects of the thickness on the elastic coefficients of the smart thin sandwich structure with a triangular-shaped reinforcing core. Again, the material properties and other entities are kept constant as the other structures being analyzed in this section. The extensional stiffness values in this structure are more than what was obtained in sections 6.6.3 and 6.6.2 but not as high as the values from 6.6.1

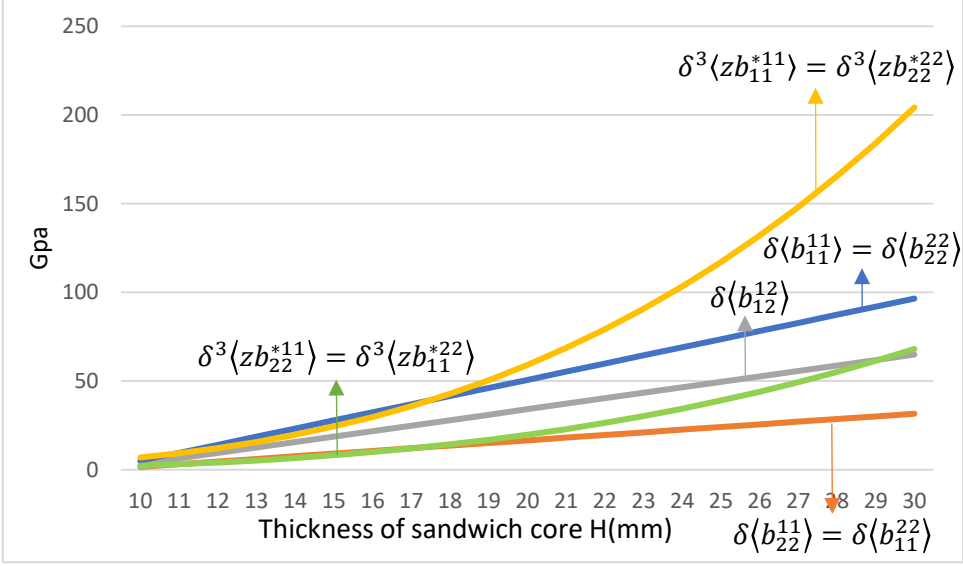


**Figure 6.48 Effective elastic coefficients of smart thin wafer structure with triangular reinforcements**

So, in comparison with the four structures being analyzed in this section, the hexagonal honeycomb core can still offer better properties compared to its counterparts. In this structure, the coupling coefficients in the $\delta^3\langle zb_{11}^{*11}\rangle$ and $\delta^3\langle zb_{22}^{*22}\rangle$ direction can give the most superior properties of all the other coefficients. The coefficients in the $\delta\langle b_{22}^{11}\rangle$ and $\delta\langle b_{22}^{11}\rangle$ direction is in the range as compared to the previous two sub-sections. In the $\delta\langle b_{12}^{12}\rangle$ direction, the values are slightly superior to the other structures except for the hexagonal honeycomb structure. On careful observation, it can be said that the

sandwich structure with the triangular reinforcements is the second-best design arrangement in these four structures.

### 6.6.5 PIEZOELECTRIC COEFFICIENTS OF VARIOUS SANDWICH SHELLS

This section represents the piezoelectric coefficients of the structure considered in this section. Figure 6.49 is a depiction of the effective piezoelectric coefficients of the hexagonal honeycomb cored structure. The proclivity of the structure to react to the electric field or any actuation applied to activate the piezoelectric material is on the higher side for the honeycomb cored structure compared to the piezoelectric coefficients seen in this section illustrated in Figure 6.51. The values being discussed here is $\delta^3\langle zd_{11}^*\rangle$ and $\delta^3\langle zd_{22}^*\rangle$. With the increase in thickness of the composite, the capability to impart piezoelectric behavior is only increased for all the values and coefficients in different directions obtained in this section. In figure 6.50, the piezoelectric coefficients for the remaining three structures are seen. These coefficients are again similar for the thin rectangular reinforced composite and diagonally restrained wafer structure. The thin triangular reinforced structure is offering coefficients slightly on the lower side with respect to others.

Figure 6.50 illustrates the values $\delta\langle d_{11}^3\rangle$ and $\delta\langle d_{22}^3\rangle$ for all the structures in the discussion. Here, the propensity of the material to be reactive to piezoelectric performance is increased with the increase in thickness which is the usual behavior for most composites. It is to be noted that the hexagonal honeycomb cored structure in this regard offers the lowest propensity for the structure to exhibit piezoelectric properties. It is capable very much of producing the piezoelectric effect, but just that, the other structures are able to offer slightly superior piezoelectricity. Here again the thin sandwich structure with triangular reinforcements. Also, the values obtained in this

section are all on the negative side, meaning that only a negative reaction can be created on the composite material. In layman terms, it can be used to create a sponge or cushioning effect when subject to loads or stresses in the required direction. This can be done by activating the piezoelectric material in the required structural orientation. The coefficients for the thin rectangularly reinforced structure and diagonally restrained wafer structure are again in this regard equal for the terms $\delta\langle d_{11}^{3}\rangle$ and $\delta\langle d_{22}^{3}\rangle$.

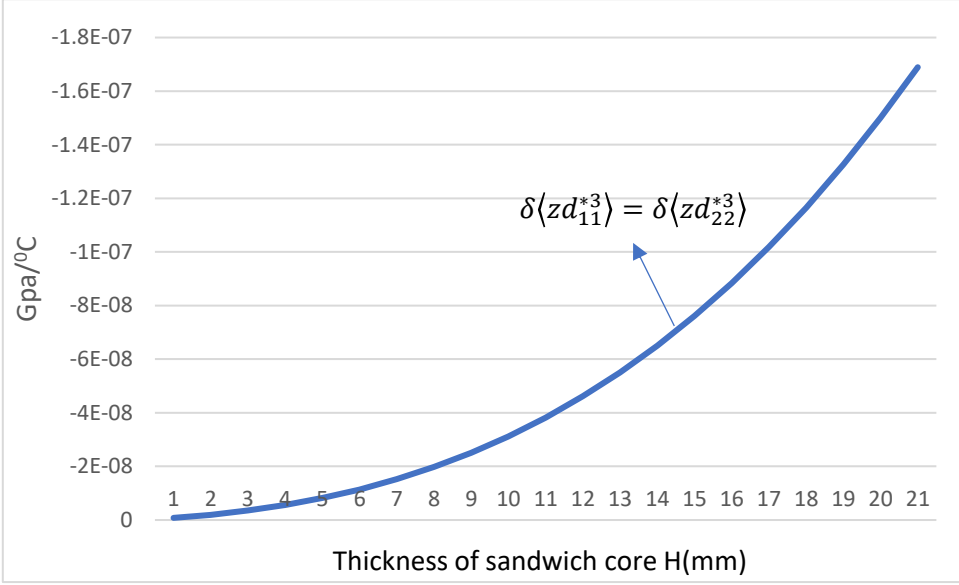


**Figure 6.49 Effective piezoelectric coefficients of hexagonal honeycomb structure**

Sandwich structures are an integral part of the composite world in today's industrial applications. It is lightweight and has a high strength-to-weight ratio. These two properties in themselves are a major contribution to industries through cost-cutting in raw material, manufacturing workforce, and also reducing the weight of their products. With the sandwich composites mostly finding their applications in aerospace, it is susceptible to damage on impacts. The impact of debris in space vehicles and bird strikes on aircraft shields or body is a common example of this. Even though it can give these certain mechanical properties, with the increase in core thickness, the laminates

used for the sandwich plates become more susceptible to damage when put under the impacts mentioned above.

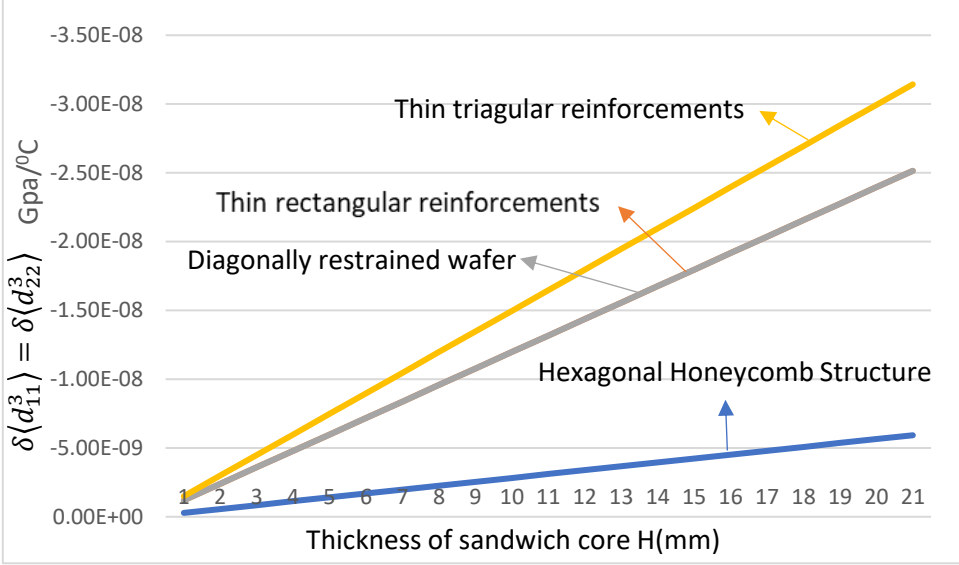


**Figure 6.50 Effective piezoelectric coefficients of various sandwich structures**

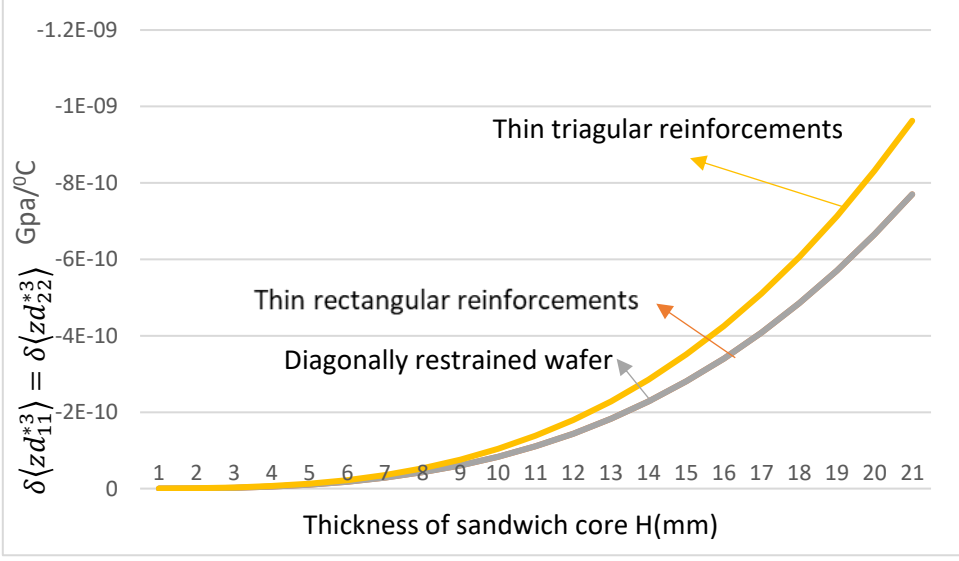


**Figure 6.51 Effective piezoelectric coefficients of various sandwich structures**

The sandwich structures used in car chassis with carbon fiber material have a usual range for stiffness of the material from 6 to 13 Gpa [73]. The results obtained are even better for the sample material used here and can be used to improve the applications further if the cost of the material allows the material to be used. The usual longitudinal

and transverse modulus is 17 Gpa for the material used in [73] and compared to E being 0.83 Gpa for the sample material H130. There is also the added effect of the high modulus piezoelectric material on the properties obtained.

Here, piezoelectricity can be of very good help in fine-tuning these properties and ironing out the shortcomings. As with the structures seen above, honeycomb cored structures offer good piezoelectricity in some directions with limitations here and there. If required, it can be used for these applications, but there are some limiting implications with the use of honeycomb, with one of them being that the impact falls on the hollow part of the sandwich panel. Then the piezoelectric effect is a bit nullified because of the absence of any material present there. So, the effect of the impact might be the same in that instance. The analysis of impacts was conducted in [69], and there are found to be catastrophic defects imparted by impact loading. Blunt objects are also seemingly more detrimental as it has more surface area and the impact increases when it is on weak hollow parts. So, several design considerations can be done to add more reinforcing elements in contact with the sandwich panels. The diagonally restrained and thin triangularly reinforced composite are good examples of these. The design can be modified in such a way as to demagnify the structure being analyzed in this section so that there will be a greater number of reinforcing components present in the structure. This will also increase the overall effect of piezoelectricity. Using the rectangularly reinforce structure even when it is able to offer coefficients similar to the diagonally retrained wafer might be a mistake. This is because of the design and alignment of the core in the rectangular reinforced sandwich structure. There are no crisscross elements in the core of this structure, and the properties or bonding offered are very much affected due to this design. As it is widely known that the properties between the elements in a

sandwich core are largely varying, the rectangular arrangement might be disadvantageous to avoid obvious problems like delamination, transverse cracking, and weakening of the core. The variety of structures seen in this section and the superior properties being given by almost all of these designs only create more streams for the composite sandwich panels to be used. For example, in [70], the sandwich composites were analyzed for application in biomedical industries as a replacement for knee joints. The composites were found to give superior properties in relation to the conventional metallic joints, and also the mechanical behavior such as resistance of wear, three-point bending, rotational capabilities were all found to be promising. This mechanical behavior creates better scope for these composites to be used in a wider range of applications.

## 6.7 SMART COMPOSITE PLATES WITH EMBEDDED ACTUATORS AND RAPIDLY VARYING THICKNESS

This section captures the effective properties in the piezoelectric and the thermal capabilities for smart composite sandwich structures. These structures are embedded with actuators meaning it exhibits piezoelectric behavior. We vary the thickness rapidly for these structures to capture the variation of properties along with the thickness. The structural display is done in section 5.7. The material properties for all the materials are taken in Gpa wherever pertinent for the analysis. It is to be noted that there is also the capability of varying the thermal piezoelectric properties by varying other parameters too such as the dimensions of the core and the laminate for the sandwich composites, and the material properties can also be varied, which will largely have an influence on the final properties of the composite material.

**Table 3 Material properties for the smart composites**

| Properties | E-glass/epoxy | PZT4 | PZT-5A |
|---|---|---|---|
| $E_1(10^9 Pa)$ | 38.6 | 81.23 | 61.0 |
| $E_2(10^9 Pa)$ | 8.27 | 81.23 | 61.0 |
| $G_{12}(10^9 Pa)$ | 4.14 | 30.6 | 22.6 |
| $G_{23}(10^9 Pa)$ | 3.281 | 25.6 | 21.1 |
| $G_{13}(10^9 Pa)$ | 4.14 | 25.6 | 21.1 |
| $\nu_{12}$ | 0.26 | 0.327 | 0.35 |
| $\nu_{21}$ | 0.055 | 0.327 | 0.35 |
| $d_{31}(10^{-10} C/N)$ | 0 | −1.238 | −1.238 |
| $d_{32}(10^{-10} C/N)$ | 0 | −1.238 | −1.238 |
| $\beta_1$ | 0.014 | | |
| $\beta_2$ | 0.29 | | |
| $\alpha_1(10^{-6}/°C)$ | 6.3 | | 1.5 |
| $\alpha_2(10^{-6}/°C)$ | 20 | | 1.5 |

Figure 6.52 and 6.53 represents the thermal properties for a smart composite structure with reinforced rib. The second structure is also that of a rib reinforced structure, but another layer of laminate is added to make it a sandwich structure. The properties can just be varied by taking the thickness of the plate which is being added to the sandwich structure. This structure offers the most typical values for these coefficients when generally considered for a composite. The range offered is also pretty good for the thicknesses being used. In practical applications, the use of these very thick cores is rare. In the $\langle \Theta_{11} \rangle$ direction, the variation of the properties is not present. The thickness does not have any effect on the reaction of the composites when exposed to thermal loads. The thermal expansion coefficients are the same from the lowest of thickness to the highest of thicknesses. In the other transverse $\langle \Theta_{22} \rangle$ direction, the variation is offered linearly with the increase in thickness, meaning an increase in the values of the thermal expansion coefficients.

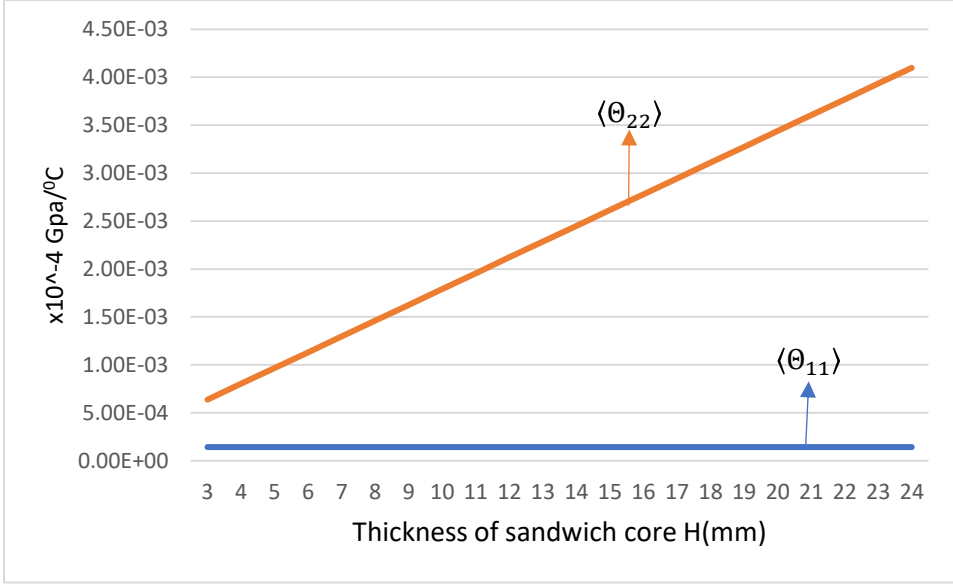


**Figure 6.52 Thermal coefficients of a sandwich rib structure**

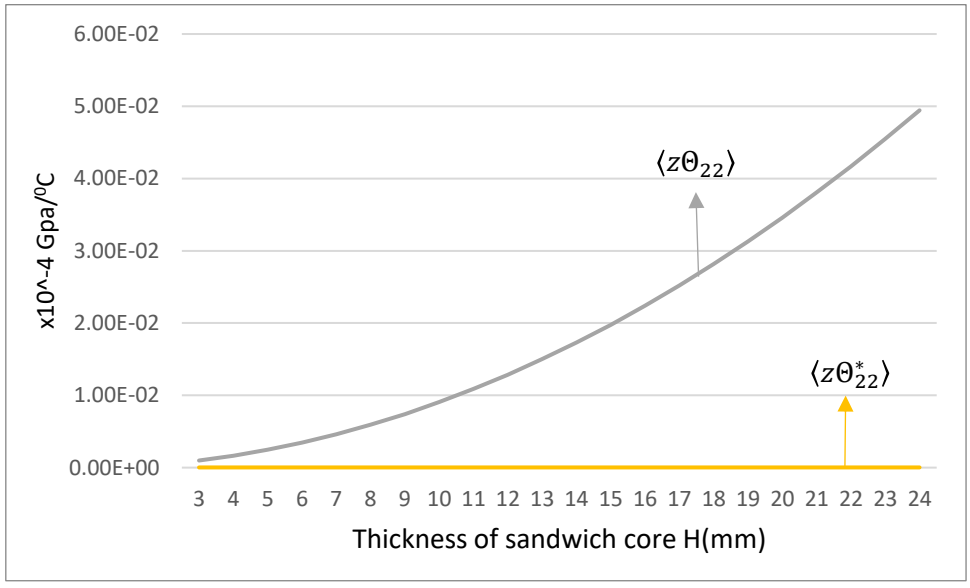


**Figure 6.53 Thermal coefficients of a sandwich rib structure**

In figure 6.53, again, the properties offered in the $\langle z\Theta^{*}_{22}\rangle$ direction is constant for all the thicknesses being analyzed. The thickness does not influence the coefficients. This is maybe because of the absence of the sandwich arrangement in the composite since all the sandwich structures give a variation with the change of the laminate thickness, and the core properties affect the thermal expansion coefficients to a large extent. In $\langle z\Theta_{22}\rangle$ direction, the composite structure offers a curved variation with a

relatively constant slope without rapidly varying the thermal coefficients. In this direction, the thickness does seem to have the most influence, and also, the proclivity of the material to be affected by thermal loading is higher. It is also noted that the thermal expansion coefficients for $\langle z\Theta_{11}\rangle$ direction is zero, and thus, the variation of any parameter does not affect the properties in this direction.

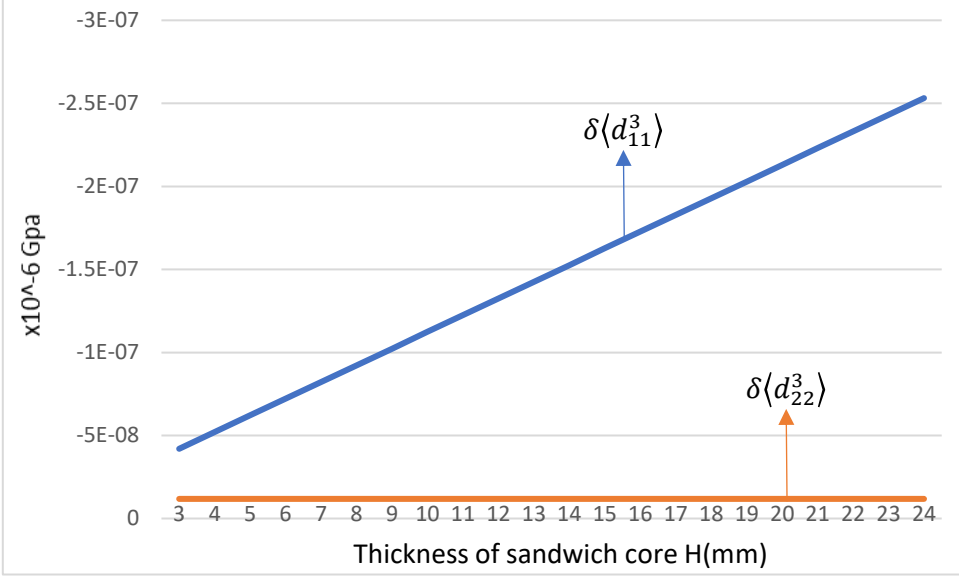


**Figure 6.54 Piezoelectric coefficients of smart composite structures**

Figures 6.54 and 6.55 represent the piezoelectric coefficients of the smart composite structures for all the pertinent structures in this analysis. All the variations are not captured in this illustration by the following figures as the properties and parameters used to procure the coefficients are the same. Here again, the piezoelectric coefficients also are not influenced by the parameters in the $\delta\langle d_{22}^3\rangle$ and $\delta\langle zd_{22}^{*3}\rangle$ direction. The variations captured along the thickness are comparable to the thermal expansion coefficients, with the values differing for piezoelectricity. In the $\delta\langle d_{11}^3\rangle$ direction, the piezoelectricity varies with the values becoming higher with the thickness getting higher.

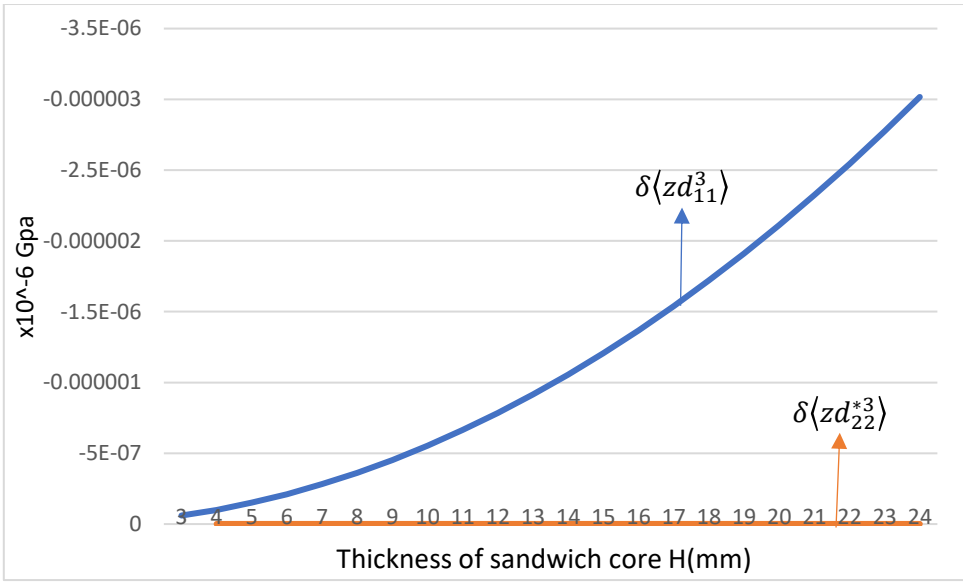


**Figure 6.55 Piezoelectric coefficients $\delta\langle zd_{11}^{3}\rangle$ and $\delta\langle zd_{22}^{*3}\rangle$ of smart composite structures**

The same goes for the properties in $\delta\langle zd_{11}^{3}\rangle$ and $\delta\langle zd_{11}^{*3}\rangle$ direction. But in the $\delta\langle zd_{11}^{*3}\rangle$ direction, there is a steep variation in the piezoelectric properties when the H becomes more than 15 mm, with the properties being relatively constant up to 15 mm.

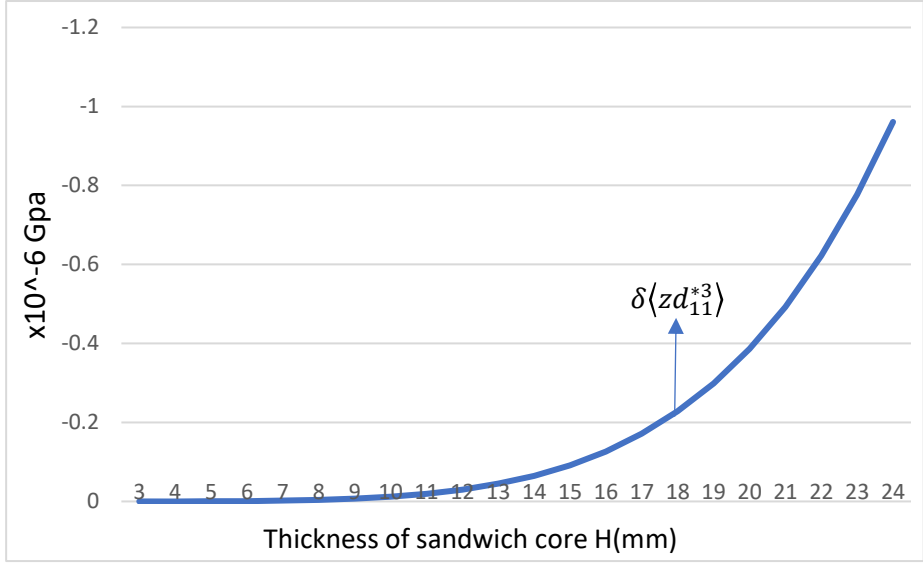


**Figure 6.56 Piezoelectric coefficient $\delta\langle zd_{11}^{*3}\rangle$ of smart composite structures**

Typical thermal expansion coefficients of carbon fiber composite structure used in aerospace grade requirements with fibers arranged at +45/-45 degrees are 0.9E-6 to 10

E-6. The coefficients obtained in this analysis for the rib reinforced structure are in the same range. In fact, the coefficients of thermal expansion illustrated in Figure 6.51 are lesser, which means it is better because it holds its structural integrity even when exposed to higher temperatures. These composite materials are also widely gaining applications in all aspects because of their superior properties, as always mentioned. The thermal expansion coefficient for traditional materials like steel is 11E-6 which is way larger than the properties offered by the composites. The piezoelectric properties offered by this plate are extremely efficient for use in practical applications. It can be actively used to control the thermal buckling and counter the vibrational effect laid on composites used in industries [72]. As seen in Figure 6.53, the thermal expansion coefficients represent the propensity of the composite to precisely undergo this buckling effect. The coefficients in the buckling are larger than that for the other directions, but the obtained properties are shown to be capable of improving by using the piezoelectric actuators. This will lead to improved properties of the composite by ensuring the structural stability of the sandwich structures. The control of these entities is possible only with the use of smart structures. These kinds of structures can be used in impact loading applications such as a gymnasium or an industrial workplace where constant lads are applied to the roofing to provide a cushioning effect. Also, the variation offered to the composite material in this direction due to piezoelectricity is the highest in these directions. One of the reasons may be the presence of more piezoelectric material being able to respond in these directions. The piezoelectric material can also be embedded with sensors to obtain data regarding stresses, vibration, and impact on the composite structure.

The alignment of the piezoelectric material being used can be changed to act in the perpendicular direction when being used for applications, as mentioned above. The

concrete grid reinforced ceilings are perfectly capable of bearing the loads, but this structure will help reduce the thickness of the ceiling and, therefore, lesser raw material and cost. The rib structure, as seen in Figure 5.11 is being used in roofing applications since the olden ages. The grid-reinforced composites then took over as years passed by. It offered more elasticity, longer life and avoided problems such as debonding, common in previous structures. But, then adding a sandwich layer to the rib reinforced structure, as seen in Figure 5.12, provides better properties as nowadays it is being used in the construction of tension bridges. As the wafers and ribs have some shortcomings in certain areas due to the absence of reinforcing elements, cores are redesigned in truss format to provide more load-bearing capabilities and efficient load dissipation.

## 6.8 PRISMATIC SMART COMPOSITE STRUCTURES

In this section, we consider a prismatic smart structure with reinforcements. We see two prismatic structures with 0- and 90-degree reinforcements and a rhombic prismatic structure with reinforcements in 30-, 90- and 150-degree angles.

**Table 4 Properties of E-glass/epoxy**

| Coefficient | E-glass/epoxy |
|---|---|
| $E_1$ (MPa) | 39,000 |
| $E_2$ (MPa) | 8600 |
| $G_{12}$ (MPa) | 3800 |
| $\alpha_{11}$ ($10^{-6}$/°C) | 7.0 |
| $\alpha_{22}$ ($10^{-6}$/°C) | 21 |
| $\alpha_{33}$ ($10^{-6}$/°C) | 21 |

The material taken as reinforcement is mostly taken as an orthotropic material in this analysis. The thickness of the reinforcement F is varied through the analysis, and the length and other dimensions are kept constant. In this case, an E-glass/ epoxy composite is taken, and the properties are depicted in the table above.

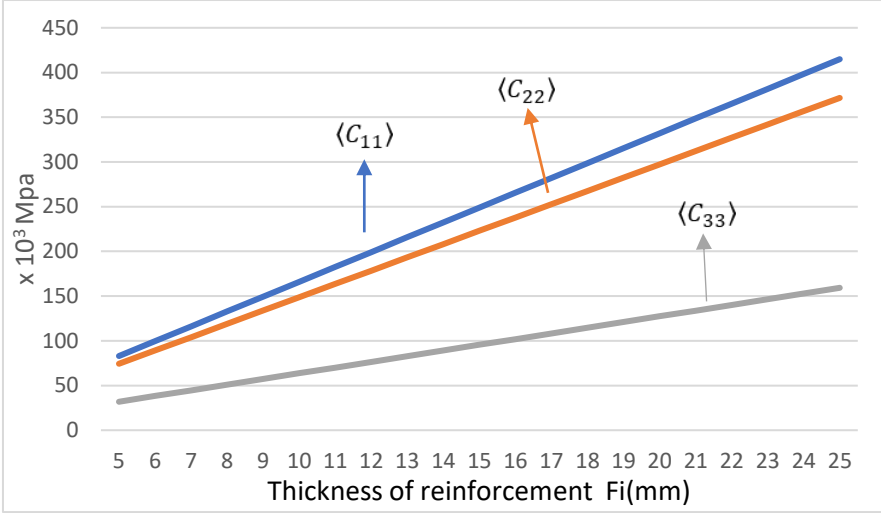


**Figure 6.57 Elastic coefficients of prismatic with $0^0$ and $90^0$ structure**

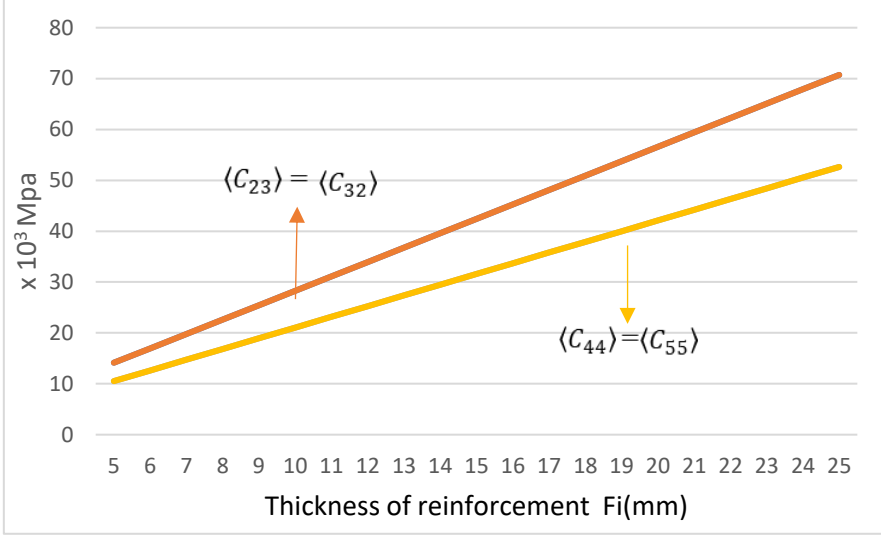


**Figure 6.58 Elastic coefficients of prismatic with $0^0$ and $90^0$ reinforcement**

In the prismatic structure with $0^0$ and $90^0$ reinforcement, the variation of elastic properties is shown in Fig 6.57 and 6.58. As expected, the elastic coefficient in the $\langle C_{11} \rangle$ direction is the highest of all the other properties while the $\langle C_{22} \rangle$ direction is not that far behind in the chart. It is also noticeable that the properties in the $\langle C_{23} \rangle \, and \langle C_{32} \rangle$ direction and $\langle C_{44} \rangle \, and \langle C_{55} \rangle$ direction are similar to each other while the former offer superior coefficients than the latter. These coefficients are well suited for mid-level applications.

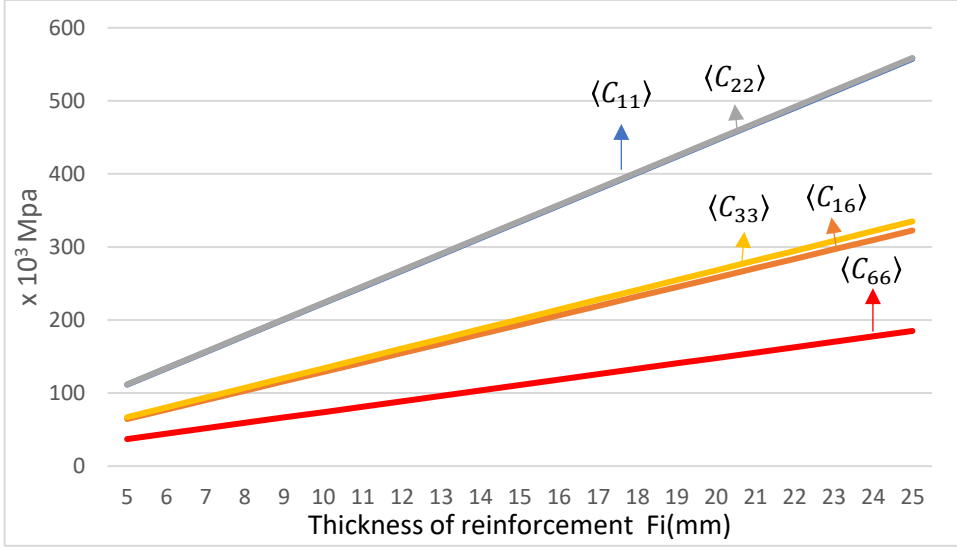


**Figure 6.59 Elastic coefficients $\langle C_{11}\rangle$ , $\langle C_{22}\rangle$ , $\langle C_{33}\rangle$ $\langle C_{16}\rangle$ $and\langle C_{66}\rangle$ of prismatic rhombic structure**

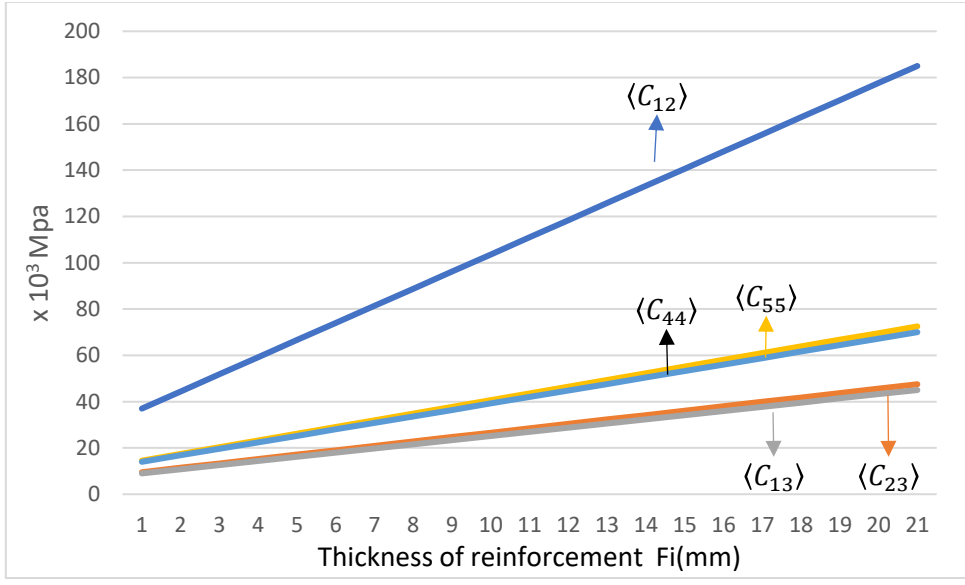


**Figure 6.60 Elastic coefficients $\langle C_{12}\rangle$ , $\langle C_{13}\rangle$ , $\langle C_{23}\rangle$ $\langle C_{44}\rangle$ $and\langle C_{55}\rangle$ of prismatic rhombic structure**

Figures 6.59 and 6.60 represent the elastic coefficients of the prismatic rhombic structure with 30-, 90- and 150-degree reinforcements. It is significant that this structure can offer a wide range of properties in many different directions compared to other structures. Here, $\langle C_{11}\rangle$ and $\langle C_{22}\rangle$ are nearly equal, which will expand its usage to a wide variety of applications as many other structures cannot attain this feature. $\langle C_{13}\rangle$ and $\langle C_{23}\rangle$

are the lowest among the set of variables discussed for this structure. It should not affect the applications of this structure as most industrial applications do not demand high-stiffnesses in these directions and will be satisfying to most of the requirements. $\langle C_{12} \rangle$ as expected, it is also able to offer comparatively significantly better properties than the other directions.

Compared to the first structure considered here, the rhombic configuration change can offer a higher set of stiffness values. This is because of the varied configuration of the fundamental constituents in the structure being able to manipulate the properties in certain directions. There is also the consideration of more reinforcing elements being added to the rhombic configuration being able to offer more superiority.

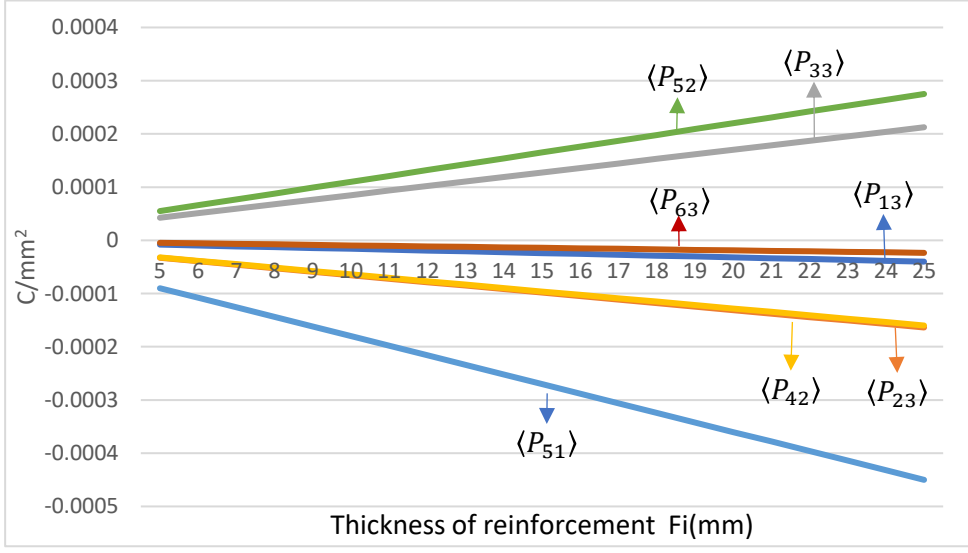


**Figure 6.61 Piezoelectric coefficients of prismatic rhombic structure**

Figure 6.61 can offer the variation of properties in the piezoelectric scale. Here, the negative and positive coefficients will trigger an expanding or a contracting dimensional change in the structure being used. This piezoelectric behavior is triggered by an electric pulse, as described before in the previous sections. Here, the coefficient $\langle P_{51} \rangle$ can offer the biggest variation of dimension in the structure since its's value is the

highest. The dimensional change in the structure is directly proportional to the value of the piezoelectric coefficient. $\langle P_{63} \rangle$ and $\langle P_{13} \rangle$ are the coefficients which can have the least effect on the composite structure, while the other coefficients are well-suited to offer decent variations to the composite structure.

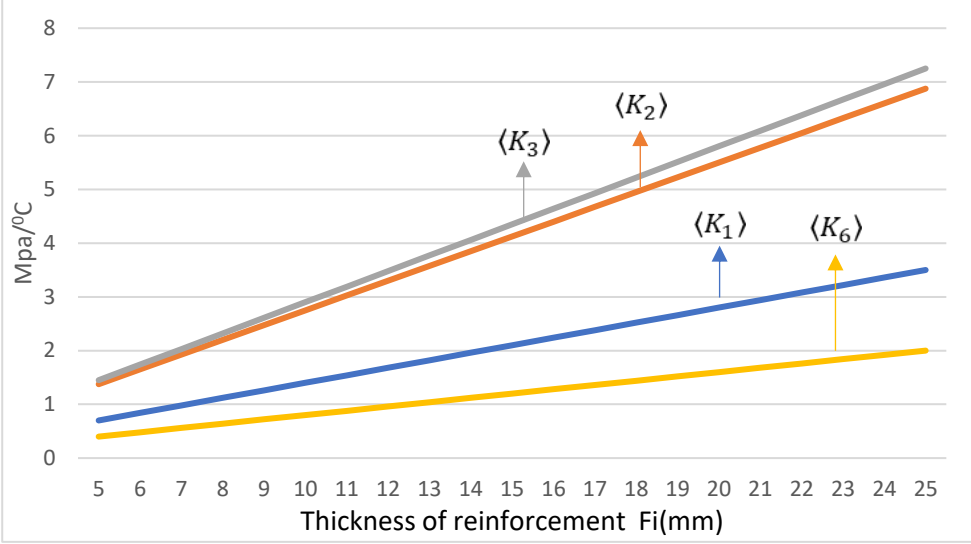


**Figure 6.62 Thermal coefficients of prismatic rhombic structure**

The thermal coefficients of a prismatic structure with a rhombic configuration, the same being analyzed in the previous figure, are portrayed in Fig 6.62. We capture the variation of these coefficients with the thickness of the reinforcements. We observe that the coefficients $\langle K_2 \rangle$ and $\langle K_3 \rangle$ offer similar properties and can offer superiority over others. These properties are also offering a higher variation in properties along with the thickness of the reinforcement, while the differential for $\langle K_1 \rangle$ and $\langle K_6 \rangle$ is relatively less.

The design of the prismatic structures is more of an open concept one and is easy to manufacture. The challenging part for manufacturing the prismatic composites we have seen in this analysis is that there is more contact between the reinforcements and the matrix layer. As we have seen in sandwich structures, there are bonding issues between the reinforcements and the sandwich laminates because of the vast variation in

properties between the core and the laminates. Here, there is more surface area under contact between the two layers of the composite material. The stiffness values indigenous to a polymer matrix composite are around 12-24 Gpa [73]. The values obtained here for the stiffness coefficients are lesser than that, adding to the problems discussed above. Piezoelectricity offered is good for these structures in comparison to other structures in this chapter. So, these composites can be used in more civil engineering applications where we will be able to avoid the question of delamination or debonding. The most common examples of this design are pavements and tiled panels. The tiles are laid on the floor, and a layer of cement acts as a resin to hold the tiles in their place. The arrangement of reinforcements in the prismatic structures also reminds us of the construction of brick walls. Thus, these composites can produce good soundproofing, high strength, and toughness, with drawbacks being their impact performance. Prismatic composites are also very promising in giving applications to transforming nanomaterials that will adjust themselves to the external effects exerted on them in a strategic manner, meaning they are where these effects are imparted can be separately made to react to them the loads. Because of its simple design and the versatility of offering piezoelectricity, these composites can also be used in dye fittings and clamps. The materials and resins used can be varied to provide better off-coming properties than cast-iron dyes, and the piezoelectric effect can easily loosen the finished product from the die. The piezoelectric effect is capable of being imparted in both the positive and negative phases in a certain direction, as seen in Figure 6.58. It lets us some space to provide some space for the natural expansion or contraction occurring after the product is cured. This also involves high temperatures because of the nature of the application, and phenolic resins can be used as it pretty much incapable of burning.

Manufacturing of these prismatic composites in itself can be problematic in the curing stages. Since the material arrangement is different from laminates and there is more exposure to air for the layers of resin. The formation of pores and inadequate bonding is a major concern. So, curing must be carried out slowly in different temperatures rather than exposing it directly to room temperature.

## 6.9 SMART COMPOSITE PLATES WITH GENERALLY ORTHOTROPIC REINFORCING NETWORKS

This section will conduct a parametric observation of properties for a thin smart composite reinforced plate reinforced with orthotropic bars, which may also exhibit piezoelectric behavior. Therefore, we consider the piezoelectric properties of the material PZT-5A as shown in Table 5. These reinforcements are homogenous and, for the sake of analysis, are taken to be in the 45-degree angle with the $y_1$ direction. This orientation angle, along with many other properties, can be varied for different uses. We assume $A_1=A_2=1$ and calculate the outcomes based on the variation of the volume of the structure.

**Table 5 Properties of PZT-5A**

| Coefficient | Value |
|---|---|
| $C_{11}^{(p)} = C_{22}^{(p)}$ (MPa) | 119 899.13 |
| $C_{33}^{(p)}$ (MPa) | 109 892.37 |
| $C_{12}^{(p)}$ (MPa) | 74 732.01 |
| $C_{13}^{(p)} = C_{23}^{(p)}$ (MPa) | 74 429.92 |
| $C_{44}^{(p)} = C_{55}^{(p)}$ (MPa) | 21 052.63 |
| $C_{66}^{(p)}$ (MPa) | 22 573.36 |
| $P_{13}^{(p)} = P_{23}^{(p)}$ (C mm$^{-2}$) | $-5.45 \times 10^{-6}$ |
| $P_{33}^{(p)}$ (C mm$^{-2}$) | $1.56 \times 10^{-5}$ |
| $P_{42}^{(p)} = P_{51}^{(p)}$ (C mm$^{-2}$) | $2.46 \times 10^{-5}$ |
| $\alpha_{11}^{(p)} = \alpha_{22}^{(p)}$ (°C$^{-1}$) | $-1.704 \times 10^{-10}$ |
| $\alpha_{33}^{(p)}$ (°C$^{-1}$) | $3.732 \times 10^{-10}$ |

In the analysis of this structure, we only capture the parametric variations of the piezoelectric coefficients and the thermal coefficients of the structure. Figures 6.63 and 6.65 are a representation of the piezoelectric coefficients for the thin reinforced structure.

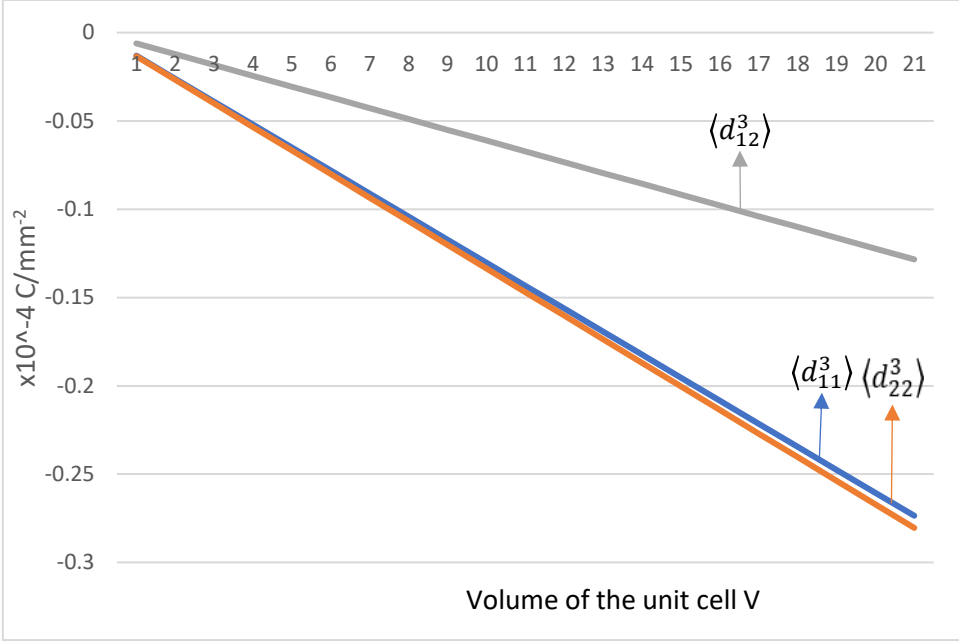


**Figure 6.63 Piezoelectric coefficients of thin reinforced structure**

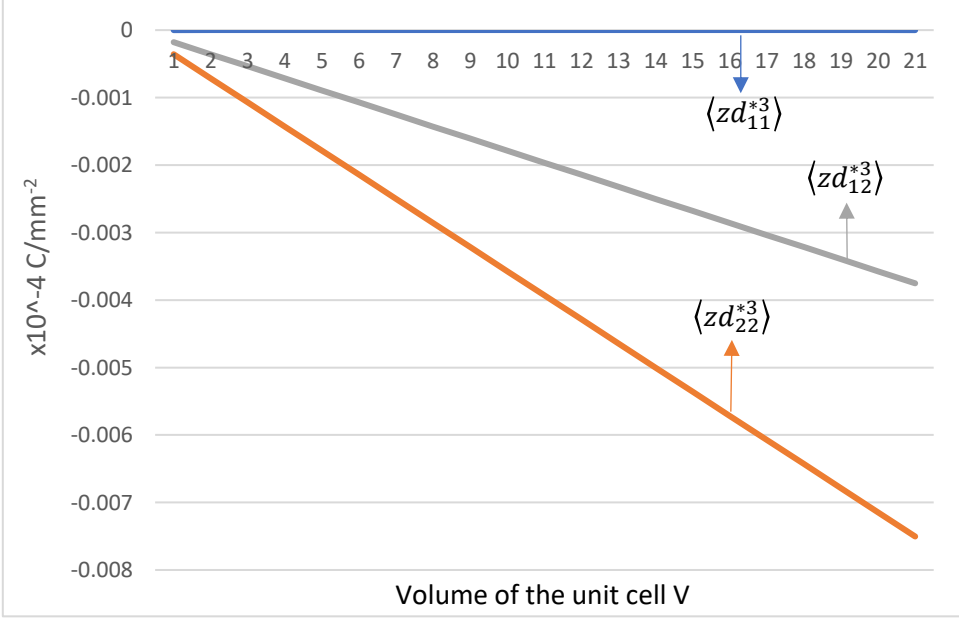


**Figure 6.64 Piezoelectric coefficients of thin reinforced structure**

The coefficients obtained are mostly in the negative direction overall in this analysis. The coefficients $\langle d_{11}^3 \rangle$ and $\langle d_{22}^3 \rangle$ are both nearly equal and offer more versatile piezoelectricity in terms of the other directions. All directions show a linear variation in

the negative direction, among which $\langle d_{12}^{3} \rangle$ varies the least in variation with the volume of the structure in question.

The coefficients $\langle zd_{22}^{*3} \rangle$ is again offering more piezoelectricity similar to the coefficient $\langle d_{22}^{3} \rangle$. It is also important to note that in the $\langle zd_{11}^{*3} \rangle$ direction, there is very less piezoelectricity offered in comparison to the other directions. Here, there is a variation of almost two times through the increment of the volume of the structure, but it has not been depicted as such because of the small outcomes shown in that direction. The coefficients in the $\langle zd_{12}^{*3} \rangle$ direction is in the mid-range and shows a variation averaging the other directions. The material's piezoelectricity in different directions will decide the extent of its ability to actuate and differ its properties through this actuation. So, the more the piezoelectricity, the better, as we will be able to modify the properties as required by passing a pulse or charge of some kind to the structure.

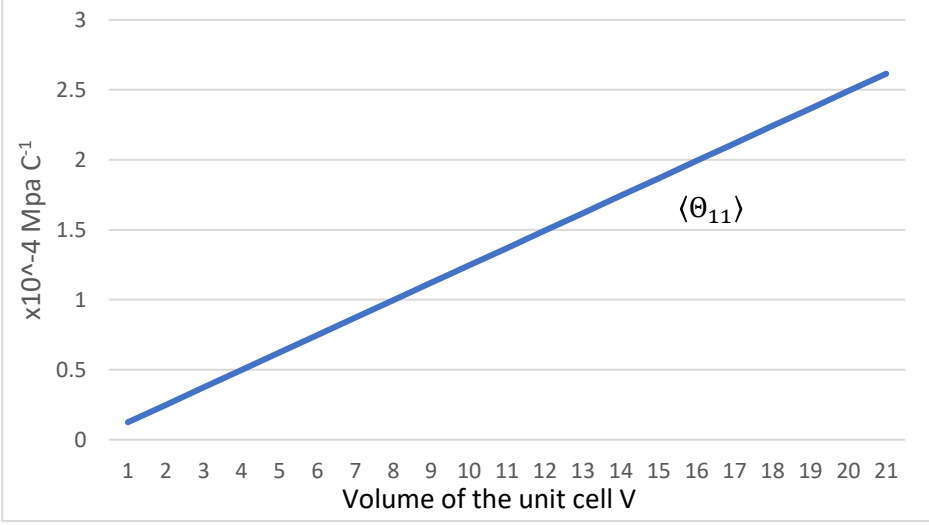


**Figure 6.65 Thermal coefficient $\langle \Theta_{11} \rangle$ of thin reinforced structure**

In figures 6.65 and 6.66, we represent the thermal coefficients of the thin reinforced homogenous structure. Figure 6.65 just represents the thermal coefficient $\langle \Theta_{11} \rangle$. This direction is unique as it offers a positive coefficient through the volume of

the structure. This coefficient also increases with the positive change in the volume of the structure.

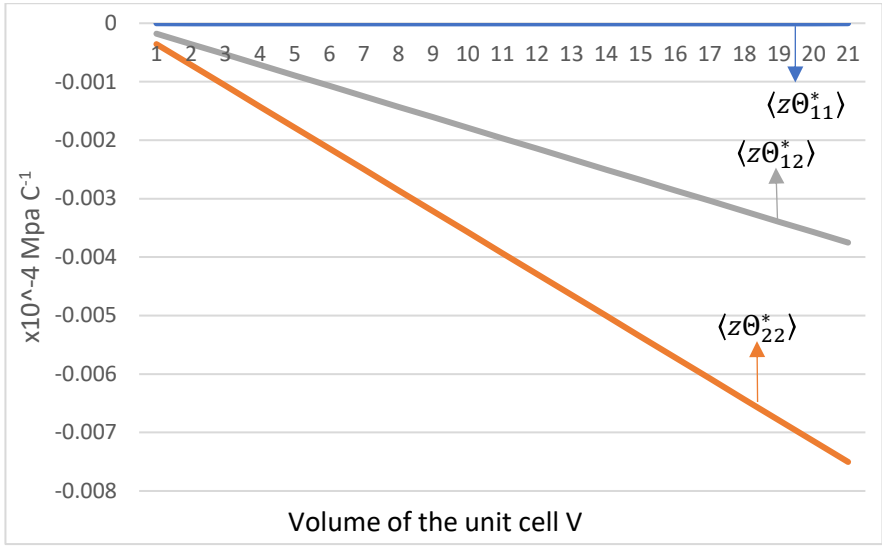


**Figure 6.66 Thermal coefficients of thin reinforced structure**

In figure 6.66, the plot captures the variations of the remaining thermal coefficients. In sync with the other coefficients obtained in this analysis, these coefficients also give values in the negative axis. Here, there does exist a variation of $\langle z\Theta_{11}^{*}\rangle$ by almost two times through the increment of the volume of the structure, but it has not been depicted as such because of the small outcomes shown in that direction. $\langle z\Theta_{22}^{*}\rangle$ shows the maximum variation among these coefficients and are giving decent values in comparison with other coefficients. The most important point to note is that these coefficients can be highly influenced according to the application by differing the input parameters such as volume fraction, materials used, type, size, geometrical parameters to obtain the desired coefficients.

The unit cell analyzed in this analysis is that of a thin orthotropic bar network reinforced structure. When these bar-reinforced structures combine to form a composite plate or shell, there are many design considerations to perform. This differs from the

standard grid reinforced structure in terms of the number of reinforcing elements being used. Thin smart composite structures can be used for applications involving single-bar reinforcements and standard plain alignment without e dimensional overlap. Barrels with single bar reinforcements can be helpful when carrying heavy materials. Design can be considered for the reinforcing framework to come from the bottom of the barrel to the barrel's walls. This will reduce the peel stress induced in the barrel when carrying heavyweights. But the most problematic issue with structures like this is the fracture and breakage properties.

Since these barrels are required to be hollow, and the lid does not help the structural integrity of the barrel, it tends to fracture on impact. So, in the search for replacements, military-grade thermoplastics were used to reduce breakage, and because of the elastic nature of plastic, it also tends to come back to its original shape. Tin barrels were also used, which on impact gets bent and does not fracture unless it is put to a very high load. These are some material considerations to be done for these types of composite structures. Thin bar reinforcements can also be an important consideration for use in roofing or ceiling applications. The bars can reinforce false roofing structures and act as a framework for proper bonding of the roofing material. This cannot be done with a concrete ceiling and can be used for lightweight materials like gypsum plaster. These bars can also be added to automobile roofs as a safety feature to ensure that the roof or body does not fracture on high impact in accidents. This will put a lot of compressive force on the roof, and the joints of this roof must be bolstered due to the increased weight of the reinforcing bars and to provide failure of joints. Thin, highly rigid materials can be added to tin sheets used in roofing to bolster the structural integrity of the roof. Most of the structures support the edges or, for that matter, just the corners are fully capable of

being reinforced using the orthotropic bars considered in this section. Industrial worktables can be reinforced using a network of bars to better suit the requirements to heavy impacts and constant stresses due to work being carried out. Bar reinforced cylindrical shells were considered for the application of being used as a marine pile, and the stresses are strains induced discussed in [71]. The results were satisfactory for the composite bars being used, and there was no buckling observed up to approximately 9000 KN of loading. Thermal properties obtained also suggest that the propensity of the object to undergo structural changes is lesser. Piezoelectric properties obtained show that it can be used to positively impact the load-bearing or impact resistance 70 capability of the structure.

## 6.10 WAFER REINFORCED PIEZOELECTRIC PLATE

In this section, we perform the data analysis of a wafer reinforced piezoelectric plate. The structural appearance of this plate is discussed in section 5.10, and the formulae from which the data has been derived is also described in that section. Here, we make some assumptions to help perform the analysis being that the reinforcing elements in this plate are considered to display piezoelectric properties, which in the case of a non-piezoelectric analysis may be kept to zero. Multiple coefficients are calculated and put forth further in the section. We take a laminate with elastic and piezoelectric properties, as shown in the table below.

The figures 6.67 and 6.68 are the illustration of the thermal coefficients of the wafer composite plate. Here, we see that the thermal properties are more on the higher side in comparison with the other plates in this analysis. The coefficients in the preliminary direction $\delta\langle\Theta_{11}\rangle$ is the lowest in this structure.

**Table 6 Elastic and Piezoelectric properties of $0^0$ PVDF**

| Material | 0° PVDF |
|---|---|
| $C_{11}$ (GPa) | 238.24 |
| $C_{12}$ (GPa) | 3.98 |
| $C_{13}$ (GPa) | 2.19 |
| $C_{22}$ (GPa) | 14.6 |
| $C_{23}$ (GPa) | 4.4 |
| $C_{33}$ (GPa) | 10.64 |
| $C_{44}$ (GPa) | 2.15 |
| $C_{55}$ (GPa) | 2.15 |
| $C_{66}$ (GPa) | 6.43 |
| $e_{31}(Cm^{-2})$ | –0.130 |
| $e_{32}(Cm^{-2})$ | –0.145 |
| $e_{33}(Cm^{-2})$ | –0.276 |
| $e_{24}(Cm^{-2})$ | –0.009 |
| $e_{15}(Cm^{-2})$ | –0.135 |

It can reach a value of 25*10^-6/$^0$C at the maximum h value used in this analysis when in the other direction, we can get properties on about 18*10^-5/$^0$C. In the $\delta\langle\Theta_{22}\rangle$ direction, the values are higher than the longitudinal direction but are the second-best of all in terms of its ability to resist expansion. Expansion of these plates is tolerable up to an extent, but the values of thermal expansion obtained from this composite plate overall are only suited to low temperatures and cannot be used in high heat applications such as engines, brake plates, etc. The properties also of interest is in the direction $\delta\langle\Theta_{11}^{*}\rangle$ as it increases steeply with an increase in thickness, offering highly unfavorable properties. It is unfavorable because it is highly desirable that the variation of the thickness of the composite plate does not have much impact on the thermal expansion coefficient of the plate. The $\delta\langle z\Theta_{11}^{*}\rangle$ direction has the highest thermal expansion value in this structure. Overall, the observation for the wafer reinforced structure is that the propensity of the composite plate to expand is on the higher side when exposed to higher temperatures.

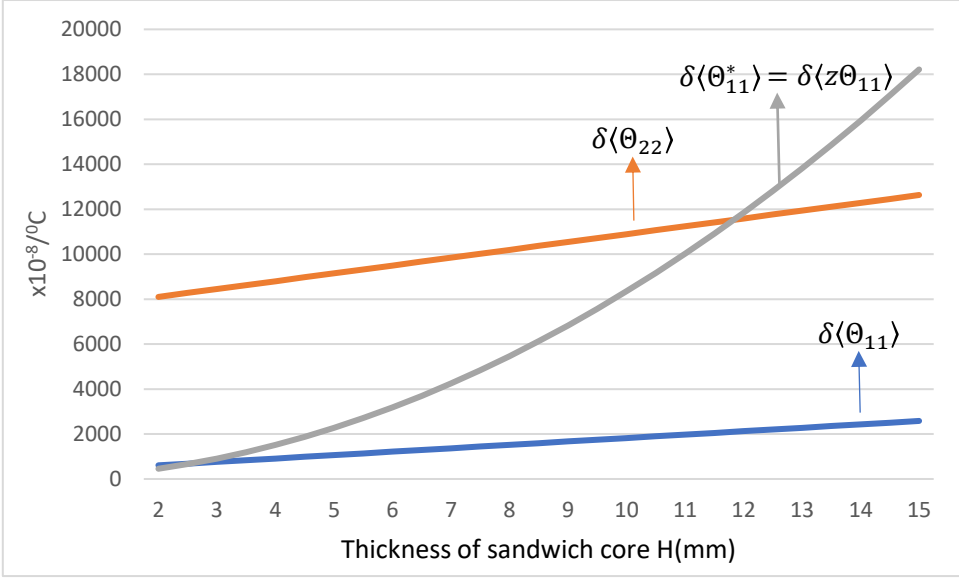


**Figure 6.67 Thermal coefficients of a wafer reinforced structure**

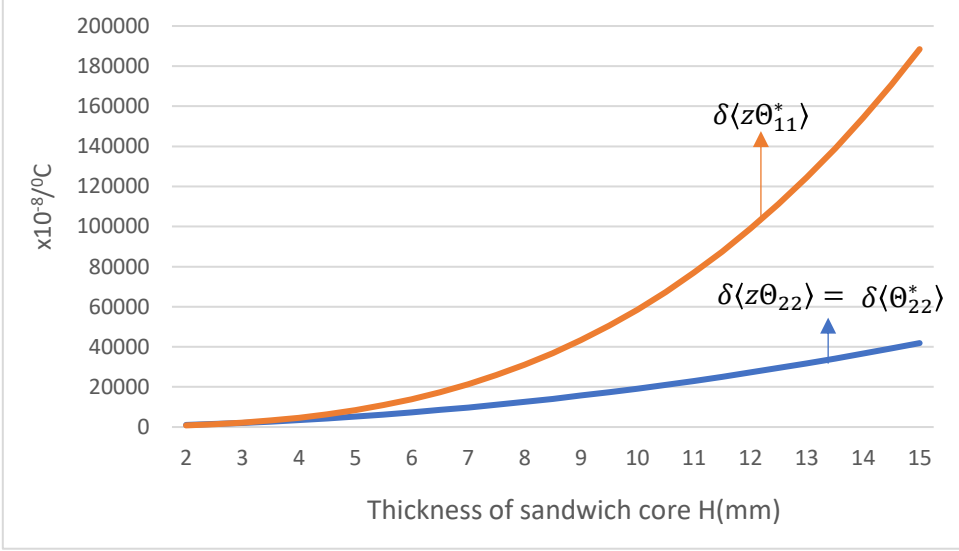


**Figure 6.68 Torsional Thermal coefficients of a wafer reinforced structure**

Figure 6.69 represents the variation of the hygroscopic coefficients along with the thickness of the composite plate. Here, it is observed that the moisture absorption is getting higher as expected when the thickness of the composites is increased. We get relatively lesser coefficients of hygroscopic in the $\delta\langle\Lambda_{22}\rangle$ direction and that is because of lower surface area in that direction, which reduces the tendency for the material to take in moisture.

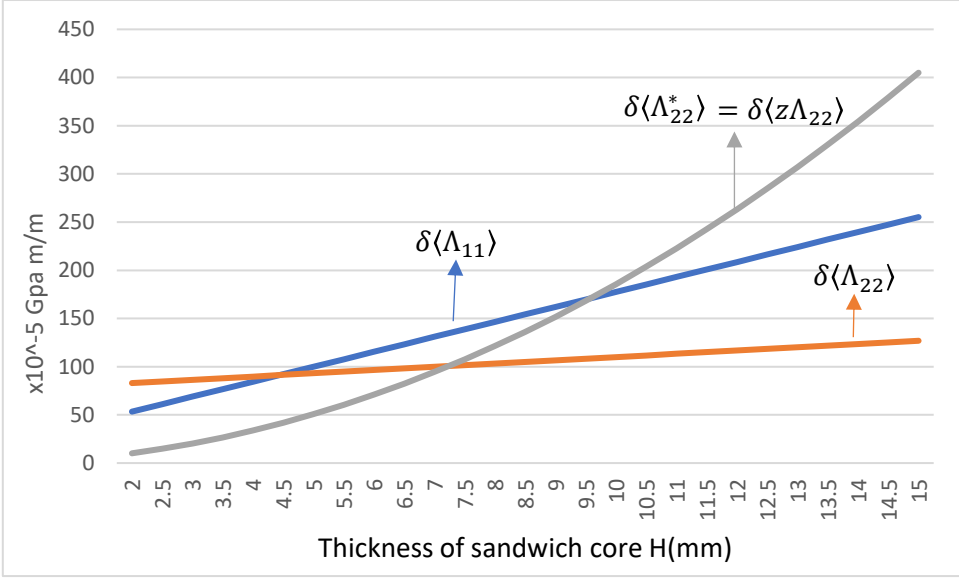


**Figure 6.69 Hygroscopic coefficients of a wafer reinforced structure**

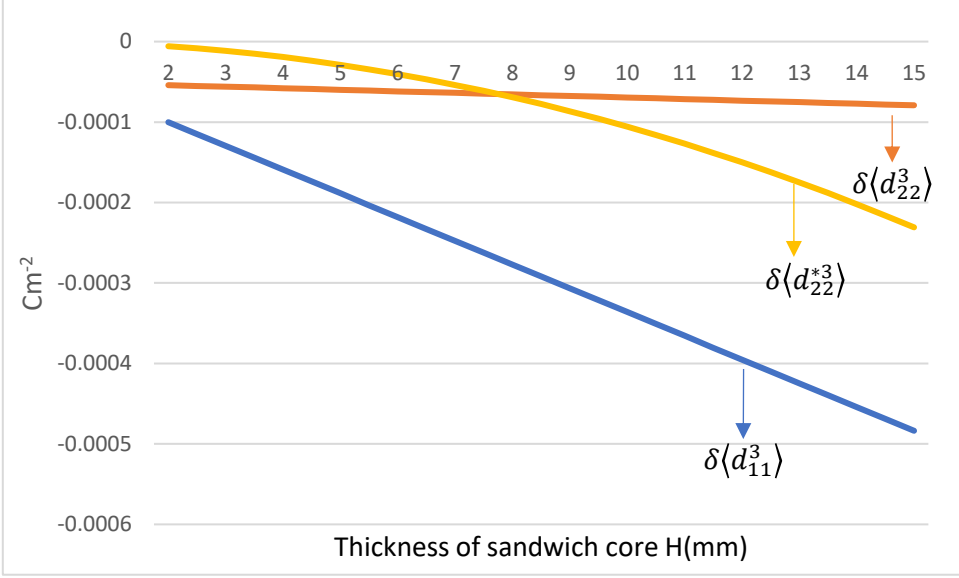


**Figure 6.70 Piezoelectric coefficients of a wafer reinforced structure**

The piezoelectric coefficients are shown in Figures 6.70 and 6.71. These coefficients represent the amount of volume change capable of being induced to the composite material. The values obtained here are all negative, meaning that we will be able to induce a negative effect on the composite, which is a contracting volume change to the composite plate. Here, as expected, the properties in the $\delta\langle d^3_{11}\rangle$ direction is the

most capable of being modified. It gives a constant rate of change through the increase of thickness, leading to a higher capability of modification with higher thickness. The $\delta\langle d_{22}^{3}\rangle$ direction is also able to give similar properties and variation as the $\delta\langle d_{11}^{3}\rangle$ direction but with a lesser capability of change in all thicknesses. It is also interesting to see that the $\delta\langle d_{22}^{3}\rangle$ the direction does not vary with the change in thickness, meaning that the piezoelectricity has zero effect on the nature of the composite plate in this direction.

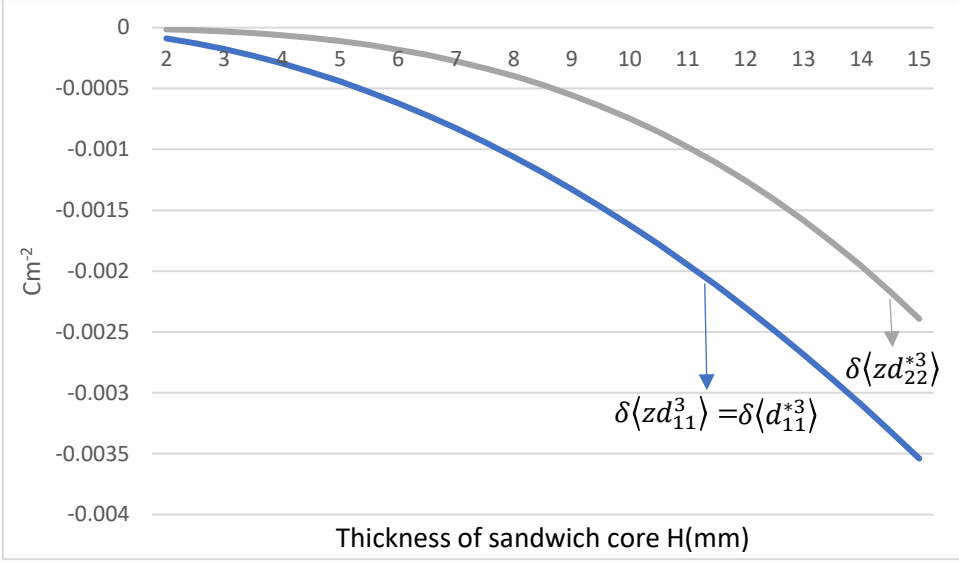


**Figure 6.71 Torsional piezoelectric coefficients of a wafer reinforced structure**

Figure 6.71 is a representation of the torsional piezoelectric coefficients of this structure. These torsional coefficients have more effect on the composite than the previous set of coefficients. The values are given nearly start from the highest possible effect created by the coefficients in Figure 6.70 and increases gradually with the increase in thickness. The properties in the $\delta\langle d_{11}^{*3}\rangle$ is the highest of all in terms of piezoelectricity.

Figures 6.72 and 6.73 illustrate the variation of elasticity with the increase in thickness of the composite plate. Here, the general observation is similar to the piezoelectricity in that the torsional elastic coefficients are higher than that in the preliminary directions.

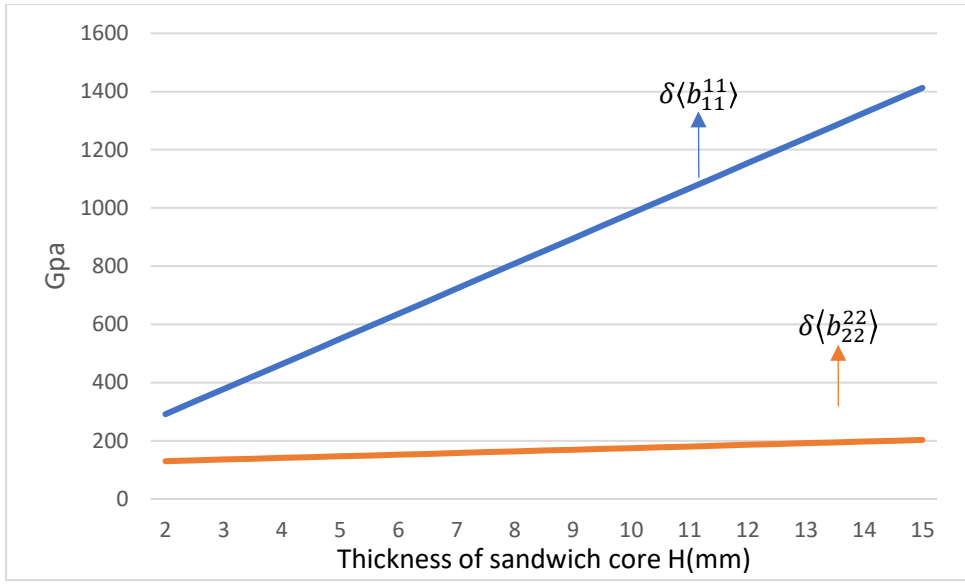


**Figure 6.72 Elastic coefficients of a wafer reinforced structure**

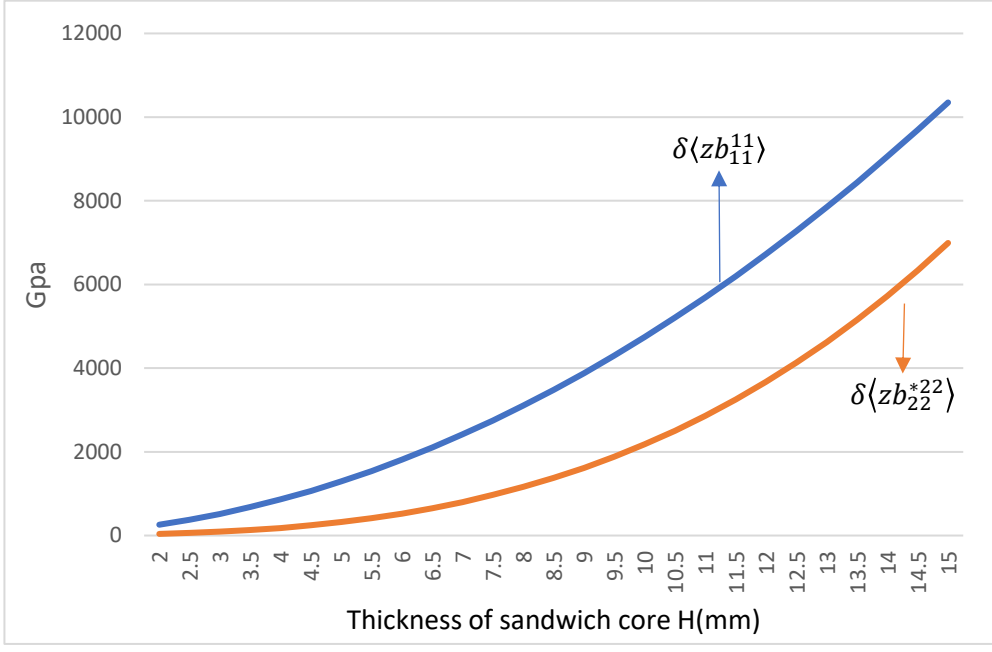


**Figure 6.73 Coupling elastic coefficients of a wafer reinforced structure**

The $\delta\langle b_{11}^{11}\rangle$ direction similar to most other structures offers higher coefficients than the $\delta\langle b_{22}^{22}\rangle$ counterpart. The $\delta\langle b_{11}^{11}\rangle$ direction also varies at a constant rate with an increase in thickness while the $\delta\langle b_{22}^{22}\rangle$ direction does not offer many variations and remains relatively standard for the thickness values.

In the figure above, the properties in the $\delta\langle \mathrm{zb}_{11}^{11} \rangle$ and $\delta\langle \mathrm{zb}_{22}^{*22} \rangle$ direction is shown. Both these directions start with elastic coefficients similar to each other and slowly increase with the thickness variation. With higher thicknesses, the $\delta\langle \mathrm{zb}_{11}^{11} \rangle$ direction can give a larger coefficient value than the other one.

In the above section, the hygroscopic coefficients, thermal coefficients, and piezoelectric coefficients for a wafer reinforced composite structure were analyzed. Common applications for these types of structures are insulation, false ceilings, waterproofing, etc. Applications like insulation and false ceiling are not subject to much loading, and their uses can be based upon the calculated coefficients rather than the calculation of the values of coefficients for the stiffness matrix of the composite since its effect on this will be very negligible. In these applications, the effect of moisture plays a very important role in deciding the use of the composite in these applications. The typical hygroscopic expansion coefficients for the polymers are between 0.002 and 0.005, and the composite plate is also in that range, with thickness increasing the moisture absorption of the plate. This is advantageous as the moisture does not hinder the use of the composite in these applications. The properties can also be extended by using a protective layer of resin on the top of the sandwich plate, which will provide water resistance to the composite. This is already being put to use in boats and ships to make the structure lightweight. The obtained piezoelectric coefficients are relatively high for the material being used, and this piezoelectricity can be used very well when these plates are being used for soundproofing or insulation purposes by creating a smart soundproof wall that will be able to absorb the sound frequencies by creating the piezoelectric reaction to the incoming soundwave. When used as insulating panels, the

thermal properties are also an important part to consider. Values ranging from 5*10^-6/K to 8*10^-6/K were obtained when a composite with cobalt was considered, and the coefficient of thermal expansion is higher than that. The thermal expansion propensity can be reduced by varying some factors during the design stages, such as the thickness of the core, the material sued for the reinforcement of the core, etc. This value also tends to increase with the decrease in Poisson's ratio of the material in use. The tendency of the sandwich composite plate must be within permissible limits to be used in the application. The values coinciding with the stiffness matrices are very good in the longitudinal direction, with it not offering a change transversely being a drawback. When carbon fiber is being used in a +45/-45-degree configuration, the stiffness coefficient is in the range of 70-100 Gpa concerning resins and other manufacturing factors. The material analyzed is also in the range and above. It is not practical as the higher modulus values are given, with the higher thickness being a disadvantage. The problem of porosities and cracks in the composites also affects the thermal conductivity of any material.

Damage and problem detection in sandwich structures are an integral part of ensuring its long-term usage. Since it is very new, the characteristics of the structures in the long term are unknown. Therefore, the manufacturing of the composites expected to be having the calculated value of coefficients, the process must be highly controlled in view of the reduction of any defects in the composite material. It will ensure the validity of the properties when the structure is put to use in reality.

## 6.11 GRID REINFORCED COMPOSITE SHELL WITH A NETWORK OF REINFORCEMENTS/ACTUATORS

In this section, we will discuss the variation of a grid reinforced shell with a network of reinforcements. The variation of the piezoelectric and the thermal properties

are captured along the volume fraction of the composite plate, which is defined as $\rho=V/h_1h_2$. There are also some stresses involved in this plate, which are not considered, assuming that it would not affect the overall properties when varying it along the volume fraction. There are also some other assumptions in this model, as described in Georgiades et al. [49]. Some of the important assumptions are that the reinforcements are made of fully orthotropic material. They are much stiffer than the matrix being used to bond the composite plate. The bonding of the composite layer is also taken to be in perfect order with no deficiencies. The properties of the reinforcements taken in this analysis are given in Table 6. For the sake of analysis, we take $A_1=A_2=1$ and thickness $\delta=0.5$ mm. The volume fraction of the composite is varied by varying the input dimensions, but the overall material properties are kept standard for the analysis.

**Table 7 Properties of the orthotropic reinforcements [49]**

| Coefficient | Value |
|---|---|
| $C_{11}^{(p)} = C_{22}^{(p)}$ (MPa) | 119899.13 |
| $C_{33}^{(p)}$ (MPa) | 109892.37 |
| $C_{12}^{(p)}$ (MPa) | 74732.01 |
| $C_{13}^{(p)} = C_{23}^{(p)}$ (MPa) | 74429.92 |
| $C_{44}^{(p)} = C_{55}^{(p)}$ (MPa) | 21052.63 |
| $C_{66}^{(p)}$ (MPa) | 22573.36 |
| $P_{13}^{(p)} = P_{23}^{(p)}$ (C/mm$^2$) | −5.45E−6 |
| $P_{33}^{(p)}$ (C/mm$^2$) | 1.56E−5 |
| $P_{42}^{(p)} = P_{51}^{(p)}$ (C/mm$^2$) | 2.46E−5 |
| $\alpha_{11}^{(p)} = \alpha_{22}^{(p)}$ (°C$^{-1}$) | −1.704E−10 |
| $\alpha_{33}^{(p)}$ (°C$^{-1}$) | 3.732E−10 |

Figures 6.74 and 6.75 illustrate the piezoelectric coefficients of the grid reinforced composite shell. In the $\langle d_{11}^3 \rangle$ direction, we get typical coefficients for the units of properties used, and as expected, there is the capability to create the maximum variation in this direction followed by the $\langle d_{22}^3 \rangle$ direction. Both directions have the

coefficients in the negative direction proportionally, creating a variational impact of the composite plate in the negative direction. We can create the maximum change of volume of the composite material in these aforementioned directions. These variations are multiplied with the increase in the volume fraction of the composite shell being used. There is a very minimal impact for the smallest dimensions used in the shell and nearly six times improved capability of variation for the highest volume fraction captured in the illustration below.

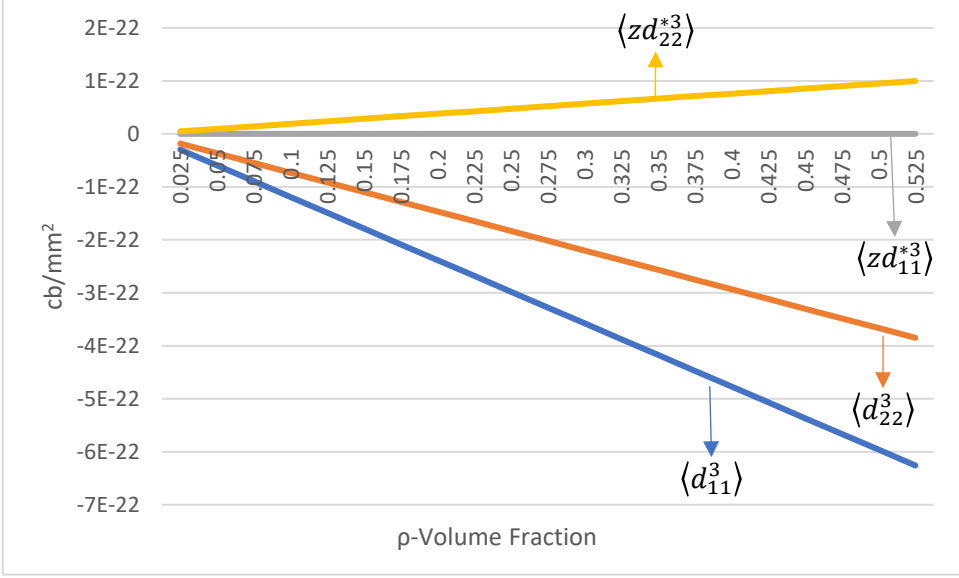


**Figure 6.74 Piezoelectric coefficients of a grid reinforced shell**

The other properties to be noted are the ones in $\langle zd_{11}^{*3} \rangle$ and $\langle zd_{22}^{*3} \rangle$ direction. These coefficients are in the positive direction of the x-axis are capable of inducing a positive volume change in the composite shell. It is noted that these coefficients are lesser than the other two directions in this graph and are only able to create a lesser volume change in the composite shell. Also, the $\langle zd_{11}^{*3} \rangle$ directional properties are very minimal and cannot offer significant variation to the composite shell compared to the other properties in the same shell.

Figure 6.75 captures the torsional piezoelectric coefficient of this composite shell. It is in the negative direction, and hence the negative contracting volume change can be induced. The torsional coefficient means that it can induce a twisting effect and can be used to counter the forces induced by external loads applied to the plate.

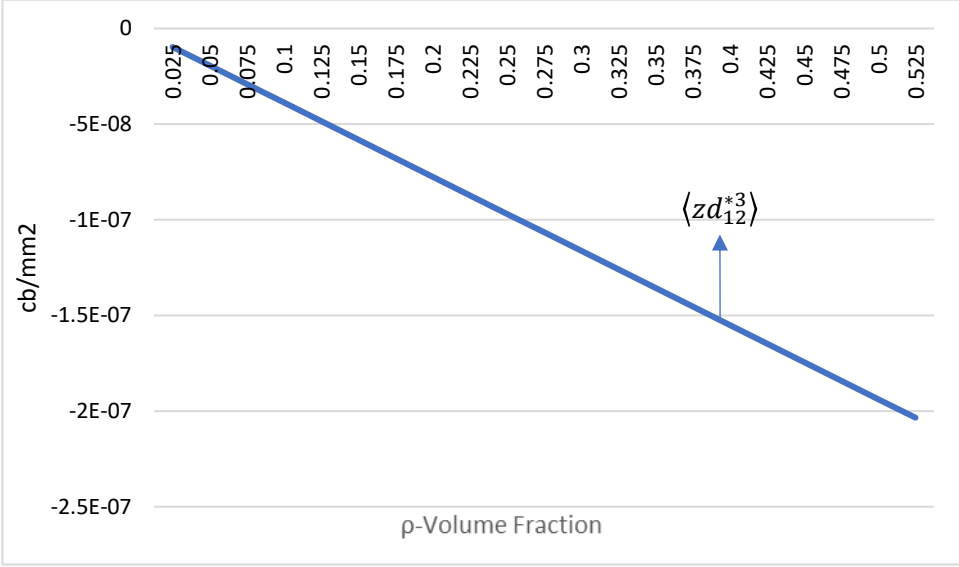


**Figure 6.75 Piezoelectric coefficient $\delta\langle zd_{11}^{*3}\rangle$ of a grid reinforced shell**

The following figures depict the thermal properties of the grid reinforced shell. Overall, the changes in the properties between directions are very high and significant. So, the usability of this shell in thermal applications involves complexity. The same material properties are considered for the calculation of these properties, and the values of the thermal coefficients are captured in Table 6. Using these coefficients, we try to capture the propensity for the composite shell to change its structural integrity in reaction to the thermal loading to the shell. The $\langle\theta_{22}\rangle$ direction, as captured in Figure 6.76, is also in the negative direction. The coefficients vary at a standard rate along the volume fraction of the composite shell, with more volume of the plate meaning more contraction to the plate. The preliminary directions are capable of contracting variations, whereas in

the $\langle\theta_{12}\rangle$ direction as shown in Figure 6.78, the material expands in reaction to thermal loading. The rate of change induced in this direction is also significantly higher than in the preliminary two directions.

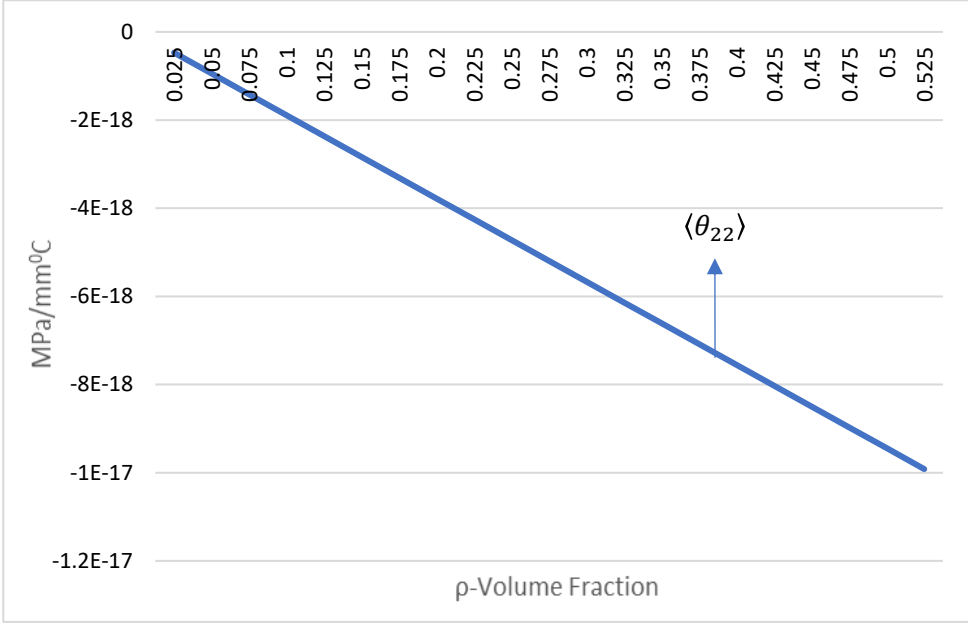


**Figure 6.76 Thermal coefficient $\theta_{22}$ of a grid reinforced shell**

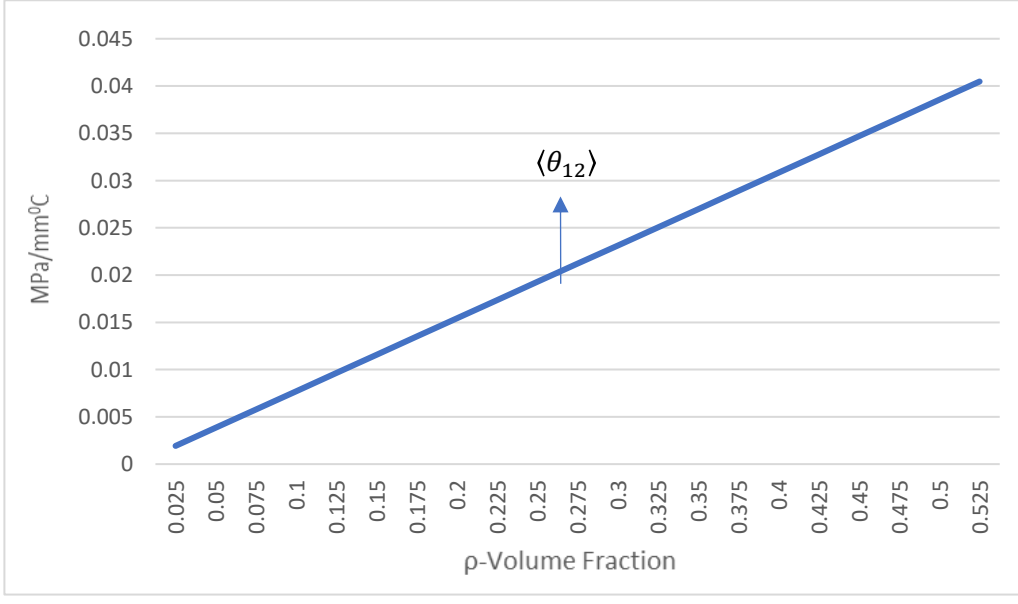


**Figure 6.77 Thermal coefficient $\theta_{12}$ of a grid reinforced shell**

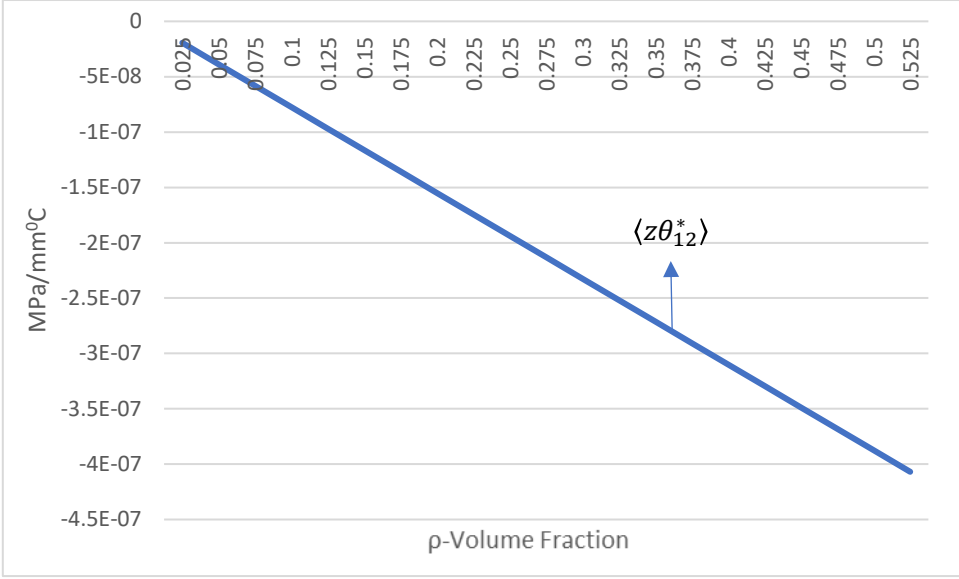


**Figure 6.78 Thermal coefficient $z\theta_{12}^{*}$ of a grid reinforced shell**

In figure 6.78, we also capture the variation of properties in the direction of $\langle z\theta_{12}^{*}\rangle$. In similarity with most other properties in this analysis, these coefficients are on the negative side. It is also able to create more variation in the shell than the preliminary two directions.

The grid reinforced composites are mainly used for construction and other reinforcement purposes. When we consider a plate, as we see in Figure 5.20, the scope of changing the design to complex shapes is very limited. So, these composites are well off being used as plates or bars. The most common application in this area is the composites used for ceilings, pillars, and beams in civil engineering applications. According to the thermal coefficients obtained for this structure for the material used in this analysis, the values are very pertinent as these parts are not exposed to much of the thermal impacts. There is also the piezoelectric capability possible in this structure by using a piezoelectric material. This will come in handy when used in more spontaneous applications such as bulletproof vests. The design idea must be changed for these vests

from the mundane alignment being used until this time. The reinforcements can be arranged in more of a criss-cross manner than the traditional $0/90^0$ alignment, which will increase its versatility to be used as a bulletproof vest. The coefficient of thermal expansion for these types of application differs from a -1E-6 to 1E-6 in-in/F. The coefficients obtained here are nearly in the range, with it slightly on the upper side with unit conversion. Normally, Kevlar extensively used in these applications has a negative coefficient of thermal expansion. When used along with a resin with a positive matrix, the coefficient of thermal expansion can be canceled out and made to be zero, with thermal impacts not affecting the structure. For example, a $-45^0/+45^0$ arrangement stacked upon each other has a very good capability of absorbing high impact than the $0^0/90^0$. The piezoelectric material can be used for making a smart vest through which we can apply an electric field to this material as a response to the impact created by a bullet on the vest. There are some complexions as the reaction is needed must be highly spontaneous, but the achievement of this is capable of triggering much-needed counter stress to increase the effectiveness of the bulletproof vest. As shown in Figures 6.75 to 6.78, it is observed that the propensity of the material to react to thermal impact or loading is very marginal. Still, these properties are for the material we used for the analysis, which may be disadvantageous in other aspects. Kevlar is the most used material for bulletproof vests, and the material we used can provide good thermal expansion coefficients comparable to Kevlar.

# CHAPTER 7 CONCLUSION

The present thesis outlines the importance and uses of composites and helps gain knowledge about the different types of composite materials available for use. Current disadvantageous trends leading to the sparse use of composites in layman applications due to the lack of long-term usage statistics were put forth. The asymptotic homogenization method was discussed in the hope of providing this valuable data to the engineers. Input data is given to these structures, and the properties were captured and discussed with its variation to dimensional parameters H and, in some cases, the volume fraction. Suitable applications in comparison to the material properties obtained were put forward.

The variation in properties along the thickness is almost always increasing, with some special cases being constant. The change does not influence the properties in some structures in thickness. But, various other parameters are varied to obtain the required properties like size, thickness of core, thickness of laminate, directional configuration of laminate, material properties, etc. In the parametric analysis, the independence of the properties in $\delta\langle b_{11}^{11}\rangle$ direction from the Poisson's ratio is noted. In these directions, the reinforcements lay more influence on the elastic properties. A general hypothesis among engineers, researchers, and this thesis is that the addition of reinforcing elements to a composite structure will positively impact the properties of the composite. But in opposition to the general hypothesis, there is observation in some cases that a greater number of reinforcements does not necessarily mean better properties, as noted in section 6.6. This was found when one of those structures had a greater number of reinforcing

elements than the other, suggesting that it is important to use the structure with better reinforcing elements to prevent defects.

The analysis of the piezoelectric composites was optimistic, and we were able to create more impact with the use of more piezoelectric material in the loading directions. Some of the properties obtained were negligible to create much impact on the properties. But, there is positive scope for modification of the behavior for the composite structures using this phenomenon. The properties were very promising to be used extensively in the future, capable of offering a variety of reactions to the load being applied on it. Most of the properties obtained through the analysis conducted in this thesis were also better than traditional materials like in smart rib, sandwich, and grid reinforced structures. The thermal reactivity of these composites was also explored for some of the composite structures. The coefficients observed for the materials and structure used were generally optimal and did not show any catastrophic behavior. This will create a more positive impact among engineers and use the composites where thermal loading might be involved. The thermal coefficients for prismatic structures were also observed, and they were able to offer properties comparable to smart rib structures. It was due to the similar construction of the structures analyzed.

In conclusion, the thesis achieves the solution to the lack of data for different composite structures. Data is also provided for smart composite structures, which can be a huge reckoning force in a myriad of applications in the current era and, most importantly, in the future. There is also hope that the data made available through this thesis will encourage the engineers to use composites for more common applications to benefit everyone with more flexibility.

## REFERENCES


[1] A.L. Kalamkarov, F.Tornabene, P. M. C. L. Pacheco, M. A. Savi, and G. C. Saha (2017)"Geometrically non-linear elastic model for a thin composite layer with wavy surfaces"

[2] A.V.Georgiades (2002)Experimental and Analytical Studies of Smart Composite Reinforcement and Structures

[3] V. V. Novozhilov, Thin Shell Theory (Noordhoff, Groningen, 1964)

[4] J. N. Reddy, Mechanics of Laminated Composite Plates and Shells: Theory and Analysis, 2nd ed. (CRC Press, Boca Raton, 2004)

[5] K.S Challagula, A.L.Kalamkarov et al. (2010) "Asymptotic homogenization modeling of smart composite generally orthotropic grid-reinforced shells: Part I theory., European Journal of Mechanics A/Solids,29(2010),530-540

[6] https://en.wikipedia.org/wiki/Fiber-reinforced_composite

[7] Seçkin Erden, Kingsley Ho(2017) in Fiber Technology for Fiber-Reinforced Composites

[8] https://www.intechopen.com/books/fiber-reinforced-polymers-the-technology-applied-for-concrete-repair/introduction-of-fibre-reinforced-polymers-polymers-and-composites-concepts-properties-and-processes

[9] http://www.materials.unsw.edu.au/tutorials/online-tutorials/5-particle-reinforced-composites

[10] https://www.explainthatstuff.com/composites.html

[11] Marya Raji, Hind Abdelloui et al., Prediction of the cyclic durability of woven-hybrid composites, 2019, pp 27-62

[12] ErcanSevkat, MalekBrahimi, Bearing strength of pin-loaded woven composites manufactured by vacuum-assisted resin transfer molding and hand lay-up techniques, Vol 10, 2011, pp 153-158

[13] Quanjin Ma et al., Filament winding technique: SWOT analysis and applied favorable factors, SCIREA Vol 3, 2019

[14] A.M.Fairuz et al., Pultrusion Process of Natural Fibre-Reinforced Polymer Composites, 2015, pp 217-231

[15] C.J.G. Plummer et al., Polymer Matrix Composites: Matrices and Processing, 2016, pp 7388-7396

[16] D.A. Hadjiloizi, A.L. Kalamkarov, G.C. Saha, K.G. Christoforidis, A.V. Georgiades, Micromechanical modeling of thin composite and reinforced magnetoelectric plates – Effective elastic, piezoelectric and piezomagnetic coefficients, 2017,pp-102-118

[17] D. A. Hadjiloizi, A. L. Kalamkarov, Ch. Metti, and A. V. Georgiades, Analysis of Smart Piezo-Magneto-Thermo-Elastic Composite and Reinforced Plates, DE Gruyter, 2014, Vol 1, pp 11-31

[18] Demetra A. Hadjiloizi, Alexander L. Kalamkarov & Anastasis V.Georgiades (2018) Micromechanical analysis of piezo-magneto-thermo-elastic T-ribbed and Π-ribbed plates, Mechanics of Advanced Materials and Structures, 25:8, 657-668, DOI:10.1080/15376494.2017.1308602

[19] K.S. Challagulla, A.V.Georgiades, A.L.Kalamkarov Asymptotic homogenization modeling of smart composite generally orthotropic grid-reinforced shells, EJMSOL, 2010, pp 530-540

[20] GOBINDA C. SAHA, ALEXANDER L. KALAMKAROV, Micromechanical Thermoelastic Model for Sandwich Composite Shells made of Generally Orthotropic Materials, Journal of SANDWICH STRUCTURES AND MATERIALS, Vol. 11—January 2009

[21] K.S. Challagulla, A.V. Georgiades, G.C. Saha, A.L. Kalamkarov, Micromechanical analysis of grid-reinforced thin composite generally orthotropic shells, Composites: Part B 39,2008, pp 627–644

[22] R. V. Kohn and M. Vogelius, A new model for thin plates with rapidly varying thickness, Int. J. Solids Struct. (UK) 20, 333–350(1984).

[23] R. V. Kohn and M. Vogelius, A new model for thin plates with rapidly varying thickness II: a convergence proof, Q. Appl. Math.(USA) 43, 1–22 (1985).

[24] R. V. Kohn and M. Vogelius, A new model for thin plates with rapidly varying thickness III: comparison of different scalings, Q.Appl. Math. (USA) 44, 35–48 (1986).

[25] D. Caillerie, Thin elastic and periodic plates, Math. Methods Appl. Sci. (UK) 6(1), 159–191 (1984).

[26] A. L. Kalamkarov, On the determination of effective characteristics of cellular plates and shells of periodic structure, Mech. Solids (USA) 22, 175–179 (1987).

[27] A. L. Kalamkarov, Asymptotic Homogenization Method and Micromechanical Models for Composite Materials and Thin-Walled Composite Structures, Chapter 1 in “Mathematical Methods and Models in Composites,” pp. 1–60 (Imperial College Press, London, 2014).

[28] A. L. Kalamkarov and A. Kolpakov, Analysis, Design, and Optimization of Composite Structures (Wiley, Chichester, N-Y, 1997).

[29] A.L. Kalamkarov, G.C. Saha, A.V. Georgiades, General micromechanical modeling of smart composite shells with application to smart honeycomb sandwich structures, Composite Structures 79, 2007, pp 18–33

[30] Gobinda C Saha, Alexander L Kalamkarov and AV Georgiades, Micromechanical analysis of effective piezoelastic properties of smart composite sandwich shells made of generally orthotropic materials, Smart Mater. Struct. 16, 2007, pp 866–883

[31] A.V. Georgiades, K.S. Challagulla, A.L. Kalamkarov, Modeling of the thermopiezoelastic behavior of prismatic smart composite structures made of orthotropic materials, Composites: Part B 37, 2006, pp 569–582

[32] Dominick V. Rosato, ... Matthew V. Rosato, in Plastic Product Material and Process Selection Handbook, 2004

[33] Azmi, M. Azham & Abdullah, Hasan & Idris, Maizlinda. (2013). Properties of polyurethane foam/coconut coir fiber as a core material and as a sandwich composites component. IOP Conference Series: Materials Science and Engineering. 50. 10.1088/1757-899X/50/1/012067.

[34] Gobinda C. Saha, Alexander L. Kalamkarov *, Anastasis V. Georgiades, Effective elastic characteristics of honeycomb sandwich composite shells made of generally orthotropic materials, Composites: Part A 38,2007, pp 1533–1546

[35] Navid Niknafs Kermani, Pavel Simacek, Suresh G.Advani, Porosity predictions during co-cure of honeycomb core prepreg sandwich structures, https://doi.org/10.1016/j.compositesa.2020.105824, Composites Part A: Applied Science and ManufacturingVolume 132, May 2020, 105824

[36] Hassan EM, Georgiades AV, Savi MA, Kalamkarov AL. Analytical and numerical analysis of 3D grid-reinforced orthotropic composite structures. International Journal of Engineering Science. 2011 Jul 1;49(7):589-605.

[37] Maricherla, Dinesh, "Advanced Grid Stiffened composite structures" (2005). LSU Master's Theses. 916. https://digitalcommons.lsu.edu/gradschool_theses/916

[38] Kalamkarov AL. On the determination of effective characteristics of cellular plates and shells of the periodic structure. Mech Solids 1987;22: 175–9.

[39] Kalamkarov AL. Thermoelastic problem for structurally non-uniform shells of regular structure. J Appl Mech Tech Phys 1989;30:981–8.

[40] Kalamkarov AL. Composite and reinforced elements of construction. New York: Wiley; 1992.

[41] S.L.Ogin, P.Potluri, Textile-reinforced composite materials, Volume 2: Technical Textile Applications, 2016, Pages 1-26

[42] D. A. Hadjiloizi, A. L. Kalamkarov, and A. V. Georgiades, Plane stress analysis of magnetoelectric composite and reinforced plates: Applications to wafer- and rib-reinforced plates and three-layered honeycomb shells, ZAMM · Z. Angew. Math. Mech. 97, No. 7, 786–814 (2017) / DOI 10.1002/zamm.201500228

[43] A.L.Kalamkarov and A.G.Kolpakov, On the analysis and design of Fiber-reinforced composite shells, Journal of Applied Mechanics, December 1996, Col 63/939

[44] Gobinda C. Saha, Alexander L. Kalamkarov_, Anastasis V. Georgiades, Asymptotic homogenization modeling and analysis of effective properties of smart composite reinforced and sandwich shells, International Journal of Mechanical Sciences 49 (2007) 138–150

[45] K.S. Challagulla, A.V. Georgiades, A.L. Kalamkarov, Asymptotic homogenization modeling of thin composite network structures, Composite Structures 79 (2007) 432–444

[46] A. L. KALAMKAROV, A. V. GEORGIADES, K. CHALLAGULLA AND G. C. SAHA, Micromechanics of Smart Composite Plates with Periodically Embedded Actuators and Rapidly Varying Thickness, Journal of THERMOPLASTIC COMPOSITE MATERIALS, Vol. 19—May 2006, DOI: 10.1177/0892705706062182

[47] A V Georgiades, A L Kalamkarov and K S Challagulla, Asymptotic homogenization model for generally orthotropic reinforcing networks in smart composite plates, Smart Mater. Struct. 15 (2006) 1197–1210, doi:10.1088/0964-1726/15/5/006

[48] A. V. Georgiades & A. L. Kalamkarov, Asymptotic Homogenization Models for Smart Composite Plates with Rapidly Varying Thickness: Part II—Applications, International Journal for Multiscale Computational Engineering, 2(1) 149–172 (2004)

[49] A.V.Georgiades, K.S.Challagulla , A.L.Kalamkarov, Asymptotic homogenization modeling of smart composite generally orthotropic grid-reinforced shells: Part II – Applications, European Journal of Mechanics A/Solids29(2010)541e556

[50] Ramani, Satyen. (2016). Analytical Study for Impact Strength Evaluation of Composite Circular Plate as per ISO 6603-I. International Journal of Emerging Technologies & Innovative research. 3. 156-164.

[50] Quantian Luo, Liyong Tong, High precision shape control of plates using orthotropic piezoelectric actuators, Finite Elements in Analysis and Design, Volume 42, Issue 11,2006,Pages 1009-1020,ISSN 0168-874X

[51] D.B. Koconis, L.P. Kollar, G.S. Springer, Shape control of compositeplates and shells with embedded actuators I: voltage specified, J. Compos.Mater. 28 (1994) 415–458.

[52] D.B. Koconis, L.P. Kollar, G.S. Springer, Shape control of compositeplates and shells with embedded actuators II: desired shape specified, J.Compos. Mater. 28 (1994) 459–482.

[53] Nguyen, Quan, and Tong, Liyong. "Shape Control of Smart Composite Plate with Non-rectangular Piezoelectric Actuators." Composite Structures 66.1 (2004): 207-14. Web.

[54] Choi, Sup, and Lee, Jung Ju. "The Shape Control of a Composite Beam with Embedded Shape Memory Alloy Wire Actuators." Smart Materials and Structures 7.6 (1998): 759-70. Web.

[55] Bravo-Castillero, Julián, Rodríguez-Ramos, Reinaldo, Mechkour, Houari, Otero, José A, and Sabina, Federico J. "Homogenization of Magneto-electro-elastic Multilaminated Materials." Quarterly Journal of Mechanics and Applied Mathematics 61.3 (2008): 311-32. Web.

[56] Igor V Andrianov, Vladimir I Bolshakov, Vladyslav V Danishevs'kyy, and Dieter Weichert. "Higher Order Asymptotic Homogenization and Wave Propagation in Periodic Composite Materials." Proceedings of the Royal Society. A, Mathematical, Physical, and Engineering Sciences 464.2093 (2008): 1181-201. Web.

[57] Yi, Yeong-Moo, Park, Sang-Hoon, and Youn, Sung-Kie. "Asymptotic Homogenization of Viscoelastic Composites with Periodic Microstructures." International Journal of Solids and Structures 35.17 (1998): 2039-055. Web.

[58] Cheng, Zhen-Qiang, Lim, C.W, and Kitipornchai, S. "Three-dimensional Asymptotic Approach to Inhomogeneous and Laminated Piezoelectric Plates." International Journal of Solids and Structures 37.23 (2000): 3153-175. Web.

[59] He, Zhelong, and Pindera, Marek-Jerzy. "Locally Exact Asymptotic Homogenization of Viscoelastic Composites under Anti-plane Shear Loading." Mechanics of Materials 155 (2021): 103752. Web.

[60] Avila-Pozos, O, Klarbring, A, and Movchan, A.B. "Asymptotic Model of Orthotropic Highly Inhomogeneous Layered Structure." Mechanics of Materials 31.2 (1999): 101-16. Web.

[61] Zinno, A, Fusco, E, Prota, A, and Manfredi, G. "Multiscale Approach for the Design of Composite Sandwich Structures for Train Application." Composite Structures 92.9 (2010): 2208-219. Web.

[62] Birman, Victor, and Kardomateas, George A. "Review of Current Trends in Research and Applications of Sandwich Structures." Composites. Part B, Engineering 142 (2018): 221-40. Web.

[63] Kim M, Choe J, Lee DG. Development of the fire-retardant sandwich structure using an aramid/glass hybrid composite and a phenolic foam-filled honeycomb. Compos Struct 2016;158:227–34.

[64] Berggreen, Christian, Quispitupa, Amilcar, Costache, Andrei, and Carlsson, Leif A. "Face/core Mixed Mode Debond Fracture Toughness Characterization Using the Modified TSD Test Method." *Journal of Composite Materials* 48.16 (2014): 1939-945. Web.

[65] Shen, Wei, Luo, Bailu, Yan, Renjun, Zeng, Haiyan, and Xu, Lin. "The Mechanical Behavior of Sandwich Composite Joints for Ship Structures." Ocean Engineering 144 (2017): 78-89. Web.

[66] Zhao, J.; Li, F.; Cao, X.; Li, H. Wave Propagation in Aluminum Honeycomb Plate and Debonding Detection Using Scanning Laser Vibrometer. *Sensors* 2018, *18*, 1669. https://doi.org/10.3390/s18061669

[67] Aviles, F, and Aguilar-Montero, M. "Mechanical Degradation of Foam-cored Sandwich Materials Exposed to High Moisture." Composite Structures 92.1 (2010): 122-29. Web.

[68] Fang, Hai, Zou, Fang, Liu, Weiqing, Wu, Chao, Bai, Yu, and Hui, David. "Mechanical Performance of Concrete Pavement Reinforced by CFRP Grids for Bridge Deck Applications." Composites. Part B, Engineering 110 (2017): 315-35. Web.

[69] He, Y., Zhang, X., Long, S. *et al.* Dynamic mechanical behavior of foam-core composite sandwich structures subjected to low-velocity impact. *Arch Appl Mech* 86, 1605–1619 (2016). https://doi.org/10.1007/s00419-016-1138-4

[70] Polisetti, Veerababu, and Ray, Paramita. "Thin Film Composite Nanofiltration Membranes with Polystyrene Sodium Sulfonate–polypiperazinetrimesamide Semi-interpenetrating Polymer Network Active Layer." Journal of Applied Polymer Science 137.44 (2020): 49351-N/a. Web.

[71] https://www.fhwa.dot.gov/publications/research/infrastructure/geotechn/04017

[72] Li, Jinqiang, Li, Fengming, and Narita, Yoshihiro. "Active Control of Thermal Buckling and Vibration for a Sandwich Composite Laminated Plate with Piezoelectric Fiber-reinforced Composite Actuator Facesheets." The Journal of Sandwich Structures & Materials 21.7 (2019): 2563-581. Web.6.8

[73] https://www.performancecomposites.com/about-composites-technical-info/124-designing-with-carbon-fiber.pdf

[74] D. Dai, M. Fan,1 - Wood fibers as reinforcements in natural fibre composites: structure, properties, processing and applications,Editor(s): Alma Hodzic, Robert Shanks,Natural Fibre Composites,Woodhead Publishing,2014,Pages 3-65,ISBN 9780857095244, https://doi.org/10.1533/9780857099228.1.3.

[75] Novo, P.J, Silva, J.F, Nunes, J.P, and Marques, A.T. "Pultrusion of Fibre Reinforced Thermoplastic Pre-impregnated Materials." Composites. Part B, Engineering 89 (2016): 328-39. Web.75

[76] Wanhill, Russell. (2017). Carbon Fibre Polymer Matrix Structural Composites. 10.1007/978-981-10-2134-3_14.

[77] Kainer, K.U. (2006). Basics of Metal Matrix Composites. In Metal Matrix Composites, K.U. Kainer (Ed.). https://doi.org/10.1002/3527608117.ch1